

STUDIA UNIVERSITATIS BABEȘ-BOLYAI, CLUJ-NAPOCA, ROMÂNIA

CHEMIA

Volume 55 (2010) No. 3

3/2010



STUDIA UNIVERSITATIS
BABEȘ-BOLYAI

STUDIA UNIVERSITATIS BABEȘ-BOLYAI

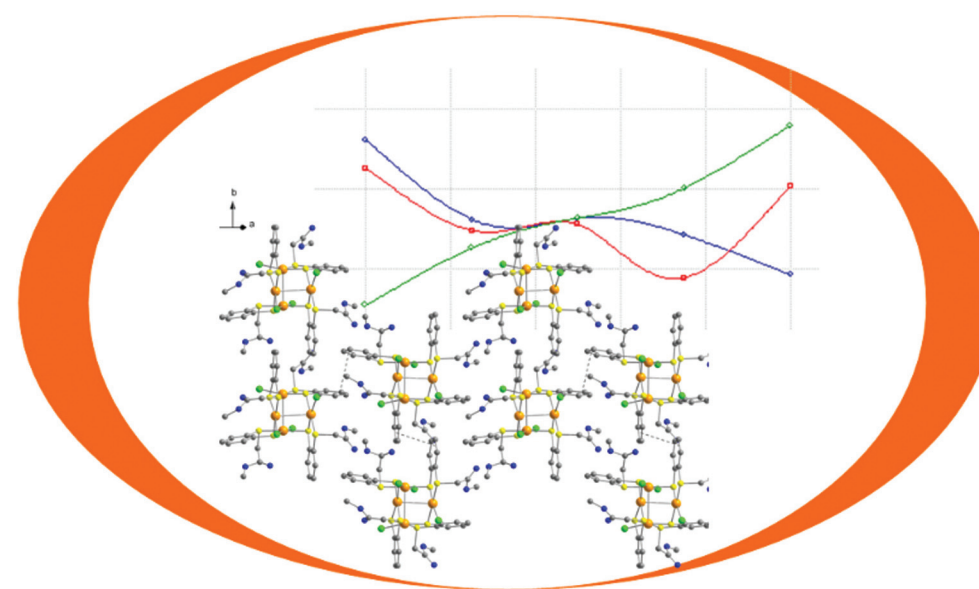
Other titles in the series are:

AMBIENTUM
BIOETHICA
BIOLOGIA
CHEMIA
DRAMATICA
EDUCATIO ARTIS GYMNASTICAE
EPHEMERIDES
EUROPAEA
GEOGRAPHIA
GEOLOGIA
HISTORIA
HISTORIA ARTIUM
INFORMATICA
IURISPRUDENTIA
MATHEMATICA
MUSICA

NEGOTIA
OECONOMICA
PHILOLOGIA
PHILOSOPHIA
PHYSICA
POLITICA
PSYCHOLOGIA-PAEDAGOGIA
SOCIOLOGIA
THEOLOGIA CATHOLICA
THEOLOGIA CATHOLICA LATINA
THEOLOGIA GRAECO-CATHOLICA
VARADIENSIS
THEOLOGIA ORTHODOXA
THEOLOGIA REFORMATA
TRANSYLVANICA

www.studia.ubbcluj.ro
office@studia.ubbcluj.ro

STUDIA UNIVERSITATIS BABEȘ-BOLYAI - CHEMIA



CHEMIA



ISSN: 1224-7154



CLUJ UNIVERSITY PRESS
51 B.P. Hasdeu Street, 400371
Cluj-Napoca, ROMANIA

3/2010

STUDIA UNIVERSITATIS BABEŞ-BOLYAI

SERIES

CHEMIA

EDITORIAL OFFICE: 11, Arany Janos Str., Cluj-Napoca, ROMANIA, Phone: +40 264 593833

HONORARY EDITOR:

IONEL HAIDUC, Member of the Romanian Academy

EDITOR-IN-CHIEF:

LUMINIŢA SILAGHI-DUMITRESCU

EDITORIAL BOARD:

PAUL ŞERBAN AGACHI, Babeş-Bolyai University, Cluj-Napoca, Romania
LIVAIN BREAU, UQAM University of Quebec, Montreal, Canada
HANS JOACHIM BREUNIG, Institute of Inorganic and Physical Chemistry,
University of Bremen, Bremen, Germany
JEAN ESCUDIE, HFA, Paul Sabatier University, Toulouse, France
ION GROSU, Babeş-Bolyai University, Cluj-Napoca, Romania
EVAMARIE HEY-HAWKINS, University of Leipzig, Leipzig, Germany
FLORIN DAN IRIMIE, Babeş-Bolyai University, Cluj-Napoca, Romania
FERENCZ KILAR, University of Pecs, Pecs, Hungary
BRUCE KING, University of Georgia, Athens, Georgia, USA
ANTONIO LAGUNA, Department of Inorganic Chemistry, ICMA,
University of Zaragoza, Zaragoza, Spain
JURGEN LIEBSCHER, Humboldt University, Berlin, Germany
KIERAN MOLLOY, University of Bath, Bath, UK
IONEL CĂTĂLIN POPESCU, Babeş-Bolyai University, Cluj-Napoca, Romania
CORNELIA MAJDIC, Babeş-Bolyai University, Cluj-Napoca, Romania
CRISTIAN SILVESTRU, Babeş-Bolyai University, Cluj-Napoca, Romania

EXECUTIVE EDITOR:

GABRIELA NEMEŞ

STUDIA

UNIVERSITATIS BABEȘ-BOLYAI

CHEMIA

3

Desktop Editing Office: 51ST B.P. Hasdeu, Cluj-Napoca, Romania, Phone + 40 264-40.53.52

CUPRINS – CONTENT – SOMMAIRE – INHALT

ANUAR KASSIM, HO SOON MIN, ATAN SHARIF, SARAVANAN NAGALINGAM, X-Ray Diffraction and Atomic Force Microscopy Studies of Chemical Bath Deposited FeS Thin Films	5
BOGDAN TUTUNARU, ADRIANA SAMIDE, ADINA CIUCIU, MIRCEA PREDA, Anticorrosive Protection of Carbon Steel by Electrosynthesis of Polyaniline	13
ADINA CIUCIU, ADRIANA SAMIDE, BOGDAN TUTUNARU, MIRCEA PREDA, Corrosion Behavior of Stainless Steel Coated with Poly(vinyl Alcohol) Film Doped with Strontium Ranelate	23
MARIA LOREDANA SORAN, SIMONA CODRUTA COBZAC, CODRUTA VARODI, ILDIKO LUNG, EMANOIL SURDUCAN, VASILE SURDUCAN, Extraction and Chromatographic Determination of Essentials Oils from <i>Ocimum Basilicum L.</i> Leaves	31
LÁSZLÓ SZÉLL, VALENTINA CETEAN, LUCIA GAGEA, ANIKÓ TÓTH, ROMAN CECILIA, ROMAN MARIUS, GOG ADRIANA, Recovery Possibilities of Power Plant Fly Ash from Zalău	39
LACRIMIOARA SENILA, ADRIANA GOG, MARIN SENILA, CECILIA ROMAN, FLORIN DAN IRIMIE, Analysis of Glucose Obtained from Wood Carbohy- drates by Gas Chromatography-Mass Spectrometry	51

MARIA GOREA, RODICA CREȚ, DELIA MARIA SIMUȚ, Characterization of Some SnO ₂ Ceramics with ZnO and Sb ₂ O ₃ Additives.....	57
SILVIA IMRE, SZENDE VANCEA, GRIGORE DOGARU, CARMEN CĂLDĂRARU, CAMIL-EUGEN VARI, MARIA TITICA DOGARU, New Liquid Chromatography Coupled with Mass Spectrometry Method for Ciprofloxacin Monitoring in Human Plasma.....	65
LIVIA PATRASCU, IRINA DOBRE, PETRU ALEXE, K-Carrageenan Effects on Texture Characteristics of Meat Emulsified Systems.....	75
MIRELA MICLEAN, ERIKA LEVELI, ADRIANA GOG, LUDOVIC FERENCZI, CORNELIA MAJDIK, CARMEN PUIA, CECILIA ROMAN, Determination of Total Petroleum Hydrocarbons in Contaminated Soil by FTIR and GC-FID Methods.....	83
ALEXANDRA-GERTRUD HOSU-PRACK, IOAN PETEAN, GEORGE ARGHIR, LIVIU-DOREL BOBOS, MARIA TOMOAI-COTISEL, Particulate Matters Found in Urban Street Dust.....	93
RODICA DOMNICA NAȘCU-BRICIU, COSTEL SÂRBU, The Lipophilicity Determination of some Pesticides by High Performance Thin-Layer Chromatography and Various Computing Methods.....	105
JULIA SZAKÁCS, DAN RUSU, MARIANA RUSU, New Perspectives in Polyoxomolybdates Chemistry Containing Large {Mo ₁₃₂ } Clusters.....	119
TONK SZENDE, CERASELLA INDOLEAN, SILVIA BURCĂ, ANDRADA MĂICĂNEANU, KOCSIS BELA, MAJDIK CORNELIA, Biosorption of Cd ²⁺ Ions by Immobilized Cells of <i>Saccharomyces Cerevisiae</i> . Adsorption Equilibrium and Kinetic Studies.....	129
NICU BORȘ, ANDRA TĂMAȘ, The Testing and Calibration of a Rotating Rheometer.....	139
LACRIMIOARA SENILA, MIRELA MICLEAN, MARIUS ROMAN, MIRCEA CHINTOANU, GABRIEL KATONA, CECILIA ROMAN, CORNELIA MAJDIK, Starch Hydrolysis with Commercial Enzyme Preparates.....	145
GABRIEL KATONA, MIRELA MICLEAN, MIRCEA CHINTOANU, MARIUS ROMAN, EMIL LUCA, LACRIMIOARA SENILA, CORNELIA MAJDIK, CECILIA ROMAN, The Cellular Biodegradation of Di- and Trihydroxybenzenes.....	151
ALIN MIHIȘ, LIGIA MIRABELA GOLBAN, ELENA BOGDAN, ANAMARIA TERC, ION GROSU, Synthesis, Structure and Reactivity Investigations of Some New Mono- and Bis(5,5-Dibromomethyl-1,3-Dioxan-2-yl) Derivatives.....	157
GORAN JANJIĆ, PREDRAG PETROVIĆ, DRAGAN NINKOVIĆ, DUŠAN VELJKOVIĆ, AGNEŠ KAPOR, SNEŽANA D. ZARIĆ, Stacking Interactions between Pyridine Fragments in Crystal Structures of Terpyridyl Complexes.....	165

CORNELIA OPREA, VLAD PAȘCANU, CRINA CISMAȘ, ANAMARIA TERC, RICHARD ATTILA VARGA, ION GROSU, Tri-Armed Podands as Efficient Precursors for Supramolecular Systems	177
MONICA CÎRCU, VLAD NISTE, RICHARD ATTILA VARGA, EMESE DÉNES, ELENA BOGDAN, CRINA CISMAȘ, ION GROSU, Synthesis, Separation and X-Ray Diffractometry Investigations of <i>Trans, Trans</i> 1,4-bis(5'-hydroxymethyl-2',5'-dimethyl-1',3'-dioxan-2'-yl)benzene	183
CLAUDIU TĂNĂSELIA, STANKO ILIK-POPOV, DANA POP, BELA ABRAHAM, CECILIA ROMAN, TRAJČE STAFILOV, LEONTIN DAVID, MARIANA UDRESCU, Preliminary Investigation of Mocs Meteorite by Lead Isotopic Ratio Using Quadrupole Inductively Coupled Plasma Mass Spectrometry	191
MARIAN MIHAIU, CONSTANTIN BELE, ALEXANDRA LAPUSAN, ROMOLICA MIHAIU, SORIN DANIEL DAN, CARMEN TAULESCU, CRISTIAN MATEA, Seasonal Variations in the Biochemical Composition of Buffalo Milk.....	197
RADU SILAGHI-DUMITRESCU, Assays for Peroxidase Activity: the HRP Case.....	207
RALUCA SEPTELEAN, PETRONELA M. PETRAR, IULIA COMAN, GABRIELA NEMES, Structural Study of New Cyclo-1, 3-Diphosphabutanes	223
ADRIAN PÎRNĂU, MIRCEA BOGDAN, CĂLIN G. FLOARE, DANA ALINA MĂGDAȘ, ² H NMR Spectroscopy of some Romanian Comercial Wines	235
IOANA GEORGETA GROSU, SANTIAGO GOMÉZ-RUIZ, LUMINITA SILAGHI-DUMITRESCU, EVAMARIE HEY-HAWKINS, Inorganic Rings: Eight-Membered Pd ₄ S ₄ Ring In [Pd ₄ Cl ₄ {1-S-2-SCH ₂ COOMe-C ₆ H ₄ -κ ² S,S'} ₄].....	241
TAMAS LOVASZ, EMESE GAL, LUIZA GĂINĂ, IOANA SAS, CASTELIA CRISTEA, LUMINIȚA SILAGHI-DUMITRESCU, Synthesis and Characterization of New Phenothiazinyl-Diphenyl-Phosphines.....	249
EMESE GAL, LUIZA GĂINĂ, CASTELIA CRISTEA, LUMINIȚA SILAGHI-DUMITRESCU, Microwaves Asssited Cycloaddition Reactions of Unsaturated Phenothiazine Derivatives.....	257
ATTILA-ZSOLT KUN, ALEXANDRU LUPAN, RADU SILAGHI-DUMITRESCU, PM6 Modeling of Alpha Helical Polypeptide Structures	265

Studia Universitatis Babes-Bolyai Chemia has been selected for coverage in Thomson Reuters products and custom information services. Beginning with V. 53 (1) 2008, this publication is indexed and abstracted in the following:

- Science Citation Index Expanded (also known as SciSearch®)
- Chemistry Citation Index®
- Journal Citation Reports/Science Edition

X-RAY DIFFRACTION AND ATOMIC FORCE MICROSCOPY STUDIES OF CHEMICAL BATH DEPOSITED FeS THIN FILMS

ANUAR KASSIM^{*a}, HO SOON MIN^a, ATAN SHARIF^a,
SARAVANAN NAGALINGAM^b

ABSTRACT. FeS thin films were deposited onto indium tin oxide glass substrates by chemical bath deposition method. The main objective of the paper was to investigate the influence of the bath temperature on the properties of thin films. The structural and morphological properties of the thin films were studied using X-ray diffraction and atomic force microscopy, respectively. According to XRD results, the number of FeS peaks increased to four peaks and the intensities of these peaks were improved for the films deposited at higher bath temperature. The AFM analysis showed that an increased in bath temperature allowed more materials to be deposited onto the substrate and thicker films to be formed.

Keywords: *chemical bath deposition, thin films, iron sulphide, X-ray diffraction*

INTRODUCTION

Iron sulphide thin films have been the subject of intensive research in the past decade. These thin films have found important applications such as photoelectrochemical and solar cell applications. Several preparative routes of synthesis of iron sulphide thin films were reported in the literature such as metal organic chemical vapour deposition [1], molecular beam deposition [2], reactive DC magnetron sputtering [3], flash evaporation [4], electrodeposition [5] and chemical bath deposition [6]. From the methods used for the preparation of iron sulphide thin films, the chemical bath deposition method is often preferred because it is simple, economic and offers a possibility for large area deposition. The chemical bath deposition method has frequently been used for the deposition of thin films such as PbS [7], PbSe [8], CdTe [9], Ni₄S₃ [10], AgIn₅S₈ [11] and Cd_{0.5}Zn_{0.5}Se [12]. So far, to our knowledge, a study on the properties of the chemical bath deposited iron sulfide thin films has not been reported by other researchers except Anuar et al. [6]. They found that the pH played an important role in the process of deposition of FeS₂ thin films in the presence of triethanolamine solution.

^a Department of Chemistry, Faculty of Science, University Putra Malaysia, 43400 Serdang, Selangor, Malaysia.

^b Department of Bioscience and Chemistry, Faculty of Engineering and Science, University Tunku Abdul Rahman, 53300 Kuala Lumpur, Malaysia.

*email: soonminho@yahoo.com

In this work, for the first time, the FeS thin films have been chemically deposited on indium tin oxide glass substrate in the presence of sodium tartrate as a complexing agent. The effect of bath temperature (50-80 °C) on the properties of these films is investigated. These thin films have been characterized using X-ray diffraction and atomic force microscope for structural and surface morphological properties studies.

RESULTS AND DISCUSSION

Figure 1 shows the X-ray diffraction patterns of the iron sulphide thin films deposited under different bath temperatures. The XRD patterns from all the samples have shown a major diffraction peaks at 2θ equal to 29.9° and 43.6° , which are corresponding to (200) and (202) orientation of hexagonal structure of FeS. For the films deposited at higher bath temperature (60-80 °C), in addition to the (200) and (202) planes, we also observed other peaks such as (112) and (220) peaks which are corresponding to the FeS phase [13]. The observed d -spacing values are in good agreement with the standard d -spacing values (Reference code: 01-080-1028). The lattice parameter values for the dominant structure are: $a=b=6.958 \text{ \AA}$, $c=5.824 \text{ \AA}$. It is found that the intensities of FeS peaks enhanced with the increase of the bath temperature indicating the degree of crystallinity of the films increases. It is also observed that the films show a most preferred orientation along (202) plane.

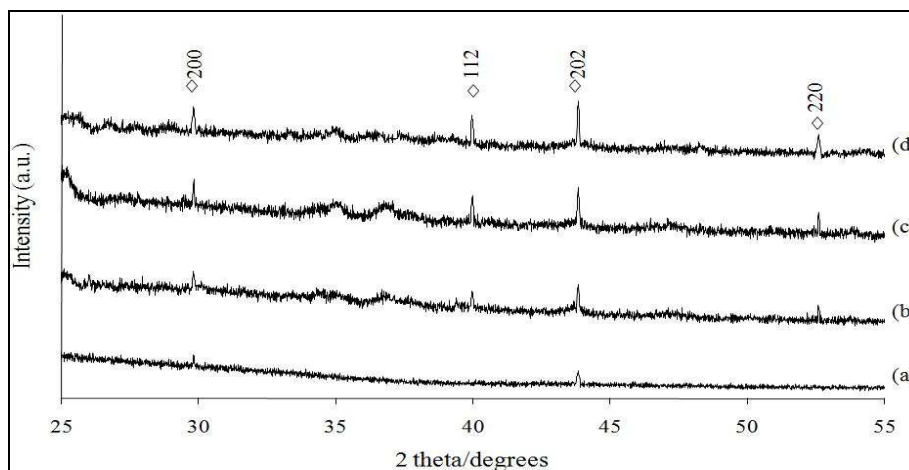


Figure 1. X-ray diffraction patterns for FeS thin films deposited at various bath temperatures. (a) 50 °C (b) 60 °C (c) 70 °C (d) 80 °C

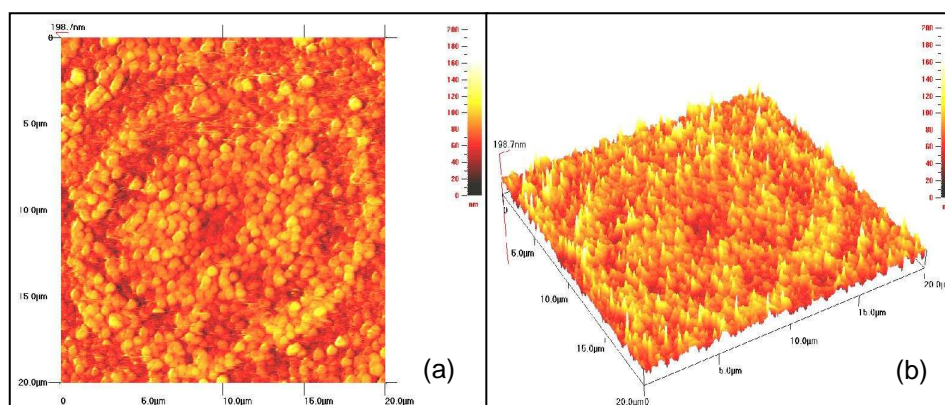


Figure 2. Atomic force microscopy images for FeS thin films deposited at 50 °C
(a) 2-dimensional (b) 3-dimensional

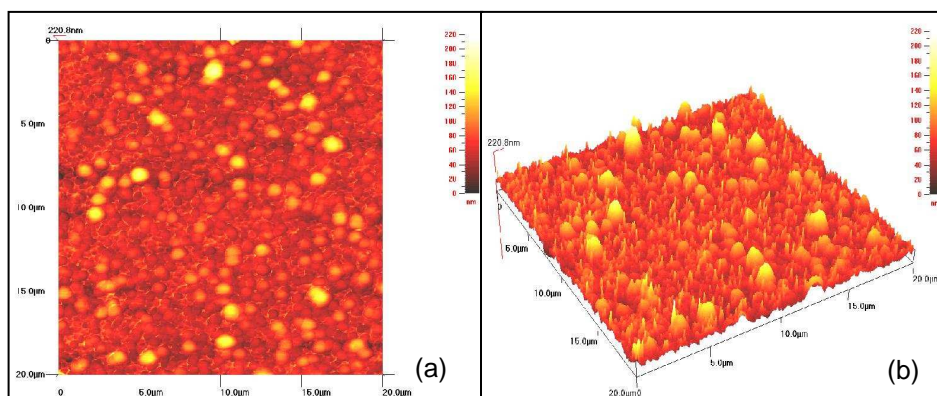


Figure 3. Atomic force microscopy images for FeS thin films deposited at 60 °C
(a) 2-dimensional (b) 3-dimensional

The surface morphology of FeS thin films deposited under various bath temperatures was investigated using atomic force microscopy (AFM) technique. Figure 2 shows a typical two-dimensional (Figure 2a) and three-dimensional (Figure 2b) AFM images of the FeS thin films deposited at 50 °C. These films revealed that grains were very small in size (0.4-0.5 μm) with no well-defined grain boundaries. It is known that the lower the bath temperature, smaller crystal size could be observed. From AFM analysis, it is observed that the FeS thin films are non-uniform when the bath temperature is increased to 60 °C (Figure 3a and 3b) and 70 °C (Figure 4a and 4b), respectively. We

observed that the surface morphology of these films is more or less the same and the average grain size is around 0.5-1.0 μm . When the deposition temperature is further increased to 80 $^{\circ}\text{C}$, the growth morphology is relatively better with more homogeneous spherical FeS grains with their size ranging from 1.8-2.0 μm as shown in Figure 5 (Figure 5a and 5b).

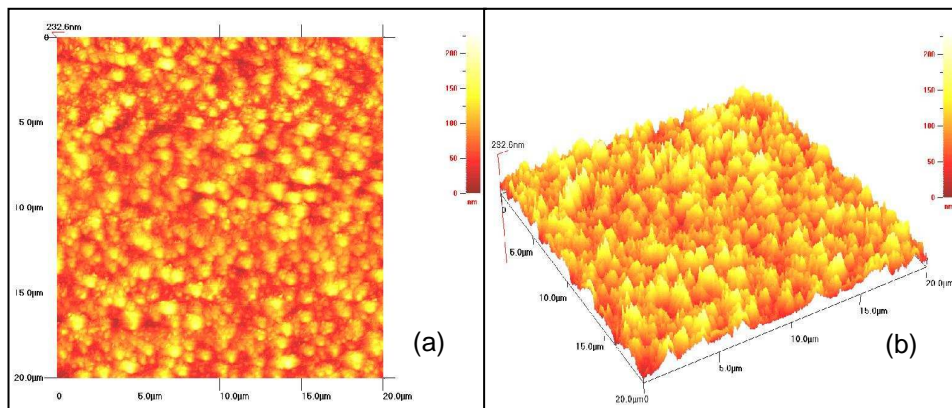


Figure 4. Atomic force microscopy images for FeS thin films deposited at 70 $^{\circ}\text{C}$
(a) 2-dimensional (b) 3-dimensional

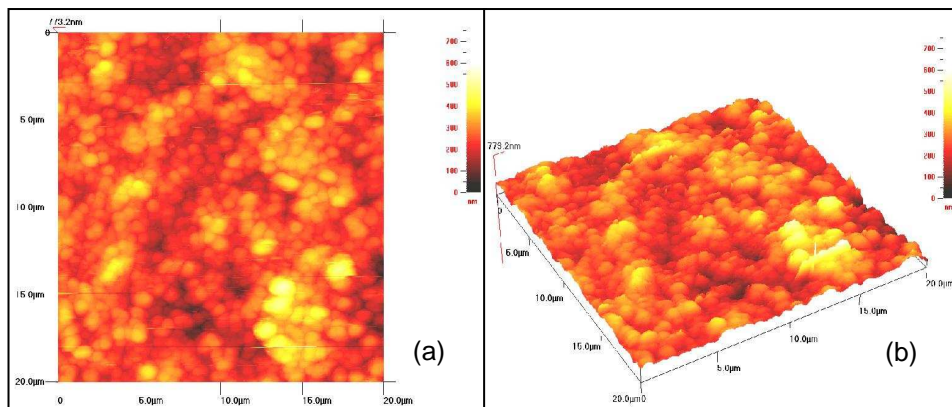


Figure 5. Atomic force microscopy images for FeS thin films deposited at 80 $^{\circ}\text{C}$
(a) 2-dimensional (b) 3-dimensional

The investigation on the surface roughness and the thickness of thin films from AFM images was carried out by many researchers [14-16]. Root mean square (RMS) roughness is defined as the standard deviation of the

surface height profile from the average height, is the most commonly reported measurement of surface roughness [17]. The surface roughness is 16, 20, 30 and 63 nm for the films deposited at 50, 60, 70 and 80 °C, respectively. The surface roughness of the film is unavoidable since grains are grown with different sizes and spherical in shapes.

On the other hand, at the right side of the AFM images, an intensity strip is shown, which indicates the depth and height along the z-axis. The thickness values of 199, 221, 233 and 773 nm have been observed for samples deposited at 50, 60, 70 and 80 °C, respectively. This result shows that an increase in bath temperature allows more materials to be deposited onto indium tin oxide substrate and thicker films to be formed. The AFM results suggested that the influence of bath temperature on the surface morphology of thin films is significant.

CONCLUSIONS

The FeS thin films were successfully deposited on indium tin oxide glass substrates using chemical bath deposition technique from acidic medium in the presence of sodium tartrate solution. Structural studies showed polycrystalline nature of deposited films with hexagonal structure for all samples. According to XRD results, the number of FeS peaks increased and the intensities of these peaks were much better for the films deposited at higher bath temperature. The smaller grain was observed for lower bath temperature while a larger grain was obtained for higher bath temperature based on AFM analysis. Uniform morphology with spherical shaped grains was seen through AFM images for the films deposited at 80 °C. Therefore, deposition at 80 °C was found to be the best bath temperature to prepare good quality thin films under the current conditions.

EXPERIMENTAL SECTION

Iron sulphide thin films were deposited on indium tin oxide (ITO) glass substrates using chemical bath deposition method. Prior to deposition, the substrate was degreased in ethanol for 10 min, followed by ultrasonically cleaned with distilled water for another 15 min and finally dried in air. During the deposition process, an aqueous solution of iron nitrate was used as iron source, sodium thiosulfate as sulfide source and sodium tartrate as complexing agent. All these chemicals used for the deposition were analytical grade. All the solutions were prepared in deionised water (Alpha-Q Millipore). For deposition, 25 ml of 0.2 M iron nitrate was complexed with 25 ml of 0.25 M sodium tartrate. To this, 25 mL of 0.2 M sodium thiosulphate was added slowly

to the reaction mixture. The pH was adjusted to 1.5 by addition of hydrochloric acid with constant stirring. The clean glass substrate was vertically immersed into the chemical bath solution with the temperatures of 50, 60, 70 and 80 °C, respectively. After the deposition time of 120 min, the glass substrate was taken out of the bath, washed with distilled water and dried in desiccators for further characterization.

X-ray diffraction (XRD) analysis was carried out using a Philips PM 11730 diffractometer for the 2θ ranging from 25° to 55° with CuK α ($\lambda=1.5418$ Å) radiation. The surface morphology, thickness and roughness were examined by recording atomic force microscopy (AFM) images in contact mode (commercial Si₃N₄ cantilever) with Q-Scope 250. Contact mode imaging employed a soft cantilevered beam that had a sharp tip at its end which was brought in contact with the surface of the sample. Values of root mean square (RMS) roughness were calculated from the height values in the atomic force microscopy images using the commercial software.

ACKNOWLEDGMENTS

The authors would like to thank the Department of Chemistry, University Putra Malaysia (UPM) for the provision of laboratory facilities and Ministry of Science, Technology and Innovation (MOSTI) for the National Science Fellowship.

REFERENCES

1. B. Thomas, C. Hopfner, K. Ellmer, S. Fiechter, H. Tributsch, *J. Cryst. Growth*, **1995**, *146*, 630.
2. M. Bronold, S. Kubala, C. Pettenkofer, W. Jaegermann, *Thin Solid Films*, **1997**, *304*, 178.
3. D. Lichtenberger, K. Ellmer, R. Schieck, S. Fiechter, *Appl. Surf. Sci.*, **1993**, *70-71*, 583.
4. C. Heras, C. Sanchez, *Thin Solid Films*, **1991**, *199*, 259.
5. A.S. Arico, V. Antonucci, P.L. Antonucci, E. Modica, S. Ferrara, N. Giordano, *Mater. Lett.*, **1992**, *13*, 12.
6. K. Anuar, W.T. Tan, N. Saravanan, S.M. Ho, S.Y. Gwee, *Pac. J. Sci. Technol.*, **2009**, *10*, 801.
7. L. Raniero, C.L. Ferreira, L.R. Cruz, A.L. Pinto, R.M.P. Alves, *Phys. Rev. B*, **2010**, *405*, 1283.
8. K. Anuar, W.T. Tan, K.A. Dzulkafly, H. Md. Jelas, S.M. Ho, M. Shanthi, N. Saravanan, *Jurnal Kimia*, **2010**, *4*, 1.

9. K.M. Garadkar, S.J. Pawar, P.P. Hankare, A.A. Patil, *J. Alloy Compd.*, **2010**, 491, 77.
10. K. Anuar, N. Saravanan, W.T. Tan, S.M. Ho, D. Teo, *Leonardo J. Sci.*, **2010**, 16, 1.
11. K.W. Cheng, C.M. Huang, G.T. Pan, P.C. Chen, T.C. Lee, T.C.K. Yang, *Mater. Chem. Phys.*, **2008**, 108, 16.
12. R.B. Kale, C.D. Lokhande, R.S. Mane, S.H. Han, *Appl. Surf. Sci.*, **2007**, 253, 3109.
13. F. Keller-Besrest, G. Collin, *J. Solid State Chem.*, **1990**, 84, 194.
14. F. Iacomi, M. Purica, E. Budianu, P. Prepelita, D. Macovei, *Thin Solid Films*, **2007**, 515, 6080.
15. W.Y. Li, X. Cai, Q.L. Chen, Z.B. Zhou, *Mater. Lett.*, **2005**, 59, 1.
16. M. Kwoka, L. Ottaviano, J. Szuber, *Thin Solid Films*, **2007**, 515, 8328.
17. T. Jiang, N. Hall, A. Ho., S. Morin, *Thin Solid Films*, **2005**, 417, 76.

ANTICORROSIVE PROTECTION OF CARBON STEEL BY ELECTROSYNTHESIS OF POLYANILINE

BOGDAN TUTUNARU^a, ADRIANA SAMIDE^{a,*},
ADINA CIUCIU^a, MIRCEA PREDA^a

ABSTRACT. The corrosion of carbon steel in 0.5 M H₂SO₄ and its inhibition in presence of electrosynthesized film of polyaniline (PAN) were investigated by using Tafel polarization (TP) and electrochemical impedance spectroscopy. The surface morphology of the carbon steel before and after aniline electropolymerization was also investigated. TP showed a significant shift of the corrosion potential towards more negative values at the same time with the decrease of the corrosion current density. This fact suggests that the polymeric film behaves as a mixed inhibitor, acting predominantly on the cathodic process. Microscopic images showed a clear modification of the surfaces morphology when the carbon steel was corroded in presence of the inhibitor.

Keywords: carbon steel; anticorrosive protection; electropolymerization

INTRODUCTION

Quite recently in electrochemistry is a growing interest in conducting polymers, particularly polyaniline, polypyrrole, polythiophen or mixed polymers of these ones, for the fabrication of anticorrosive protective coatings [1-10].

The polyaniline (PAN) can be easily obtained electrochemically on electrodes in the iron group, without any pretreatment, because the passive layer is a conducting one. From the other hand, the aniline (ANi) polymerization on metallic electrodes covered with insulating passive layers does not take place or only some cristalizing centres are formed. Under particular conditions, the mechanism of nucleation and growth for conducting polymers was found to be a three dimensional (3-D) instantaneous one [11-15].

The polymerization reaction of ANi, carried out by chemical or electrochemical methods, gives several products such as: leucoemeraldine (the completely reduced form), protoemeraldine, emeraldine (the neuter form), nigraniline, pernigraniline (the completely oxidated form). These forms of PAN are differentiated through the number of protons associated with the nitrogen atom, a number which also determines the degree of polyaniline oxidation. It has been observed that the electrochemical properties of PAN are directly

^a University of Craiova, Faculty of Chemistry, 107 Calea București, Craiova, Romania.

* samide_adriana@yahoo.com

influenced by many parameters such as: the nature of the anion associated to the protoning agent; the nature of the sublayer; the molecular mass; the solvent nature; the current density; the applied potential; the agitation; the temperature; the electronegativity and the solvation degree [16-20].

DeBerry [21] found that a decrease in the corrosion rate occurred for a prepassivated steel coated with an electrochemically generated PAN film. In this case, the polymer acts as a redox catalyst and a more noble metal with respect to iron.

Wessling [22] has established a general reaction mechanism, according to which PAN intervenes in the reaction between oxidizable metal and oxygen/water to form a passivating oxide layer.

RESULTS AND DISCUSSION

Tafel polarization

Tafel polarizations curves were recorded with a carbon steel electrode (surface area was 2 cm^2) immersed in $0.5 \text{ M H}_2\text{SO}_4$ and $0.5 \text{ M H}_2\text{SO}_4$ solutions containing different concentrations of ANi, at room temperature and scan rate of 10 mV/sec . The extrapolation of anodic and cathodic Tafel lines, corresponding to the corrosion domain controlled by charge transfer, gives the corrosion current density, i_{corr} and the corrosion potential, E_{corr} (Figure 1).

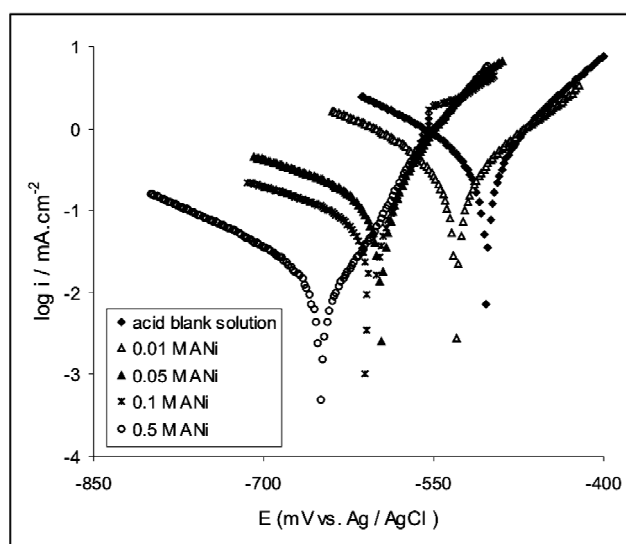


Figure 1. Tafel diagram of carbon steel corroded in $0.5 \text{ M H}_2\text{SO}_4$ solutions in absence and in presence of ANi inhibitor.

The cathodic and anodic polarization curves exhibit a typical Tafel behavior. The addition of ANi increased both the cathodic and anodic overvoltages and caused mainly parallel displacement to the more negative and positive values, respectively. The corrosion current density (i_{corr}) decreased with the increase of ANi concentration, indicating that this compound acts as an inhibitor, and the degree of inhibition depends on the inhibitor concentration. The degree of coverage (θ) of the surface of carbon steel was calculated using the following relation:

$$\theta = \frac{i'_{corr} - i_{corr}}{i'_{corr}} \quad (1)$$

where i'_{corr} and i_{corr} are the corrosion current densities in absence and in presence of inhibitor, respectively. These values were obtained by the extrapolation of the anodic and cathodic Tafel lines to the corrosion potential. The degree of coverage increases with the inhibitor concentration, while the density of corrosion current decreases with the inhibitor concentration (Figure 2).

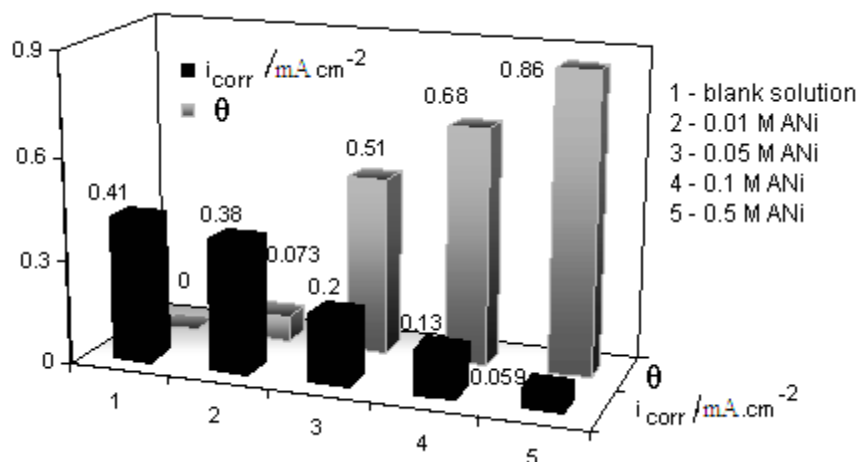


Figure 2. Variation of the corrosion current and the degree of coverage with the concentration of aniline for the carbon steel corroded in 0.5 M H_2SO_4 , at room temperature.

The presence of inhibitor molecules can change the texture of carbon steel by electro-polymerization of aniline, which consequently results in the formation of impermeable layer. This layer restrains faradic processes such as electrode oxidation and the exchange of electrons between the electrode and solution. The behavior of this blocking film is attributed to its compactly packed structure, which obstructs the approach of solution SO_4^{2-} ions to the electrode surface. This behaviour shows that the addition of ANi reduces

anodic dissolution and also retards the hydrogen evolution reaction. This suggests that although inhibition is of mixed type, it is predominantly cathodic. The inhibition efficiency (IE %) was calculated using the relation:

$$IE = \theta \cdot 100 \quad (2)$$

The corrosion current densities decreases from a high value of 0.41 mA/cm^2 , corresponding to unprotected carbon steel, to 0.059 mA/cm^2 for PAN protected carbon steel in presence of 0.5 M aniline and $0.5 \text{ M H}_2\text{SO}_4$. This behaviour proves the inhibition of the corrosion process by the polymer coating. The magnitude of this protective effect is proportional to aniline concentration.

As it can be observed from figure 3, the decrease of the corrosion current densities is associated with a shift of the corrosion potential towards more negative values. This fact suggests that polyaniline is a mixed inhibitor which acts predominantly cathodically.

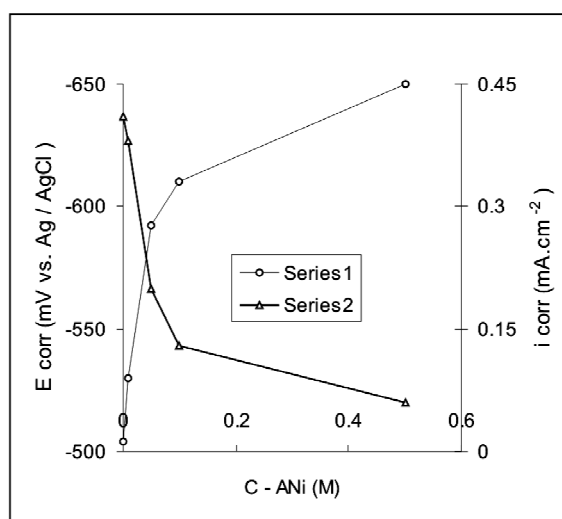


Figure 3. Variation of the corrosion potential and the corrosion current with the concentration of aniline for the carbon steel corroded in $0.5 \text{ M H}_2\text{SO}_4$, at room temperature.

Adsorption isotherm

Different adsorption isotherms were found to describe the adsorption of the inhibitors on steel. In the case of our results, it was found that the experimental data fitted well to the thermodynamic-kinetic model of El-Awady *et al.* [23] (figure 4), which is a modification of the Flory-Huggins adsorption isotherm. The model may be formulated as equations 3:

$$\log \theta / 1 - \theta = \log K' + 1/n \log c \quad (3)$$

where c is the concentration of the adsorbate, θ is the coverage degree and n is the number of inhibitor molecules occupying one active site. The binding constant K is given by:

$$K^{(1/n)} = K' \quad (4)$$

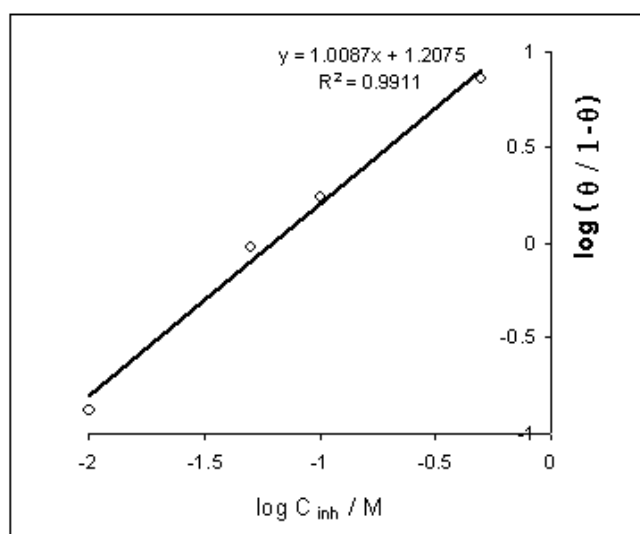


Figure 4. El-Awady *et al.* thermodynamic-kinetic model for mild steel in 0.5 M H₂SO₄ solution containing aniline.

The efficiency of a given inhibitor is a function of both the magnitude of its binding constant K and the number of active sites (n) which it is able to block, the first parameter being the most important [23]. Large values of K mean better and strong interaction, while small values of K mean that the interaction between the inhibitor molecules and the metal is weaker [24, 25]. Hence, according to the obtained numerical value of K (1.2), weak surface interactions occur between the inhibitor molecules and the carbon steel. The value of n obtained was practically one, suggesting that an inhibitor molecule will occupy one active site on the surface of carbon steel [23].

Electrochemical impedance spectroscopy (EIS)

In order to investigate the polyaniline coated carbon steel surface, measurements using electrochemical impedance spectroscopy were performed too (figure 5).

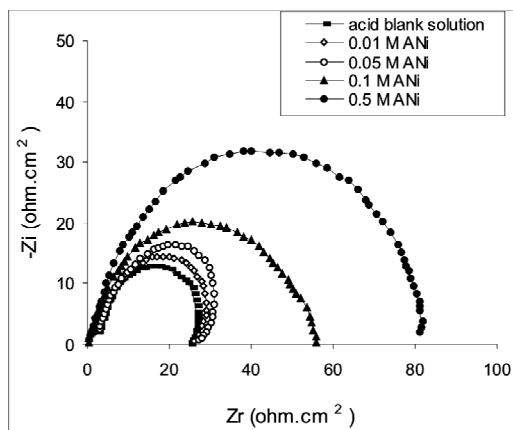


Figure 5. The electrochemical impedance spectra of carbon steel corroded in 0.5 M H_2SO_4 solutions in absence and in presence of ANi inhibitor.

Figure 5 shows the impedance measurements of a carbon steel electrode in 0.5 M H_2SO_4 solution and in 0.5 M H_2SO_4 containing ANi in different concentrations vs. Ag/AgCl reference electrode, in the frequency range from 10^5 to 10^{-1} Hz with a value of 10 mV for the amplitude. In the case of the inhibitor film, the impedance spectrum is represented like a Nyquist diagram with a capacitive arc of circle more or less leveled, which presents a phase shift comparative with the real axe. This phase shift is due to the density variations or to the composition of the film or of the electrode surface coating. The size of the capacitive arcs of circles phase differed comparative with the axes is increasing in the case of solution containing the inhibitor. The formed film is not tridimensional; the impedance diagram would be more complex. For an enough thick film (some μm), the impedance spectrum from the Nyquist plot is formed from two capacity arcs of circles more or less uncoupled at certain frequencies. As shown in the Figure 5 a typical Nyquist diagram is obtained. As shown in Figure 5 when polyaniline film is deposited from 0.5 M H_2SO_4 solution on the carbon steel electrode a semicircle with a different diameter is obtained, in higher frequency region related to charge transfer process. This region is electrically described by a resistance in parallel with a capacitor related to the double-layer. In this region the reaction is purely kinetically controlled. For the description of EIS measurements an equivalent circuit is suggested in figure 6, where (R_s) is the solution resistance of the bulk electrolyte, (C_{dl}) represents the double layer capacitance of the electrolyte at the metal surface and (R_p) is the polarization resistance of the metal. The impedance parameters derived from EIS measurements and respective fitting results (e.g. C-steel / 0.5 M H_2SO_4 solution / 0.5 M ANi) are given in Table 1 and figure 6. The fitting results show that R_s and C_{dl} decrease and R_p increases, suggesting that the amount of inhibitor molecules absorbed increases.

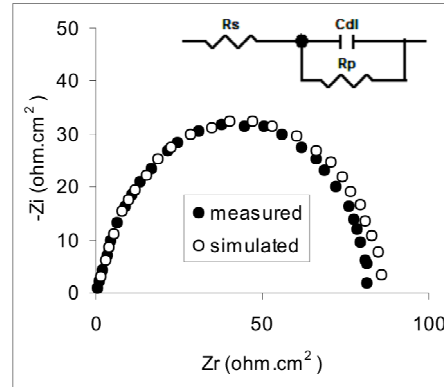


Figure 6. Equivalent circuit model for the studied inhibitor and the fit results for C-steel in 0.5 M H₂SO₄ solution containing 0.5 M ANi.

According to the data obtained from Nyquist plot it can be observed that R_p increases with increasing ANi concentration. It is clear that the presence of PAN film produced a higher R_p value, which is an indication of the formation of an effective protective layer that hindered corrosion, which indicates that this film is formed by aniline polymerization. The electrode coverage (θ) is a key factor, which can be used to estimate the surface state of the electrode and it is related to the charge transfer resistance. According to this assumption, the following equation for the apparent fractional coverage of the electrode can be used:

$$\theta = 1 - \frac{R_p^0}{R_p} \quad (5)$$

where R_p^0 is the polarization resistance of carbon steel corroded in acidic medium in absence of the inhibitor and R_p is the polarization resistance of carbon steel corroded in acidic medium in presence of the inhibitor. The variation of R_p , the degree of coverage (θ) and EI(%) with the concentration of ANi for the carbon steel electrode in 0.5 M H₂SO₄ is presented in Table 1. These results are consistent with those obtained by Tafel polarization.

Table 1. Electrochemical parameters obtained from impedance measurements for C- steel in 0.5 M H₂SO₄ solution containing ANi.

<i>c</i> -ANi (M)	R_s ($\Omega \text{ cm}^2$)	C_{dl} ($\mu\text{F cm}^{-2}$)	R_p ($\Omega \text{ cm}^2$)	θ	IE (%)
0	2.897	478.4	39.4	0	0
0.01	2.627	459.1	46.47	0.15	15
0.05	2.468	443.5	70.6	0.44	44
0.1	1.959	339.2	161.82	0.75	75
0.5	1.798	259.7	264.3	0.85	85

Surface characterization

The morphology of carbon steel surface after corrosion in 0.5 M H_2SO_4 solution (Figure 7a), and in 0.5 M H_2SO_4 solutions containing aniline was examined with a metallographic microscope. Figure 7 shows the evidence of formation of a thick film on the surface of carbon steel. In "b", "c", "d", "e" cases the formation of specific layers of electrodepositions are observed; it is difficult to assess that they would be characteristic of a PAN or PAN/ANi. The corrosion spots are reduced in intensity in the case of carbon steel corroded in 0.5 M H_2SO_4 containing ANi (Figure 7b, 7c, 7d, 7e).

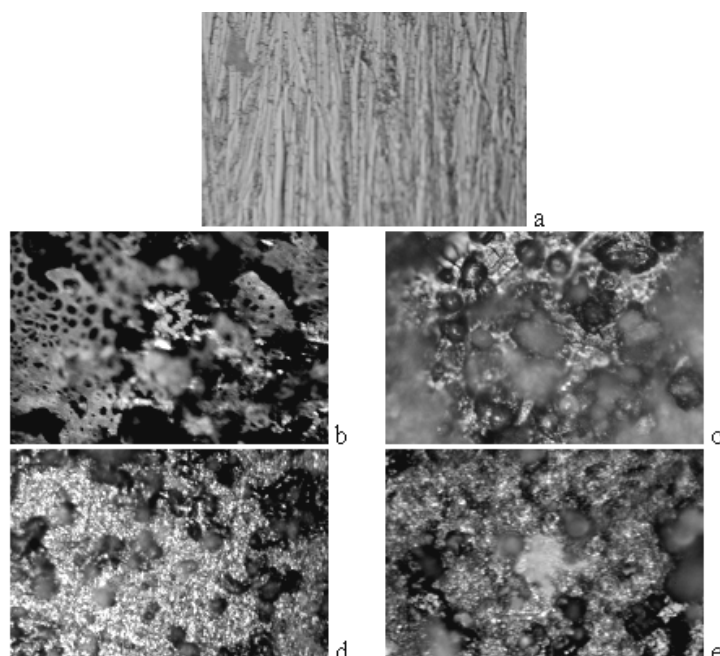


Figure 7. Microscopic images of unprotected carbon steel (a) and protected carbon steel with PAN or PAN/ANi coatings for different aniline concentrations: 0.01 M (b), 0.05 M (c), 0.1 M (d) and 0.5 M (e).

CONCLUSIONS

The corrosion and inhibition of carbon steel in 0.5 M H_2SO_4 in absence and presence of PAN electrosynthesized film was investigated using electrochemical measurements such as, Tafel polarization and electrochemical impedance spectroscopy. The cathodic and anodic curves obtained exhibit

a Tafel type behavior. Addition of ANi increased both the cathodic and anodic overvoltages and caused mainly parallel displacement to the more negative and positive values, respectively. The corrosion current density ($i_{corr.}$) decreased with increasing the concentration of ANi, which indicates that this compound acts as inhibitor. This behavior shows that the addition of ANi reduces anodic dissolution and also retards the hydrogen evolution reaction. This suggests that although inhibition is of mixed type, it is predominantly cathodic.

According to the data obtained from Nyquist plot it can be observed that R_p increases with increasing ANi concentration. It is clear that the presence of PAN film produced a higher R_p value, which is an indication of the formation of an effective protective layer that hindered corrosion, which indicates that this film is formed by aniline polymerization.

The values of R_p , degree of coverage (θ) and EI (%) obtained from Nyquist diagram are consistent with those obtained by Tafel polarization.

Microscopic images show the evidence of formation of a thick film on the surface of carbon steel and the specific electrodeposited layers were observed too. It was difficult to assess that they are characteristic to PAN or PAN/ANi system.

EXPERIMENTAL SECTION

The present study aims to determine the role of aniline in providing the protection film in the case of generalized corrosion of carbon steel in sulphuric acid.

For electrochemical measurements a standard cell has been used with a plate working electrode (surface 2 cm²) made of carbon steel, a platinum auxiliary electrode (surface 1 cm²) and a Ag/AgCl reference electrode. The electrode made of carbon steel (wt %: C 0.13; Mn 0.35; Si 0.03; P 0.04; S 0.04; Al 0.0045; Fe balance) was polished with metallographic paper, washed in distilled water, degreased in acetone and dried in warm air. For each determination the samples were introduced for 4 minutes, at room temperature, in the following media: 0.5 M H₂SO₄ solution blank and 0.5 M H₂SO₄ solutions containing different concentrations of ANi (Fluka): 0.01 M; 0.05 M; 0.1 M; 0.5 M, at room temperature. A potentiostat VoltaLab 40 connected to a Computer with VoltaMaster 4 software was used in the measurements. Five determinations were made for each solution, taking into consideration the most reproducible responses for the same conditions, at room temperature.

The surface morphology of the substrate and polymer film was examined using Euromex microscope, having a Canon camera and the specific software included.

REFERENCES

1. P. Herrasti, P. Ocon, A. Ibanez, E. Fatas, *J. Appl. Electrochem.*, **2003**, *33*, 533.
2. D. Huerta-Vilca, S. R. Moraes, A. J. Motheo, *J. Braz. Chem. Soc.*, **2003**, *14*, 52.
3. D.E. Tallman, G. Spinks, A. Dominis, G. G. Wallace, *J. Solid State Electrochem.*, **2002**, *6*, 73.
4. M.T. Galkowski, P. J. Kulesza, K. Miecznikowski, M. Chojak, H. Bala, *J. Solid State Electrochem.*, **2004**, *8*, 430.
5. V. Vrusic, M. Angelopoulos, T. Graham, *J. Electrochem. Soc.*, **2002**, *144*, 436.
6. G. Mengoli, M. M. Mussiani, *Electrochim. Acta*, **1986**, *31*, 201.
7. B. Wessling, *Adv. Mater.*, **1994**, *6*, 226.
8. M.C. Bernard, A. Hugot-LeGoff, S. Joiret, N.N. Dinh, N.N. Toan, *J. Electrochem. Soc.*, **1999**, *146*, 995.
9. U. Rammelt, P. T. Hguyen, W. Plieth, *Electrochim. Acta*, **2001**, *46*, 4251.
10. G. Torres-Gomez, S. Skaarup, K. West, P. Gomez-Romero, *J. Electrochem. Soc.*, **2000**, *147*, 2513.
11. A. Hamnet, A. R. Hillman, *J. Electrochem. Soc.*, **1998**, *135*, 2517.
12. A. J. Downard, D. Pletcher, *J. Electroanal. Chem.*, **1986**, *206*, 139.
13. M. L. Marcus, I. Rodrigues, J.G. Velsaco, *Electrochim. Acta*, **1987**, *32*, 1453.
14. G. Dian, N. Merlet, F. Outurquin, C. Pulimer, *J. Electroanal. Chem.*, **1987**, *238*, 225.
15. F. Beck, *Electrochim. Acta*, **1988**, *33*, 839.
16. S. Ivanov, V. Tsakova, *J. Appl. Electrochim.*, **2002**, *32*, 709.
17. S. Ivanov, V. Tsakova, *J. Appl. Electrochim.*, **2002**, *32*, 701.
18. V. Tsakova, D. Borissov, B. Rangelov, Ch. Stomberg, J.W. Schultze, *Electrochim. Acta*, **2001**, *46*, 4213.
19. B. Sari, M. Talu, F. Yildirim, *Russ. J. Electrochim.*, **2002**, *38*, 707.
20. R. C. Patil, S.F. Patil, I. S. Mulla, K. Vijayamohanan, *Polym, Int.*, **2000**, *49*, 189.
21. D. W. DeBerry, *J. Electrochem. Soc.*, **1985**, *132*, 1022.
22. B. Wessling, *Mater. Corros.*, **1996**, *47*, 439.
23. El-Awady, B. A. Abd-El-Nabey, S.G. Aziz, *J. Electrochem. Soc.*, **1992**, *139*(8), 2149.
24. P. C. Okafor, E. E. Ebenso, *Pigm. Res. Tech.*, **2007**, *36*(3), 134.
25. N. Khalil, F. Mahgoub, B. A. Abd-El-Nabey, A. Abdel-Aziz, *Corros. Eng. Sci. Technol.*, **2003**, *38*(3), 205.

CORROSION BEHAVIOR OF STAINLESS STEEL COATED WITH POLY(VINYL ALCOHOL) FILM DOPED WITH STRONTIUM RANELATE

**ADINA CIUCIU^a, ADRIANA SAMIDE^{a,*}, BOGDAN TUTUNARU^a,
MIRCEA PREDA^a**

ABSTRACT. The aim of this paper is to investigate the role of the poly (vinyl alcohol) film, doped with strontium ranelate, on the corrosion behavior of stainless steel in contact with physiological serum. The corrosion behavior was studied using two electrochemical methods: the Tafel polarization and the polarization resistance. The small current densities and high polarization resistances were obtained for stainless steel surfaces covered with PVA doped with strontium ranelate, electrochemically deposited from 0.1 M HCl solutions. It was found that the protection efficiency increased when stainless steel was electrochemically modified with strontium ranelate.

Keywords: *poly(vinyl alcohol) film, strontium ranelate, protection efficiency, stainless steel corrosion*

INTRODUCTION

Metals and their alloys are widely used as biomedical materials and they became indispensable for medical field. One of the most important properties of the biomaterials is their safety. Therefore, corrosion resistant materials are required, such as stainless steel [1-6].

Poly(vinyl alcohol) (PVA), a water-soluble synthetic polymer, has been produced for many industrial applications. It is used as emulsifier, colloid stabilizer, sizing agent, protection colloid, replacing material for leather, soil conditioner, coating in the textile, adhesives and house building industries etc. All these end-uses of PVA are based on its exceptional properties such as: water solubility, good thermal stability, good film forming, high tensile strength, no static charge, resistance to organic solvents and oils, non toxicity and non carcinogenicity and good biodegradability [7-9].

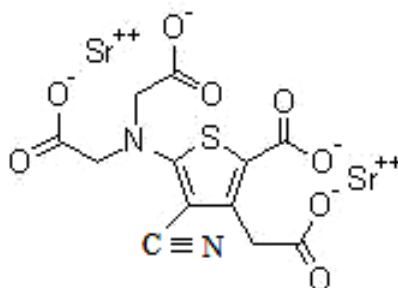
The surface roughness texture and localized corrosion resistance are the most important requirements for stabilizing stainless steel / medium interface. This inconvenient can be surpassed by covering the metallic

^a *University of Craiova, Faculty of Chemistry, Calea Bucuresti No. 107 I, Craiova, Romania*

* *samide_adriana@yahoo.com*

substrate with polymer coatings. The use of polymers as corrosion inhibitors has attracted considerable attention. Polymers such as poly(vinyl pyrrolidone), polyethylenimine, polyaniline and polysiloxane, poly(ethylene glycol) methyl ether have been widely investigated [10-13].

A new therapeutic agent, strontium ranelate (Osseor), was recently introduced for the treatment of postmenopausal osteoporosis [6]. It contains two strontium stable atoms connected to an organic core represented by ranelic acid.



5-[Bis(carboxymethyl)amino]-2-carboxy-4-cyano-3-thiopheneacetic acid strontium salt

It could be mentioned that approximately 26 strontium salts were investigated during the development of this agent and the ranelate salt was selected due to its physical and chemical characteristics (purity, solubility, chelating properties absence, stability) and, not lastly, due to the safety.

Multiple evidences showed that strontium ranelate has various effects in boned metabolism. Its usage in osteoporosis treatment is based on a double action mechanism: increasing bone formation and decreasing bone resorption [6].

The aim of this paper is to investigate the role of the poly (vinyl alcohol) film, doped with strontium ranelate, on the corrosion behavior of stainless steel in contact with physiological serum.

RESULTS AND DISCUSSION

Linear sweep voltammetry

The polarization curves of the stainless steel in 0.1 M HCl in absence and in presence of strontium ranelate, after the deposition of poly (vinyl alcohol) film from 2% PVA solution (by two and three immersions) are presented in Figure 1.

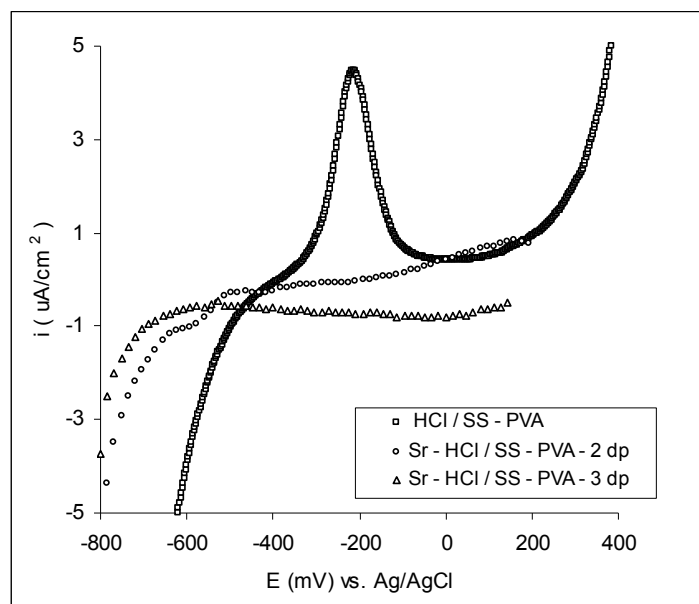


Figure 1. The polarization curves of the modified stainless steel surface with PVA film in 0.1 M HCl solution in absence and in presence of strontium ranelate (potential scan rate, 100 mV / s)

From Figure 1 it can be noticed that in the case of poly(vinyl alcohol) film the polarization curve exhibits three domains: the first part is an active region between -600 mV and -200 mV, the current densities reaching high values; then the curve presents a passive region until approximately 200 mV, while the current densities values are maintained constantly at zero. This is followed by a transpassive domain. In case of PVA films doped with strontium ranelate the active region is shifted between -800 mV and -600 mV, and is followed by the surface passivation, indicating the electrodeposition of strontium.

Tafel polarization

For the modified stainless steel surface with PVA film and PVA film doped with strontium ranelate, deposited at different pulling speeds (0.045 cm/s and 0.065 cm/s) and electrodeposited from 0.1 M HCl solution, the corrosion tests were recorded in physiological serum (PS).

The anodic and cathodic Tafel lines corresponding to the stainless steel corroded in physiological serum solution were represented in figure 2.

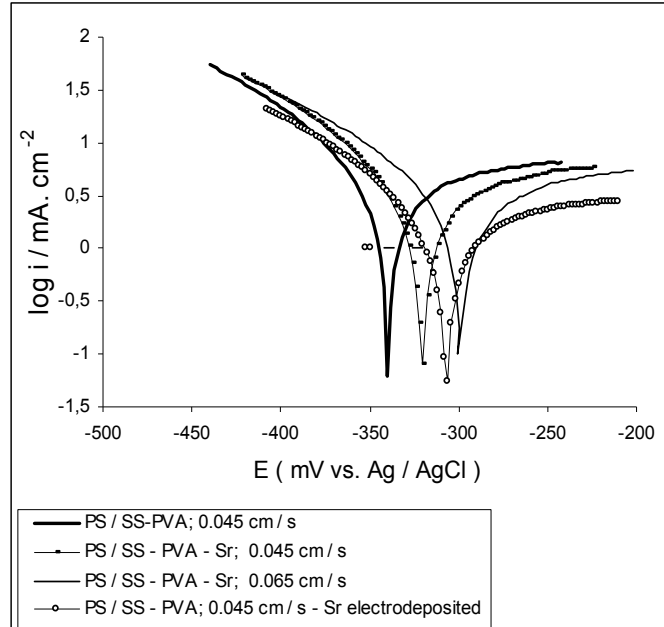


Figure 2. Tafel plot of the modified stainless steel surfaces with PVA and Sr-PVA films, corroded in physiological serum solution (potential scan rate of 10 mV/s)

From Figure 2 it can be noticed that the corrosion potential (E_{corr}) shifts to less negative values when the speed of pulling from 2 % PVA solutions containing 1 % strontium ranelate increases. At the same time, the current densities decrease for the modified surfaces with Sr-PVA film. Sr-PVA film increased both the cathodic and anodic overvoltages and caused mainly a parallel displacement to the more negative and positive values, respectively. The corrosion current density (i_{corr}) decreased in the case of Sr-PVA film, with increasing the pulling speed for deposition of PVA, and shifts towards lower values for the modified stainless steel surface with PVA – strontium ranelate electrodeposited, which indicates that the degree of protection depends on the film type and deposition method (Figure 3).

The protection efficiency (P) of Sr-PVA film was also determined from the polarization measurements according to the following equation:

$$P = \frac{i'_{corr} - i_{corr}}{i'_{corr}} \times 100 \quad (1)$$

where i'_{corr} and i_{corr} are the corrosion current densities for stainless steel in presence of PVA film and in presence of PVA doped with strontium ranelate film, respectively. These values were obtained by extrapolation of the anodic and cathodic Tafel lines to the corrosion potential.

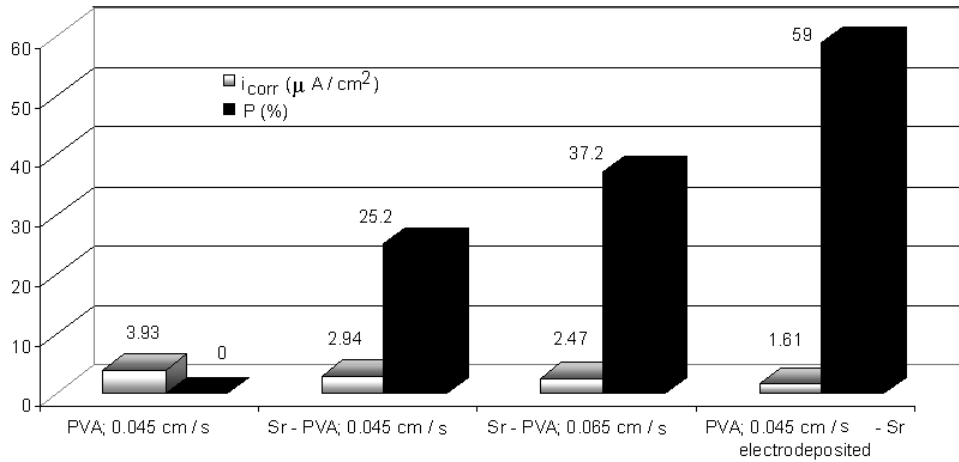


Figure 3. Variation of corrosion current density and protection efficiency (estimated using Tafel polarization) on the deposition method of Sr-PVA films.

Polarization resistance technique (Stern Method)

The polarization curves corresponding to the potential domain close to the corrosion potentials were recorded with a scan rate of 10 mV/s. Their linearizations were performed in the domain of overvoltages values of ± 10 mV (Figure 4).

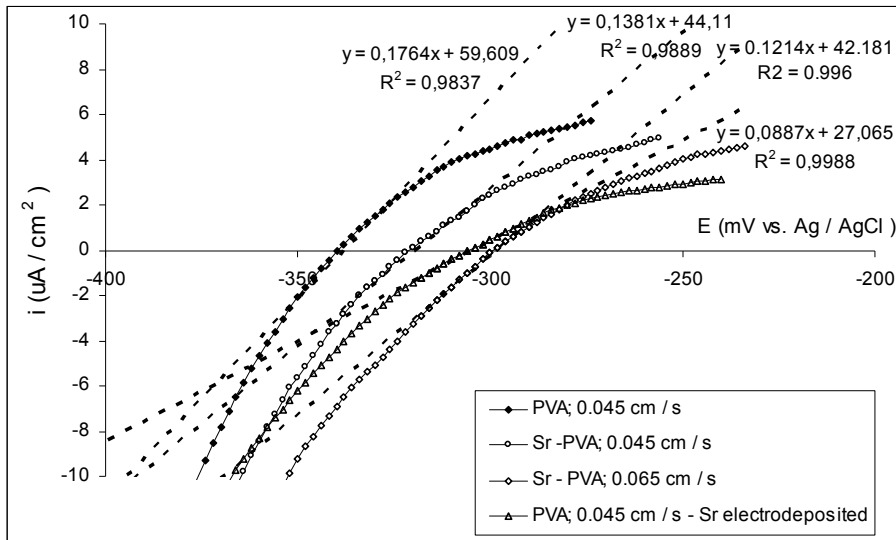


Figure 4. Polarization resistance (R_p) of the stainless steel surfaces modified with PVA and Sr-PVA films, corroded in physiological serum solution.

The slopes $(di/dE)_{E \rightarrow E_{corr}}$ of the lines from Figure 4, represent the polarization conductance. Polarization resistance (R_p , $k\Omega \cdot cm^2$) was calculated using relation 2:

$$\left(\frac{di}{dE} \right)_{E \rightarrow E_{corr}} = \frac{1}{R_p} \quad (2)$$

As it can be seen from figure 4, the polarization resistances increase with the increase of stainless steel pulling speed. The polarization resistance for the modified surfaces with Sr-PVA film reaches the highest values for the surfaces modified with PVA deposited at 0.045 cm/s pulling speed and for the surfaces where strontium ranelate was electrodeposited.

The protection efficiency (P') of Sr-PVA film was calculated according to the following equation:

$$P' = \left(1 - \frac{R_p^0}{R_p} \right) \times 100 \quad (3)$$

where R_p^0 is polarization resistance of the unmodified stainless steel electrode and R_p is the polarization resistance of stainless steel electrode modified with PVA doped with strontium ranelate. The numerical values of the polarization resistances (R_p) and protection efficiencies (P') are presented in Figure 5.

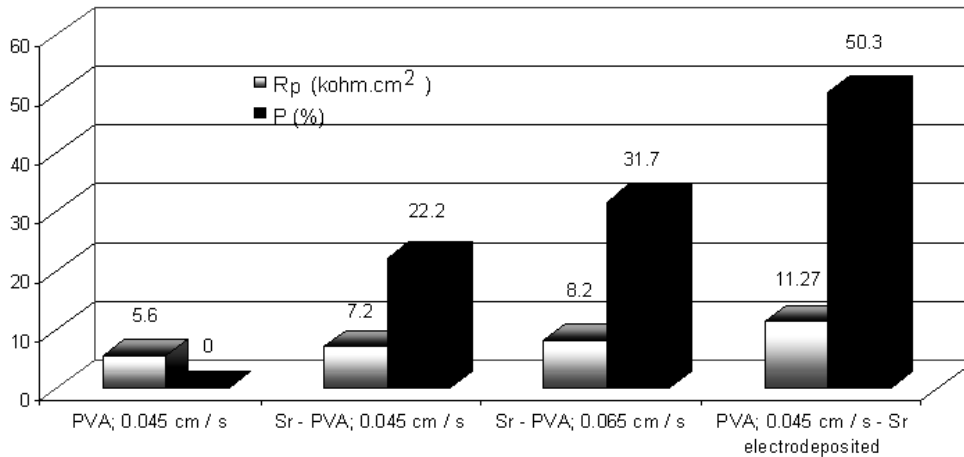


Figure 5. Variation of polarization resistance and protection efficiency (using polarization resistance technique) on the deposition method of Sr-PVA film.

The values of protection efficiency obtained from Tafel polarization and resistance polarization technique were found in good agreement.

CONCLUSIONS

The aim of this paper was to investigate the role of the poly (vinyl alcohol) film, doped with strontium ranelate, on the stainless steel corrosion behavior in contact with physiological serum.

The corrosion current density (i_{corr}) decreased in the case of Sr- PVA film, with the increase of the pulling speed for PVA deposition, and shifts to lower values for stainless steel surfaces modified with electrodeposited PVA – strontium ranelate. This behavior indicates that the protection degree depends on the film type as well as on the deposition method.

The polarization resistance for the modified surfaces with Sr-PVA film reaches the highest values for the surfaces modified with PVA deposited at 0.045 cm/s pulling speed and for the surfaces where strontium ranelate was electrodeposited.

The values of protection efficiency obtained from Tafel polarization are in good agreement with those provided by the technique of resistance polarization.

EXPERIMENTAL SECTION

Films were deposited on the stainless steel surfaces from 2 % PVA solutions containing 1 % strontium ranelate with a DipCoater at different speeds of pulling: 0.045 cm/s and 0.065 cm/s. Also, PVA films were initially deposited with DipCoater through consecutive immersions, 2 dips or 3 dips, with the same pulling speed (neclar!!). Then these were doped with strontium from 0.1 M HCl solutions containing 1% strontium ranelate by using linear sweep voltammetry. Poly (vinyl alcohol) was obtained from Fluka.

The chemical composition (wt %) of the stainless steel employed in this study was determined by using SEM/EDS analysis (Figure 6). The stainless steel contains Cr 18-20 and Ni 8-10.

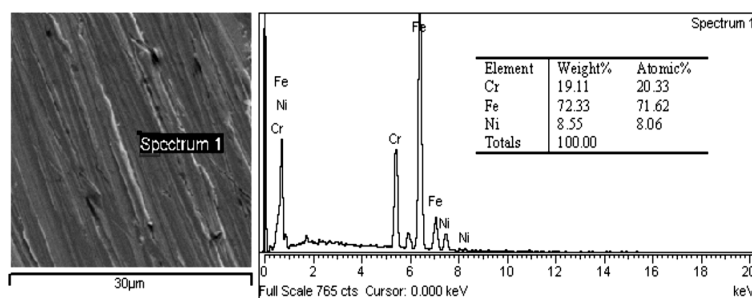


Figure 6. SEM/EDS analysis of the 304L stainless steel sample

For the electrochemical measurements, Tafel polarization and polarization resistance technique were used. For electrochemical measurements a standard cylindrical cell (made of glass) has been used, provided with a plate working electrode (surface 2 cm²) made of stainless steel, a platinum auxiliary electrode (surface 1 cm²) and an Ag/AgCl reference electrode. The stainless steel electrode was polished with metallographic paper, washed in distilled water, degreased in acetone and dried in warm air. A VoltaLab 40 potentiostat connected to a personal computer, using VoltaMaster 4 as software, were used to perform electrochemical measurements in physiological serum solution.

ACKNOWLEDGMENTS

The authors thank for the financial support to the IDEAS/Grant-Program, 422 / 2008 competition.

REFERENCES

1. I Bibicu, A. P. Samide, A. Ciuciu, M. Preda, *RSE-SEE, Rovinj, Croatia*, **2008**, 366.
2. A. Samide, I. Bibicu, A. Ciuciu, B. Oprea, C. Oprea, *ICAME, Viena*, **2009**, 110.
3. A. Ciuciu, A. Samide, M. Preda, *Analele Universitatii Craiova, Seria Chimie*, **2009**, XXXVIII, 35.
4. A. Samide, I. Bibicu, B. Oprea, N. Cioatera, A. Ciuciu, *Journal Optoelectronic and Advanced Materials*, **2008**, 10, 1431.
5. B. Tutunaru, A. Samide, I. Bibicu, M. Preda, *Journal of Optoelectronic and Advanced Materials*, **2007**, 9, 3400.
6. I. Bibicu, A. Samide, B. Oprea, B. Tutunaru, *Journal of Optoelectronics and Advanced Materials*, **2008**, 10, 2156.
7. F. Crivoi, C. Vasile, *Journal of Optoelectronic and Advanced Materials*, **2007**, 9, 3330.
8. C. A. Finch, "Polyvinyl alcohol-development", John Wiley & Sons, Bristol, UK, **1973**.
9. D. Predeteanu, *Medicina interna*, **2007**, 7, 61.
10. P. Herrasti, P. Ocón, A. Ibáñez, E. Fatás, *Journal of Applied Electrochemistry*, **2003**, 33, 533.
11. D. P. Le, Y. H. Yoo, J. G. Kim, S. M. Cho, Y. K. Son, *Corrosion Science*, **2009**, 51, 330.
12. M. Finšgar, S. Fassbender, F. Nicolini, I. Milošev, *Corrosion Science*, **2009**, 51, 525.
13. Y. Jianguo, W. Lin, V. Otieno-Alego, D. P. Schweinsberg, *Corrosion Science*, **1995**, 37, 975.

EXTRACTION AND CHROMATOGRAPHIC DETERMINATION OF ESSENTIAL OILS FROM *OCIMUM BASILICUM L.* LEAVES

MARIA LOREDANA SORAN^{a,*}, SIMONA CODRUTA COBZAC^b,
CODRUTA VARODI^a, ILDIKO LUNG^a, EMANOIL SURDUCAN^a
AND VASILE SURDUCAN^a

ABSTRACT. Three different techniques (maceration, sonication and microwave assisted extraction) were used for extraction of essential oils from *Ocimum basilicum L.* The extracts were analyzed by TLC/HPTLC technique and the fingerprint information were obtained. The GC-FID was used to characterized the extraction efficiency and for identify the terpenic bioactive compounds. The most efficient extraction technique was maceration followed by microwave and ultrasound. The best extraction solvent system was ethyl ether - ethanol (1:1, v/v). The main compounds identified in *Ocimum basilicum L.* extracts were: α and β -pinene (mixture), limonene, citronellol, and geraniol.

Keywords: essential oils, *Ocimum basilicum L.*, extraction, chromatography

INTRODUCTION

Basil (*Ocimum basilicum L.*) is an aromatic herb that is used extensively to add a distinctive aroma and flavor to food. The leaves can be used fresh or dried for use as a spice. Essential oils extracted from fresh leaves and flowers can be used as aroma additives in food, pharmaceuticals, and cosmetics [1]. The interest in medicinal plants and their biologically active derivatives has increased in recent years, in relation to the possible development of novel potential drugs [2]. Traditionally, basil has been used as a medicinal plant in the treatment of headaches, coughs, diarrhea, constipation, warts, worms, and kidney malfunction. Major aroma compounds from volatile extracts of basil present anti-oxidative activity [1].

Any changes of metabolism equilibrium cause the alteration of volatile oil extracts compositions, which might be called 'aroma profile characteristics' by analogy with the fingerprint [3].

^a National Institute for Research and Development of Isotopic and Molecular Technologies, 65-103 Donath, 400293 Cluj-Napoca, Romania, * loredana.soran@itim-cj.ro

^b Babes-Bolyai University, Faculty of Chemistry and Chemical Engineering, 11 Arany Janos, 400028 Cluj-Napoca, Romania

Conventional essential oil extraction techniques include maceration (passive extraction) [4], steam distillation (SD) [5-7], purge and trap (P&T) [8], static and dynamic headspace [9] and head-space solid-phase microextraction (HS-SPME) [10, 11]. Steam distillation is the routine method recommended by pharmacopoeias for controlling the quality of plant materials as essential oil sources [12]. These classical methods require long extraction time, large amounts of solvents and multiple steps. Moreover, many unstable volatiles compounds would be thermally decomposed and degraded during thermal extraction. Due to the relative simplicity SD and SDE are still extensively used for essential oils extraction. In recent years, some advanced extraction techniques, such as headspace solvent drop microextraction (HSME) [13], pressurized liquid extraction (PLE) [14], supercritical fluid extraction (SFE) [15], solvent free microwave extraction [16], microwave assisted hydrodistillation extraction and ultrasound-assisted extraction [17] were used. Among these extraction techniques, high-temperature water extraction of herb like basil is of particular interest because the water extraction is performed around to 100°C and therefore may mimic the cooking process in the kitchen. The extraction in the microwave field has the same practical importance, as well.

The essential oils extracts are analyzed by various chromatographic techniques such as: high - performance liquid chromatography (HPLC) [18, 19] and thin layer chromatography (TLC) [19, 20]. Due to the high volatility of the analytes, the specific technique is GC. The more precisely information in qualitative analysis are obtained by gas-chromatography coupled with mass spectrometry (GC-MS) [21]. For quantitative determination gas-chromatography with flame ionization detector (GC-FID) and GC-MS are preferred [1, 2, 20, 22].

The main goal of our investigations was to evaluate the extraction efficiency of essential oils from basil using various techniques and solvent systems. The chromatographic determinations were performed by TLC and GC-FID. The resulting chromatograms were analyzed. Some essential oils were identified using standard solutions

RESULTS AND DISCUSSION

In the case of plant extracts TLC/HPTLC is used to provide fingerprint information [23, 24]. Only when a very good resolution and no doubt about the identity of compounds are achieved a quantitative analyze is possible.

For identification of some essential oils, HPTLC was used. The E6 extraction solvent was chose because it has the capacity to extract the compounds with different polarities. After separation the plates were pulverized with anisaldehyde, heated for spots coloring and inspected in UV at 366 nm (figure 1a) and in visible range (figure 1b).

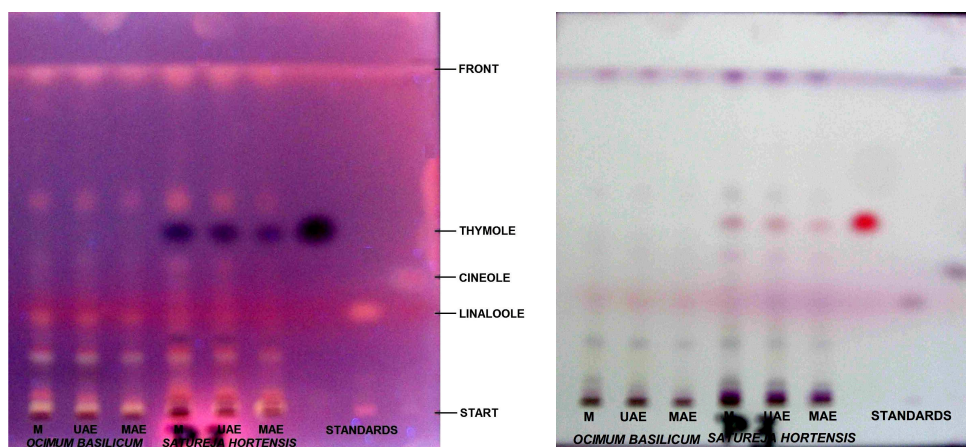


Figure 1. Identification chromatograms of linalool and cineole in *Ocimum basilicum* L. extracts E6 after reaction with anisaldehyde, UV at 366 nm and daylight inspection.

The R_f values were determined and compared with those existent in literature (table 1). Based on this it is possible that the *Ocimum basilicum* L. extracts to contain cineole and linalool. The presence of linalool is confirmed by [23, 25]. The TLC fingerprint of extracts obtained with different techniques – M, MAE and UAE showed to be similar, that means that no degradations processes happens or no new compounds were extracted.

Table 1. Identification of some terpenoidic compounds from *Ocimum basilicum* L. extracts

Compound	R_f value		
	Standard	Sample	Reference [25]
Cineole	0.39	0.38	0.40
Linalool	0.30	0.3	0.30

Another goal was to determine which solvent and which technique is more suitable for extraction of essential oils from *Ocimum basilicum* L. leaves. In figure 2 is presented the chromatogram of all extracts.

It can be observed that E1 shows the lowest efficiency. Better results were obtained with E3, E4 and E6, the spots being more intense. Even so we cannot choose the best extraction condition (solvent and technique), because that together with essential oils, some other compounds were extracted. In this case is indicated to be employed GC as analytical technique.

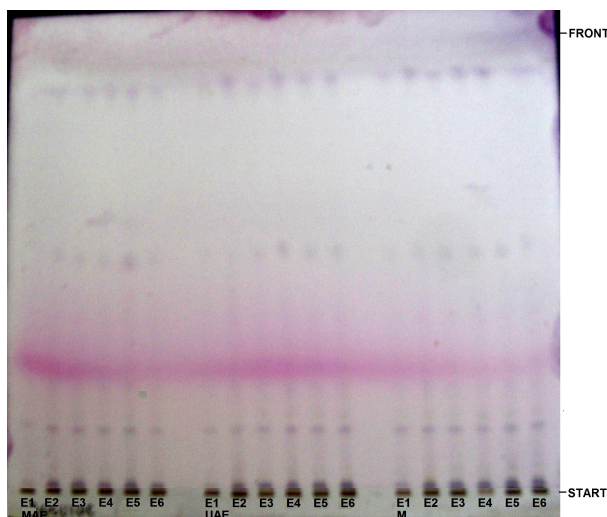


Figure 2. The chromatogram of *Ocimum basilicum* L. extracts obtained with solvent system E1-E6 using M, MAE and UAE techniques

The chromatograms of extracts E1-E6 obtained by MAE and some standards were registered by GC-FID (figure 3).

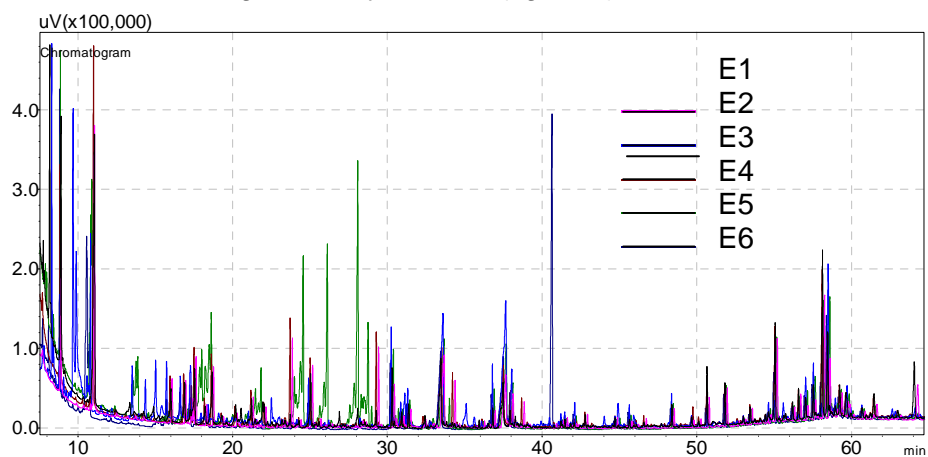


Figure 3. The chromatograms of *Ocimum basilicum* L. extracts obtained by MAE in various solvents mixtures.

It is very obvious that the extracts E5 has a different fingerprint, beginning with a R.T. = 15 min the shape of chromatogram is changed. The maximum area of the peak was obtained using the E5 mixture as extraction solvent. The chromatograms for E5 extracts obtained with the studied techniques were compared (figure 4).

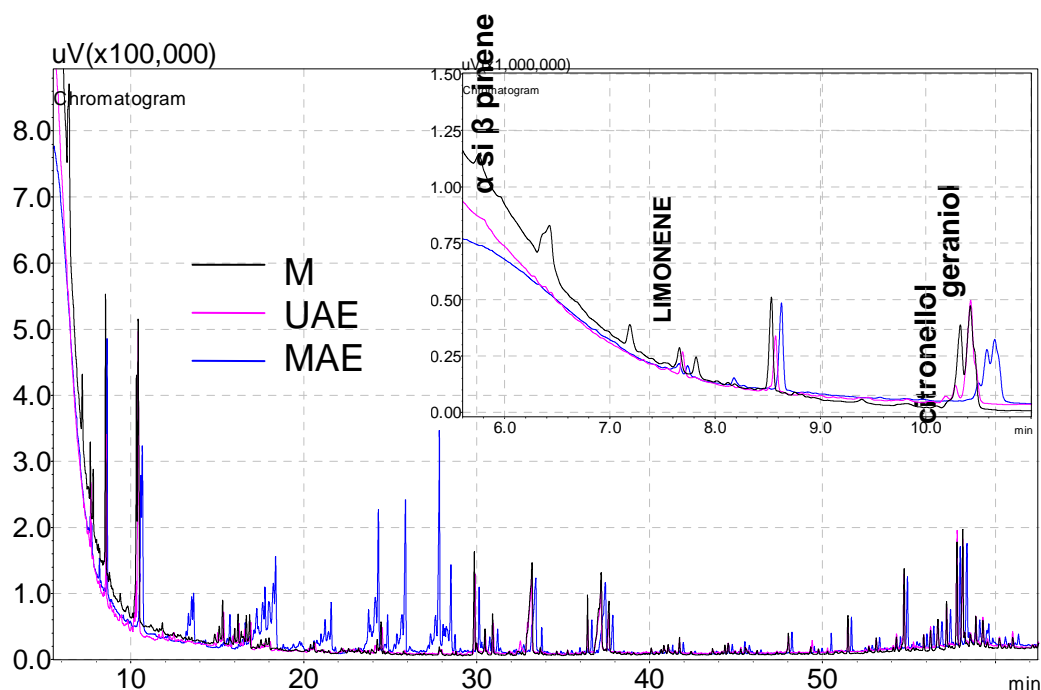


Figure 4. The chromatograms of *Ocimum basilicum* L. extracts E5 obtained by MAE and M, extracts E6 obtained by UAE

This reveals that M and UAE extracts are similar. Maceration is more efficient but more time consuming, which is a huge drawback. First part of chromatogram of the extracts obtained by MAE and M (the reference technique) are similar, but in the second one, after 14 min, are quite different. More probably this is done by some decomposition reaction induces by microwave than because some new extracted compounds.

Good results were obtained by MAE and M techniques. A great advantage of extraction in microwave field was the short time for extraction comparing with maceration or sonication.

By over layering the standards and extracts chromatograms some essential oils were identified: α and β -pinene (mixture), limonene, citronellol and geraniol.

There may be observed from other papers as well, that the essential oils fingerprint depend on extraction technique, solvent system and operation conditions. The modern techniques are advantageous, but they can change the composition of extract, enhancing some compounds and depleting other [26, 27].

CONCLUSIONS

The extracts were analyzed by TLC/HPTLC technique and the fingerprint information was obtained. The GC-FID was used for to establish the best conditions for extractions and for identifying the essential oils. The best extraction of essential oils was obtained by maceration using the mixture ethyl ether + ethanol (1:1, v/v) as extraction solvent. In *Ocimum basilicum* L. extracts were identified: α and β -pinene (mixture), limonene, citronellol, and geraniol.

EXPERIMENTAL SECTION

Materials

The plant material was commercially purchased. The essential oils standards were obtained from Fluka (Germany). The chromatographic plates were from Merck (Germany). All the solvents were from Chimopar (Bucharest, Romania). All chemicals were of analytical grade. Stock solutions were prepared in ethanol at $100 \mu\text{g ml}^{-1}$.

Extraction Procedure

The vegetal material of *Ocimum basilicum* L. for culinary purpose was purchase from Kotany, Austria as dried leaves. After grinding with a hand mill (grinder), the powder was exactly weighed in portions of 0.5 g and subjected to solvent extraction with different systems and techniques. Following solvent were chose to perform the extraction: E1 – hexane; E2 – ethyl ether; E3 – ethanol; E4 – hexane + ethyl ether (1:1, v/v); E5 – ethyl ether + ethanol (1:1, v/v) and E6 – hexane + ethyl ether + ethanol (1:1:1, v/v). Each extraction procedure was optimized with respect the principal factors.

Maceration (M) was performed 14 days at room temperature with 15 ml extraction solvents E1-E6. After filtration and washing the final volume was adjusted at 25 ml.

Ultrasound solvent assisted extraction (UAE) was performed in two steps using a Transsonic T 310 bath at 35 kHz and an installed power of 95 W. In the first step sample was soaked 10 min with 10 ml extraction solvent (E1-E6). After 15 min of sonication the extract was separated (by decantation) and the sample was once again subjected for other 15 min sonication with 10 ml solvent (E1-E6). The sample was finally filtered and the residuum washed. The extracts were reunited and than the final volume were adjusted at 25 ml. For avoiding solvent leaks the extraction temperature was established at 4°C (ice bath) and the extraction vessels were tightly closed.

Microwave solvent assisted extraction (MAE) was performed using a home made apparatus [28]. The device has the possibilities to control the operation time, temperature and duty cycle. Sample (0.5g) together with extraction solvent (20 ml) was placed into the extraction cell. In concordance with sonication the extraction procedure consist in two steps, 10 min soaking followed by microwave extraction. Taking in account the specificity of plant material the following parameter were selected: maximum temperature 30°C, action time 1 min and duty coefficient of 40% at an installed power of 900 W. Depending of the absorption capacity of the solvent, the entire extraction time takes more than 1 min because the cell needs to cool down bellow 30°C. Because of the low operation temperature, the solvent systems used do not boiled, so the extraction can be conducted at atmospheric pressure. After filtration and washing the final volume was adjusted at 25 ml.

TLC analysis

TLC analyses were performed on two kinds of plates: TLC Sil G F₂₅₄ and HPTLC Sil G F₂₅₄ pre-coated plates. Prior using, the TLC plates were conditioned with methanol and dried at 110°C for 3 h. The samples were applied with a Linomat 5 device as 5 mm bands, 20 µl for plant extracts and 7 µl for standards. In the case of HPTLC plates the applied volume was decreased at 10 µL for extracts and at 5 µl for standards. Every time a mixture of toluene-ethyl acetate (93:7, v/v) was used as mobile phase. The developed plates were sprayed with anisaldehyde and than heated 3 min at 110°C when red-bluish bands appear. The plates were inspected in daylight and also at 366 nm in UV range [25].

GC-FID analysis

GC analysis was performed with a Shimadzu GC-2010 gas chromatograph with flame- ionization detection (FID). Compounds were separated on a methyl silicone column OV-17 (2m x 3.16 mm, 80-100 Mesh). Helium was used as carrier gas at 15 ml/min flow rate. The oven temperature was programmed 2 min at 80°C increased to 200°C with 4°C/min, maintained 1 min and then with 20°C/min to 260°C and held for 35 min. The injection port and detector temperature were 260°C and 240°C respectively. The injection volume was 2 µl for extract samples and standards (100 mg/ml).

ACKNOWLEDGMENTS

Financial assistance provided through the Ministry of Education and Research of Romania (PN II Research Program, Project 51-098/2007) is gratefully acknowledged.

REFERENCES

1. S.J. Lee, K. Umano, T. Shibamoto, K.G. Lee, *Food Chem.*, **2005**, *91*, 131
2. Lampronti, A.M. Saab, R. Gambari, *Int. J. Oncol.*, **2006**, *29*, 989
3. E. Klimánková, K. Holadová, J. Hajšlová, T. Čajka, J. Poustka, M. Koudela, *Food Chem.*, **2008**, *107*, 464
4. Y. Yang, B. Kayan, N. Bozer, B. Pate, C. Baker, A.M. Gizir, *J. Chromatogr. A*, **2007**, *1152*, 262
5. Z.M. Zhang, G.K. Li, *Microchem. J.*, **2007**, *86*, 29
6. B.P. Quinn, U.R. Bernier, M.M. Booth, *J. Chromatogr. A*, **2007**, *1160*, 306
7. C. Siani, I.S. Garido, S.S. Monteiro, E.S. Carvalho, M.F.S. Ramos, *Biochem. Syst. Ecol.*, **2004**, *32*, 477
8. S. Sinyinda, J.W. Gramshaw, *Food Chem.*, **1998**, *62*, 483
9. S. Texteira, A. Mendes, A. Alves, L. Santos, *Anal. Chim. Acta*, **2007**, *584*, 435
10. E. Stashenko, B.E. Jaramillo, J.R. Martinez, *J. Chromatogr. A*, **2004**, *1025*, 93
11. L. Rosillo, M.R. Salinas, J. Garijo, G.L. Alonso, *J. Chromatogr. A*, **1999**, *847*, 155
12. *** *European Pharmacopoeia 1997*
13. B. Seidani, A. Jabbari, Y. Yamini, *Anal. Chim. Acta*, **2005**, *530*, 155
14. L. Dawidowicz, E. Rado, D. Wianowska, M. Mardarowicz, J. Gawdzik, *Talanta*, **2008**, *76*, 878
15. S.M. Pourmorizavi, S.S. Hajmirsadeghi, *J. Chromatogr. A*, **2007**, *1163*, 2
16. M.E. Lucchesi, F. Chemat, J. Smadja, *J. Chromatogr. A*, **2004**, *1043*, 323
17. C. Kimbaris, N.G. Siatis, D.J. Daferera, P.A. Tarantilis, C.S. Pappas, M.G. Polissiou, *Ultrason. Sonochem.*, **2006**, *13*, 54
18. S. Rauber, S.S. Guterres, E.E.S. Schapoval, *J. Pharm. Biomed. Anal.* **2005**, *37*, 587
19. F. Buiarelli, G.P. Cartoni, F. Coccioli, E. Ravazzi, *Chromatographia*, **1991**, *31*, 489
20. E. Háznagy-Radnal, S. Czigle, I. Máthé, *J. Planar. Chromatogr.*, **2007**, *20*, 189
21. Z. Cong, Q. Meiling, S. Qinglong, Z. Shan, F. Ruonong, *J. Pharm. Biomed. Anal.* **2007**, *44*, 464
22. S.Y. Wang, C.L. Wu, F.H. Chu, S.C. Chien, Y.H. Kuo, L.F. Shyr, S.T. Chang, *Holzforschung*, **2005**, *59*, 295
23. M. Wicht, „*Herbal Drugs and phytopharmaceuticals*“, Medpharm Scientific Publ., CRC Press, Stuttgart, **1994**, pp 104-105.
24. Sz. Nyiredy, K. Glowniak, „*Planar Chromatography – A Retrospective view for the third millennium*“, Springer, Debrecen, **2001**, pp 550-568.
25. H. Wagner, S. Bladt, E.M. Zgainski, „*Drogen Analyse, Dunnsichtchromatographische Analyse von Arzneidrogen*“, Springer, Berlin, **1983**, pp 5-26
26. E.E. Stashenko, B.E. Jaramillo, J.R. Martinez, *J. Chromatogr. A*, **2004**, *1025*, 93
27. M. Vinatoru, *Ultrason. Sonochem.*, **2001**, *8*, 303
28. E. Surducan, V. Surducan, „*Procedure and device for dynamic processing of materials*“, Romanian Patent, **2008**, RO-00112063 B1

RECOVERY POSSIBILITIES OF POWER PLANT FLY ASH FROM ZALĂU

LÁSZLÓ SZÉLL^a, VALENTINA CETEAN^b, LUCIA GAGEA^c, ANIKÓ TÓTH^a,
CECILIA ROMAN^d, MARIUS ROMAN^d, ADRIANA GOG^d

ABSTRACT This paper presents a detailed study on the properties of power plant fly ash from Zalău and the recovery possibilities in concrete slabs. The fly ash chemical and mineralogical composition, the particle size distribution and the thermal behaviour were established. The changes on the hardened concretes properties induced by the fly ash introduced in concrete compositions were studied. It was observed that 10 wt% replacement of cement by ash improved the mechanical features of the products.

Keywords: fly ash, concrete, mortar

INTRODUCTION

From economically point of view the use of fly ash has several advantages: the ash is an inexpensive raw material which introduced in compositions contributes to the manufacturing cost price decrease of the products, without compromising their quality. The ash use is justified by the construction products long-term mechanical strengths and durability improvement, therewith leading to increase their life cycle [1-3]

The study of the power plant fly ash recovery options as well as the establishment of the different products manufacturing technologies with this material require detailed knowledge of the fly ash properties and its complex characterization.

Knowing the properties of fly ash is important, being known the interdependence between the chemical-mineralogical composition, physical properties and hydraulic activity of ashes, which in turn influences the concrete products features. [4-6]

^a S.C. Procema Cercetare S.R.L., Punct de lucru Cluj-Napoca, Str. Beiuşului, Nr. 1, RO-400394 Cluj-Napoca, Romania, officecj@procema-cercetare.ro

^b S.C. Procema Geologi S.R.L., B-dul Preciziei, Nr. 6, RO-062203 Bucureşti, Romania, procema.geologi@clicknet.ro

^c Universitatea Babeş-Bolyai, Facultatea de Chimie şi Inginerie Chimică, Str. Arany János, Nr. 11, RO-400084 Cluj-Napoca, Romania, gagea@chem.ubbcluj.ro

^d INCDO-INOE2000 filiala ICIA, str Donath, Nr. 67, RO-400293 Cluj-Napoca, Romania, icia@icia.ro

RESULTS AND DISCUSSIONS

The granulation of power plant fly ash is of particularly interest regarding the preparation of concretes with imposed properties and appearance (the quality of sides and edges for example) by the local applications.

The results of the sieve analysis are presented in Table 1:

Table 1. Grain size distribution.

Fraction	Percent [wt %]
> 2mm	6,33
> 1mm	5,58
> 500 μ m	12,00
> 200 μ m	42,52
> 100 μ m	25,29
< 100 μ m	8,28

The average results of the chemical analysis obtained on replicate samples, are given in Table 2.

Table 2. The chemical composition of power plant ash from Zalau (%)

Major oxides (%)								
SiO ₂	Al ₂ O ₃	TiO ₂	Fe ₂ O ₃	CaO	MgO	Na ₂ O	K ₂ O	L.I.
59,71	21,62	0,62	7,10	4,48	1,02	0,60	2,60	1,31

It notes an important content of main oxides: SiO₂, Al₂O₃, Fe₂O₃ and CaO.

The sum SiO₂+Al₂O₃+Fe₂O₃ amounts to 88,43%, which allows to classify the analysed fly ash in F class [3], for which the minimum percentage of these oxides is 70.0%. The ashes from this class result in the burning process of bituminous coal and anthracite and they are characterized by pozzolanic properties.

The calcium oxide content, an important parameter when using ash as additive in concrete, is of 4.48%; in this case the ash may be classified in type F, for which the CaO content is less than 8%.

RECOVERY POSSIBILITIES OF POWER PLANT FLY ASH FROM ZALĂU

In conclusion, the chemical composition of Zalău power plant fly ash is situated between the normal limits for this material. It notes that this material has a carbon content which slowly exceeds the recommended upper limit, which shows an incomplete process of preparation and burning of fuel in the thermoelectric power plant.

The mineralogical composition of the fly ash was determined by X-ray diffraction. The X-ray diffraction spectra, as it was recorded, are shown in Figure 1.

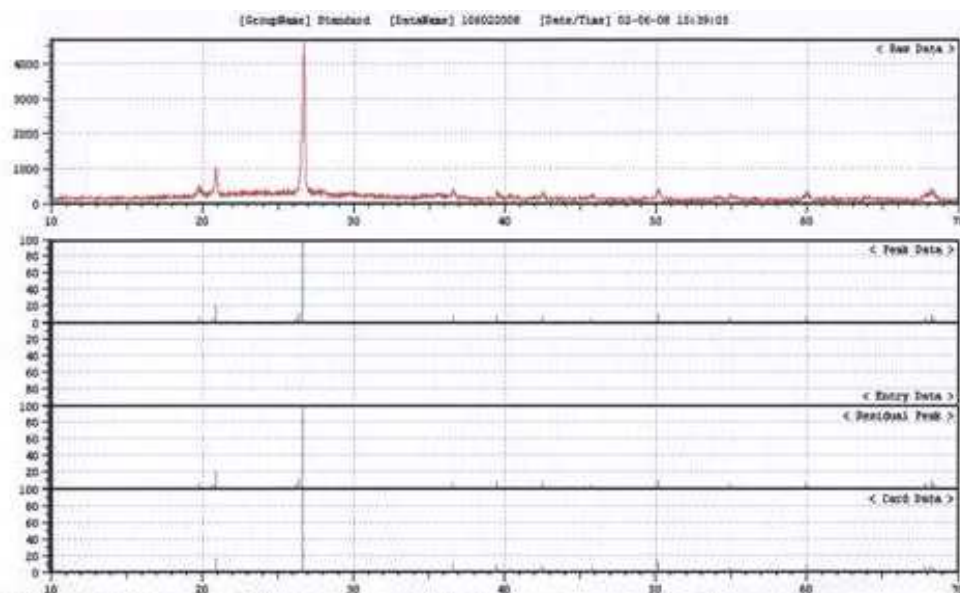


Figure 1. – The X-ray diffraction spectra

It notes a spectrum poor in reflexes, with a single mineral content. The X-ray spectra analysis established that the reflexes perfect match for quartz. Reflexes of other minerals were not recorded which indicate the presence of the silicon dioxide only in this mineralogical form. It is very interesting that minerals from clays, feldspars or iron oxides groups or other crystalline species that are possible to be present in ashes, derived from fossil fuels combustion as coal, are not revealed. Any crystalline form of carbon is not revealed, although the loss on ignition of the ash exceeds 10%. There is a small amount of vitreous phase, betrayed by the slightly lift, in the form of dome, of the spectra recorded between 18 and 30 degrees of 2θ angles.

For a more detailed study of the mineralogical composition the X-ray spectra of the fly ash sample, treated at 900°C for two hours was recorded. In Figure 2 are given the spectra performed under the same conditions as for original ash.

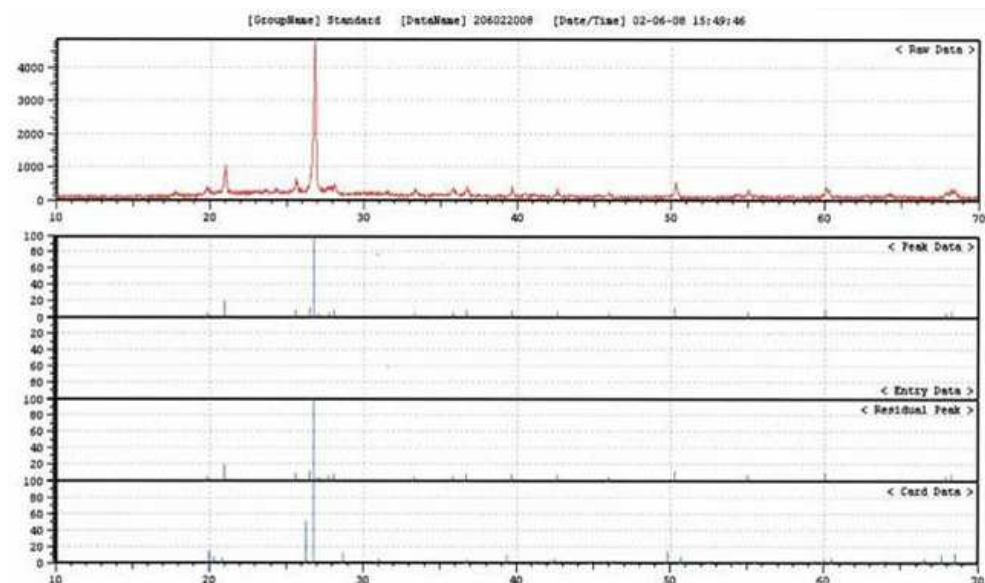


Figure 2. – The X-ray diffraction spectra of the calcinated ash

It notes the remarkable similarity of the two spectra, which leads to the conclusion that the minerals present are common and during the ash calcinations are not occurred essential changes in the mineralogical composition. The transformations of the minerals undergone during the coal combustion in the power plant at 1600°C, remained as definitive.

The stability related aspects of a material can be obtained with the aid of thermal analysis, especially for applications that allow operation at temperatures higher than the ambient temperature. In figure 3 is given the derivatogramm for Zalău power plant fly ash. The dried material was heated in device until the temperature of 1500°C.

The recorded curves do not show pronounced thermal effects. The residual carbon combustion occurs in a narrow temperature range of 400°-610°C, with a maximum of the DTA curve at 410,38°C, in a broad exothermic effect. The thermal effects curve presents an endothermic effect with a maximum at 1250,22°C. This occurs without a change in weight – recorded on TGA curve - and is assigned to the ash soaking itself, a process that occurs in the temperature range of 1120°-1270°C.

RECOVERY POSSIBILITIES OF POWER PLANT FLY ASH FROM ZALĂU

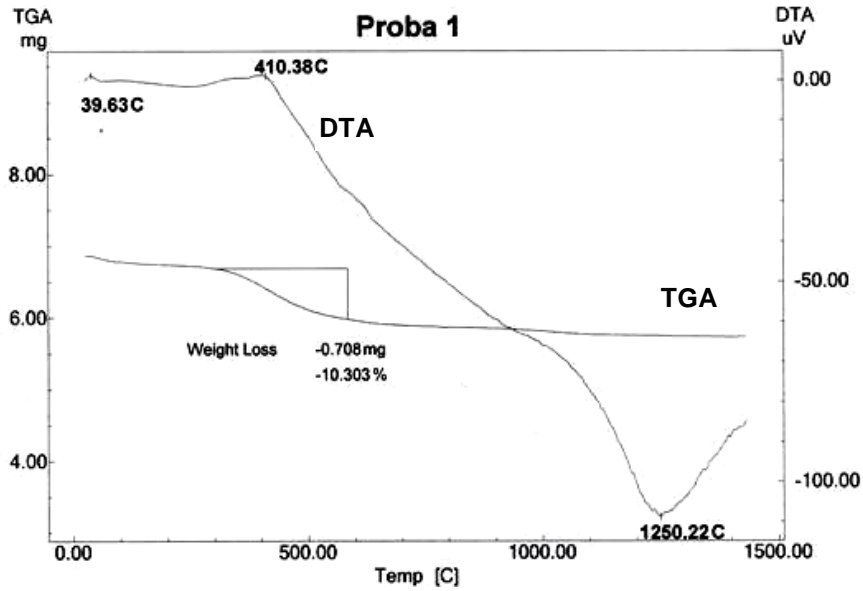


Figure 3. – Thermal behaviour of the ash

In conclusion, the fly ash presents a thermal resistance up to 410°C, when begins the residual carbon burning.

After 28 days of hardening the density and water absorption of the concrete compositions were determined.

The results are shown in the figures nr 4 and 5.

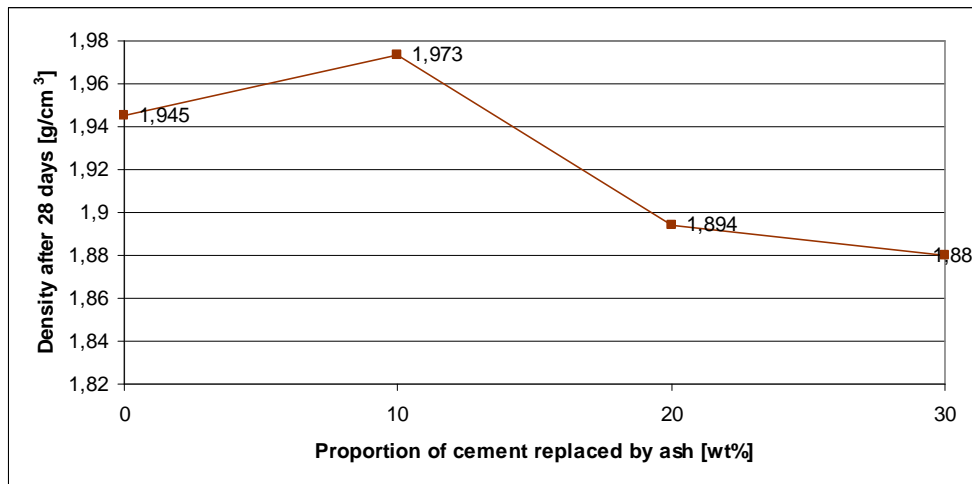


Figure 4. Density variation in function of cement replaced by ash.

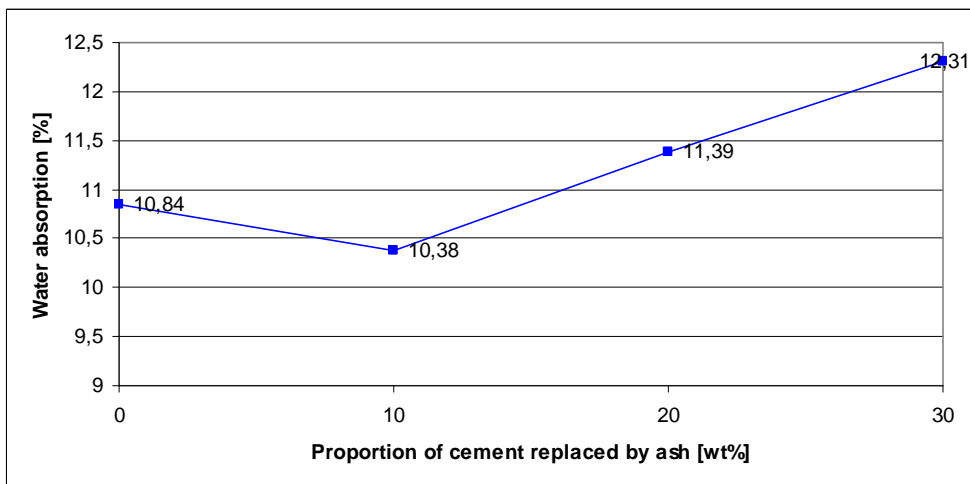


Figure 5. Water absorption variation in function of cement replaced by ash.

The flexural and compressive strength of the compositions were determined after 28 days of hardening. In the figure 6 and 7 is presented the evolution of the strength in function of proportion of cement replaced by ash.

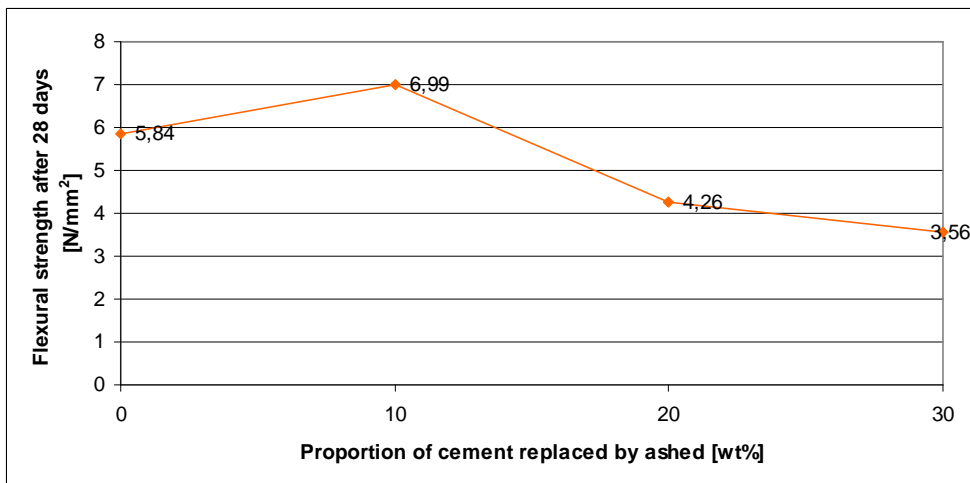


Figure 6. Flexural strength variation in function of proportion of cement replaced by ash.

RECOVERY POSSIBILITIES OF POWER PLANT FLY ASH FROM ZALĂU

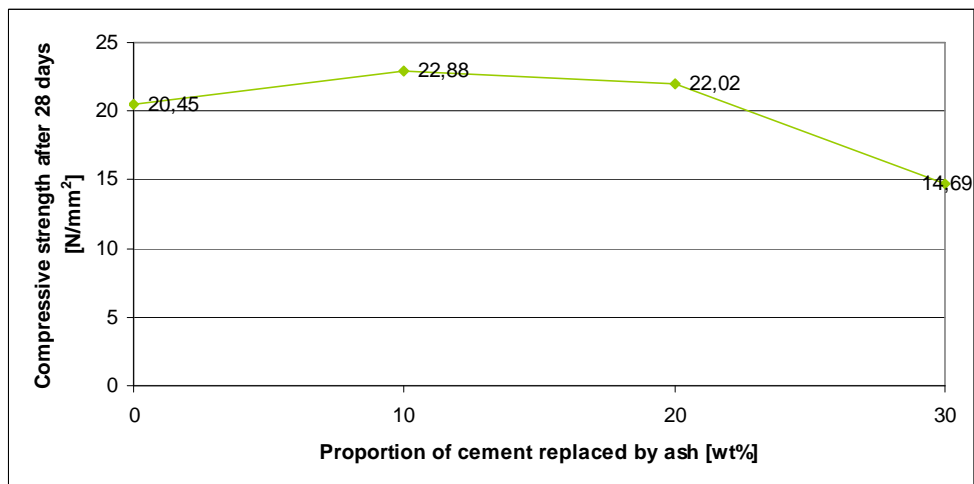


Figure 7. Compressive strength variation in function of proportion of cement replaced by ash.

It is a known fact that the mechanical strength of the mortars and concretes with ash content is lower after 28 days and a beneficial effect it is observed only after 56 or 91 days. To demonstrate the evolution of the strength, mechanical tests were repeated after 56 days (fig. 8 and 9).

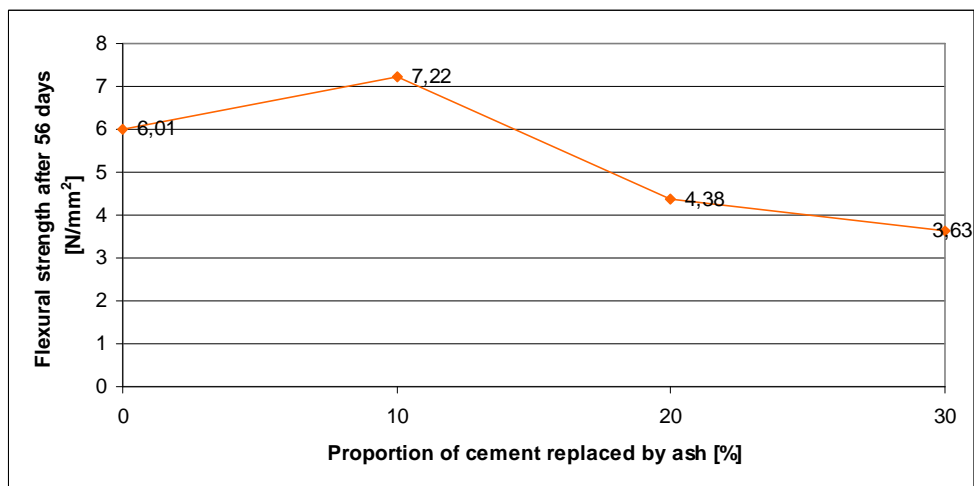


Figure 8. Flexural strength variation in function of proportion of cement replaced by ash.

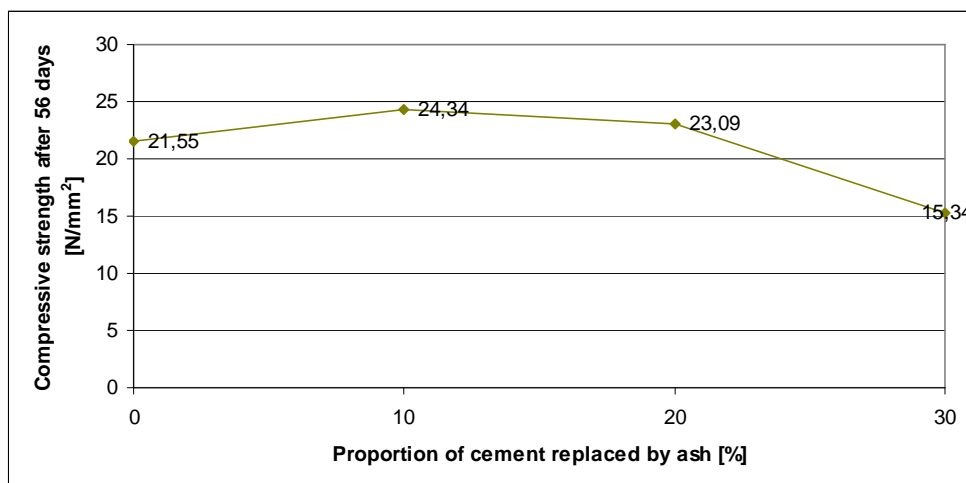


Figure 9. Compressive strength variations in function of proportion of cement replaced by ash

From the figures presented above it can be concluded that it is possible to use ashes in concrete compositions, respectively a part of the cement can be replaced by ashes. The replacement of cement in proportion of 10, 20 and 30 wt% was experimented (composition 2, 3 and 4).

The density increases slowly by replacing 10% of cement, after that a decrease is observed, every sample densities being under the density of the standard composition. The water absorption is in agreement with the results obtained for the densities. The water absorption decrease from 10,84 % for the standard composition to 10,38% for composition 2 with 10wt% ash. For the other compositions the value of absorption increases to 12,31 %, while the ash proportion was increased to 30 wt%.

The values for the mechanical strength state the observations at the density and absorption determination. Thus an increase in strength, both flexural and compressive, was observed for the composition no. 2 with 10 wt% ash. While the ash content was increased the mechanical strength decreased and it is situated below the standard composition strength.

The mechanical test after 56 day of hardening shows that the strength increase is higher for the compositions with ash.

Microscopic images of the studied concretes were realised. In all samples it can be distinguished the presence of binder, which is the basis of the concrete pieces, giving their size and shape. The binder is composed of Portland cement, whose chemical components re-crystallized, immediately and in time, in the form of gels of hydrated calcium silicate crystals or fine granules of calcium hydroxide by reaction with water.

RECOVERY POSSIBILITIES OF POWER PLANT FLY ASH FROM ZALĂU

Microscopic sections were prepared to be examined by transmission. The sections were prepared from the composition containing 10% fly ash and from the standard composition.

For both sample (standard and experimental sample) a highly uniform matrix can be observed, in the finely ground cement, hardened by water, fine particles of crystalline silicate components are dispersed. Especially quartzite crystals are present, in smaller proportions feldspar and limestone and rarely inclusions of mica contained by the sand introduced as aggregate. The particle content is clear and every mineral exhibit specific optical characteristics.

Unevenly distributed small and rare pores are present, more often in the standard sample (Figure 10a-11a).

In the figures 10b-11b intensely colored, small and isolated granules of fly ash can be observed. They are placed between the aggregate particles, increasing the mass compactness. All granular phases are well connected and embedded by the binder matrix

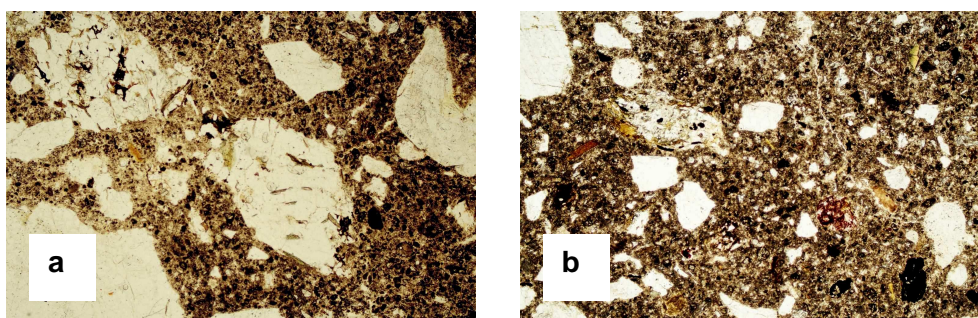


Figure 10. – Samples of slabs in natural polarized light
a - standard concrete slab, b – concrete slab with 10% fly ash

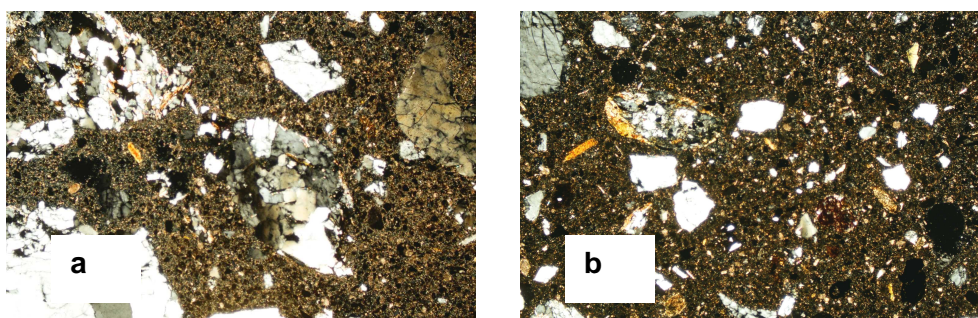


Figure 11. - Samples in transmitted (refracted) polarized light
a - standard concrete slab, b – concrete slab with 10% fly ash

CONCLUSIONS

It can be concluded that the Zalău power plant ash can be used in concrete compositions. 10 wt% replacement of cement by ash brings both economical and qualitative benefits.

Ashes fill in the minute voids that no other part of the mix can fill, thus creating a denser and less absorptive concrete with improved mechanical features. On short term mechanical strengths are lower than plain concrete, after 28 days they equalized and after a long period of hydration products with ashes presents 15-20% higher mechanical strength than classic concrete. Ashes use – recovered wastes – reduces the natural resources use. They also reduces the energy-intensive production of other concrete ingredients, leading to energy saving and “greenhouse gas” emission decrease. Replacing one tone of cement with fly ash it would save enough electricity to power an average home for 24 days, and reduce carbon dioxide emissions equal to a two months use of an automobile.

The enormous quantities and the increasingly wider using opportunities, promoting economic, technical and ecological criteria, make the fly ash an important industrial by-product whose recovery is a national necessity.

EXPERIMENTAL SECTION

Chemical analysis was performed by disaggregating the sample by alkaline fusion of the fine grounded and calcined in platinum crucible. The silica gel was filtered out and separate from the filtrate by double insolubilisation and the oxidic constituents of the mineral mass were determined by complexometric techniques. The second stage in power plant ash composition analysis consisted in careful measurements of the contents of secondary elements. The finely pulverized material, fully passed through a sieve no. 0063 was subjected to mineralization in a mixture of aqua regia and hydrofluoric acid for 30 minutes in a microwave facility and the residual material was filtrated. The contents of the secondary elements were measured by the ELAN DRC II spectrophotometer produced by the Perkin Elmer Company.

The mineralogical composition of the ash was investigated with a SHIMADZU 6000 X-ray diffractometer, using $\text{CuK}\alpha$ radiation (40.0 kV, 30.0 mA).

The thermal behaviour of the ash was investigated by a SHIMADZU derivatographe.

In this experimental works (4) compositions of concrete were prepared replacing the cement with different amounts of ash. In the table 3 are presented the proportions of the raw materials used in the compositions. The first composition, without ash is the standard composition. The hardened concrete characteristics were investigated.

RECOVERY POSSIBILITIES OF POWER PLANT FLY ASH FROM ZALĂU

From the experimentally realized monolithic pieces, some of them with standard composition, without fly ash, others with the addition of 10% ash, thin sections were prepared for microscopic investigations. The used method of investigation was polarizing microscopy in transmitted light with a Yenapol microscope.

Table 3. Concrete compositions

	1	2	3	4
CEM I 42,5 R %	40	36	32	28
Ash %	0	4	8	12
Sand 0-4 %	45	45	45	45
Gravel 4-8 %	15	15	15	15
+ Water %	18,30	18,30	18,30	18,30

The aim was to highlight the role of the ash granules as dispersed phase in the concrete matrix.

REFERENCES

1. Gao Pei-wei, Lu Xiao-lin, Lin Hui, Li Xiaoyan, Hou Jie, *Fuel*, **2007**, *86*, 1208.
2. Tsong Yen, Tsao-Hua Hsu, Yu-Wen Liu, Shin-Ho Chen, *Construction and Building Materials*, **2007**, *21*, 458.
3. L. Széll, V. Cetean, A. Tóth, L. Gagea, C. Roman, M. Roman, A Gog, *Studia Universitatis Babeş-Bolyai Chemia*, **2009**, *LIV*, *1*, 59
4. Serdar Aydın, Halit Yazıcı, Hüseyin Yigiter, Bülent Baradan, *Building and environment*, **2007**, *42*, 717.
5. N.P. Rajamane, J. Annie Peter, P.S. Ambily, *Cement & Concrete Composites*, **2007**, *29*, 218.
6. Takeshi Yamamoto, Tsutomu Kanazu, Masateru Nambu, Takao Tanosaki, *Fuel*, **2006**, *85*, 2345.

ANALYSIS OF GLUCOSE OBTAINED FROM WOOD CARBOHYDRATES BY GAS CHROMATOGRAPHY-MASS SPECTROMETRY

LACRIMIOARA SENILA^a, ADRIANA GOG^a, MARIN SENILA^a,
CECILIA ROMAN^a, FLORIN DAN IRIMIE^b

ABSTRACT. The aim of this study was the development and validation of a new method for glucose analysis obtained from woody biomass by steam-explosion and enzymatic hydrolysis. Quantification of glucose was made by liquid-liquid extraction, oximation and silylation and, finally, analysis by gas chromatography-mass spectrometry (GC-MS). Glucose derivatives obtained were identified by their GC retention time and the corresponding MS fragmentation. BSTFA was used as derivatization reagent to prepare the trimethylsilyl derivatives of glucose.

Keywords: *glucose, wood carbohydrates, derivatization, GC-MS*

INTRODUCTION

Ethanol production from woody biomass is a second generation biofuel process. It is necessary to find energy alternatives to petroleum due to the fossil fuel price and environmental requirements of the Kyoto protocol [1, 2]. The woody biomass is formed from cellulose, hemicellulose and lignin. Cellulose and hemicellulose are carbohydrates who can be converted into ethanol by saccharification and fermentation of glucose [3].

The bioconversion of woody feedstock to glucose contains three steps: pretreatment, hydrolysis, and glucose recovery/analysis. Cellulose is hydrolyzed to glucose, while hemicellulose is hydrolyzed to a mixture of pentoses and hexoses (glucose, mannose, galactose, xylose and arabinose). Cellulose can be chemically or enzymatically converted to glucose [4, 5].

The most used analytical techniques for glucose quantification are high-performance liquid chromatography (HPLC), gel permeation, thin layer, ion exchange and gas chromatography (GC). Derivatization is needed to produce

^a INCDO-INOE 2000, Research Institute for Analytical Instrumentation, Donath 67, 400293, Cluj-Napoca, Romania; E-mail: lacri.senila@icia.ro

^b "Babes-Bolyai" University, Faculty of Chemistry and Chemical Engineering, Arany Janos 11, 400028, Cluj-Napoca, Romania

more volatile compounds for gas chromatographic analyses of glucose [6, 7]. This technique was used for sugars quantification from food and soil. Usually, identification of sugar from lignocellulosic material was done by HPLC. The resolution of HPLC is not always sufficient to separate all mono and oligosaccharide of inters, and also quantification is limited. Gas chromatography coupled with mass spectrometry has the advantage of rapid identification of unknown compounds [8, 9].

The purpose of this paper is the development of a new analysis method based on GC-MS for quantification of glucose obtained by enzymatic hydrolysis of cellulose from wood. The method employed for glucose quantification is liquid-liquid extraction, followed by oximation and silylation with BSTFA.

RESULTS AND DISCUSSION

Glucose was obtained from woody biomass by steam-explosion pretreatment and enzymatic hydrolysis of cellulose. Wood is a renewable source of glucose [3]. Cellulose separation of hemicellulose requires a hard pretreatment. Steam-explosion is a physico-chemical pretreatment, used for cellulose separation.

The solid fraction obtained after steam explosion pretreatment was enzymatically hydrolyzed using cellulase enzymes complex. The solid material was assumed to consist of lignin and cellulose only.

The glucose concentration was determined by two steps derivatization procedure: oximation and silylation, followed by GC-MS determination. Fig.1 shows the chromatogram of glucose using hydroxylamine hydrochloride in pyridine and BSTFA obtained by GC-MS.

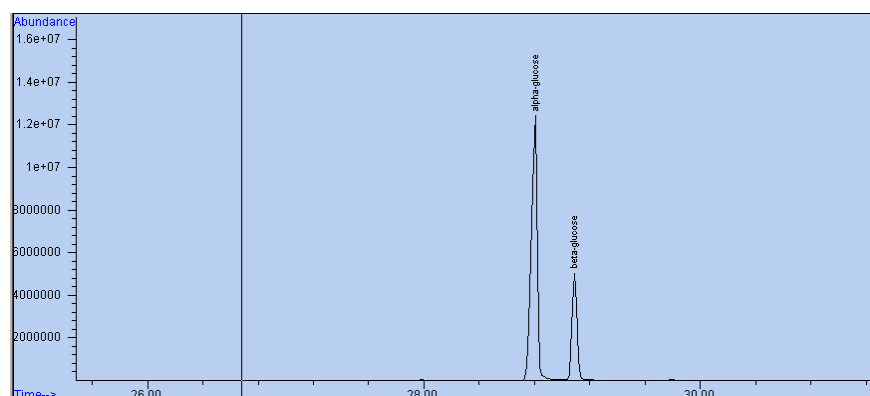


Figure 1. The SIM chromatogram of the glucose after oximation and silylation with BSTFA

Glucose contains six hydroxyl-groups thus the hexa-TMSi derivatives are formed. In SIM chromatogram, hexa-TMSi derivatives are evidenced by the presence of the two GC peaks due to the both 1 α - and 1 β - compounds. A good chromatographic separation was obtained with a resolution better than 1.5 for 1 α - and 1 β - glucose.

The mass spectra of hexasilylated derivatives are mainly characterized by the m/z 319, 205 and 147, respectively. Mass [(CH₃)₃Si⁻, m/z , 73] was obtained that corresponds to the mono-TMS⁺ ion.

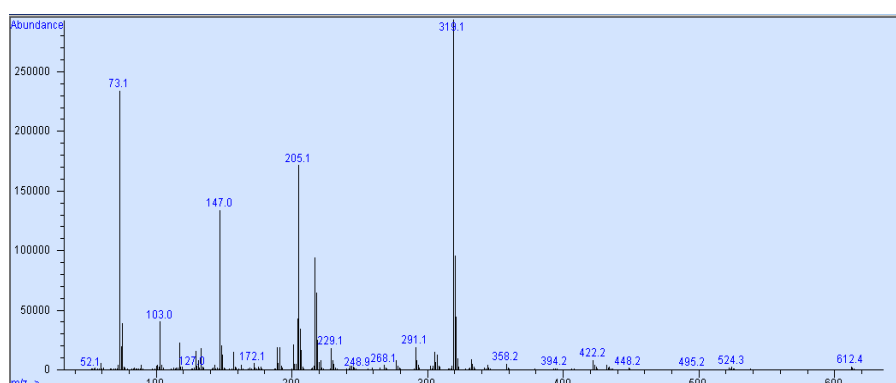


Figure 2. The MS spectra of the ions for the quantitative and qualitative analysis of the silylated derivatives of glucose

Retention time is the parameter used for correct identification of the glucose isomers obtained by extraction and derivatization of the enzymatic hydrolysates. The peaks that corresponded to the 1 α - and 1 β -glucose appear at the retention time 28.709 and 29.004 min.

For glucose quantification, external calibration was used. Standard solutions of glucose were prepared at five different concentrations (1 mg/ml, 3mg/ml, 5mg/ml, 7mg/ml and 10mg/ml), derivatised and analyzed by GC-MS. The limit of detection (LOD) for glucose was calculated as the concentration that corresponds to the three times the standard deviation of the blanks (3s criterion, 10 independent blanks for each analyte) [8]. The limit of detection was calculated as being 0.222 μ g for 1 α -glucose and 0.171 μ g for 1 β -glucose, respectively.

The chromatogram of the glucose resulted from enzymatic hydrolysates after oximation and silylation derivatization process is shown in Fig. 3.

The recovery of glucose from samples was evaluated by using a glucose solution. Six experiments were done in parallel. Glucose was extracted, filtrated and concentrated as presented at experimental section. 1 mg extract was dissolved in 1 ml hydroxylamine hydrochloride solution and derivatized, followed by GC-MS analysis. The calculated degree of recovery was 91 \pm 5.2 %.

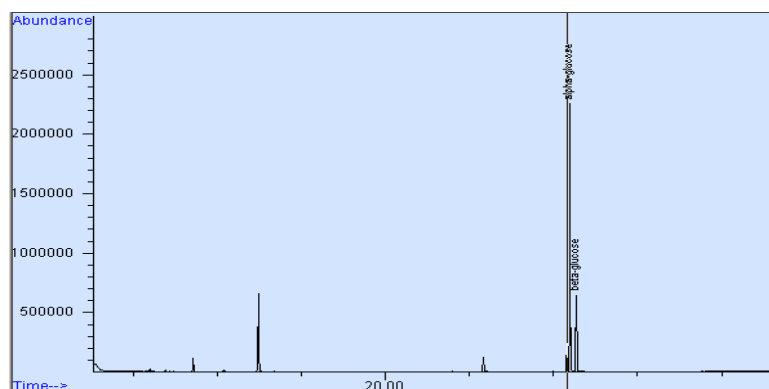


Figure 3. The chromatogram of the glucose-TMS oxime obtained from enzymatic hydrolysates

The relative standard deviation (RSD) of the peak area of the glucose derivatives in the chromatogram (calculated for 6 replicates of a solution containing glucose derivatives) was less than 1%.

CONCLUSIONS

The analytical results show that oxime-TMS derivatization of glucose is a suitable method for GC-MS identification. The products of derivatization can be easily identified by combination of their retention time and mass spectra. Derivatization of carbohydrates allows the quantitative determination of glucose in different cellulose and hemicellulose fractions. Glucose obtained from wood can be easily fermented to bioethanol, a renewable fuel that can replace gasoline.

Extraction of glucose from enzymatic hydrolysates, oximation and silylation with BSTFA is a simple and fast analytical method.

Both recovery and LOD values obtained for glucose using the method described here is comparable with those obtained by other authors [7].

EXPERIMENTAL SECTION

Glucose was obtained from wood by steam-explosion pretreatment and enzymatic hydrolysis of cellulose according to Sassner method with modifications [10].

Steam-explosion involves separating the cellulose as a solid fraction at high temperature and pressure. The pretreated material was separated by filtration in two fractions: a solid material and a liquid phase. The solid material (cellulose and lignin) is enzymatically hydrolyzed to glucose. The glucose content was determined by GC-MS.

The optimal parameters of the derivatization method used in this study (temperature, derivatization time, extraction time) were selected according to other studies [7, 8].

Analytical methods

Glucose obtained after enzymatic hydrolysis was extracted from the solution in 30 ml mixture of dichloromethane:methanol (2:1 v/v). The extract was concentrated by rotary evaporator; total extract was dried using a stream of filtered nitrogen gas. 1 mg extract or standard glucose was dissolved in 1 ml hydroxylamine hydrochloride solution (2.5%), heated to 80°C for 30 min. After oximation, the derivatives were silylated by adding 300 µL BSTFA and the reaction mixture was heated at 80°C for 10 min. One microliter of silylate derivative was injected to the gas chromatograph [7, 8].

Chemicals

All chemicals were of analytical reagent grade. Glucose, pyridine, hydroxylamine hydrochloride (NH₂OH.HCl), dichloromethane, methanol were purchased from Merck (Darmstadt, Germany). The derivatization agents N, O-bis(trimethylsilyl) trifluoroacetamide (BSTFA) were purchased from Sigma–Aldrich.

Instrumentation

A gas chromatograph 6890N (Agilent Technologies) coupled with a mass spectrometer 5973N MSD (Agilent Technologies) and a capillary column HP-5 MS (30 m×0.25 mm×0.25 µm) were used to analyze the glucose concentration.

GC-MS analysis

For quantitative determination of glucose, the MS system was operated in SIM mode. The carrier gas was helium at constant flow rate of 1.0 mLmin⁻¹. The GC column temperature program applied was as following: the initial oven temperature was set at 65 °C, held for 2 min, temperature increase of 6 °C.min⁻¹ to 300 °C, followed by the isothermal hold at 300° C for 15 min.

ACKNOWLEDGEMENTS

This work was supported by the NUCLEU Program No. PN 09 27 03 02/2009/OPTRONICA III, (ANCS Program).

REFERENCES

1. Ó.J. Sánchez, C.A. Cardona, *Bioresource Technology*, **2008**, *99*, 5270-5292.
2. L.C. Lau, K.T. Tan, K.T. Lee, A.R. Mohamed, *Energy Policy*, **2009**, *37*, 4771-4778.
3. E. Araque, C. Parra, J. Freer, D. Contreras, J. Rodríguez, R. Mendonça, J. Baeza, *Enzyme and Microbial Technology*, **2008**, *43*, 214-219.
4. H. Li, N. Kim, M. Jiang, J.W. Kang, H.N. Chang, *Bioresource Technology*, **2009**, *100*, 3245-3251.
5. Y. Teramoto, S. Lee, T. Endo, *Bioresource Technology*, **2008**, *99*, 8856-8863.
6. B. Kamm, M. Kamm, M. Schmidt, I. Starke, E. Kleinpeter, *Chemosphere*, **2006**, *62*, 97-105.
7. P.M. Medeiros, B.R.T. Simoneit, *Journal of Chromatography A*, **2007**, *1141*, 271-278.
8. E. Rojas-Escudero, A.L. Alarcón-Jiménez, P. Elizalde-Galván, F. Rojo-Callejas, *Journal of Chromatography A*, **2004**, *1027*, 117-120.
9. P.N. Wahjudi, M.E. Patterson, S. Lim, J.K. Yee, C.S. Mao, W.-N.P. Lee, *Clinical Biochemistry*, **2010**, *43*, 198-207.
10. P. Sessner, C.-G. Mårtensson, M. Galbe, G. Zacchi, *Bioresource Technology*, **2008**, *99*, 137-145.

CHARACTERIZATION OF SOME SnO₂ CERAMICS WITH ZnO AND Sb₂O₃ ADDITIVES

MARIA GOREA^a, RODICA CRET^b, DELIA MARIA SIMUȚ^a

ABSTRACT. The paper concerns obtaining SnO₂ ceramics with addition of 1, respectively 2 % mol ZnO, and of 0.01 %, 0.05 % and respectively 0.1 % mol Sb₂O₃. The oxides were mixed in wet state, in ethanol. The thermal treatment was experimented at three temperatures (1150, 1200 and 1250 °C) defined based on the results of the dilatometric analysis. Apparent density, compactness and electrical characteristics of ceramics depend on both sintering temperature, and the dopant type and amount. By doping, ceramics with about 85 % of the theoretic density were obtained. Electrical resistivity increases with the amount of dopant.

Keywords: *ceramics, tin dioxide, dopant*

INTRODUCTION

Tin dioxide, SnO₂, represents an n-type semiconductor with a rutile-type crystalline structure. Semiconductors may be used for detecting gases such as H₂, CO, hydrocarbons, other gases and organic vapours. They have become part of modern life, ceramic sensors being preferred due to their chemical and physical stability in aggressive environments, to their easy-processing, and to the possibility of achieving pre-defined properties in their case. The n-type semiconductor sensors are based on the superficial adsorption of oxygen leading to an increase of electrical resistance, which then decreases if a reducing gas reacts with the adsorbed oxygen. A lot of oxides (SnO₂, ZnO, TiO₂, ZrO₂) have been studied as materials for obtaining sensitive ceramics, however this research involving the identification of new methods and materials is still on top as consequence of the need of solving specific requirements – such as sensibility, selectivity, feedback time, density, and less but not least, the fabrication costs [1-5]. SnO₂-based ceramics are used for the fabrication of gas sensors, but their disadvantage is a low density (about 50 % from the theoretical one). The level of densification for such ceramics can be improved by adding dopants like CoO, MnO, ZnO, CuO or Bi₂O₃. By adding 0.5-1 % mol of dopant, the ceramics' density may increase

^a Babeş-Bolyai University, Faculty of Chemistry and Chemical Engineering, 11 Arany Janos Str., RO-400084, Cluj-Napoca, Romania, mgorea@chem.ubbcluj.ro

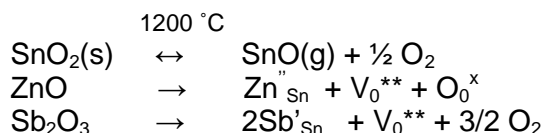
^b Technical University, Faculty of Electrical Engineering, 26-28 G. Barițiu Str. RO-400027, Cluj-Napoca, Romania, rodica_cret@yahoo.fr

up to 95 % from the theoretical one [6-9]. Doping with an oxide of divalent and one of a pentavalent metal may lead to densification of ceramics and in the same time to its varistor-type electrical behaviour (nonlinear pattern of resistivity). Oxide systems based on SnO₂ and ZnO were intensely studied as both gas sensors, and varistors [10,11]. Under normal circumstances, this leads first to an increase of the resistance of the circuit, then to its decrease due to the reaction of the reducing gas with the adsorbed oxygen [12-13]. In the case of dense ceramics with SnO₂, the role of ZnO used as dopant is to realize oxygen vacancies, *i.e.* Zn^{''}_{Sn}+ V^{**}_O type defects that lead to the formation of Schottky barriers and finally, to the densification of the material [14]. Doping is also an effective mean for controlling the crystallites size. By using dopants such as Pd, Pt, Sb₂O₃, or MgO, the sensibility and sensitivity of the sensor can be highly improved [15, 16].

This paper concerns SnO₂-containing ceramics with addition of ZnO and Sb₂O₃ from the point of view of sintering temperatures, compactness characteristics and correlation with electrical properties.

RESULTS AND DISCUSSION

Tin dioxide (SnO₂) represents an n-type semiconductor with a rutile-type crystalline structure; after sintering the powders, the final ceramic products show low densities. The high diffusion coefficient of oxygen even at low temperatures, and the stability of Sn²⁺ oxidation state may promote loss of oxygen and vacancies creation. Also, during the thermal treatment, in the presence of dopants, substitutions occur in the crystalline network of SnO₂, influencing the electrical properties of ceramics, and densification of the material.



The influence of ZnO and Sb₂O₃ on the sintering process has been investigated by using dilatometric analysis. By observing the dilatometric results on samples with ZnO vs. those with both ZnO and Sb₂O₃ in a ratio of 0.1 % mol (table 5), one can notice that an increase of ZnO content from 1 to 2 % mol leads to an increase of the maximum sintering temperature from 1178.5 °C to 1203.9 °C, while the addition of Sb₂O₃ does not significantly influence the results. Thus, three sintering temperatures for the mixtures have been chosen, as follows: 1150 °C (samples M₁, M₂, M₅ and M₆), 1200 °C (samples M₁-M₈) and 1250 °C (samples M₃, M₄, M₇ and M₈). In the case of all compositions, an incipient sintering was noticed around 900 °C.

Table 1. Compactness characteristics of the studied ceramics

Sample no.	T _{sintering} (°C)	Apparent density (g/cm ³)	Relative density (% of d _{theoretic})	Water adsorption (%)	Apparent porosity (%)	Firing shrinkage (%)
M ₁	1150	5.429	78.115	6.439	34.879	3.555
M ₂		4.457	64.129	7.344	32.716	2.557
M ₅		4.398	63.281	7.213	31.675	2.644
M ₆		3.845	55.320	6.901	27.233	3.029
M ₁	1200	4.610	66.331	6.425	29.604	4.098
M ₂		4.608	66.330	7.296	29.997	3.415
M ₃		5.269	75.813	3.759	19.741	8.546
M ₄		5.274	75.885	3.763	19.846	7.618
M ₅		4.484	64.518	6.752	30.257	3.415
M ₆		4.426	63.683	7.129	25.686	3.660
M ₇		4.799	69.050	5.678	27.26	5.236
M ₈		4.727	68.014	5.565	26.292	5.832
M ₃	1250	5.779	83.150	1.627	9.380	10.595
M ₄		5.615	80.790	2.392	13.424	9.772
M ₇		4.864	69.986	4.944	23.971	6.848
M ₈		5.594	80.489	4.434	24.222	7.496

Taking into account that the sensors' mechanism is mainly associated with adsorption-desorption processes, the specific surface of ceramics becomes an important factor that defines its sensitivity. Porosity may improve specific surface, so that the porous ceramics are suitable materials when it comes to sensors.

The compactness characteristics of the experimental compositions are presented in table 1.

When examining the analytical data, it can be noticed that apparent density and compactness are higher in the case of samples M₃ and M₄ fired at 1200 °C (about 76 % of the theoretic density and an apparent porosity of 20 %), and respectively at 1250 °C (more than 80 % of the theoretic density and 10 % apparent porosity). A high porosity was noticed in samples M₁ and M₂ fired at 1150 °C.

The current density– electric field intensity characteristics were plotted at logarithmic scale – $\log J = f(\log E)$ – by measuring the intensity of the electrical field crossing the sample at a specific value of the applied voltage. These characteristics, according to the content of ZnO and Sb₂O₃ in samples fired at different temperatures are presented in figure 1a, b, c and d, while the ceramics' resistivities (calculated based on the values for the voltage, current intensity and geometrical features of the samples) are indicated in tables 2 and 3.

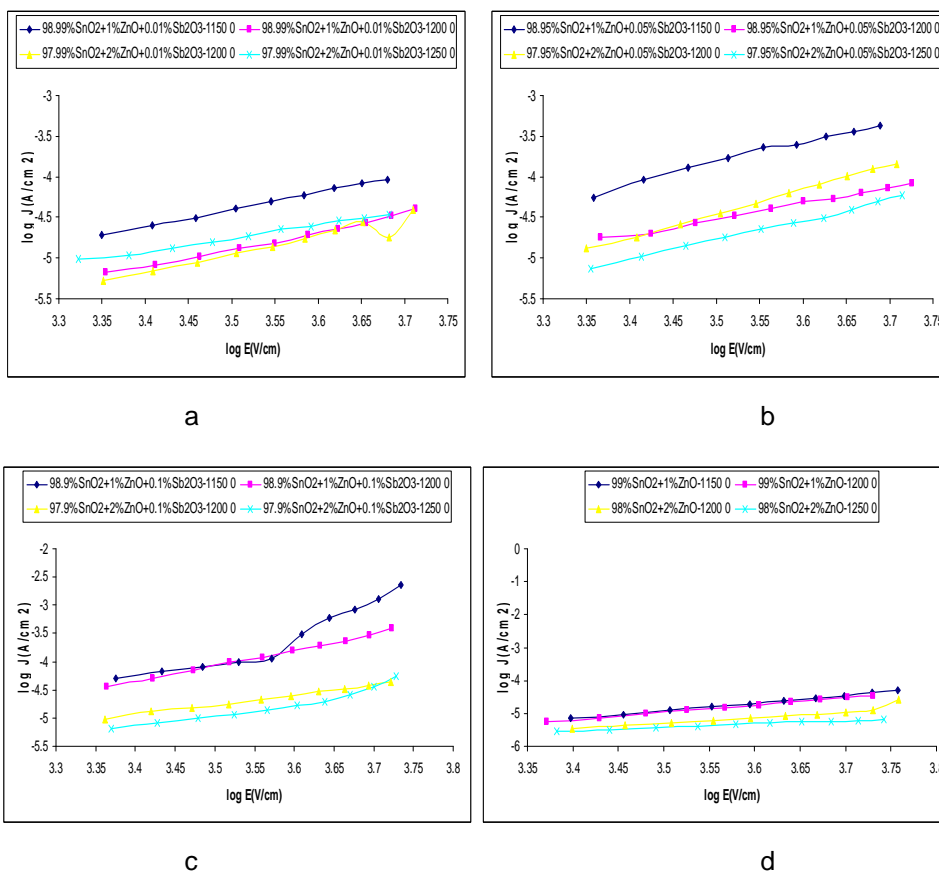


Figure 1. Current density with respect to the applied electrical field for different ZnO and Sb_2O_3 concentrations

It can be noticed that an amount of 1% mol ZnO does not influence the values of the electrical field in the case of the samples fired at 1150 °C and 1200 °C, while 2 % mol ZnO in samples fired at 1200 °C and 1250 °C slightly modifies them (figure 1 d). Significant changes of the electrical characteristics were noticed in samples doped with 1 % mol ZnO, and 0.01 respectively 0.05 % mol Sb_2O_3 fired at 1150 °C and 1200 °C; in the case of samples containing 2 % mol ZnO fired at 1200 °C and 1250 °C, the variation is minimal (figures 1 a, b). With the increase of Sb_2O_3 content to 0.1 % mol, the values of the electrical characteristics are grouped in the case of samples with 1 and respectively 2 % mol ZnO, while those with 2 % mol ZnO show higher values for the electrical resistances.

Table 2. Electrical resistivity for samples fired at 1150 °C and 1250 °C

No.	U(V)	Resistivity (MΩ·m)							
		Samples fired at 1150 °C				Samples fired at 1250 °C			
		M1	M2	M5	M6	M3	M4	M7	M8
1	700	3.4524	0.4814	0.4131	1.1719	8.5148	3.6173	3.0726	2.1949
2	900	2.5172	0.3714	0.2295	0.9216	8.3110	3.0492	2.0819	2.0131
3	1200	1.8351	0.1325	0.1601	0.6507	8.2356	2.3481	1.4302	1.5803
4	1500	1.2799	0.0395	0.1127	0.5157	8.3724	1.4044	0.9675	1,4525

Table 3. Electrical resistivity for samples fired at 1200 °C

No.	U(V)	Resistivity (MΩ·m)							
		Samples fired at 1200 °C							
		M1	M2	M3	M4	M5	M6	M7	M8
1	700	4.1499	0.6354	7.0817	2.3869	1.2964	3.3600	1.6884	4.1984
2	900	3.1171	0.4152	6.4929	1.9180	1.1147	2.7428	1.1073	3.2452
3	1200	2.2140	0.2553	5.2968	1.6088	0.8061	2.0389	0.6127	2.2162
4	1500	1.5751	0.1686	4.2834	1.2847	0.6755	1.4769	0.3819	2.6725

The electrical resistivity increases with firing temperature. The densest samples, M3 and M4, show the highest values for resistivity.

CONCLUSIONS

The sintering temperatures and the linear shrinkages of ceramic samples in the SnO₂ – ZnO – Sb₂O₃ system can be established by performing dilatometric analysis. The addition of Sb₂O₃ to SnO₂ ceramics with 1 and respectively 2 % mol ZnO influences densification and values of electrical resistivity. Electrical characteristics depend on the dopant concentration and on sintering temperature, the amount of Sb₂O₃ playing the leading role. Doping resulted in ceramics with densities up to 85 % from the theoretical density and in an increase of the electrical resistivity.

EXPERIMENTAL SECTION

In the view of obtaining the ceramics, oxides (SnO₂, Sb₂O₃ and ZnO) with high analytical purity (over 99.5 %) were used, because impurities can alter the microstructure, thus implicitly the properties – mainly the electric ones - of the final product. For a suitable processing of the mixtures, the particle size is an important factor, due to the fact that the dopants diffusion and the sintering take place in solid state, at high temperatures. The oxide particles used in these experiments have to be micrometric in size. The molar composition of the investigated system is presented in table 4.

Table 4. Experimental compositions

Composition no.	Oxide (% mol)		
	SnO ₂	ZnO	Sb ₂ O ₃
M ₁	99.00	1	-
M ₂	98.90	1	0.10
M ₃	98.00	2	-
M ₄	97.90	2	0.10
M ₅	98.95	1	0.05
M ₆	98.99	1	0.01
M ₇	97.95	2	0.05
M ₈	97.99	2	0.01

For the experiments, the proper ratios of raw materials were homogenised by using a laboratory ball mill in ethanol for 2 h. Then the samples were dried in an oven at 105 °C for 48 h. The powders were submitted to grain size analysis by using a Counter Coulter WING-SALD 7101 equipment. The particles for the tested compositions ranged between 0.35–6 microns in size, having an average particle size of about 2 microns.

Afterwards, the powders have been granulated and pressed as pellets by using an uniaxial press under a pressure of 800 kgf/cm². The dried samples have been sintered at different temperatures by the means of a laboratory furnace, the sintering temperatures being established based on dilatometric measurements. The starting and maximum sintering temperatures, as well as the linear shrinkages in the case of compositions M₁-M₄ are presented in table 5. The dilatometric analysis has been achieved on a Linseis L 75HX1400 unit, up to a maximum temperature of 1300 °C, with a heating rate of 10 °C/min, in normal atmosphere. The linear shrinkages for raw mixtures with various concentrations of dopants are presented in figure 2.

Table 5. Starting (T_{is}) and maximum (T_{max}) sintering temperatures for the studied samples

Composition (%mol)	T _{is} (°C)	Linear shrinkage (%)	T _{max} (°C)	Linear shrinkage (%)
M ₁ . 99 %SnO ₂ +1% ZnO	912.8	0.54	1178.5	2.39
M ₂ . 98.9 %SnO ₂ +1% ZnO+0.1% Sb ₂ O ₃	922.1	0.57	1177.3	1.66
M ₃ . 98 % SnO ₂ +2% ZnO	907.2	0.54	1203.9	3.14
M ₄ . 97.9 %SnO ₂ +2% ZnO+0.1% Sb ₂ O ₃	878.9	0.52	1190.1	2.51

The thermal treatment was performed in a Nabertherm laboratory-type furnace for 9 h and with 30 minutes dwell at maximum temperature; the cooling was slow, provided by the furnace's ventilation system.

CHARACTERIZATION OF SOME SnO₂ CERAMICS WITH ZnO AND Sb₂O₃ ADDITIVES

The compactness characteristics of the thermally-treated samples were investigated by using the Archimedes method.

In the view of the electrical characteristics measurements (current intensity – voltage, I-V), the samples have been metallised, by covering with an Ag paste on their surface.

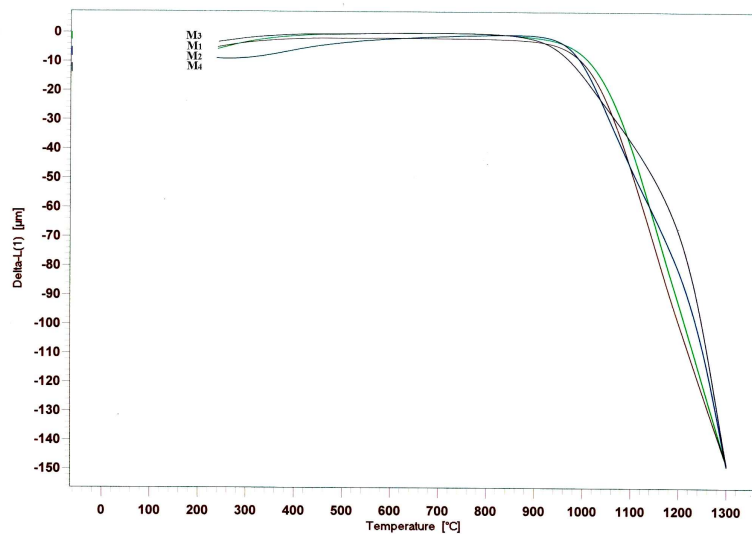


Figure 2. Linear shrinkage of the investigated samples

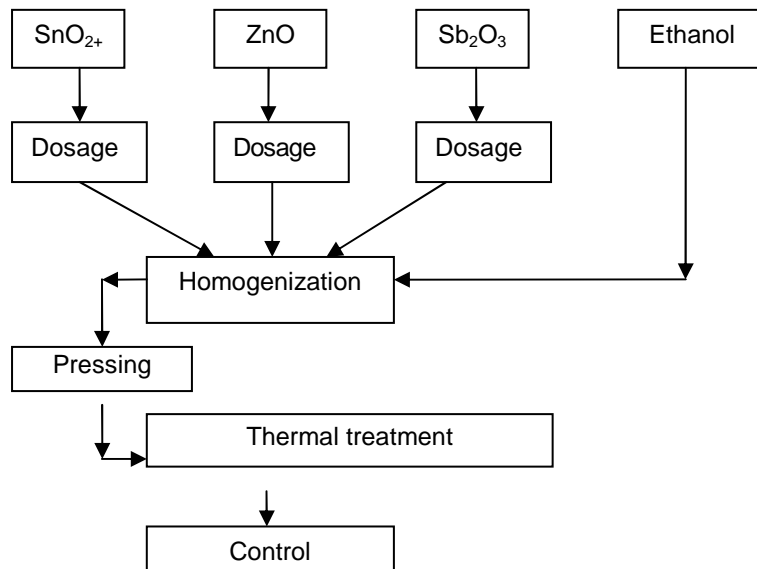


Figure 3. The schematic flux for obtaining the ceramics

The technological flux for obtaining the semiconductor ceramics with sensitive properties (figure 3) focused on reduction, as much as possible, of the possibilities for impurities to enter the system, on diminishing the loss of material, on a very good homogenization and milling of the components, in the view of obtaining an uniform microstructure following thermal treatment.

REFERENCES

1. Kim Hye-Kyung, S.D. Sathaye, Y.K. Hwang, S.H. Jhung, J-S. Hwang, S.H. Kwon, S-E. Park, J-S. Chang, *Bull.Korean Chem.Soc.*, **2005**, 26 (11), 1881.
2. D.D. Vuong, G. Sakai, K. Shimanoe, N. Yamazoe, *Sensors and Actuators*, **2005**, 105, 437.
3. G.G. Lee, L.S-J. Kang, *Sensors and actuators*, **2005**, 107, 392.
4. Y. Shimizu, A. Jano, T. Hyodo, M. Egashira, *Sensors and Actuators*, **2005**, 108, 56.
5. T.P. Hulser, H. Wiggers, A. Lorke, *Sensors and Actuators*, **2005**, 109, 13.
6. Fan Jiwei, et al., *Journal of the European Ceramic Society*, **2010**, 30, 545.
7. H.C. Wang, M.J. Yang, Y. Li, *Sensors and Actuators*, **2006**, 119, 380.
8. W. Dang, H. Ping, D. Xiaowen, P. Qungyi, *Sensors and Actuators*, **2005**, 140, 383.
9. M. Hayashi, T. Hyodo, Y. Shimitzu, M. Egashira, *Sensors and Actuators*, **2009**, 141, 465.
10. A. Somăcescu, E. Andronescu, C. Somăcescu, *Rev. Rom. de Materiale*, **2003**, XXXIII (2), 85.
11. E.A. Gușă, I. Teoreanu, A. Petrescu, M. Ionescu, M. Bârlădeanu, *Rev. Rom. de Materiale*, **2009**, 39 (1), 57.
13. D.E. Dyshel, *Power Metallurgy and Metal Ceramics*, **2001**, 40 (5-6), 282.
14. M.A.L. Margionte, A.Z. Simoes, C.S. Riccardi, F.M. Filho, A. Ries, L. Perazolli, J.A. Varela, *Ceramics International*, **2006**, 32, 713.
15. Li Laifeng, Pan Xiaoqing, *Chinese Journal of Materials Research*, **2000**, 14 (1), 42.
16. V. Geraldo, et al., *Materials Research*, **2003**, 6 (4), 451.

NEW LIQUID CHROMATOGRAPHY COUPLED WITH MASS SPECTROMETRY METHOD FOR CIPROFLOXACIN MONITORING IN HUMAN PLASMA

SILVIA IMRE^a, SZENDE VANCEA^a, GRIGORE DOGARU^a,
CARMEN CĂLDĂRARU^a, CAMIL-EUGEN VARI^a, MARIA TITICA DOGARU^a

ABSTRACT A new simple, sensitive and selective liquid chromatography coupled with mass spectrometry (LC-MS) method for quantification of ciprofloxacin in human plasma was validated. Ciprofloxacin and ofloxacin, as internal standard, were analysed on a SB-C18 column (Agilent Technologies, 100 mm x 3 mm I.D., 3.5 μ m) under isocratic conditions using a mobile phase of a 70:30 (v/v) mixture of 0.1% (v/v) formic acid in water and acetonitrile. The flow rate was 0.5 mL/min at the column temperature of 25 °C. The detection of the analyte was in SIM mode using a triple quadrupole mass spectrometer with electrospray positive ionisation. The monitored ions were m/z 332 for ciprofloxacin and m/z for 362 for ofloxacin. The sample preparation was very simple and consisted of protein precipitation from 0.2 mL plasma using 0.4 mL of 0.05% acetic acid solution in methanol containing 0.5 μ g/mL internal standard. Linear calibration curves were generated over the range of 25-5000 ng/mL with values for coefficient of determination greater than 0.999 and by using a weighted (1/c) linear regression. The lowest limit of quantification was 10 ng/ml. The values of precision (RSD%) and accuracy (relative error%) were less than 8.7% and 11.9%, for within- and between-run, respectively. The recovery of the analyte ranged between 82.5 and 91.1%. Ciprofloxacin demonstrated good stability in various conditions. The validated LC-MS method allows ciprofloxacin monitoring in human plasma during clinical treatment or other pharmacokinetics investigation.

Keywords: *ciprofloxacin, LC-MS, human plasma, pharmacokinetics, therapeutic drug monitoring*

INTRODUCTION

As it is known, ciprofloxacin (CPR) or 1-cyclopropyl-6-fluoro-4-oxo-7-(piperazin-1-yl)-1,4-dihydroquinoline-3-carboxylic acid belongs to the second generation of fluoroquinolones with activity against both Gram-positive and Gram-negative bacteria and other microorganisms [1], having a large applicability in clinical practice.

^a *Drugs Testing Laboratory, University of Medicine and Pharmacy, Gheorghe Marinescu street 38, RO-540139, Târgu-Mureş, Romania, silista@yahoo.com*

During ciprofloxacin treatment, the status of the patient's renal and hepatic function must be taken into consideration to avoid an accumulation that may lead to an overdose and the development of toxicity. Modification of the dosage is recommended for those patients with impaired kidney function by a precise monitoring of the plasma concentration.

Therapeutic drug monitoring (TDM) is an essential tool for a positive management therapy. The preferred laboratory strategy is immunoassay. Due to the cross-reactivity to other components, alternative approaches, such as liquid chromatography coupled with mass spectrometry (LC-MS), are continuously under investigation. The main application area of LC-MS in the analysis of antibiotic and antibacterial compounds is the confirmation of their identity in animal food products for human consumption at maximum residue levels, set by the regulatory authorities.

However, in the past years there are many applications of LC-MS regarding fluoroquinolones determination in human plasma, but only a few are dedicated to ciprofloxacin.

In two articles, ciprofloxacin, together with other drugs, was LC-MS detected in human plasma. Ciprofloxacin and dexamethasone were monitored in blood by a LC-MS method in order to describe the pharmacokinetics of ciprofloxacin and dexamethasone after administration of CIPRODEX Otic Suspension into the middle ears of children [2]. Tigecycline and ciprofloxacin were employed as the model compounds to study the effect of the anticoagulant ethylenediamine tetra-acetic acid (EDTA) on the determination of pharmacokinetic parameters [3], drug concentrations being quantified by LC-MS/MS analysis.

There are also two works, published only as abstracts, in which LC-MS analysis of ciprofloxacin after protein precipitation is described. Bugge and col. [4] validated a LC-MS/MS method with lomefloxacin as internal standard. Acetonitrile was used to precipitate plasma proteins, but a portion of the extract was evaporated and reconstituted in mobile phase. The detection was in positive ion multiple reaction monitoring (MRM) mode. In the other paper, a rapid, sensitive, selective, accurate LC-MS method for the determination of ciprofloxacin in human plasma was developed and validated after protein precipitation [5], the detection being also in MRM mode.

Taking in account to those present above, we attempted to develop and validate a new and fast LC-MS method able to quantify ciprofloxacin in human plasma during drug therapy or pharmacokinetic investigations by applying a simple and consistent plasma sample preparation by protein precipitation, ofloxacin (OFL) being the internal standard.

RESULTS AND DISCUSSION

No significant interference at the retention time of CPR (3.19 min) and OFL (2.3 min) was observed in different plasma blank samples chromatograms due to the specificity of the selected signals against endogenous compounds.

The analytes were well separated under the proposed chromatographic conditions in less than 3.5 min (Figure 1). The analyte carryover was verified using a blank injection made right after the injection of the calibration solution with the most elevated level of concentration (Figure 2, curve a). The interference at the retention times of analytes due to carryover was less than 1/10 of the signal corresponding to the lower limit of quantification - LLOQ (Figure 2, curve b).

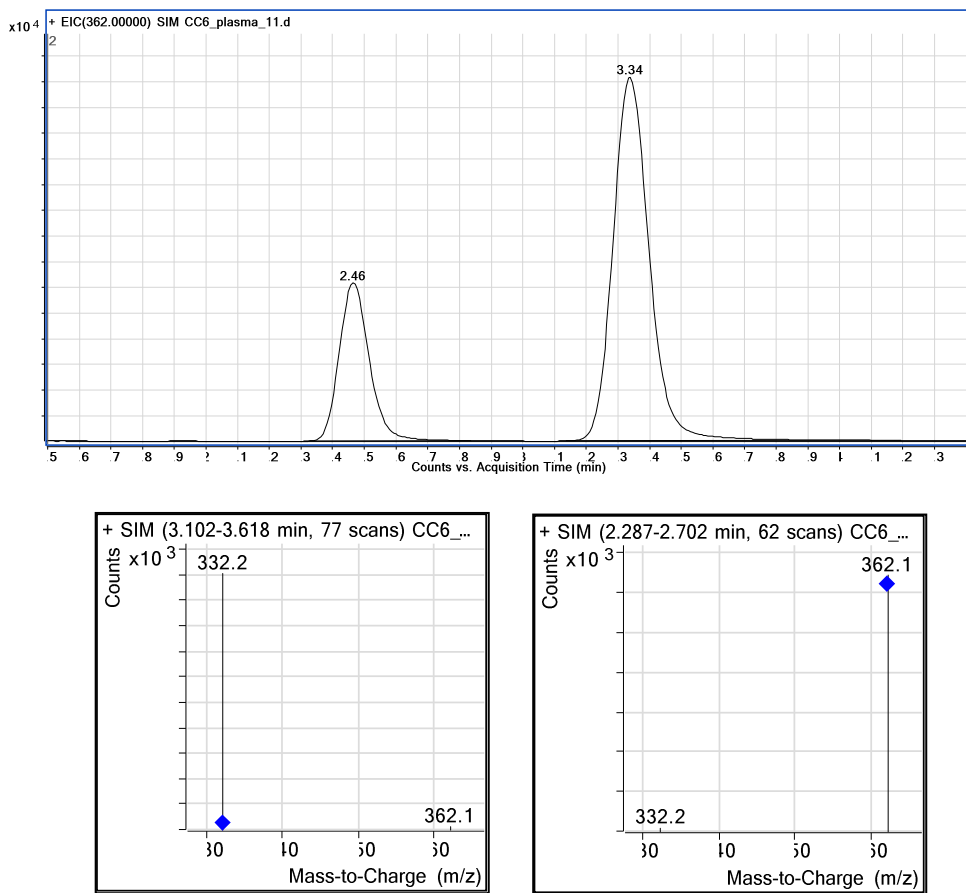


Figure 1. Chromatograms of a plasma standard with 5000 ng/ml CPR and 1000 ng/ml OFL (upper image) and SIM mass spectra of CPR and OFL (lower images)

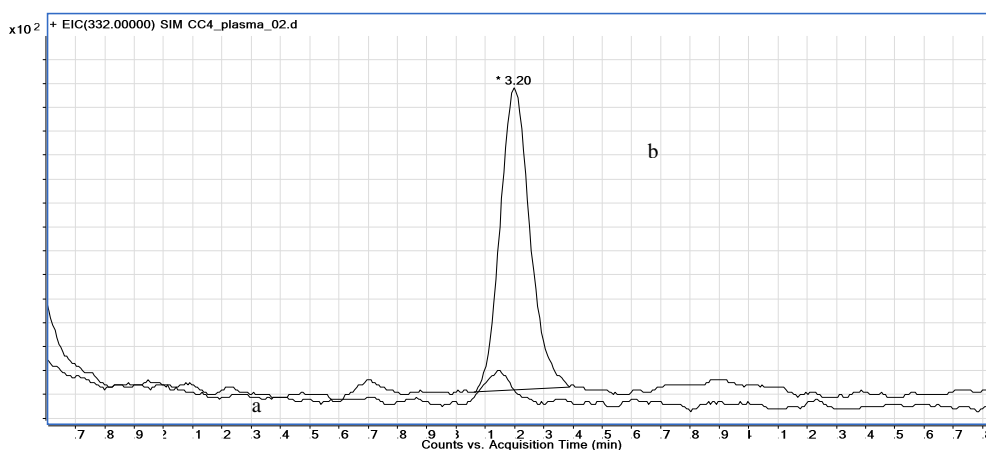


Figure 2. Chromatograms of blank plasma (a) and the LLOQ plasma standard with 25 ng/ml CPR (b)

The applied calibration curve model proved to be accurate over the concentration range 25 - 5000 ng/mL, with the coefficient of correlation greater than 0.999. The mean calibration curve, $y = a(\pm SD) x + b (\pm SD)$, where SD is the standard deviation, was: $y = 0.5655 (\pm 0.0218) x + 0.0013 (\pm 0.0031)$, $N = 10$ calibration points, $n = 5$ determinations for each calibration point. The residuals had no tendency of variation with concentration and were less than 13.4%.

The method had within- and between-run accuracy and precision (Tables 1 and 2), in agreement to the international regulations regarding bioanalytical methods validation [7-9]. The lower limit of the linearity domain was established at 25 ng/mL CPR, with accuracy and precision less than 5.2%. The lowest limit of quantification, corresponding to a signal to noise ratio of ten, was established at 10 ng/mL.

The recovery was consistent (87%) and reproducible (CV of 5%).

Table 1. Within-run accuracy and precision results

Level	QCA	QCB	QCC
Nominal concentration, ng/mL	100	2000	3200
Found mean, n=5	109	2040	3093
Accuracy, %	8.7	1.9	-3.4
CV, %	2.6	1.4	2.4

Table 2. Between-run accuracy and precision results

Level	QCA	QCB	QCC
Nominal concentration, $\mu\text{g/mL}$	100	2000	3200
Found mean, n=5	112	1979	3185
Accuracy, %	11.9	-1.1	-0.5
CV, %	5.7	5.6	5.2

The analytes proved their stability under various conditions, the Bias% of found concentration against concentration of the reference QC sample being less than 10%.

The method was finally verified by analyzing plasma samples obtained from a healthy volunteer after oral administration of a single dose of 500 mg CPR (Figure 3). As it can be seen, the proposed method is able to quantify CPR concentration with accuracy and precision after at least four half-times in order to obtain an adequate plasma concentration profile for pharmacokinetic or bioequivalence studies.

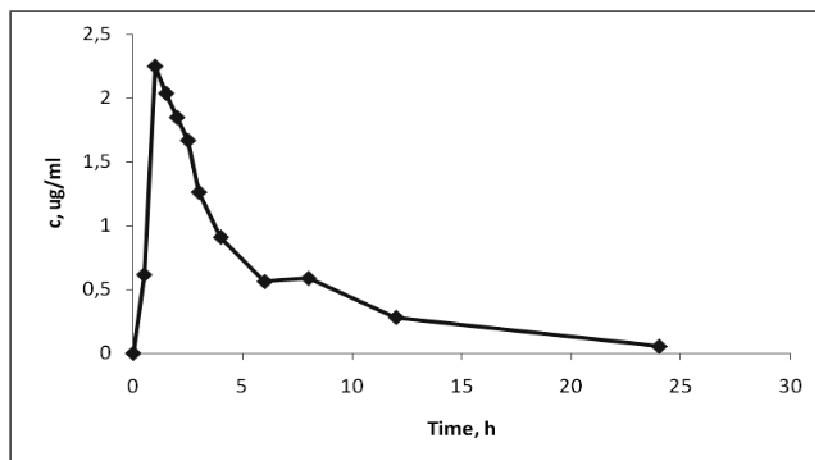


Figure 3. The time - concentration profile of ciprofloxacin in a healthy volunteer after oral administration of 500 mg CPR

As far as we are aware, there are only two works published as abstracts in which ciprofloxacin determination in human plasma by LC-MS is made after protein precipitation, alone or combined with other extraction procedure (Table 3). In comparison, the proposed method has some advantages: the sensitivity (the lowest limit of quantification of 10 ng/mL at 7 pg injected); a better recovery of the analyte (over 80%) in comparison with the cited method

in which only protein precipitation was applied [5]. This is the first full text paper about ciprofloxacin LC-MS determination in human plasma in which the sample preparation consisted of protein precipitation.

Table 3. Comparison of the actual work with already published methods in which the plasma protein precipitation was applied

Work	Method	Sample treatment	Recovery, %	Linearity domain, ng/ml / pg injected	LstLOQ, ng/ml / pg injected	Run time, min
Current	ESI+, SIM, isocratic elution	PP	87	25-5000 / 16	10 / 7	3.5
Bugge & col. (2005) [4]	ESI+, MRM, isocratic elution	PP + solvent evaporation	Extraction was quantitative	25-10000 / ?	?	2
Peng & col. (2008) [5]	ESI+, MRM, gradient elution	PP	53	25-2000 / ?	?	4.5

PP – protein precipitation; ? – no data available; LstLOQ - Lowest Limit of Quantification

CONCLUSIONS

The proposed method provides accuracy and precision for quantitative monitoring of ciprofloxacin in human plasma during therapy or pharmacokinetics investigation. The simple sample preparation by protein precipitation, while using less organic solvent with small amounts of sample plasma volume, the relatively short run time and the selected signals for monitoring allow a specific and efficient analysis of plasma samples, making the method more productive and thus more cost effective.

EXPERIMENTAL SECTION

Reagents

Ciprofloxacin and ofloxacin (OFL - internal standard) were analytical standards purchased from Fluka (Sigma-Aldrich Chemicals, UK) and Riedel-De Haën (Germany), respectively. Acetonitrile, methanol, acetic acid were Merck products (Merck KgaA, Germany) and formic acid was Scharlau (Scharlau Chemie S.A., Spain) reagent grade. Ultrapure, deionised water was produced by a Millipore Direct Q5 water system (Millipore SA, France). The human blank plasma was supplied from healthy volunteers.

Standard solutions

Two stock solutions of CPR and OFL, respectively, with concentration of 1 mg/mL were prepared by dissolving appropriate quantities of reference substances (weighed on an analytical balance AB54S, Mettler-Toledo, Switzerland) in 10 mL solution of 0.05% acetic acid in methanol. Ten calibration working solutions of 0.125 - 25 µg/mL CPR were then obtained by diluting specific volumes of stock solutions with the same solvent. Then these were used to spike 0.16 mL plasma blank, providing finally ten plasma standards with the concentrations ranged between 25 and 5000 ng/mL. Accuracy and precision of the method was verified using plasma standards with concentrations of 100, 2000 and 3200 ng/mL. Quality control samples (QC) with the same concentrations 100 (QCA), 2000 (QCB) and 3200 (QCC) ng/mL analyte will be used during clinical samples analysis.

Chromatographic and mass spectrometry systems and conditions

The HPLC system was an 1100 series model (Agilent Technologies, USA) consisted of a quaternary pump, an in-line degasser, an autosampler, a column thermostat, and a triple quadrupole mass spectrometer detector 6410 (Agilent Technologies). Chromatograms were processed using MassHunter software (Agilent Technologies).

The detection of the analyte was in single ion monitoring (SIM) mode using an electrospray positive ionization (ESI positive). The monitored ions were m/z 332 for CPR and m/z 362 for OFL. Other detector parameters: dry temperature 350 °C, nebulizer 50 psi, dry gas – nitrogen at 10 L/min.

Chromatographic separation was performed at 25°C on a Zorbax SB-C18, 100 x 3 mm, 3.5 µm column (Agilent Technologies), protected by an in-line filter.

Mobile phase

The mobile phase consisted of a mixture of water containing 0.1% formic acid and acetonitrile (70:30 v/v), each component being degassed, before elution, for 10 minutes in a Elma Transsonic T700 ultrasonic bath (Germany). The pump delivered the mobile phase at 0.5 mL/min.

Sample preparation

Standard and test plasma samples were prepared as follows in order to be chromatographically analyzed. In an Eppendorf tube 0.2 mL plasma with 0.4 mL internal standard methanolic solution (0.5 µg/mL OFL) was vortex-mixed for 30 seconds (Mix20, Falc Instruments, Italy). After 10 minutes, the tube was centrifuged for 10 minutes at 10000 rpm (Sigma 2K15 centrifuge, Germany). The supernatant was transferred in an autosampler vial and 2 µL were injected into the LC-MS system.

Validation

As a first step of method validation [7-9], specificity was verified using six different plasma blanks obtained from healthy human volunteers who had not previously taken any medication.

The concentration of analytes was determined automatically by the instrument data system using the internal standard method. Calibration was performed using singlicate calibration standards on five different occasions. The calibration curve model was determined by the least squares analysis. The applied calibration model was a linear one: $y = ax + b$, weight $1/x$, where y – peak area ratio and x – concentration ratio. Distribution of the residuals (% difference of the back-calculated concentration from the nominal concentration) was investigated. The calibration model was accepted, if the residuals were within $\pm 20\%$ at the lower limit of quantification (LLOQ) and within $\pm 15\%$ at all other calibration levels and at least 2/3 of the standards met this criterion, including highest and lowest calibration levels.

The lower limit of quantification was established as the lowest calibration standard with an accuracy and precision less than 20%. The lowest limit of quantification was investigated at a signal to noise ratio of ten.

The within- and between-run precision (expressed as coefficient of variation, CV%) and accuracy (expressed as relative difference between obtained and theoretical concentration, Bias%) of the assay procedure were determined by analysis on the same day of five different samples at each of the lower (100 ng/mL), medium (2000 ng/mL), and higher (3200 ng/mL) levels of the considered concentration range and one different sample of each on five different occasions, respectively.

The relative recoveries at each of the previously three levels of concentration were measured by comparing the responses of the final solutions obtained after preparation of plasma standards (N=3 replicates) with the responses of the standard solutions with the same concentrations of analytes.

The stability of stock solutions of CPR and OFL for four hours at room temperature was verified by comparing the responses of the diluted solutions (1000 ng/ml) with those obtained from stock solutions kept in the refrigerator ($t \leq 8$ °C).

The stability of the analytes in human plasma was investigated in three ways, in order to characterize each operation during the process of bioanalytical studies: room-temperature stability (RTS), post-preparative stability (PPS) in the autosampler, freeze-thaw stability (FTS). For all stability studies, plasma standards at each of the lower (100 ng/mL), and higher (3200 ng/mL) levels were used. Five plasma standards at each of the three levels were prepared and let at room temperature four hours before processing (RTS study).

Other five pairs were prepared, immediately processed and stored in the HPLC thermostated autosampler (20 °C) (PPS study). The samples were injected after 22 hours, the expected longest storage times of the samples in autosampler before injection. For the freeze-thaw stability (FTS), aliquots at the same low and high concentrations were prepared. These samples were subjected to three cycles of freeze-thaw operations. After the third cycle the samples were analyzed against calibration curve of the day. The mean concentration calculated for the samples subjected to the cycles and the nominal ones were compared. For long-term stability (LTS), we appreciated it over 40 days as we verified previously in the same freezing device of the laboratory [6]. However, the same types of lower and higher concentration standards were used in order to evaluate analytes stability over two months of storage below -20°C. The requirement for stable analytes was that the difference between mean concentrations of the tested samples in various conditions and nominal concentrations had to be in $\pm 15\%$ range.

Acknowledgments

The work was supported by the Romanian national grant with ID 2041, research contract nr. 1154/2008 CNCSIS, awarded under "Idei" competition 2008.

REFERENCES

- [1] Physician's Desk Reference, Medical Economics Company, Inc at Montvale, NJ, USA, **2001**, sec. 5, 848.
- [2] Z. Spektor, M.C. Jasek, D. Jasheway, D.C. Dahlin, D.J. Kay, R. Mitchell, R. Faulkner, G.M. Wall, *Int. J. Pediatr. Otorhinolaryngol.*, **2008**, 72, 97.
- [3] Q. Chen, E.C. Tung, S.L. Ciccotto, J.R. Strauss, R. Ortiga, K.A. Ramsay, W. Tang, *Xenobiotica*, **2008**, 38, 76.
- [4] C. Bugge, M. Sullivan, M. Tan, *AAPS J.*, **2005**, http://www.aapsj.org/abstracts/AM_2005/AAPS2005-001539.pdf
- [5] X. Peng, J. Lee, A. Pinnawala, G. de Boer, S. Ostonal, E. Chung, G. van der Gugten, *AAPS J.*, **2008**, http://www.aapsj.org/abstracts/AM_2008/AAPS2008-003100.PDF
- [6] S. Imre, M.T. Dogaru, C.E. Vari, T. Muntean, L. Kelemen, *J. Pharm. Biomed. Anal.*, **2003**, 33, 125.
- [7] The European Agency for the Evaluation of Medicinal Products, Note for Guidance on the Investigation of Bioavailability and Bioequivalence, CPMP/EWP/QWP/1401/98, July 2001, London, UK, <http://www.emea.europa.eu/pdfs/human/qwp/140198enfin.pdf>

S. IMRE, S. VANCEA, G. DOGARU, C. CĂLDĂRARU, C.-E. VARI, M. TITICA DOGARU

- [8] U. S. Department of Health and Human Services, Food and Drug Administration, Center for Drug Evaluation and Research. Guidance for Industry. Bioavailability and Bioequivalence studies for orally administered drug products - general considerations, March 2003, Rockville, USA, <http://www.fda.gov/cder/guidance/5356f1.pdf>
- [9] U.S. Department of Health and Human Services, Food and Drug Administration, Guidance for Industry – Bioanalytical Method Validation, May 2001, <http://www.fda.gov/cder/guidance/4252f1.pdf>

K-CARRAGEENAN EFFECTS ON TEXTURE CHARACTERISTICS OF MEAT EMULSIFIED SYSTEMS

LIVIA PATRASCU^a, IRINA DOBRE^a, PETRU ALEXE^a

ABSTRACT. A sausage mix with different quantities of k-carrageenan was tested out in order to determine their effect on the admixture rheology. Four levels of polysaccharide were used (0.25%, 0.5% 0.75% and 1%) with 30% and 40% brine percentages. The used proportion of meat to fat was 70/30. Viscoelasticity of the samples was observed with an AR2000ex rheometer and after cooking a texture analyzing test was performed in order to determine the Warner - Bratzler shear force. Results showed a big impact of ratio of added hydrocolloid on the rheological behavior and on cooking yield but there was no impact on batters' texture.

Keywords: *K-carrageenan, creep, rheology, temperature ramp, Warner - Bratzler.*

INTRODUCTION

One of the most important characteristics of processed meat products is their texture [1], [2]. It depends on the structure of the matrix formed by the proteins gel and the moisture content. Lots of factors are involved in the matrix formation, such as protein, water holding capacity, salt, pH and non meat ingredients.

There is a tendency to equilibrate the quality with costs of the products, so manufacturers add different non meat ingredients in comminuted meat products in order to supplement the binder effect of the proteins and to replace meat and added fat with soya protein concentrate or hydrocolloids such as starch, xanthan or carrageenan [3], [4].

Polysaccharides are largely used in food products as they form a variety of different gels at room temperature. They are widely used as food thickening and stabilizing agents.

Obtained from red and brown seaweeds carrageenan is large, highly flexible molecules which curl forming helical structures. They are divided into three commercial groups: Kappa - a linear sulphated polysaccharide with strong, rigid gels that interfere with potassium ions and reacts with dairy proteins, obtained mainly from *Eucheuma cottonii*. Iota carrageenan provides soft gels,

^a Department of Biochemistry, "Dunarea de Jos" University, Domneasca Street, 800201, Galati, Romania. E-mail: livia.mantoc@uqal.ro

with calcium ions. Produced mainly from *Eucheuma spinosum*; and Lambda group that does not gels, mostly used to thicken dairy products [5]. A particular advantage is that carrageenan is pseudoplastic - they thin under shear stress. This means that they are easy to pump but stiffen again afterwards. The effect of the carrageenan addition on the functional properties of meat products is the subject of numerous studies.

Some researchers [6] have found that k-carrageenan addition caused an increase in solid like behavior of the product, hardness, gel strength and water holding capacity but they decline the carrageenan ability for the build-up of a three-dimensional gel network. In other case [7] was detected an increase in cooking yield and hardness when adding up to 2% k-carrageenan to low fermented meatballs.

The aim of this study was to observe the effect of different levels of added k-carrageenan and water content on texture characteristics of meat emulsion systems.

RESULTS AND DISCUSSION

Physico - chemical characteristics

Table 1. Meat batters physical characteristics

Sample composition		Dry matter, %	WHC cm ² /g	pH
Brine %	k-carrag., %			
Blank	-	35.64±1.2	4.6±0.5	5.7±0.5
30	0	30.63±0.9	0.6±0.02	5.6±0.4
30	0.25	30.62±0.8	0.4±0.02	5.6±0.5
30	0.5	30.59±0.5	0.1±0.01	5.7±0.5
30	0.75	31.85±0.9	-	6.0±0.2
30	1	31.99±1.2	-	6.1±0.3
40	0	29.62±0.9	0.8±0.01	5.5±0.4
40	0.25	29.74±0.8	0.2±0.02	6.0±0.3
40	0.5	29.88±0.6	0.2±0.01	5.7±0.2
40	0.75	30.17±1.0	-	5.6±0.3
40	1	30.25±1.1	-	5.9±0.2

For all samples, water holding capacity (Table 1) was very high ($p < 0.05$), namely there was found a little area of the released water for most of the samples, even for those with 40 % of added brine. In both cases the best water holding capacity with no water released was found in mince with 0.75% and 1% of added hydrocolloid. It can be observed an accession of dry matter values with the increasing rate of added k-carrageenan.

Cooking yield

The results of cooking yield are given in Figure 1. There can be seen that at 40% added brine, the yield was better for all cases.

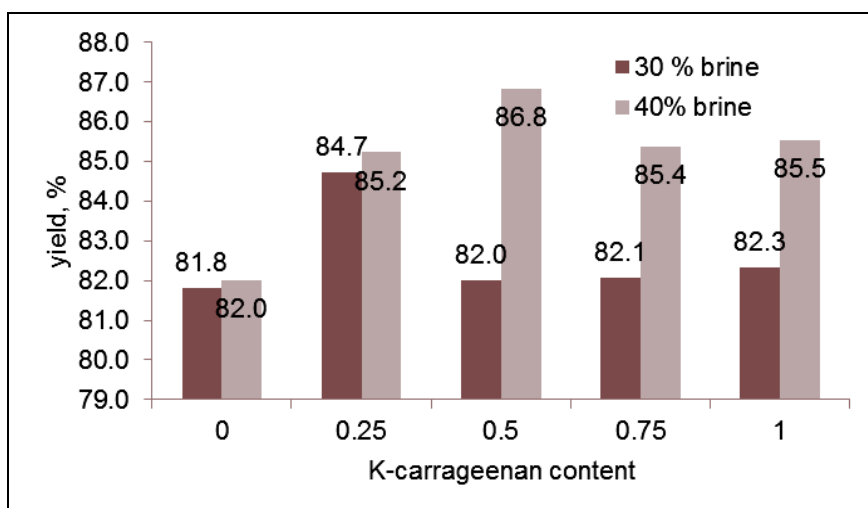


Figure 1. Graphical resemblance of cooking yield

This phenomenon can be explained in that at lower water content the structure of the admixture is denser which creates an expelling of water from the batters than at bigger percentages of content water. Another cause can be that at higher water content the gelling capacity of k-carrageenan is better, [8], [9], [10], [11], researchers have suggested that polysaccharide chains exist as a very weak, sparsely cross-linked network. On the other hand, the double helix model [12] and later modified to the domain model [13] is widely accepted. The domain model assumes that in the sol state at high temperature the carrageenan molecules exist as random coil and a temperature decrease induces the formation of double helices. Intermolecular association through double helices leads to the formation of small independent domains involving a limited number of chains. Aggregation of helices in different domains via cations enables more long-range cross-linking for the gel formation.

Rheological characteristics

The viscoelastic storage G' modulus, representing the elastic behavior of the sample, was measured over a frequency range of 0.1 to 10 Hz and a maximum strain of 1%. The results exposed in Figure 2 and Figure 3 shows a perfect correlation between G' values and the hydrocolloid concentration for both cases.

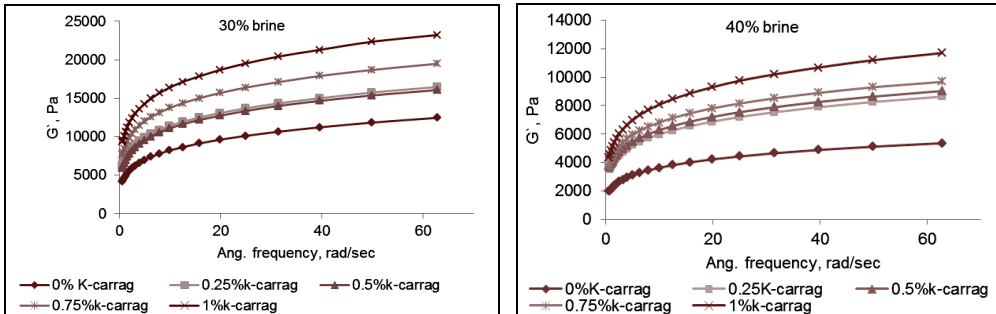


Figure 2. Storage modulus (G'), depending on angular frequency during oscillation test

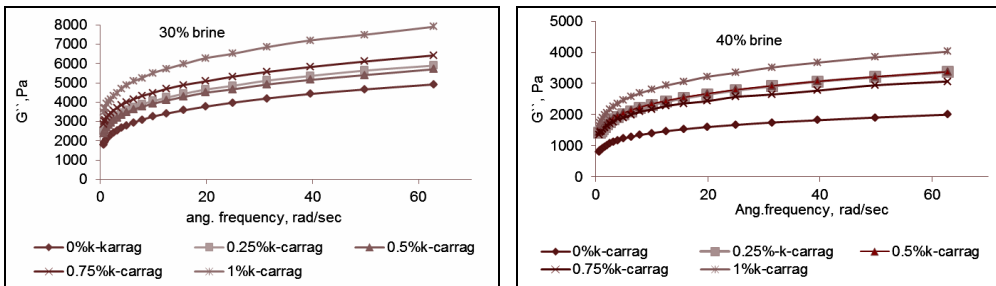


Figure 3. Loss modulus (G'') depending on angular frequency during oscillation test

But as opposed to samples with 30% of added brine with a maximum 24000 Pa for G' (1% k-carrageenan), those with 40% had a softer structure, with a maximum value of G' of 12000 Pa (1% k-carrageenan).

However the G'' values, representing the viscous behavior of a sample [14] were below G' values, indicating that the material is behaving more like a solid.

In the temperature ramp test, both moduli (Figure 4 and Figure 5) initially decreased until the coagulation point of the proteins at 40°C, when G' reached the lowest values, then it began to grow again as the protein mixture formed a strong structure till 70°C. The dynamic G' moduli was (as in previous test) larger than G'' . The influence of the added k-carrageenan is visible in the differences between tendency of G' curves as much as between G'' curves. Researchers who studied hydrocolloid's rheology found a similar behavior in gels subdued to temperature sweeping [15], [16], [17].

The biggest G' values had admixtures with the highest content of k-carrageenan, thus the ratio of hydrocolloid addition has a big impact in the solid like behavior of the samples at low temperatures but after heating all the samples had a similar behavior. That could mean that k-carrageenan loses its rheological characteristics after heating by entering in a rubbery zone and at high temperatures it remains there rather than crossing back into the terminal region [11].

K-CARRAGEENAN EFFECTS ON TEXTURE CHARACTERISTICS OF MEAT EMULSIFIED SYSTEMS

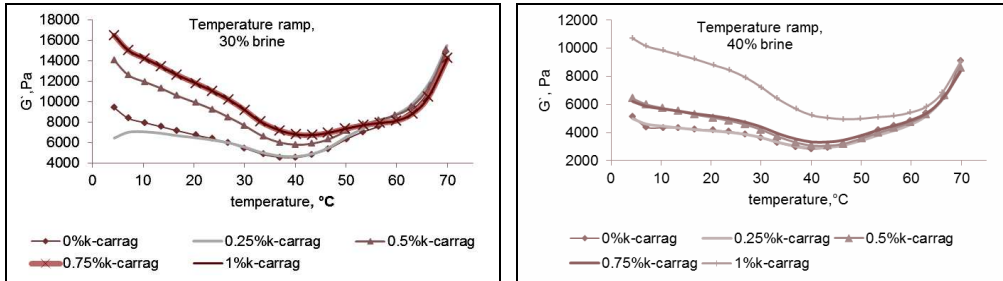


Figure 4. Storage modulus (G') variation with temperature ramping.

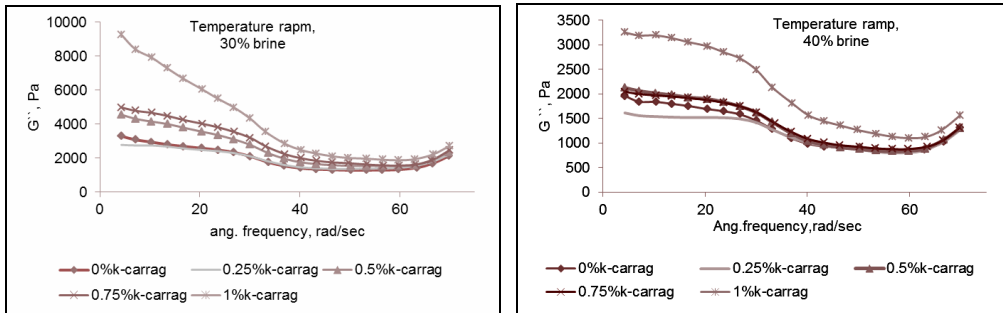


Figure 5. Loss modulus (G'') variation with temperature ramping.

The viscoelasticity characteristics of the samples were given by the rheological parameter δ , that represents the ratio of G''/G' [18]. The $\tan(\delta)$ values obtained in the temperature ramp test (Table 2) showed a more solid like behavior of the materials. The best case for meat filling mixtures would be a range more closely to 45° , when the samples would have a purely elastic behavior. The biggest value of the shift angle had the sample with 40% brine and no k-carrageenan at all (17.49°), however admixtures with more brine had larger values of $\tan(\delta)$ approaching more to elastic behavior.

Table 2. The average of shift angle ($\tan(\delta)^\circ$), values during temperature sweep.

Brine conc.,%	0%k-carrag	0.25%k-carrag	0.5%k-carrag	0.75%k-carrag	1%k-carrag
30 %	16.07	16.48	15.79	15.51	14.87
40 %	17.49	16.53	16.54	16.20	15.74

Texture analysis

The results from the WB test showed significant differences for cutting force [19]. The averages of all data represented in Figure 6 as the firmness shows two tendencies, a growing in firmness for batters with 30% of added brine and a descendent one for those with 40 % of added brine.

The same behavior is seen for cooking yield, when batters with more brine for same amounts of k-carrageenan had the biggest values of yield.

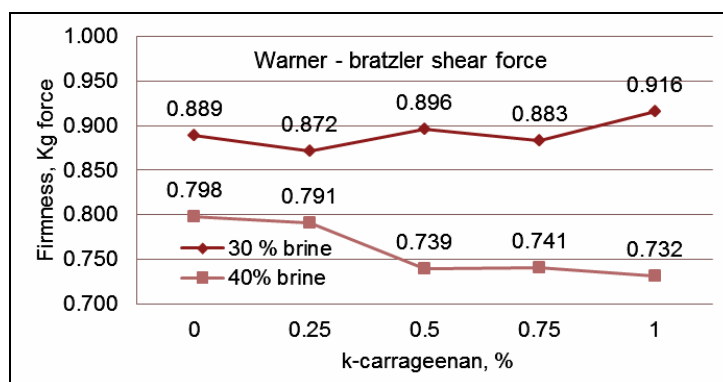


Figure 6. The firmness of butters expressed in Kg force.

CONCLUSIONS

The results of the present study show that the addition of k-carrageenan appeared to affect the rheological properties of the emulsified meat systems. The impact is seen at low temperatures, but after 40°C when the protein gelation starts there is no difference between samples. However, k-carrageenan appears to have a great impact on the cooking yield of butters at high quantities of brine, phenomenon that leads to a decrease in WB shear cutting force.

EXPERIMENTAL SECTION

Preparation of meat composition

In this study pork *gluteus maximus* muscle was used and back fat at a ratio of 70% to 30%. The materials were comminuted at 3000 rot/min for 3 minutes in a home chopper. A commercial k-carrageenan flower was added in four levels: 0%; 0.25%; 0.5%; 0.75% and 1%. There are studies in which k-carrageenan was used up to 3% [20], but they observed that carrageenan level of 3% negatively affected the firmness of the sausages.

The brine was then prepared from ice water, 2.5% of sodium chloride, 15 ppm sodium nitrite, 0.5% sodium polyphosphate, 0.015% ascorbic acid and 0.05% sucrose and the latest mentioned quantities of k-carrageenan in order to have a brine content of 30% and 40% from meat muscle. So that we had one blank probe with no brine and ten others with different levels of carrageenan in duplicate. The butters were let for 24 hours at 5°C prior to

processing. Then they were manually stuffed into polyethilen casings, cooked for approximately 60 min until reaching an internal temperature of 72 ± 2 °C.

Physico - chemical characteristics

Water holding capacity of the batters was measured with the filter paper press method [21], [22], with some modifications. A meat sample (0.3 g) was placed on a piece of filter paper, then placed between two Plexiglas plates and subjected to a force of 1Kg for 10 min. The water released (area of the moisture ring around the meat film area) was expressed per unit weight of meat sample (cm^2/g). Low value of cm^2/g means that the meat has superior water holding properties to meat with a high value of cm^2/g .

Cooking yield

The weight of each sample was taken before and after cooking and cooling. Cooking yield was calculated as:

$$\text{Cooking yield} = \frac{\text{cook weight}}{\text{initial weight}} \times 100\% \quad (1)$$

Rheological characteristics

Rheological development of batters was tested out with an AR2000ex Rheometer from TA instruments. Rheological measurements were performed at 4°C, using parallel plates of 40mm diameter and a 1.5 mm gap. First the linear domain was determined with a *strain sweep step* by observing the γ_c (critical strain), the subsequent oscillation tests were carried out using a strain % below γ_c where the structure is intact [23]. A *frequency sweep step* was performed for further characterization of the structure of the material. This provides more information about the effect of colloidal forces and the interactions among particles.

At last a *temperature ramp* step was carried out by rising the temperature with 5°C/min, from 4°C to 70°C by using a Peltier plate. Then the G' , G'' and $\tan(\delta)$ were stored in order to observe the rheological behavior of the admixtures.

For every step was used another sample so that we would prevent errors that could interfere from conformation damages. Edges of samples were covered with light silicone oil to prevent drying out.

Texture analysis

After cooking, samples were cooled at room temperature and the texture of the batters was determined by using a TA-XT plus Texture Analyzer with a Warner Bratzler blade set (HDP/BS) and a 25 Kg load cell [19] at a crosshead speed of 2 mm/s. The cutting force in compression was stored and the average value of each sample was recorded (mean of five replicates).

Statistical and data analysis

Where necessary, the test data were statistically analyzed by Anova single factor analysis of variance.

REFERENCES

1. Flores, M., Giner, E., Fiszman, S.M., Salvador, A., Flores, J., *Meat Science*, **2007**, 76, 9.
2. Foegeding, E.A., Lanier, T.C., *Cereal Foods World*, **1987**, 32, 202-205.
3. Bernal, V.M., Smajda, C.H., Smith, J.L., Stanley, D.W., *Journal of Food Science*, **1987**, 52(5), 1121, 1136.
4. Xiong, Y.L., Noel, D.C., Moody, W.G., *Journal of Food Science*, **1999**, 64(3), 550.
5. Giese, J. *Food Technology*, **1992**, 46(4), 100.
6. Verbeken, D., Neirinck, N., Meeren, P., Dewettinck, K., *Meat Science*, **2005**, 70, 161.
7. Hsu, S.Y., Chung, H.Y., *Journal of Food Engineering*, **2001**, 47(2), 115.
8. Whittaker, L. E., Al-Ruqaie, I.M., Kasapis, S., Richardson, R.K., *Carbohydrate Polymers*, **1997**, 33, 39.
9. Evageliou, V., Kasapis, S., Hember, M.W.N., *Polymer*, **1998**, 39, 3909.
10. Kasapis, S., Al-Marhoobi, I.M.A., Giannouli, P., *Journal of Agriculture and Food Chemistry*, **1999**, 47, 4944.
11. Nickerson M.T., Paulson, A.T., *Carbohydrate Polymers*, **2005**, 61, 231.
12. Anderson, N.S., Campbell, J.W., Harding, M.M., Rees, D.A., Samuel, J.W.B., *Journal of Molecular Biology*, **1969**, 45, 85.
13. Morris, E.R., Rees, D.A. & Robinson, G., *Journal of Molecular Biology*, **1980**, 138, 349.
14. Mezger, T.G., The rheology handbook: for users of rotational and oscillatory rheometers. In Ulrich Zorll (Ed.), **2002**, Germany: Hannover.
15. Kohyama, K., Lida, H., Nishinari, K., *Food Hydrocolloids*, **1993**, 7, 213.
16. Lundin, L., Hermansson, A. M., *Polymers*, **1997**, 34, 365.
17. Norziah, M.H., Foo, S.L., Karim, A.Abd., *Food Hydrocolloids*, **2006**, 20, 204.
18. Nunez-Santiago, M.C., Tecante, A., *Carbohydrate Polymers*, **2007**, 69, 763.
19. Arino, B., Hernandez, P., Blasco, A., *Meat Science*, **2006**, 73, 687.
20. Koutsopoulos, D.A., *Meat Science*, **2008**, 79, 188.
21. Grau, R. & Hamm, R., *Naturwissenschaften*, **1953**, 40, 29.
22. Stadnik, J., Dolatowski, Z.J., Baranowska, H.M., *Food Science and Technology*, **2008**, 41, 2151.
23. Bourbon, A.I., Pinheiro, A.C., Ribeiro, C., Miranda, C., Maia, J.M., Teixeira, J.A., Vicente, A.A., *Food Hydrocolloids*, **2010**, 24, 184.

DETERMINATION OF TOTAL PETROLEUM HYDROCARBONS IN CONTAMINATED SOIL BY FTIR AND GC-FID METHODS

MIRELA MICLEAN^{a,c}, ERIKA LEVEL^a, ADRIANA GOG^a,
LUDOVIC FERENCZI^a, CORNELIA MAJDIK^b,
CARMEN PUIA^c, CECILIA ROMAN^a

ABSTRACT. This paper presents the results obtained for total petroleum hydrocarbons (TPH) in contaminated soil by two methods: one based on conventional extraction with 1,1,2-trichloro-1,2,2-trifluoroethane and determination by Fourier Transform Infrared Spectrometry (FTIR) and the other based on ultrasonic extraction with a mixture of hexane and acetone followed by determination using gas chromatography with flame ionization detection (GC-FID). In general, TPH concentrations in soil measured with FTIR were higher than those measured with GC-FID. The obtained TPH concentrations exceeded the intervention level for non-sensitive soils, according to Romanian legislation.

Keywords: TPH, soil, GC-FID, FTIR

INTRODUCTION

Contamination of soil with petroleum hydrocarbons is a major concern due to their potential to spread into soil and aquatic environments. Thus, the determination of hydrocarbon contaminants is one of the most frequently performed analyses in the study of contaminated sites [1, 2].

Despite the large number of hydrocarbons found in petroleum products, only a relatively small number of compounds have been characterized for toxicity [3]. The most important chemicals of concern are benzene, toluene, ethylbenzene, and polycyclic aromatic hydrocarbons (PAHs), that could pose significant cytotoxic, immunotoxic, mutagenic and/or carcinogenic risks to different organisms [4], in addition to sublethal effects which include morphological, histopathological and genetic damage [5-6], physiological and stress effects [7], endocrine disruption [8, 9] and ecological effects [10]. Certain crude oils or aromatic fractions are considered to be responsible for adverse health effects on the reproductive system in mussels, goldfish (*Carassius auratus*) and rainbow trout [11, 12].

^a National Institute for Research and Development of Optoelectronics Bucharest - Research Institute for Analytical Instrumentation, Cluj-Napoca, 67 Donath, 400293, Romania, icia@icia.ro

^b Faculty of Chemistry and Chemical Engineering, Babes-Bolyai University, 11 Arany Janos, 400028, Cluj-Napoca, Romania

^c University of Agricultural Sciences and Veterinary Medicine, 3-5 Manastur, Cluj-Napoca, Romania

Due to the great number of compounds that exists in petroleum hydrocarbons (hexane, jet fuels, mineral oils, benzene, toluene, xylenes, naphthalene, fluorine), it is impossible to assess the extent of contamination by separately measuring the concentration of each hydrocarbon contaminant. To express the total concentration of non-polar petroleum hydrocarbons in soil the term total petroleum hydrocarbon (TPH), mineral oil or hydrocarbon oil index is used [13-15].

No single analytical method is capable of providing comprehensive chemical information on petroleum contaminants in soil. Non-specific methods can be used to obtain information on the type and total amount of hydrocarbons present in soil, whereas specific methods are required to give detailed information on individual contaminants [16]. There are many analytical techniques available that measure TPH concentrations in soil, with different extraction, clean up and detection methods, each technique measuring slightly different subsets of the petroleum-derived hydrocarbons present in the sample. Gas chromatography and infrared spectroscopy are the most used techniques for the TPH determination but the interpretation of analytical results requires an understanding of how the determination was made.

The objective of this study was to assess the TPH contents from 12 soil samples contaminated with petroleum hydrocarbons using gas chromatography with flame ionization detection (GC-FID) and Fourier transform infrared spectrometry (FTIR) methods.

RESULTS AND DISCUSSION

The FTIR method determines the infrared absorbance of hydrocarbons present in the extracts. There are two absorbance maxima, at 2925 and 2958 cm^{-1} , the first corresponding to $-\text{CH}_2-$ and the second to $-\text{CH}_3$. The $-\text{CH}-$ absorbance bands corresponding to the aromatic groups located at wave numbers higher than 3030 cm^{-1} are absent from the samples due to retention on Florisil used in the clean-up process (Figure 1). The 1,1,2-trichloro-1,2,2-trifluoroethane (CFE) is the preferred extraction solvent for the FTIR determinations because it is nonflammable, relatively nontoxic and is transparent in the infrared region of interest, but in accordance with the Montreal Protocol on Substances That Deplete the Ozone Layer, Class I chlorofluorocarbons, which include CFE are phased out [17].

TPH determination by FTIR is a non specific method that estimates the contents of TPH but does not provide information on the composition of the hydrocarbon mixture. Other limitations of FTIR method are the loss of highly volatile compounds during analysis, the incomplete extraction of heavy hydrocarbon molecules and can give false positive results in the presence of organic matter.

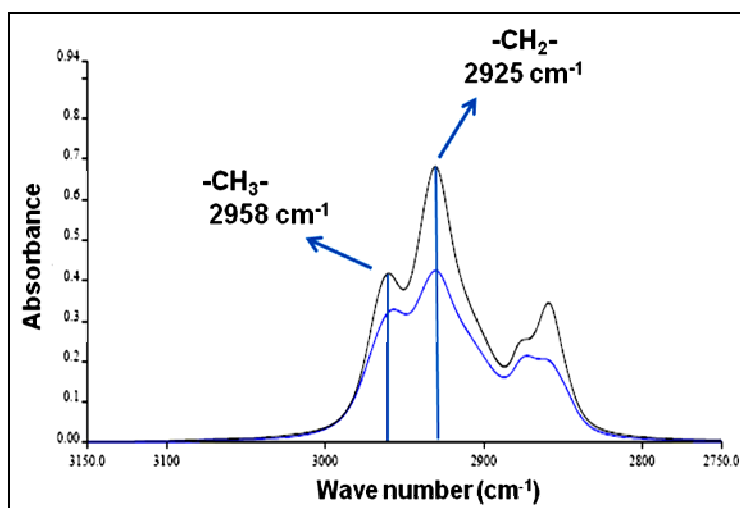


Figure 1. FTIR spectrum of TPH

Compared to FTIR method, TPH determination with GC-FID is an expensive, time consuming procedure that requires highly trained personal. The advantage of GC-FID method is that produces highly accurate results and in addition to the TPH concentration, it can also provide useful qualitative information about the type of contaminant. The disadvantages of this method are that does not determine resins, asphaltenes, and some other components with higher molecular weight that do not pass through the column, the temperatures required for the determination challenge the durability of the columns and causes column bleed, which deteriorates the analytical precision. Moreover, the lack of detailed description of the gas chromatographic settings for measuring total petroleum hydrocarbons may result in a wide range of GC operating settings that make difficult the comparisons of the results obtained by different laboratories [18].

The amount of TPH was determined as a sum parameter of resolved and unresolved components eluted from the GC capillary column between the retention times of *n*-decane and *n*-tetracontane [19, 20]. The integration window was determined using an *n*-alkanes standard solution containing C5 to C40 hydrocarbon components dissolved in carbon disulfide.

Figure 2 overlays the chromatogram of *n*-alkanes standard (red signal) with the chromatogram for TPH analysis of a soil sample extract (blue signal). The integration markers, C10 and C40, are clearly separated, thus the total area between the peak of C10 and the peak of C40 contribute to the signal, calculated after background subtraction. The integration area is presented in grey, between C10 eluted at 7.07 min and C40 eluted at 46.5 min.

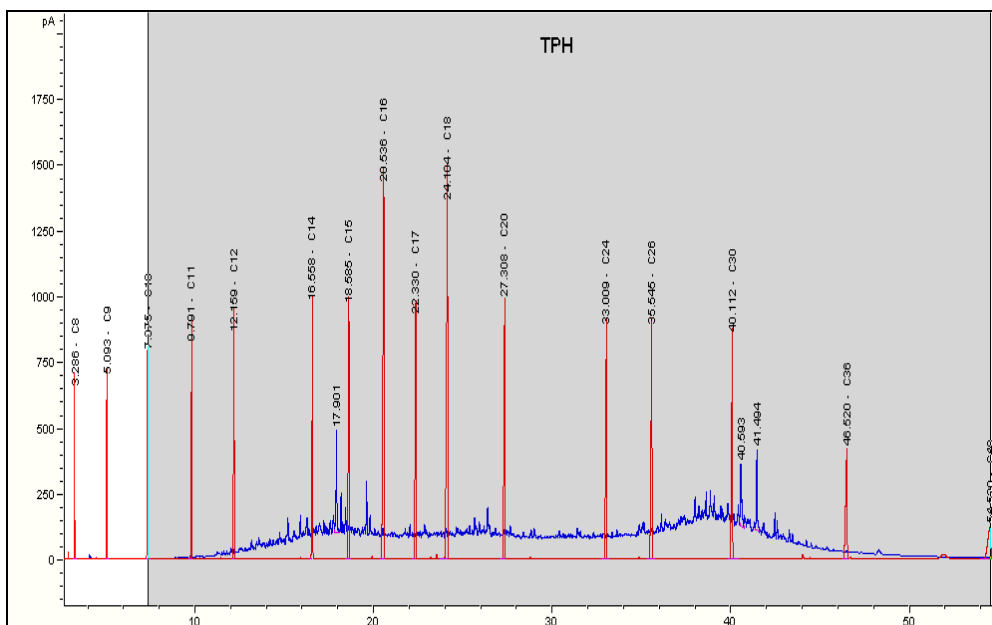


Figure 2. The chromatogram of n-alkanes standard (red signal) overlaid with the chromatogram of a soil sample extract (blue signal) in order to define the integration area (grey)

The TPH concentration in the soil samples varied between 3400-48000 mg/kg determined by FTIR method and between 3100-45000 mg/kg determined by GC-FID method (Figure 3). In the 1-6 samples a high level of contamination with crude oil was noticeable visually and olfactory.

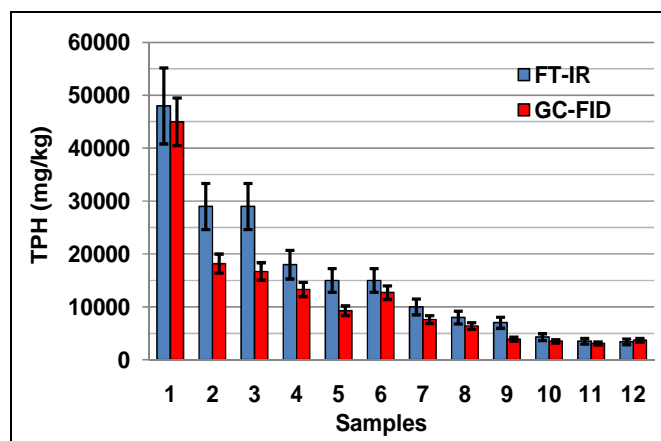


Figure 3. TPH concentrations in soil determined by GC-FID and FTIR methods

Both methods revealed significant amounts of TPH in all samples that exceeded the intervention level for non-sensitive soils (2000 mg/kg) according to Romanian legislation [21].

The TPH results obtained by the two methods are difficult to compare due to differences in analytical procedures, natural organic matter interferences, and different extraction and/or clean-up procedures.

The accuracy and precision in the studied methods was checked by the determination of TPH in two certified reference materials. No significant differences were found between the obtained results (mean value \pm standard deviation of three replicates) and the certified values (Table 1).

Table 1. The determined and certified values for the TPH concentration in CRM 358-100 and CRM PR 9583, expressed as mean value \pm standard deviation (n=3)

CRM	Reference value	Confidence Interval (95%)	Prediction Interval (95%)	Determined value
	mg/kg			
CRM 358-100				
GC-FID	3650 \pm 1160	2790-4510	1070-6230	4190 \pm 1510
FTIR	3650 \pm 1160	2790-4510	1070-6230	3580 \pm 1190
CRM PR 9583				
GC-FID	9510 \pm 2155	8858-10162	5237-13783	9340 \pm 1978
FTIR	6721 \pm 1462	6036-7406	3584-9857	6250 \pm 1400

CONCLUSIONS

The obtained results showed that the TPH concentrations in all samples exceeded the intervention level for non-sensitive soils, according to Romanian legislation, indicating a highly contaminated area and a potential environmental and health risk. Therefore, the use of decontamination methods to decrease the risks by reducing the TPH concentration in the site is mandatory.

Both analytical methods used were found to be effective for the determination of TPH concentration in contaminated soil samples, although the obtained results are dependent on the analytical method. Despite the fact that TPH determination by FTIR method is simple, quick and inexpensive, its use is currently decreasing due to the worldwide ban of CFE production. In contrast to FTIR method, GC-FID method for TPH determination in soil supports green chemistry principles, by the use of non-halogenated solvents.

EXPERIMENTAL SECTION

Reagents and Samples

All reagents were purchased from Merck (Darmstadt, Germany) or Supelco (Bellafonte, USA) and were at least p.a. quality. Chromatographic grade n-hexane and acetone and IR grade 1,1,2-trichloro-1,2,2-trifluoroethane (CFE)

were used for extraction. Anhydrous sodium sulfate was used for drying, while Florisil® (60–100 mesh) was used for purifying the extracts. Calibration solutions were prepared using a mixture of 1:1 (m/m) additive-free diesel oil/motor oil.

A standard mixture of normal paraffins containing n-alkanes from C5 to C40 was used to determine the retention times of n-decane (C10) and n-tetracontane (C40). CRM 358-100 TPH in soil (RTC, Laramie, USA) and CRMPR 9583 TPH in soil (RIZA Institute for Inland Water Management and Waste Water Treatment, Netherlands) certified reference materials was used for the quality control of the determinations.

Twelve soil samples from a contaminated area of NW Romania were collected from 0-20 cm depth and stored in glass jars for transport to laboratory, in the autumn of 2009 [22].

Instrumentation

An Agilent 7890N gas chromatograph with a flame ionization detector (FID) equipped with automatic liquid sampler (HP Model 7673) and HP-5 fused-silica capillary column from J&W Scientific and a Perkin Elmer Spectrum BX II Fourier Transformation Infrared Spectrometer (FTIR) equipped with DTGS detector and single beam sample compartment were used for TPH determination. The LABOSHAKE 500 LS (Gerhardt, Germany) reciprocating shaker and a SONOREX Longlife RK 103H ultrasonic bath (Bandelin, Germany) was used for the extractions. All extraction steps were carried out in a CHEMFREE 2000 (Faster, Italy) fume hood equipped with appropriate filters.

TPH determination by GC-FID following ultrasonic extraction

Approximately 10 g soil was dried with anhydrous sodium sulfate in a 100 ml glass beaker. The sample was sonicated with 20 ml of 1:1 (v/v) hexane : acetone mixture for 15 min [23, 24]. The extract was transferred into a 20 ml volumetric flask, through a glass funnel packed with Florisil to retain more polar solutes. The solvent level was brought up to the 20 ml marker with hexane/acetone mixture. A volume of 1 µl aliquot of the final solution was injected

Table 2. Instrumental configuration and experimental conditions used for GC-FID analysis of TPH

Injector	Split/Splitless
Column	HP-5 (fused-silica capillary column coated with cross-linked 5% phenyl methyl siloxane) 30 m x 320 µm x 0.25 µm
Detector	FID
Inlet temperature	290°C
Injection mode	Splitless
Injection volume	1 µl

DETERMINATION OF TOTAL PETROLEUM HYDROCARBONS IN CONTAMINATED SOIL ...

Carrier gas	He 2,5 ml/min
Oven temperature	Initial 50°C for 2 min 6°C/min to 300°C, 16 min
Detector temperature	300°C
Detector gases	H ₂ : 40 ml/min; Air: 450 ml/min; He make-up: 30 ml/min

in the gas chromatograph in splitless mode. The instrumental configuration and the experimental conditions are summarized in Table 2. For TPH quantification, calibration standards were prepared by contamination of clean soil with 20 g/l 1:1 (m/m) mixture of additive-free diesel oil/motor oil in hexane-acetone mixture at concentrations between 100 and 5000 mg/kg TPH.

TPH determination by FTIR following classical extraction

About 10 g of sample was weighted and chemically dried with anhydrous sodium sulfate, then shaken two times with 20 ml CFE in screw capped glass bottles for 30 minutes. Sodium sulfate was added to the extract in order to eliminate any existing moisture and filtered through Whatman glass fiber disks. To eliminate polar compounds like water, vegetable oils and animal fats a clean-up step was applied passing the extracts through a 10 cm long column packed with Florisil (60-100 mesh), and filled up to 50 ml with CFE. The extracts spectrum was recorded between 3150-2750 cm⁻¹ (average of 8 scans) at 4 cm⁻¹ resolution using 10 mm optical path-length quartz cells in transmittance (%). Samples with absorbance bellow 0.2 were concentrated by evaporation while samples with absorbance higher than 0.8 appropriately diluted.

The calibration was made using of 8 soil standards with TPH concentrations of 10, 50, 100, 250, 500, 1000, 1500, 2000 mg/kg soil made in laboratory by contamination of clean soil with 20 g/l 1:1 (m/m) mixture of additive-free diesel oil/motor oil in CFE. The soil standards were mixed by mechanical shaking for 48 hours and subjected to the same analysis steps as the samples. TPH concentration was calculated based on calibration dependence of the peak area measured between 3100 and 2800 cm⁻¹ with the concentration of the calibration standards.

ACKNOWLEDGMENTS

The financial support provided by the Romanian Minister of Education, Research, Youth and Sports, PNCDI II Program (Project SOLPETRO no. 31038/2007) was greatly appreciated.

REFERENCES

1. C.J. Kennedy, A.P. Farrell, *Environmental Pollution*, **2008**, *153*, 638-648.
2. R. Sadler, D. Connell, Analytical Methods for the Determination of Total Petroleum Hydrocarbons in Soil, *Proceedings of the Fifth National Workshop on the Assessment of Site Contamination*, Adelaide, Australia, **2002**.
3. Research Triangle Institute, Toxicological Profile for Total Petroleum Hydrocarbons (TPH). Prepared for the US Department of Health and Human Services, **1999**.
4. J. Sturve, L. Hasselberg, H. Falth, M. Celander, L. Forlin, *Aquatic Toxicology*, **2006**, *78*, S73–S78.
5. M.G. Carls, S.D. Rice, J.E. Hose, *Environmental Toxicology and Chemistry*, **1999**, *18*, 481-493.
6. R.A. Heintz, J.W. Short, S.D. Rice, *Environmental Toxicology and Chemistry*, **1999**, *18*, 494-503.
7. C.J. Kennedy, A.P. Farrell, *Journal of Experimental Marine Biology and Ecology*, **2005**, *323*, 43-56.
8. C.J. Kennedy, A.P. Farrell, *Environmental Toxicology and Chemistry*, **2006**, *25*, 2715-2724.
9. M. Evanson, G.J. Van Der Kraak, *Comparative Biochemistry and Physiology Part C*, **2001**, *130*, 249-258.
10. C.M. Reddy, T.I. Eglinton, A. Hounshell, H.K. White, L. Xu, R.B. Gaines, G.S. Frysinger, *Environmental Science and Technology*, **2002**, *36*, 4754-4760.
11. N. Aarab, C. Minier, S. Lemaire, E. Unruh, P.D. Hansen, B.K. Larsen, O.K. Andersen, J.F. Narbonne, *Marine Environmental Research*, **2004**, *58*, 437-441
12. A. Lister, V. Nero, A. Farwell, D.G. Dixon, G. Van Der Kraak, *Aquatic Toxicology*, **2008**, *87*, 170-177.
13. D. Todd, R. Chessin, J. Colman, *Toxicological profile for total petroleum hydrocarbons, U.S. Department of Health And Human Services*, Public Health Service Agency for Toxic Substances and Disease Registry, Atlanta, Georgia, **1999**.
14. K. Ventura, M. Adam, J. Dostalek, *Journal of Liquid Chromatography and related Technologies*, **2003**, *26*, 247-259.
15. W. Weisman, Analysis of petroleum hydrocarbons in environmental media, Total Petroleum Hydrocarbon Criteria Working Group Series, Amherst Scientific Publishers Massachusetts, **1998**.
16. Z. Wang, M.F. Fingas, *Marine Pollution Bulletin*, **2003**, *47*, 423-452.
17. F. Nadim, G.E. Hoag, S. Liu, R.J. Carley, P. Zack, Detection and remediation of soil and aquifer systems contaminated with petroleum products: an overview *Journal of Petroleum Science and Engineering*, **2000**, *26*, 169-178.
18. E. Saari, P. Peramaki, J. Jalonen, *Analytical and Bioanalytical Chemistry*, **2008**, *6*, 392-398.

DETERMINATION OF TOTAL PETROLEUM HYDROCARBONS IN CONTAMINATED SOIL ...

19. prEN 14039:2004, Characterization of Waste — Determination of Hydrocarbon Content in the Range of C10 to C40 by Gas Chromatography, European Committee for Standardization, Brussels, **2004**.
20. ISO/DIS 16703:2004, Soil Quality — Determination of Content of Hydrocarbon in the Range C10 to C40 by Gas Chromatography, ISO, Geneva Switzerland, **2004**.
21. Ministerial Order 756/1997 for the Regulation approval concerning the environmental pollution assessment, MO 303/bis/06.11.1997.
22. G. Pavelescu, C. Roman, E. Pfeiffer, E.A. Levei, M. Miclean, E. Cordos, Evaluation of petroleum products in soils in Suplacu de Barcau area, Romania, 4th European Bioremediation Conference, Chania, Greece, **2008**.
23. M. J. Martin, *Environmental Laboratory*, **1992**, June/July, 34-35.
24. U.S. EPA, Ultrasonic Extraction, Test Methods for Evaluating Solid Waste, Method 3550B, Revision 3, US Environmental Protection Agency, Washington, **2000**.

PARTICULATE MATTERS FOUND IN URBAN STREET DUST

ALEXANDRA-GERTRUD HOSU-PRACK^a, IOAN PETEAN^a,
GEORGE ARGHIR^b, LIVIU-DOREL BOBOS^a,
MARIA TOMOAI-COTISEL^{a,*}

ABSTRACT. This investigation was carried out to characterize the composition of different particulate matters (PM) in urban street dust. Samples of street dust were collected on a weekly basis for three summer months from the intersection of Bucharest Avenue and Paris Street in Cluj-Napoca city, Romania. The samples were processed to determine the composition by X-ray diffraction. A large amount of minerals, such as quartz, kaolinite and calcite, and some traces of portlandite and goethite were found. Particle shape was investigated by optical transmitted light and cross polarized light microscopy. The data revealed a wide range of particle size, from a few μm to several hundred μm . The surface morphology and the size distribution of different submicron particles were confirmed by AFM on various thin films of particulate matters deposited on glass support from aqueous dispersion drops, taken out at different sedimentation times. The fine particles observed by AFM had the diameter between 100 and 180 nm and they correspond to kaolinite. Chemical characteristics of urban street dust indicate that the particulate matters have a natural and an anthropogenic origin. Particulate matters, such as $\text{PM}_{2.5}$ and PM_{10} , as well as the fine kaolinite particles found in the urban street dust are very dangerous for lung health due to the potential risk of silicosis.

Keywords: *street dust, particulate matter, particle size, morphology, chemical composition, X-ray diffraction, AFM*

INTRODUCTION

In urban areas, the pollution becomes one of the common ecological problems at world scale and particularly at Cluj-Napoca city, in Romania. For instance, street dust particles deposited on roads originate from the interaction of liquid, solid and gaseous materials produced from various sources. Chemical components and their quantity in street dust are considered indicators of the environmental pollution.

^a Babeş-Bolyai University, Faculty of Chemistry and Chemical Engineering, 11, Arany Janos Str., RO-400028 Cluj-Napoca, Romania

^b Technical University of Cluj-Napoca, Faculty of Materials Science and Engineering, Muncii Avenue, No. 103 - 105, RO-400641 Cluj-Napoca, Romania

*Corresponding author: mcotisel@chem.ubbcluj.ro

Fine microscopic particles (PM) from street dust have been shown to increase the risk of silicosis [1, 2]. These studies found that the most affected subjects are pedestrians and people working in the street. The potential risk is considerably increased by fine particles, like $PM_{2.5}$, mainly when they were burned in a combustion engine.

Usually, there are two main street dust sources, the natural one from the disaggregation of soil particles, such as kaolinitic beds erosion [3], and the anthropogenic source consisting primarily of the built space erosion, such as building facades erosion [4, 5].

The amount of dust from each source depends on the distinctiveness of the investigated area, like the degree of infrastructural development and the presence or the absence of green places in that region. On the other hand, the urban streets act like sinks for vehicle emissions caused by combustion of fuel. These emissions contain particulate matter (PM), which is released in the air and deposited on the road surface in the form of street dust.

The goal of the present investigation is to determine the chemical composition of urban street dust in Cluj-Napoca city of Romania. Samples were taken from the intersection of Bucharest Avenue and Paris Street. This area was selected because it is one of the areas in Cluj-Napoca with the most traffic and pedestrian flow, where an increased risk of PM exposure appears for humans and other living organisms. Dust samples were collected weekly during the summer time (see, Experimental Section), because summer is already recognized for high pollution in Cluj-Napoca.

RESULTS AND DISCUSSION

The representative combined sample of the urban street dust is a complex material having several minerals in its composition. Generally, the best tool for mineral analysis and crystal phase identification is the X-ray diffraction [6, 7]. The obtained X-ray diffraction data for the representative combined dust sample is presented in Figure 1.

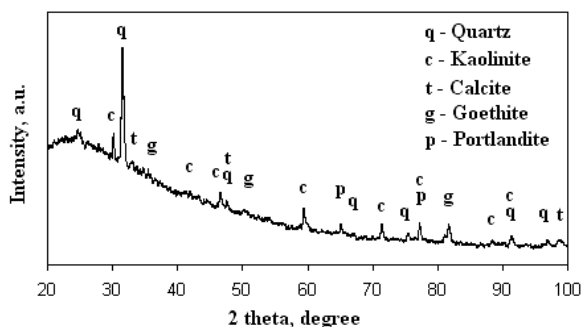


Figure 1. The X-ray diffraction data for the combined sample of urban street dust, collected from the intersection of Bucharest Avenue and Paris Street in Cluj-Napoca, during the summer time of 2009.

PARTICULATE MATTERS FOUND IN URBAN STREET DUST

The analysis of X-ray diffraction patterns (Figure 1) shows large amounts of minerals, such as quartz, kaolinite and calcite, within the combined dust sample. Additionally, trace amounts of portlandite and goethite were also found.

The dominant mineral, indicated by the most intense peak, in Figure 1, is formed by quartz particles. The chemical formula of quartz is SiO_2 , having a hexagonal crystal lattice and showing an irregular rounded aspect [8]. Because the hexagonal crystallization of quartz does not allow cleavage, the bigger quartz particles break and form very small and sharp fragments (slivers). Silica fragments are often found in nearby road soils and fallen plaster from eroded buildings.

Kaolinite ($\text{Al}_2\text{Si}_2\text{O}_5(\text{OH})_4$) is found in clay minerals [9]. It crystallizes in a monoclinic crystal system having a tabular aspect spread in a wide range of particle sizes from nanometric to large micro scale. It appears as a common component in gardening soils and also it could be found in construction materials. Thus, kaolinite is more likely found in street dust as a natural source due to the eroded soil.

Calcite (CaCO_3) is also known as limestone [10], and it is often found in soil. The calcite particles appear as a result of the disaggregation of lime stones during the marl formation. It is present in street dust via natural source.

Portlandite ($\text{Ca}(\text{OH})_2$) is not a soil component but it appears often in building plaster [11]. Its presence in the street dust sample is likely due to building erosion.

Goethite ($\text{Fe}_2\text{O}_3 \cdot \text{H}_2\text{O}$) known as rust appears in trace amounts in the combined dust sample. Its presence could be explained by the corrosion of car chassis [12]. The presence of goethite is due to anthropogenic activities.

Taking into account, the low concentration of portlandite and goethite in the combined dust sample in comparison with large amounts of quartz, it is reasonable to assume that the anthropogenic dust source has a secondary contribution in the street dust formation.

Figure 2a presents optical microscopy investigation of combined dust sample featuring a wide range of particles having different shapes. The diameter of particles varies up to 200 μm .

The shapes observed in Figure 2a vary from rounded shapes belonging to quartz to tabular one typical for kaolinite. In cross polarized light, Figure 2b, the particles appear in specific colors depending on their orientation and the position angle to the optical microscope axis. Quartz particles are colored in green-gray, kaolinite particles appear in yellow-red color, depending on the position angle, and calcite particles appear in a light yellow color [13].

Goethite usually appears in cross polarized light on a blue color, but in very thin slices it appears in blood red color. The results, shown in Figure 2, correlate substantially with the observation given in the X-ray spectrum, thus proving the goethite presence only as trace amounts.

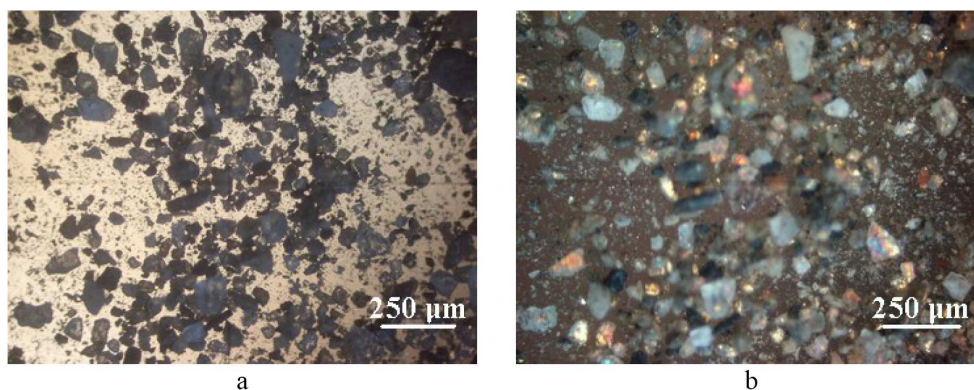


Figure 2. Optical light microphotographs of dry combined dust powder: a) in transmitted light; b) in cross polarized light.

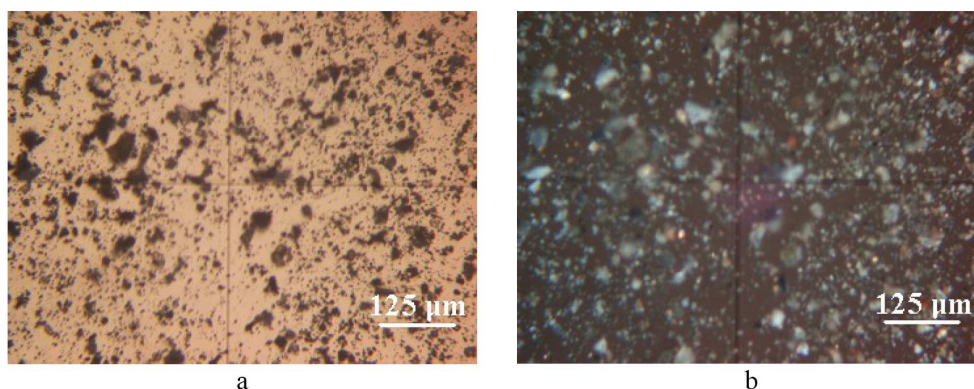


Figure 3. Optical light microphotographs of a fine fraction obtained by sieving the combined dust powder: a) in transmitted light; b) in cross polarized light.

To emphasize on the small particles from the street dust sample, the larger particles, for example those with a diameter bigger than 150 μm , were removed by sieving the initial combined dust sample through a stainless steel sieve with mesh size of 150 μm . The obtained fine dust powder was then spread as a thin layer on the glass support and it was further investigated by optical microscopy (Figure 3).

In Figure 3a, smaller particles than 150 μm in diameter are identified. Analyzing Figure 3, it seems that, the large particles have the predominant diameter between 30 and 75 μm , with specific quartzite morphology. Much smaller particles are also observed in the diameter range of 2.5 and 10 μm . In Figure 3b, the bulky particles are colored in green/ gray and are specifically identified as quartzite. The fine particles are painted in yellow and dark brown and represent kaolinite. Additionally, some trace amounts of calcite particles are identified as intense yellow colored ones.

PARTICULATE MATTERS FOUND IN URBAN STREET DUST

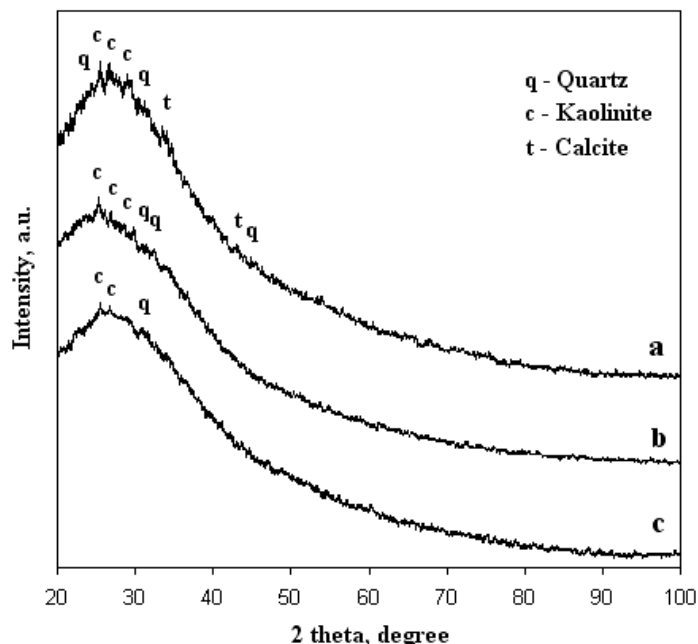


Figure 4. X – ray diffraction patterns of dry fine dust samples, taken out from dust aqueous dispersion, after several sedimentation times: a) 10 min; b) 15 min; c) 30 min.

The morphological and structural investigations of dust particles were further carried out on the fine dust obtained from the aqueous suspension of the combined dust in deionized water. For this purpose, the dilute aqueous suspension of dust was taken out at different times, namely after 10, 15 and 30 min, of sedimentation. The dried out fine dust powders obtained at different sedimentation times were used for X-ray diffractions (Figure 4) and microscopic measurements (Figures 5-7).

Structural observations (Figure 4, curve a) indicate that, for dry dust sample obtained at 10 min of sedimentation, the majority of dust parts are quartzite and kaolinite. The calcite is present in trace amounts. It is also observed that the intensity peaks are much smaller in comparison with the corresponding ones for the initial dry combined dust powder sample (given in Figure 1) and the curve shape is more bent due to the fine dust particles of micrometer size.

At 15 min of sedimentation, a complete disappearance of diffraction peaks of calcite is noted (Figure 4, curve b); the kaolinite is identified and quartzite is observed only in trace amounts. This indicates a rather quick sedimentation of calcite and quartz particles.

The X – ray diffraction patterns still remain even for dry dust, advanced processed at 30 min of sedimentation, but the quartz peaks almost disappear leaving only trace amounts of kaolinite (Figure 4, curve c).

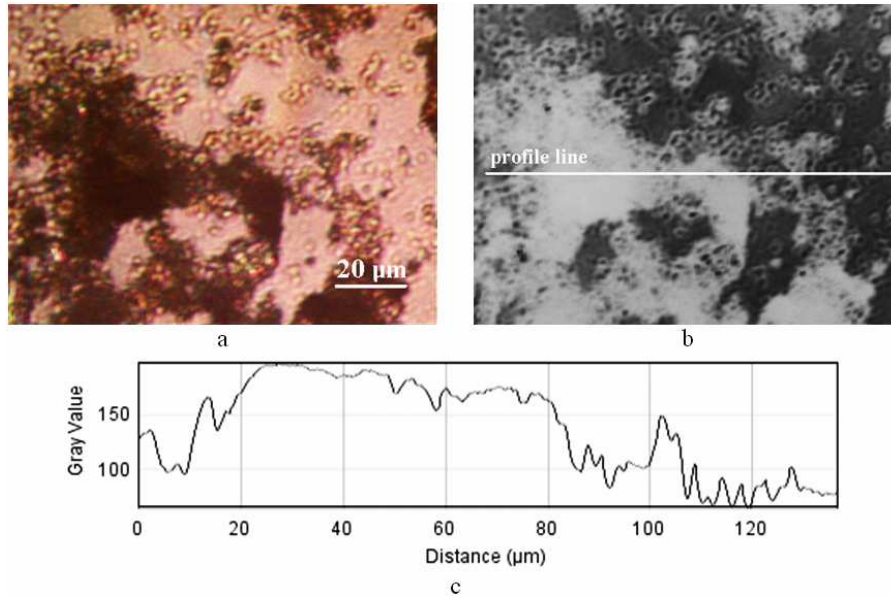


Figure 5. Optical microphotographs for the thin layer of dry fine dust, obtained after 10 min of sedimentation: a) transmitted light; b) negative gray scale representation of Figure 5a; c) profile detail on the corresponding line shown in Figure 5b.

To further explore the fine dust particles, the dust samples obtained at different sedimentation times, for 10, 15 respectively 30 min, were spread as thin films to be investigated by optic microscopy (Figures 5-7). A semi-quantitative analysis of these images was performed in order to establish an average diameter of dust particles.

In Figure 5a, two types of particles are observed, some larger particles with specific shape characteristic for quartzite and several smaller particles of kaolinitic specific form. This chemical structure is consistent with the data shown in Figure 4a.

Detailed profile (Figure 5c) shows an agglomeration of quartzite particles that is greater than 60 μm in diameter accompanied by a few fine kaolinite particles with diameter between 15 and 30 μm. The average particle diameter is about 50 μm.

The calcite particles disappear at 15 min as seen in Figure 6a, where there are some trace amounts of quartz particles with an average diameter of about 30 μm. The predominant particles are much smaller and show a specific kaolinitic habit. The profile in Figure 6c indicates an average diameter of kaolinitic particles of about 10 μm.

PARTICULATE MATTERS FOUND IN URBAN STREET DUST

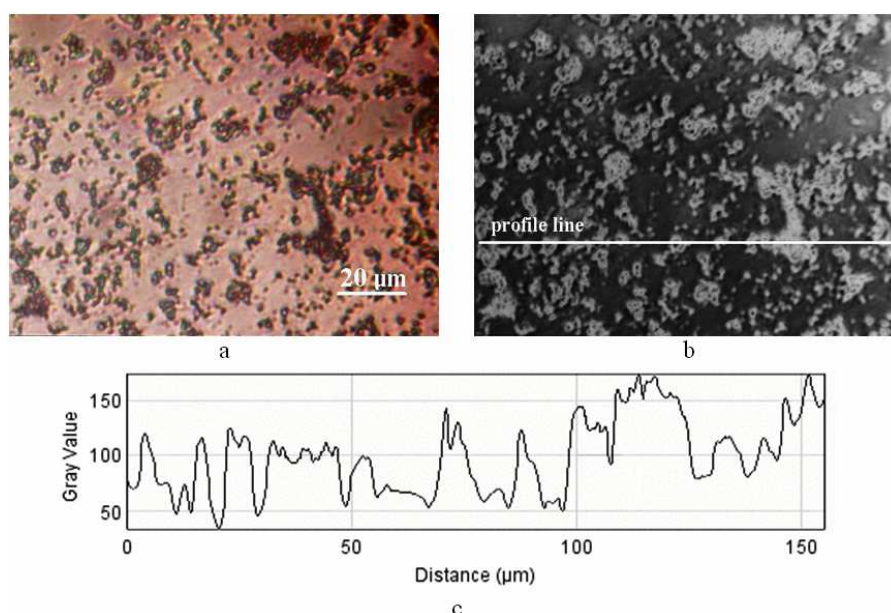


Figure 6. Optical microphotographs for the thin layer of dry fine dust, obtained after 15 min of sedimentation: a) transmitted light; b) negative gray scale representation of Figure 6a; c) profile detail on the corresponding line given in Figure 6b.

This major change (Figure 6) of particle size and shape distribution can be also seen Figure 4b, where a considerable decrease of the intensity of quartz peaks is identified. Thus, an assumption relative to a rapid sedimentation of quartz particles can be suggested. Kaolinite is a mineral with lamellar aspect susceptible to environmental factors and it can generate the very fine particles, tending to occupy an increasing space in the respective area of particles, in substantial agreement with Figure 6.

On the other hand, trace amounts of quartz show sharp corners, and they are actually broken down fragments from larger particles under the influence of environmental factors.

Details in Figure 6 are in good agreement with the information given in corresponding X-ray diffraction patterns (Figure 4b). The findings show that the kaolinite and trace amounts of quartz, in the sample obtained at 15 min of sedimentation time, can be treated as PM_{10} . Therefore, such particles show a fairly high risk factor for humans and other living beings.

Prolonged sedimentation (30 min) time of dust particles in aqueous suspension indicates that kaolinite and especially quartzite remain only as trace amounts in aqueous phase as shown in Figure 4c. In Figure 7a, the specific morphology of quartzite particles can not be identified. Only clay particles of kaolinite are identified showing varying size in agreement with data in Figure 4c.

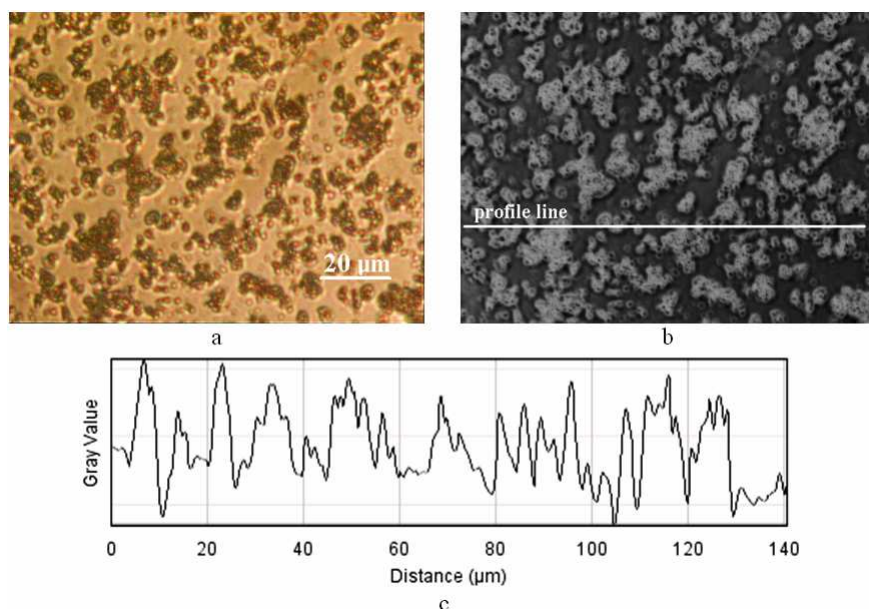


Figure 7. Optical microphotographs for the thin layer of dry fine dust, obtained at 30 min of sedimentation: a) transmitted light; b) negative gray scale representation of Figure 7a; c) profile detail on the corresponding line in Figure 7b.

Profile detail of Figure 7c shows an average particle diameter of kaolinite of about 5 μm . This size is closer to the critical value of $\text{PM}_{2.5}$, which increases the risk factor to humans.

Optical microscopy is not able to identify submicron particles for this purpose we need more profound investigation using AFM [14-16] on powders. Usually double adhesive tape allows a proper particle immobilization for AFM investigation. Dust particles deposited as thin layers on solid substrate, as glass support, confirmed to be an effective method, as also shown in optic microscopy.

For AFM investigation, a thin film of dry fine dust was deposited on glass slide, from suspension taken out at 60 min of sedimentation. The AFM images are presented in Figure 8.

The topography image, Figure 8a, present several submicron particles featuring the kaolinite aspect. On the phase image, Figure 8b, one distinct phase corresponding to kaolinite particles is observed on the glass surface. The borders of kaolinite particles are better observed in amplitude image, given in Figure 8c.

The maximum height of the thin layer of particles is shown in 3d representation of topography image (Figure 8d), and it is about 96 nm. The average diameter of particles is determined by the distance measured at the half height of the particle profile in the cross section (Figure 8e). The

PARTICULATE MATTERS FOUND IN URBAN STREET DUST

average diameter of kaolinite submicron particles is determined of about 180 nm. Similar behavior of kaolinite particles was also reported by others using SEM images [17].

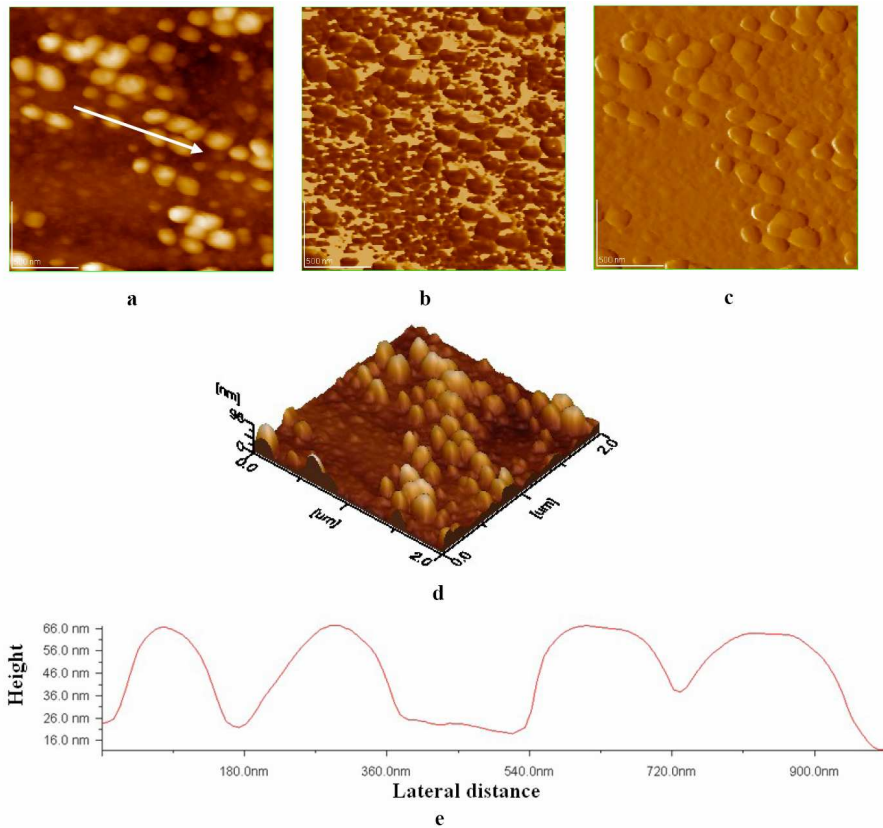


Figure 8. AFM images of the thin layer of dry fine dust, obtained at 60 min of sedimentation; a) topography; b) phase; c) amplitude; d) 3d view of image (a); e) cross section on the arrow given in image (a).

Some studies performed on fine and ultra fine particles of dust have demonstrated the implication of these particles in the shortness of breath [18, 19] which is strongly related to the cardio respiratory diseases and asthma.

CONCLUSIONS

The investigated urban street dust was formed primarily by minerals from natural sources of dust, due to soil erosion and traffic conditions, as well as by some traces of particulate matter provided from anthropogenic sources.

The urban street dust was analyzed by X-ray diffraction and it contains rather large amounts of minerals, like quartzite, kaolinite and calcite as well as goethite and portlandite, as accompanying traces of main particulate minerals. Particle shape was investigated by optical transmitted light and cross polarized light microscopy both on native dust and on thin films of dust, obtained from aqueous dispersion at different sedimentation times.

The performed sedimentation analysis revealed that the larger particles were subjected to almost immediate sedimentation, while the fine ones remained in aqueous dispersion. The data revealed a wide range of particle size, from a few μm to several hundred μm . Thus, at 10 min sedimentation time, the average diameter of quartzite particles is greater than 60 μm and for kaolinite particles is between 15 and 30 μm . The estimated average diameter of particles is about 50 μm . After that, at 15 min of sedimentation time, the kaolinite particles are predominantly detected. Their average diameter is around 10 μm . Additionally, trace amounts of quartz was also found. Then, at 30 min of sedimentation, quartz almost disappeared and only kaolinite particles remained in aqueous dispersion. The average diameter of kaolinite particles is around 5 μm .

The surface morphology and the size distribution of submicron kaolinite particles were confirmed by AFM on thin films of dust adsorbed on glass support from aqueous dispersion at 60 min sedimentation time. The average diameter of fine kaolinite particles is about 180 nm. As stated above, because of the health risk of these fine particles we recommend a proper environmental management of the streets and adjacent places in the intersection of Bucharest Avenue and Paris Street in Cluj-Napoca city.

EXPERIMENTAL SECTION

Street dust samples were collected once a week from the intersection of Bucharest Avenue and Paris Street in Cluj-Napoca, a residential and commercial area, over a period of three summer months (June 2009 - August 2009). For measurement consistency the dust samples were collected on the same day of the week using a conventional non metallic (e.g. plastic) broom and a plastic pan. This sampling procedure is similar to those reported recently [20]. Plastic containers were used to collect and store the dust samples. The samples were air dried. One average sample per month was prepared by mixing equal amounts (by mass) of dust samples from each week of the month, followed by thorough mixing. Then, a representative complex sample was obtained for the summer period by mixing equal amounts (by mass) of dust samples from each month (June, July and August of 2009), followed by thorough mixing. Portions of this representative combined sample of street dust were used for X-ray diffractions and optical microscopy observations.

PARTICULATE MATTERS FOUND IN URBAN STREET DUST

Further, X-ray diffractions and optical microscopy investigations were carried on the thin films of representative dust sample, as follows. A combined sample of about 10 g of representative street dust was immersed in deionized water and consequently subjected to sedimentation. Aqueous dispersion drops were independently taken after 10, 15 and 30 min of sedimentation time and they were spread on glass plate and dried.

For AFM studies, the dust particles were immobilized from a dilute aqueous suspension, at 60 min sedimentation time, on a freshly cleaned flat glass surface, previously optically polished. A small amount of suspension, e.g. one or two drops, was taken out from a depth of 5 cm below the water surface and placed on the glass surface. The drops were spread on the solid support. The dust particles were dried at room temperature in a desiccator overnight. Particles with weak contact to the solid surface were removed in a dry nitrogen gas stream before AFM examination.

The X-ray diffraction analysis was performed on a DRON 3 diffractometer equipped with data acquisition module and the MATMEC VI.0 soft. A monochrome Co k_{α} radiation was used for all X-ray spectra. The identification of minerals in the dust samples was carried out by comparing the obtained X-ray diffractions with the standard files of MATCH 1.0 X – ray standard data base from Crystal Impact Co.

Optical microscopy was performed on a Karl Zeiss Jena transmitted light microscope using transmitted light and cross polarized light method. Microphotographs were digital captured using a SAMSUNG 8 Mpx digital camera. The quantitative analysis of the optical microphotographs was performed by a professional soft Image J, as a free resource from National Institutes of Health, USA.

The AFM investigation was performed on a Jeol JSPM 4210 microscope in tapping operation mode using NSC 11 cantilever with resonant frequency of 330 kHz. The AFM topography, phase and amplitude images were acquired simultaneously at various scanned areas, as previously reported [21-26].

ACKNOWLEDGMENTS

One of the authors, Alexandra-Gertrud Hosu-Prack, gratefully acknowledges the financial support (the scholarship for scientific performance) from Babes-Bolyai University of Cluj-Napoca.

REFERENCES

1. R.N. Colvile, E.J. Hutchinson, J.S. Mindell, R.F. Warren, *Atmospheric Environment*, **2001**, *35*, 1537.
2. S. Seal, S. Krezoski, T.L. Barr, D.H. Petering, P.H. Evans, J. Klinowski, *Journal of Hazardous Materials*, **1997**, *53*, 57.

3. E.J. Houwing, L.C. Rijn, *Journal of Sea Research*, **1998**, 39, 243.
4. D.J. Harris, *Building and Environment*, **1999**, 34, 751.
5. A Rabl, *Environmental Impact Assessment Review*, **1999**, 19, 361.
6. G. Arghir, Caracterizarea cristalografică a metalelor și aliajelor prin difracție cu raze X, Litografia Institutului Politehnic din Cluj-Napoca, Cluj-Napoca, **1990**.
7. V. Pop, I. Chicinaș, N. Jumate, Fizica materialelor. Metode experimentale, Presa Universitară Clujeană, Cluj-Napoca, **2001**.
8. J.D. Hanawalt, H.W. Rinn, L. K. Fervel, *Anal. Chem.* **1938**, 10, 475, PDF # 01-0649, **2008**.
9. J.D. Hanawalt, H.W. Rinn, L.K. Fervel, *Anal. Chem.*, **1938**, 10, 475, PDF # 01-0527, **2008**.
10. J.D. Hanawalt, H.W. Rinn, L.K. Fervel, *Anal. Chem.*, **1938**, 10, 475, PDF # 01-0837, **2008**.
11. J.D. Hanawalt, H.W. Rinn, L.K. Fervel, *Anal. Chem.*, **1938**, 10, 475, PDF # 01-1079, **2008**.
12. W.V. Smitheringale, *Econ. Geol.*, **1929**, 24, 494, PDF # 02-0281, **2008**.
13. G. Arghir, L.M. Ghergari, Cristalografie – Mineralogie Indrumător de lucrări de laborator, Litografia Institutului Politehnic din Cluj-Napoca, **1983**.
14. M. Tomoaia-Cotisel, C. Prejmerean, Gh. Tomoaia, A. Mocanu, M. Trif, A. Badanoiu, T. Buruiana, O. Horovitz, A. Hosu, *Journal of Optoelectronics and Advanced Materials*, **2008**, 10 (4), 937.
15. C. Prejmerean, Gh. Tomoaia, M. Tomoaia-Cotisel, A. Mocanu, O. Horovitz, M. Moldovan, D. Ducea, G. Voicu, I. Petean, *Journal of Optoelectronics and Advanced Materials*, **2008**, 10 (3), 597.
16. P. Laity, A. Cassidy, J. Skepper, B. Jones, R. Cameron, *European Journal of Pharmaceutics and Biopharmaceutics*, **2010**, 74, 337.
17. M.S. Zbik, R. St. C. Smart, G.E. Morris, *Journal of Colloid and Interface Science*, **2008**, 328, 73.
18. J.J. de Hartog, G. Hoek, A. Peters, K.L. Timonen, A. Ibalid-Mulli, B. Brunekreef, J. Heinrich, P. Tiittanen, J.H. van Wijnen, W. Kreyling, M. Kulmala, J. Pekkanen, *American Journal of Epidemiology*, **2003**, 157(7), 613.
19. P. Penttinen, K.L. Timonen, P. Tiittanen, A. Mirme, J. Ruuskanen, J. Pekkanen, *European Respiratory Journal*, **2001**, 17, 428.
20. U.M. Joshi, K. Vijayaraghavan, R. Balasubramanian, *Chemosphere*, **2009**, 77, 526.
21. H. Lindgreen, J. Garnaes, P.L. Hansen, F. Besenbacher, E. Laegsgaard, I. Stensgaard, S.A.C. Gould, P.K. Hansma, *American Mineralogist*, **1991**, 76, 1218.
22. M. Zbik, R. St. C. Smart, *Minerals Engineering*, **2005**, 18, 969.
23. A. Sachan, V. Mehrotra, *Current Science*, **2008**, 95, 1699.
24. Gh. Tomoaia, C. Borzan, M. Crisan, A. Mocanu, O. Horovitz, L.-D. Bobos, M. Tomoaia-Cotisel, *Rev. Roum. Chim.*, **2009**, 54(5), 365.
25. A. Mocanu, I. Cernica, Gh. Tomoaia, L.-D. Bobos, O. Horovitz, M. Tomoaia-Cotisel, *Colloids and Surfaces A: Physicochemical and Engineering Aspects*, **2009**, 338, 93.
26. M. Tomoaia-Cotisel, N. Cioica, C. Cota, Cs. Racz, I. Petean, L.-D. Bobos, A. Mocanu, O. Horovitz, *Studia Univ. Babeș-Bolyai, Chem.*, **2010**, 55(2), 313.

THE LIPOPHILICITY DETERMINATION OF SOME PESTICIDES BY HIGH PERFORMANCE THIN-LAYER CHROMATOGRAPHY AND VARIOUS COMPUTING METHODS

RODICA DOMNICA NAȘCU-BRICIU^{a,*}, COSTEL SÂRBU^a

ABSTRACT. The lipophilicity of some emerging pesticides is investigated by reversed-phase high performance thin-layer chromatography (RP-HPTLC) on RP-18, RP-8 and CN stationary phases. The mobile phases were mixtures of methanol-water in different proportions of volume. The lipophilicity indices taken in consideration during this study are: R_{M0} , mean of R_F and R_M , b , φ_0 , scores corresponding to the first principal components of R_M and R_F . The obtained results are compared with the computed lipophilicity indices (Log P) in order to evaluate the suitability of the involved method in the lipophilicity estimation for the pesticides. The comparison is performed through correlation matrices and profiles. The obtained correlations are indicating a high statistical significance.

Keywords: Pesticides, Lipophilicity, Log P, PCA

INTRODUCTION

The pesticides are defined as being substance or mixture intended to prevent, destroy, repel or mitigate any pest including insects, rodents, and weeds [1]. The use of pesticides, in some crude forms has starting since early times but the modern use of synthetic pesticides began in the early to mid twentieth century. Nowadays the pesticides are accounting over 800 compounds that are formulated in an extremely large variety [2]. If comparing the newly synthetic pesticides with those used in 18th century, such as arsenic or mercury based pesticides, the health benefits are obvious [3]. However, even if the concern has been reduced it has been evidenced that the nowadays used pesticides have also a substantial negative impact on the environment and public health. The most significant effects are a consequence of their toxicity and endocrine activity [4]. One of the most remarkable pesticides that have illuminated the entire world regarding the negative effects was DDT, which is known as the most used insecticide of the nineteen century [5]. All the effects of pesticides, even if speaking of toxicity, is closely related to the chemical structure. These considerations were taken into account in the quantitative

^a Babeș-Bolyai University, Faculty of Chemistry and Chemical Engineering, 11, Arany Janos Str., RO-400028 Cluj-Napoca, Romania; * rodicab2003@yahoo.com

structure –property/activity relationship experiments (QSPR/QSAR). Such studies were basically involved in the pharmaceutical development, but they have gained remarkable importance in toxicology [6].

One of the most important parameter taken in consideration in the QSAR/QSPR studies is the lipophilicity. It is defining the affinity of a molecule for a lipophilic environment. The lipophilicity is connected with an increased biological activity, poorer aqueous solubility, faster metabolization and elimination, increased plasma protein binding, sometimes shorter duration of action. Recently, has been proved that it plays a significant role in the pharmacodynamic and toxicological profile of drugs and xenobiotics [7]. The lipophilicity is usually defined by the partition coefficient, denoted in few different ways, frequently depending by the determination method ($\log P$, $\log k_w$, $\log K_{ow}$, $\log K_{oc}$, R_{M0}).

According to Sangster [8] and Kaliszan [9], the lipophilicity determination methods are divided in direct and indirect methods. The most known and used direct method of determination is the “shake-flask” procedure, which is starting with the analyte repartition between two immiscible phases, usually octanol-water or hexanol-water, followed by the quantitative determination in one or both phases. Even if it is considered to be a reference method, it was almost totally replaced by the indirect methods, such as chromatographic ones, mainly because of the multiple drawbacks that characterize these methods, i.e. the analyte must have a very high purity, high consumption of solvents, involves a quantification step, and so on. On the other side, the chromatographic methods are more flexible and present some significant advantages: dynamic process, the consumption of the investigated compounds is minimal, high-purity chemicals and additional analytical quantification are not required. The lipophilicity indices are computed easily from the retention parameters (retention time, retention factor) [10]. Some previous studies have proved to be very efficient in the lipophilicity determination of pesticides [11, 12].

The purpose of this work was focused on the lipophilicity determination of some pesticides by high performance thin-layer chromatography (HPTLC). The accepted TLC lipophilicity indices (arithmetical mean of R_F : mR_F , arithmetical mean of R_M : mR_M , R_{M0} , the scores corresponding to the first principal components of R_F : $PC1/R_F$, and the scores corresponding to the first principal components of R_M : $PC1/R_M$), were analyzed and compared with the computed $\log P$ values. In addition, the scores obtained applying principal component analysis (PCA) offer the possibility to get a new lipophilicity scale, while the eigenvalues and eigenvectors (loadings) give new insights about the chromatographic mechanism and the chromatographic behaviour of the investigated compounds.

Methods. The thin layer chromatography is providing a series of lipophilicity indices starting from the retention parameter. The most popular and used lipophilicity parameter, namely retardation parameter, was defined by the Bate-Smith and Westall [13] through the following formula:

$$R_M = \log \left[\left(\frac{1}{R_F} \right) - 1 \right] \quad (1)$$

Since within this studies the used mobile phase are usually hydro-alcoholic and the solvents fraction selection does not respect a strict rule, Soczewiński-Wachtmeister [14] have developed a new equation that takes into account the concentration of the organic modifier, as follows:

$$R_M = R_{M0} + b\varphi \quad (2)$$

where R_{M0} represents the extrapolated value to pure water as mobile phase, and the same time it is considered the most relevant lipophilicity descriptor provided by the TLC. The regression slope (b) is directly related to the specific surface area of the stationary phase and also it is considered to be an alternative descriptor of lipophilicity, while φ represents the volume fraction of the organic solvent in the mobile phase.

Furthermore, Valkó [15] has proved that the fraction of the organic modifier may be also used as lipophilicity descriptors for the situation when the amount of solute in the mobile phase is equal to that in the stationary phase i. e. the retention factor is 1 ($R_M = 0$). The new indices, called index of hydrophobicity (φ_0), derived from Eq. 2, is computed through the following formula:

$$\varphi_0 = \frac{R_{M0}}{b} \quad (3)$$

More recently, the scores corresponding to the first principal components of R_F and R_M have proved to have a very high lipophilicity descriptive capacity. Even more, PCA is providing significant information about the interactions that define the separation process, and also allows the obtaining of some lipophilicity maps, both for the compounds and chromatographic stationary phases. In addition, the mean values of R_F and R_M appeared also as an illuminating alternative for the lipophilicity scales estimation [16-18].

Log P. Log P represents the computed lipophilicity indices. Many values are computed according different algorithms involved in the computer software and internet module. For the present study the compounds structures were firstly preoptimized with the Molecular Mechanics Force Field procedure included in Hyperchem version 7.5 (HyperChem, release 7.5 for Windows, Molecular Modeling System; Hypercube), and the resulting geometries were further refined by means of the semi-empirical method Parametric Method-3 using the Fletcher–Reeves algorithm and a gradient norm limit of $0.009 \text{ kcal } \text{Å}^{-1}$. On the basis of obtained geometries, the software like Chem3D Ultra 8.0, and Dragon Plus version 5.4 calculate various lipophilicity descriptors. Three of the log P values were calculated by Chem3D Ultra 8.0 (CLOGP, logPC—Crippen

method, logPV—Viswanadhan method), while two are given by the Dragon 5.4 (MLOGP-Moriguchi method, ALOGP-Ghose–Crippen method). Another seven were offered by the internet module ALOGPS 2.1-vcclab (ALOGPs, AC logP, AB/LogP, miLogP, KOWWIN, XLOGP2, XLOGP3) [19]. The investigated compounds are presented in Figure 1. All the computed values are listed in Table 1.

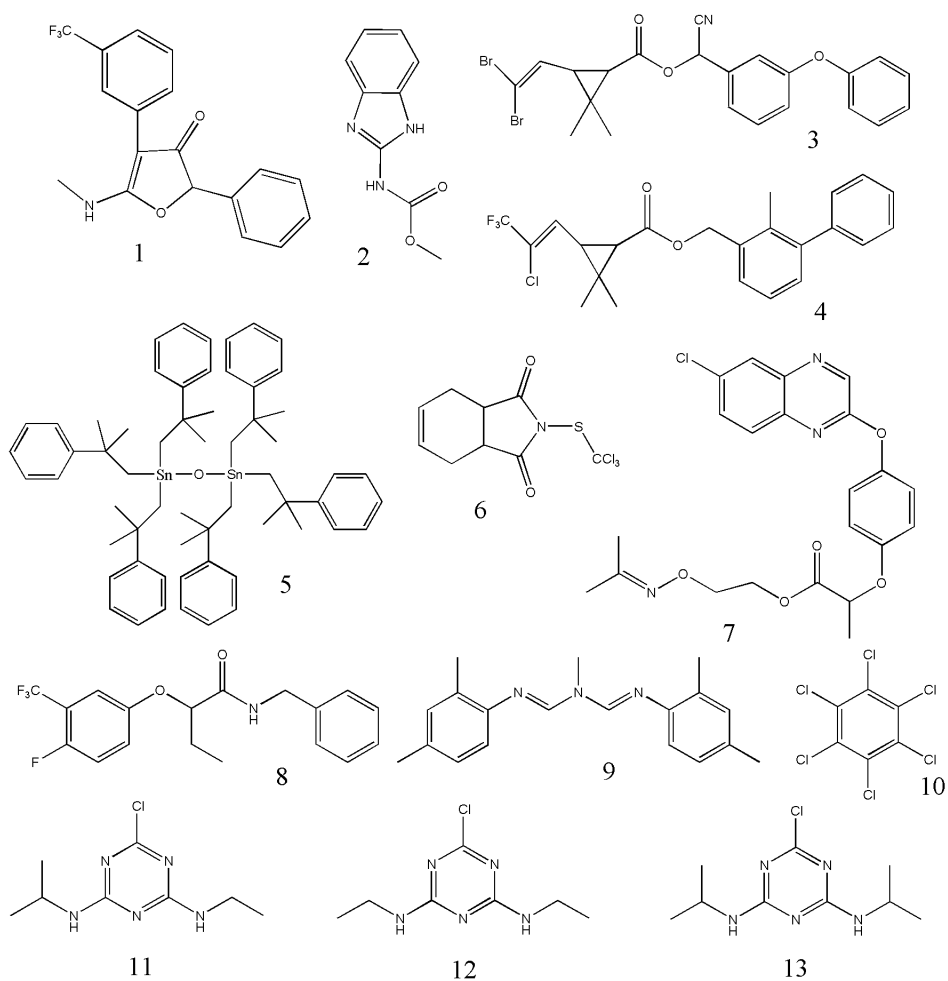


Figure 1. The chemical structure of the investigates pesticides: flurtamone (1), carbendazim (2), deltamethrin (3), bifethrin (4), fenbutatin oxide (5), captan (6), propaquizafop (7), beflubutamid (8), amitraz (9), hexachlorobenzene (10), atrazine (11), simazine (12), propazine (13).

RESULTS AND DISCUSSION

The chromatographic lipophilicity indices obtained for the investigated pesticides are presented in the Table 2 and 3. The results are indicating that the most lipophilic compound investigated in this experiment is the fenbutatin oxide. The abundance of phenyl groups founded in the molecule is favouring the lipophilic interactions. Deltamethrin, bifethrin and hexachlorobenzene are, also characterized by high lipophilicity. The group of triazine are distinguished with lower lipophilicity and within them the simazine is the most hydrophilic. Moreover, the lipophilicity level of carbendazin and amitraz is comparable to that corresponding to triazine group. The highest lipophilicity indices were obtained on the RP-8 stationary phase, closely followed by RP-18 and CN. However, all the lipophilicity indices are comparable and not very different from one stationary phase to another.

According to some authors a good correlation between slope and intercept of Eq. 2 is an indicative of a congeneric series [20, 21]. In this case the determination coefficients (R^2) were higher than 0.99 for RP-8 and CN and higher than 0.94 for RP-18. The group of investigated pesticides is not a homogeneity one and as a consequence it may not be considered a congeneric group. These results, sustained by some previously presented data [17, 18] are indicating that the correlations are not necessarily related to the chemical reality.

The regression correlation coefficients are offering information about the chromatographic behaviour related to the methanol fraction from the mobile phases. Excepting few cases (carbendazin: $r_{CN} = 0.96$; bifethrin: $r_{CN} = 0.96$; fenbutatin oxide: $r_{RP-8} = 0.95$, $r_{CN} = 0.96$; captan: $r_{RP-18} = 0.97$; amitraz: $r_{RP-18} = 0.97$), the correlations obtained were higher than 0.98, which is indicating that the chromatographic behaviour of the compounds was a linear one. All these considerations may be observed in the Figure 2. The presented profiles allow appreciating that the interactions involved into the chromatographic process during the development with mobile phases consisting of different fraction of methanol are constant and they are not modifying while the solvents ration in the mobile phases has been changed. This aspect is strongly sustained by the fact that in all situations the mean value of the retardation parameter is overlapped with the median. In addition, the symmetry observed in the correlation profiles of the lipophilicity indices (Figure 3) is suggesting that the investigated stationary phases are inducing a very similar retention mechanism. The correlations between means and PCs are indicating that the CN results are more specific than those obtained on RP-18 and RP-8 when the diagrams are indicating very high correlations. The highest differences of chromatographic behaviour in the case of RP-18/RP-8 vs. CN are observed for the bifethrin, propaquizafop and beflubutamid. In the Figure 3 C the R_{M0} values were compared with the computed Log P values and there may be easily observed that the results obtained by chromatographic analysis are comparable with

those obtained by applying different theoretical algorithms. Even more, the diagrams trend is similar in all cases. The highest differences can be identified in the case of fenbutatim oxide, when because of the Sn presence some of the computing algorithms are failing.

Table 1. The computed lipophilicity indices

No	Compound	ALOG Ps	AC logP	AB/ LogP	mi LogP	ALO GP	MLO GP	KOW WIN	XLOG P2	XLOG P3	Log P ^c	Log P ^v	CLO GP
1	Flurtamone	4,83	3,81	4,40	3,95	4,24	3,20	3,82	5,27	5,25	3,67	3,73	3,91
2	Carbendazin	1,46	2,00	1,49	1,46	1,65	1,05	1,55	1,23	1,52	1,29	1,30	1,71
3	Deltamethrin	6,13	6,02	5,71	6,65	5,63	4,11	6,18	5,84	6,20	6,47	6,40	6,79
4	Bifethrin	5,71	6,50	6,93	7,36	6,37	5,40	8,15	7,19	6,00	6,52	6,30	7,36
5	Fenbutatim O.	10,63	15,57	10,00	9,90			13,63	16,70	19,85			11,33
6	Captan	3,00	1,97	2,29	2,84	4,02	1,82	2,74	2,27	2,35	3,51	3,24	2,35
7	Propaquizafop	4,41	4,96	4,39	5,10	4,21	3,11	4,59	5,23	4,60	4,52	4,62	4,74
8	Beflubutamid	4,10	4,00	4,52	4,35	4,72	4,25	4,81	4,79	4,65	4,55	4,52	4,86
9	Amitraz	4,42	3,52	5,23	5,09	5,41	4,90	5,55	4,57	5,50	5,63	5,53	5,50
10	Hexachloro- benzene	5,70	5,66	4,90	5,72	5,82	5,21	5,86	5,75	5,73	5,38	5,15	6,06
11	Atrazine	2,70	2,48	2,52	2,55	2,54	2,59	2,82	1,66	2,61	1,95	2,06	2,70
12	Simazine	2,48	2,08	2,27	2,25	2,16	2,27	2,40	1,20	2,18	1,63	1,65	2,39
13	Propazine	2,94	2,88	2,78	2,85	2,91	2,89	3,24	2,12	2,93	2,26	2,47	3,01

Table 2. The experimentally determined lipophilicity indices on RP-18 and RP-8 HPTLC plates

No	Compound	RP-18						RP-8							
		mR _F	mR _M	R _{M0}	b	φ ₀	PC1/R _F	PC1/R _M	mR _F	mR _M	R _{M0}	b	φ ₀	PC1/R _F	PC1/R _M
1	Flurtamone	0.633	-0.239	1.98	-0.026	-75.84	-0.496	1.184	0.645	-0.270	3.85	-0.048	-79.42	-0.384	0.859
2	Carbendazin	0.545	-0.081	3.28	-0.040	-82.96	-0.302	0.825	0.645	-0.263	2.24	-0.029	-76.05	-0.383	0.861
3	Deltamethrin	0.196	0.659	6.68	-0.071	-94.30	0.480	-0.843	0.285	0.439	7.36	-0.081	-90.39	0.420	-0.749
4	Bifethrin	0.099	1.033	7.94	-0.081	-97.71	0.697	-1.683	0.178	0.734	8.15	-0.087	-93.40	0.662	-1.408
5	Fenbutatim O.	0.023	1.645	4.65	-0.035	-131.49	0.869	-3.026	0.060	1.334	10.75	-0.111	-97.04	0.926	-2.773
6	Captan	0.590	-0.161	2.39	-0.030	-79.64	-0.401	1.007	0.649	-0.278	3.79	-0.048	-79.19	-0.393	0.876
7	Propaquizafop	0.291	0.403	4.83	-0.052	-92.74	0.266	-0.261	0.402	0.185	5.72	-0.065	-87.85	0.160	-0.171
8	Beflubutamid	0.548	-0.087	3.78	-0.045	-83.09	-0.309	0.836	0.545	-0.084	4.83	-0.058	-83.55	-0.161	0.434
9	Amitraz	0.656	-0.285	2.27	-0.030	-75.53	-0.549	1.283	0.710	-0.399	3.07	-0.041	-75.23	-0.528	1.149
10	Hexachloro- benzene	0.059	1.223	4.69	-0.041	-115.01	0.788	-2.085	0.173	0.718	6.28	-0.065	-95.98	0.672	-1.349
11	Atrazine	0.570	-0.123	0.87	-0.012	-74.44	-0.354	0.932	0.625	-0.230	3.84	-0.048	-80.20	-0.338	0.771
12	Simazine	0.613	-0.201	0.59	-0.009	-63.39	-0.451	1.107	0.674	-0.324	3.26	-0.042	-77.31	-0.448	0.982
13	Propazine	0.518	-0.031	1.44	-0.017	-83.21	-0.238	0.724	0.565	-0.118	4.35	-0.053	-82.75	-0.204	0.517

Table 3. The experimentally determined lipophilicity indices on CN HPTLC plates

	Compound	CN						
		mR _F	mR _M	R _{M0}	b	φ ₀	PC1/R _F	PC1/R _M
1	Flurtamone	0.724	-0.427	2.49	-0.034	-72.56	-0.341	0.727
2	Carbendazin	0.544	-0.078	2.40	-0.029	-82.33	0.063	-0.041
3	Deltamethrin	0.449	0.094	5.15	-0.060	-86.58	0.279	-0.453
4	Bifethrin	0.528	-0.053	4.68	-0.056	-84.06	0.102	-0.123
5	Fenbutatim O.	0.087	1.088	7.71	-0.078	-98.97	1.081	-2.682
6	Captan	0.602	-0.182	2.23	-0.028	-78.60	-0.067	0.191
7	Propaquizafop	0.641	-0.256	2.74	-0.035	-77.73	-0.153	0.347
8	Beflubutamid	0.685	-0.346	2.86	-0.038	-75.85	-0.253	0.544
9	Amitraz	0.759	-0.501	1.08	-0.019	-58.12	-0.421	0.908
10	Hexachlorobenzene	0.141	0.837	6.83	-0.071	-96.86	0.964	-2.114
11	Atrazine	0.756	-0.496	1.44	-0.023	-63.28	-0.414	0.891
12	Simazine	0.754	-0.489	1.40	-0.022	-62.97	-0.409	0.877
13	Propazine	0.763	-0.514	1.83	-0.028	-66.33	-0.429	0.928

Beside of the fact that PCA is providing very efficient lipophilicity descriptors, it is offering also very important information about the compounds characteristics through the generically named "lipophilicity maps". They are in fact a 2D graphically representation of the scores corresponding to the first two principal components. The efficiency of these representations is sustained by the cumulative proportion and eigenvalues, which gave information about how the raw information of the initial data is adsorbed in the principal components. In the present case, by applying PCA on the R_F values the first principal component accounts more than 98.51%, while in the case of R_M the first principal component accounts more than 98.92%. Moreover, the first two principal components account more than 99.79% in all cases. These values are indicating that the first two principal components are retaining the majority of the variance and in the same time they are enough to be used for the compounds classification. In the Figure 4 are presented the lipophilicity maps obtained by applying PCA on the matrix of R_M values of the investigated pesticides. The triazine group is identified as linear cluster, while the rest of the compounds are more or less correlated. The hexachlorobenzene and fenbutatim oxide are distinguished as the most lipophilic compound and this may be remarked as well in the obtained lipophilicity maps.

The PCA is a very powerful tool in the chromatography, because it may be involved in the compounds and stationary phase classification, and it provides very successful lipophilicity indices. Even more, by graphical representation of PCA loadings as function of the methanol fraction used in the mobile phases, there may be obtained some pertinent information concerning the retention mechanism involved in the development process of each stationary phase. By carefully examining the patterns depicted in Figure 5, the similarity and differences between the bonded phases investigated can be clearly observed.

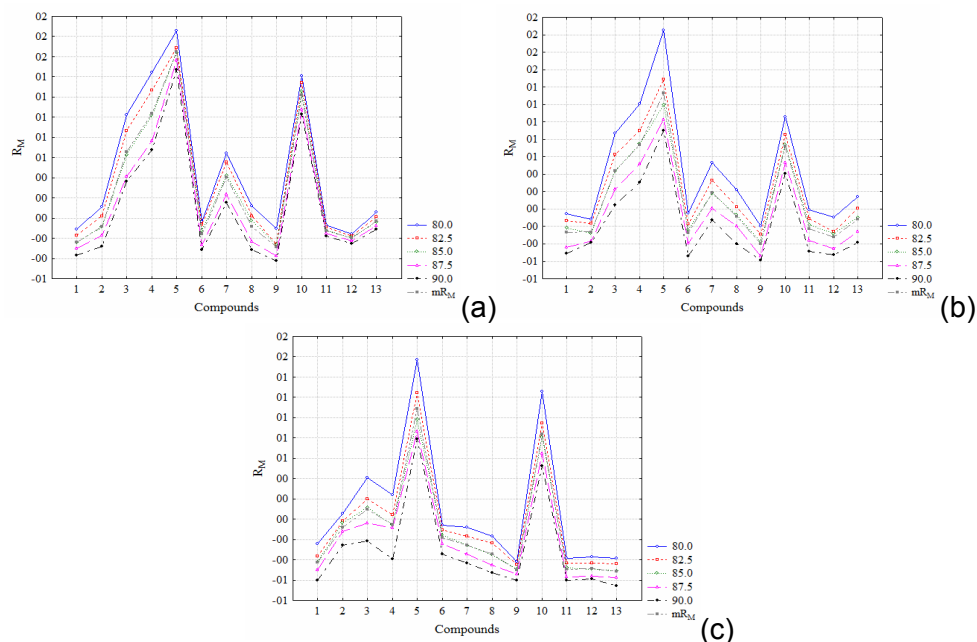


Figure 2. Profiles of R_M values for all fraction of methanol: (a) RP-18; (b) RP-8; (c)-CN.

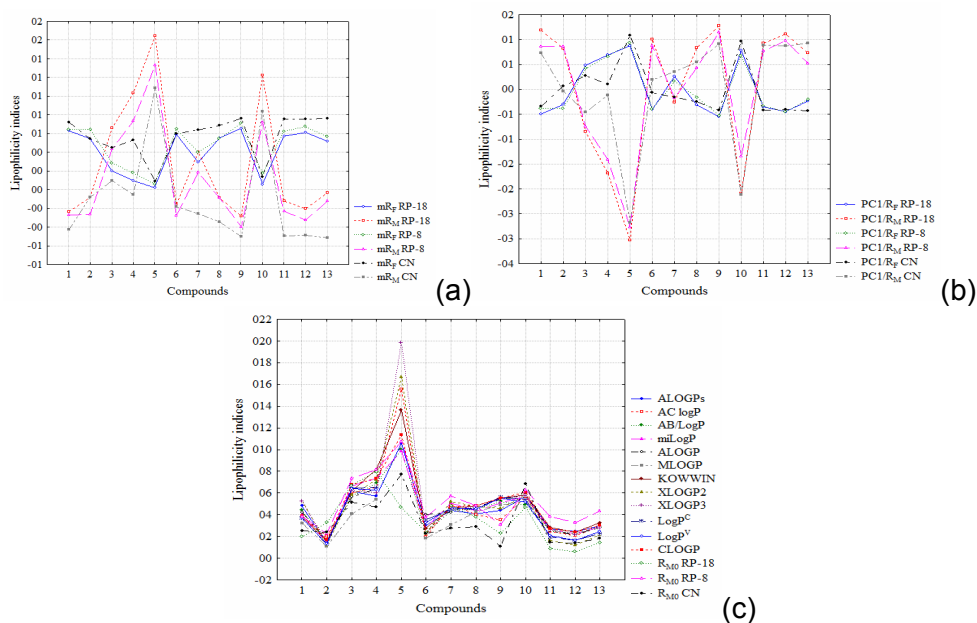


Figure 3. The correlation profiles of the lipophilicity indices: mR_F and mR_M (a), $PC1/R_F$ and $PC1/R_M$ (b), and R_{M0} and $LogP$ (c).

THE LIPOPHILICITY DETERMINATION OF SOME PESTICIDES BY HIGH PERFORMANCE ...

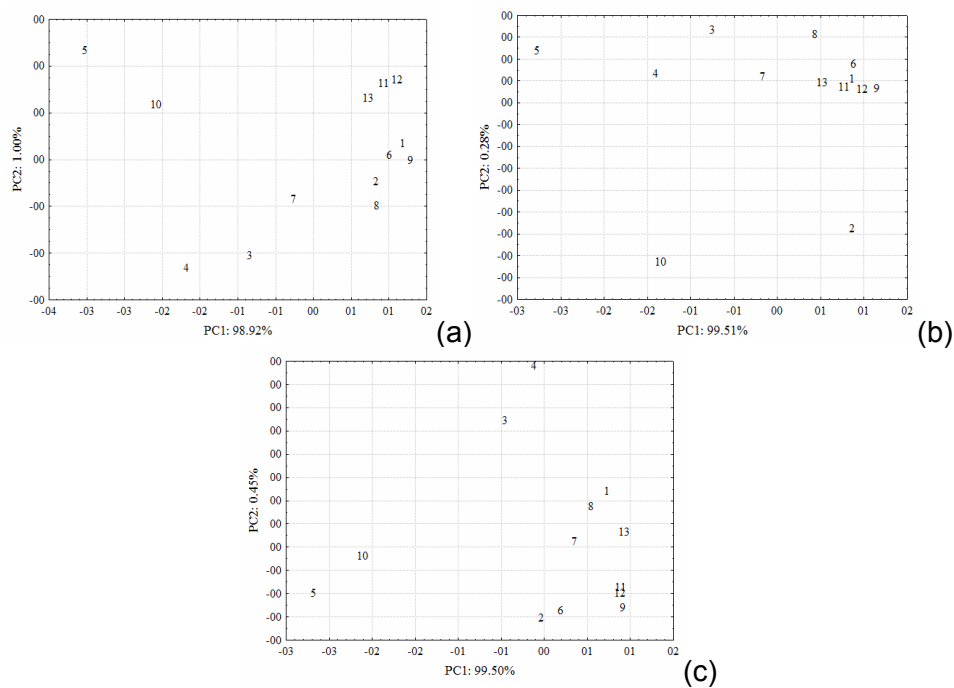


Figure 4. The lipophilicity maps of the investigated pesticides, obtained by applying PCA on the R_M values: RP-18 (a), RP-8 (b), and CN (c).

The strong lipophilic character of the RP-18 may be observed in diagrams corresponding to R_M , while the RP-8 and CN are leading to more or less similar interactions.

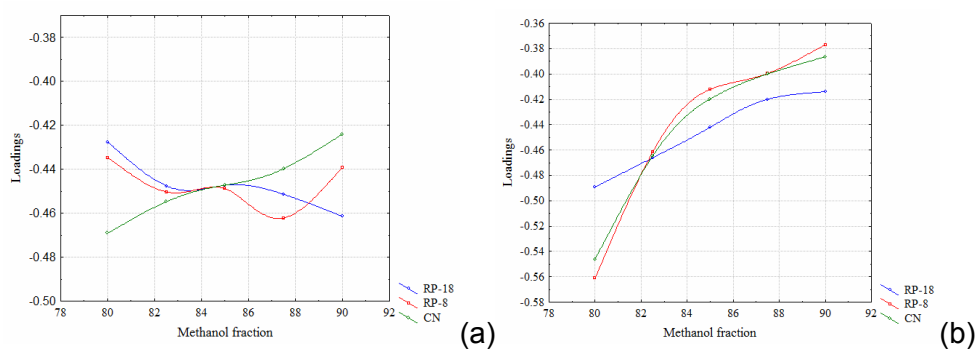


Figure 5. The loadings profiles: R_F (a), and R_M (b).

The similarities existed between the involved stationary phases are sustained by the correlation matrices (Table 4). The best correlations were obtained for the RP-8 lipophilicity indices versus those obtained on RP-18. The CN results are better correlated with the RP-8 lipophilicity indices. The highest correlation coefficients are of 0.99 and in some particular cases 1. The correlation matrix of the experimentally vs. computed lipophilicity indices may offer some information about the molecular particularities which are responsible for the chromatographic behaviour. In the Table 5 are listed the obtained correlations. The highest correlations are obtained for the $R_{M0, RP-8}$ vs. AC logP when the correlation coefficient is reaching 0.92. The AC logP index presents the highest correlations with all experimentally expressed indices. Significant correlations are obtained also, for the miLogP. Both lipophilicity indices are computed with ALOGPS 2.1 module. These significant correlations obtained ($r > 0.80$) are sustaining the experimentally obtained lipophilicity indices.

CONCLUSIONS

The lipophilicity of some emerging pesticides has been investigated on three reversed phase stationary phases using different mixtures of methanol-water as mobile phases. The most lipophilic compound has been founded to be the fenbutatim oxide, since the compound with the lowest lipophilicity is the simasine. The chromatographic behaviour of the compounds observed was constant while the mobile phase composition has been changed, for all the employed stationary phases. Once more, the PCA has been proved the power of compounds classification, as lipophilicity indices provider and the capacity if retention mechanism information support. The correlation matrices have been indicating that all the experimentally obtained lipophilicity indices are highly correlated, while the AC logP has been distinguished as the best computed descriptor.

Table 4. The correlation matrix of the experimentally obtained lipophilicity indices

Stationary phase	Index	RP-18							RP-8							CN						
		mR _F	mR _M	R _{M0}	b	φ ₀	PC1/R _F	PC1/R _M	mR _F	mR _M	R _{M0}	b	φ ₀	PC1/R _F	PC1/R _M	mR _F	mR _M	R _{M0}	b	φ ₀	PC1/R _F	PC1/R _M
RP-18	mR _F	1.00	-0.98	-0.81	0.64	0.91	-1.00	0.98	0.99	-0.96	-0.90	0.87	0.97	-0.99	0.96	0.85	-0.83	-0.92	0.93	0.85	-0.85	0.84
	mR _M		1.00	0.72	-0.53	-0.95	0.98	-1.00	-0.98	0.99	0.92	-0.89	-0.96	0.98	-0.99	-0.90	0.90	0.95	-0.95	-0.86	0.90	-0.90
	R _{M0}			1.00	-0.97	-0.64	0.81	-0.73	-0.79	0.72	0.72	-0.71	-0.75	0.79	-0.72	-0.57	0.52	0.69	-0.73	-0.70	0.57	-0.52
	b				1.00	0.45	-0.64	0.54	0.62	-0.53	-0.56	0.55	0.58	-0.62	0.53	0.37	-0.32	-0.51	0.56	0.56	-0.38	0.32
	φ ₀					1.00	-0.91	0.95	0.92	-0.95	-0.87	0.83	0.90	-0.92	0.95	0.93	-0.94	-0.94	0.93	0.89	-0.93	0.94
	PC1/R _F						1.00	-0.98	-0.99	0.96	0.90	-0.87	-0.97	0.99	-0.96	-0.85	0.83	0.92	-0.93	-0.85	0.85	-0.84
	PC1/R _M							1.00	0.99	-0.99	-0.92	0.89	0.96	-0.99	0.99	0.90	-0.90	-0.95	0.95	0.86	-0.90	0.90

THE LIPOPHILICITY DETERMINATION OF SOME PESTICIDES BY HIGH PERFORMANCE ...

Stationary phase	Index	RP-18						RP-8						CN							
		mR _F	mR _M	R _{MO}	b	φ ₀	PC1/R _F	PC1/R _M	mR _F	mR _M	R _{MO}	b	φ ₀	PC1/R _F	PC1/R _M	mR _F	mR _M	R _{MO}	b	φ ₀	PC1/R _F
RP-8	mR _F							1.00	-0.98	-0.94	0.92	0.99	-1.00	0.98	0.85	-0.84	-0.94	0.95	0.84	-0.85	0.84
	mR _M							1.00	0.96	-0.94	-0.96	0.98	-1.00	-0.87	0.88	0.95	-0.95	-0.84	0.88	-0.88	
	R _{MO}							1.00	-1.00	-0.92	0.94	-0.96	-0.75	0.75	0.87	-0.89	-0.74	0.75	-0.76		
	b							1.00	0.90	-0.92	0.94	0.70	-0.71	-0.84	0.86	0.70	-0.70	0.71			
	φ ₀							1.00	-0.99	0.96	0.81	-0.80	-0.92	0.94	0.82	-0.81	0.81				
	PC1/R _F							1.00	-0.98	-0.85	0.84	0.94	-0.95	-0.84	0.85	-0.84					
	PC1/R _M							1.00	0.87	-0.88	-0.95	0.95	0.84	-0.87	0.88						
CN	mR _F							1.00	-1.00	-0.96	0.92	0.93	-1.00	1.00							
	mR _M							1.00	0.95	-0.91	-0.91	1.00	-1.00								
	R _{MO}							1.00	-1.00	-0.93	0.96	-0.95									
	b							1.00	0.92	-0.92	0.92										
	φ ₀							1.00	-0.93	0.92											
	PC1/R _F							1.00	-1.00												
	PC1/R _M							1.00													

Table 5. The correlation matrix of the experimentally vs. computed lipophilicity indices.

Stationary phase	Index	ALOGPs	AC logP	AB/LogP	miLogP	ALOGP	MLOGP	KOWWIN	XLOGP2	XLOGP3	LogP ^C	LogP ^V	CLOGP
RP-18	mR _F	-0.70	-0.86	-0.63	-0.76	-0.63	-0.59	-0.72	-0.68	-0.60	-0.65	-0.64	-0.74
	mR _M	0.70	0.85	0.63	0.75	0.65	0.62	0.73	0.68	0.60	0.64	0.63	0.74
	R _{MO}	0.72	0.88	0.76	0.84	0.73	0.58	0.81	0.80	0.68	0.79	0.78	0.81
	b	-0.68	-0.83	-0.75	-0.81	-0.70	-0.53	-0.77	-0.78	-0.65	-0.78	-0.78	-0.78
	φ ₀	-0.65	-0.78	-0.55	-0.67	-0.64	-0.57	-0.64	-0.66	-0.58	-0.62	-0.61	-0.66
	PC1/R _F	0.70	0.86	0.63	0.76	0.63	0.59	0.72	0.68	0.60	0.64	0.64	0.74
	PC1/R _M	-0.70	-0.85	-0.64	-0.75	-0.65	-0.62	-0.73	-0.68	-0.60	-0.64	-0.63	-0.74
RP-8	mR _F	-0.75	-0.90	-0.69	-0.80	-0.69	-0.65	-0.77	-0.73	-0.65	-0.69	-0.68	-0.78
	mR _M	0.75	0.89	0.69	0.80	0.69	0.66	0.78	0.73	0.65	0.68	0.68	0.78
	R _{MO}	0.82	0.92	0.80	0.88	0.76	0.69	0.85	0.80	0.73	0.78	0.78	0.85
	b	-0.82	-0.91	-0.80	-0.88	-0.76	-0.68	-0.85	-0.80	-0.73	-0.78	-0.79	-0.84
	φ ₀	-0.76	-0.88	-0.67	-0.78	-0.68	-0.65	-0.74	-0.73	-0.65	-0.66	-0.66	-0.76
	PC1/R _F	0.75	0.90	0.69	0.80	0.69	0.65	0.77	0.73	0.65	0.69	0.68	0.78
	PC1/R _M	-0.75	-0.90	-0.70	-0.80	-0.69	-0.66	-0.78	-0.73	-0.65	-0.69	-0.68	-0.78
CN	mR _F	-0.51	-0.58	-0.34	-0.47	-0.49	-0.38	-0.43	-0.45	-0.40	-0.46	-0.43	-0.48
	mR _M	0.50	0.56	0.33	0.46	0.48	0.39	0.41	0.44	0.39	0.44	0.41	0.46
	R _{MO}	0.73	0.80	0.59	0.69	0.66	0.58	0.65	0.68	0.62	0.64	0.62	0.69
	b	-0.77	-0.84	-0.64	-0.74	-0.69	-0.61	-0.69	-0.72	-0.67	-0.67	-0.66	-0.74
	φ ₀	-0.49	-0.60	-0.34	-0.47	-0.46	-0.26	-0.40	-0.50	-0.37	-0.44	-0.42	-0.44
	PC1/R _F	0.51	0.58	0.34	0.48	0.49	0.38	0.43	0.45	0.40	0.46	0.43	0.48
	PC1/R _M	-0.50	-0.57	-0.33	-0.46	-0.49	-0.39	-0.42	-0.45	-0.40	-0.45	-0.42	-0.47

EXPERIMENTAL SECTION

All the compounds and solvents were obtained from commercial source (Merck, Fluka, and Sigma) in analytical degree purity. The stationary phases were Merck products (Nordic Invest, Cluj Napoca, Romania). The standard solutions of pesticides were prepared in acetone (1 mg mL^{-1}). The spots ($2 \text{ }\mu\text{L}$) were applied at 1.5 cm from bottom edge and at 0.7 cm from lateral edges using a Hamilton microsyringe of $10 \text{ }\mu\text{L}$. The distance between the spots was by 0.7 cm. The elution was performed on 8 cm, by ascendant development into a chromatographic chamber previously saturated for 10 min. The chemically bonded plates were by RP-18 and RP-8 silica gel 60 modified with aliphatic hydrocarbons of increasing hydrocarbon chain length resulting in increased hydrophobicity and the CN modified plate which are based on a silica gel 60 modified with cyanopropyl groups. Each stationary phase type has been developed with five mobile phases based on methanol and water. The methanol fractions used in the mobile phases were between 80 and 90% changed with 2.5% per each step. The visualization of the compounds has been realized under UV light at 254 nm.

ACKNOWLEDGEMENT

The financial support of the Ministry of Education Research, Youth and Sport of Romania (CNCSIS, IDEI 560/2007-2010) is gratefully acknowledged.

REFERENCES

1. E.R. Laws, W.J. Hayes, "Handbook of Pesticide Toxicology", Academic Press, San Diego, **1991**.
2. D.B. Barr, L.L. Needham, *J. Chromatogr. B*, **2002**, 778, 5.
3. P. Kaushik, G.J. Kaushik, *Haz. Mat.* **2007**, 143, 102.
4. R. McKinlay, J.A. Plant, J.N.B. Bell, N. Voulvoulis, *Environ. Int.* **2008**, 34, 168.
5. J. Beard, Australian Rural Health Research Collaboration, *Sci. Tot. Environ.* **2006**, 355, 78.
6. P. Baur, H. Marzouk, J. Schonherr, B.T. Grayson, *J. Agric. Food Chem.* **1997**, 45, 3659.
7. R. Kaliszan, *Chem. Rev.* **2007**, 107, 3212.
8. J. Sangster, "Octanol–Water Partition Coefficients: Fundamentals and Physical Chemistry", Wiley, West Sussex, **1997**.

9. R. Kaliszan, "Structure and Retention in Chromatography: A Chemometric Approach", Harwood Academic Publishers, Amsterdam, **1997**.
10. R.D. Briciu, A. Kot-Wasik, A. Wasik, J. Namiesnik, C. Sârbu, *J. Chromatogr. A*, **2010**, 1217, 3702.
11. C. Sârbu, B. Malawska, *J. Liq. Chromatogr. & Rel. Technol.* **2000**, 23, 2143.
12. T. Djaković-Sekulić, N. Perišić Janjić, C. Sârbu, Z. Lozanov- Crvenković, *J. Planar Chromatogr.* **2007**, 20, 251.
13. E.C. Bate-Smith, R.G. Westall, *Biochim. Biophys. Acta*, **1950**, 4, 427.
14. E. Soczewiński, C.A. Wachtmeister, *J. Chromatogr. A*, **1962**, 7, 311.
15. K. Valkó, *J. Liq. Chromatogr.* **1984**, 7, 1405.
16. R.D. Briciu, A. Kot-Wasik, J. Namiesnik, C. Sârbu, *J. Sep. Sci.* **2009**, 32, 2066.
17. R.D. Briciu, C. Sârbu, *Sep. Sci. Technol.*, **2010**, 45, 1275.
18. C. Sârbu, R.D. Briciu, *J. Liq. Chromatogr. & Rel. Technol.* **2010**, 33, 903.
19. I.V. Tetko, J. Gasteiger, R. Todeschini, A. Mauri, D. Livingstone, P. Ertl, V.A. Palyulin, E.V. Radchenko, N.S. Zefirov, A.S. Makarenko, V.Y. Tanchuk, V.V. Prokopenko, *J. Comput. Aid. Mol. Des.* **2005**, 19, 453.
20. G.L. Biagi, A.M. Barbaro, M.C. Guerra, G. Gantelli-Forti, M.E. Fracasso, *J. Med. Chem.* **1974**, 17, 28.
21. P.J. Schoenmakers, H.A.H. Billiet, L. de Galan, *J. Chromatogr.* **1979**, 185, 179.

NEW PERSPECTIVES IN POLYOXOMOLYBDATES CHEMISTRY CONTAINING LARGE {Mo₁₃₂} CLUSTERS

JULIA SZAKÀCS^a, DAN RUSU^b, MARIANA RUSU^{a,*}

ABSTRACT. The new (NH₄)₆₀{U₃C{(Mo^{VI})Mo₅^VO₂₁(H₂O)₆}₁₂{Mo₂^VO₄(SO₄)₃₀}₃₀·308H₂O spherical cluster was synthesized as ammonium salt and investigated by means of elemental analyses, FT-IR, Raman, UV-Vis and EPR spectroscopy and by magnetic measurements. The results suggest the binding of uranium cations to the SO₄²⁻ ligands and the quasi-cubic local symmetry around the uranium ions.

Keywords: Uranium (IV), metal clusters, IR, Raman, UV, Vis, RES spectroscopies, magnetic susceptibility.

INTRODUCTION

Over the past twelve years, the chemistry of the giant spherical polyoxometallate clusters has brought about spectacular changes, due to the synthesis and characterization of giant molecules with the new structures displaying a high level of symmetry and remarkable topological and electronic properties.

In 1998, Müller and his team [1] presented a very large spherical mixed-valence polyoxometallate cluster, i.e. [Mo^{VI}₇₂Mo^V₆₀O₃₇₂(CH₃COO)₃₀(H₂O)₇₂]⁴²⁻, abbreviated as {Mo₁₃₂}, [Mo^{VI}₇₂Mo^V₆₀] or [Mo₁₁]₁₂. The new dodecameric cluster was named "giant ball" (giant sphere).

The central Mo^{VI} atoms of the 12 [(Mo^{VI})Mo^V₅] pentagons define the 12 corners, while the 30 [Mo^V₂] linkers, i.e. the [Mo^V₂O₄]²⁺ units, define the 30 edges of an icosahedron. This corresponds to the formulation [(Mo^{VI})Mo^V₅O₂₁(H₂O)₆]₁₂ [Mo^V₂O₄(CH₃COO)]₃₀⁴²⁻ or [(Mo^{VI})Mo^V₅]₁₂[(Mo^V₂)]₃₀ ≡ (pentagon)₁₂(linker)₃₀. Based on a topological concept, the molecule can also be formulated as [(Mo^{VI})⁰(Mo^{VI}₅)^I(Mo^{VI}₅)^{II}]₁₂. This formulation takes formally into account the fact that the Mo atoms of each rather stable [Mo^V₂] belongs to the two adjacent [Mo₁₁] groups.

^a Babeş-Bolyai University, Faculty of Chemistry and Chemical Engineering, 11, Arany Janos Str., RO-400028 Cluj-Napoca, Romania, mrusu@chem.ubbcluj.ro

^b Iuliu Hațieganu University of Medicine and Pharmacy, Faculty of Pharmacy, 13, E. Isac Str., RO-400023, Cluj-Napoca, Romania

The cluster can be considered as being built up of 12 [Mo₁₁] units with central [MoO₇] pentagonal - bipyramidal groups, so that the fivefold symmetry axes are retained in the resulting spherical structure, which shows an overall icosahedral symmetry (I_h) [2]. The spherical nanocapsule of the type {(Mo^{VI})Mo^{VI}₅O₂₁(H₂O)₆}₁₂ has 20 sizeable pores of the {Mo₉O₉} type finely sculpturable cavity interiors. A water cluster consisting of two shells, an outer {H₂O}₆₀ Archimedian solid and an inner {H₂O}₂₀ dodecahedron, is located inside the capsule.

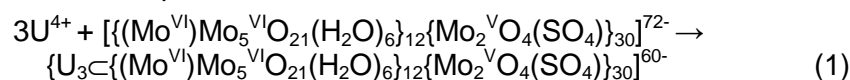
The giant sphere species can act as hosts for cations forming new types of compounds in terms of structure and properties [3-5a]. {Mo₁₃₂} exhibits a nanometer-size cavity, presenting new perspectives for novel host-guest chemistry. The most interesting challenge will be to fill the cavities of the "opened" ball-type {Mo₁₃₂} cluster, which exist as a lacunary-type system, with a variety of different guests, and also to place molecules inside the cavity of the ball-shaped clusters, which show a different reactivity to the discrete ones.

The different cations (substrates) can be fixed at a well-defined position above the {Mo₉O₉} type pores (Rb⁺), below the pores (Ce³⁺, Na⁺/Mo) and especially in the channels (urea H⁺/Na⁺, Cs⁺, Gua H⁺/Urea⁺ [6-10]).

In this paper we described the synthesis of a new, very large cluster from the {Mo₁₃₂} series which corresponds to the formula (NH₄)₆₀{U₃C} {(Mo^{VI})Mo^{VI}₅O₂₁(H₂O)₆}₁₂{Mo₂^VO₄(SO₄)₃₀}₃₀·308H₂O and which is abbreviated as {Mo₁₃₂-U^{IV}}. The new cluster was investigated by vibrational (FT-IR, Raman), electronic (UV-VISNIR) spectroscopy, magnetic susceptibility measurements, as well as EPR spectroscopy.

RESULTS AND DISCUSSIONS

The reaction of U⁴⁺ ions with {Mo₁₃₂-sulphate} in water can be described by eq. (1). The isolation of the products as ammonium salts resulted in relatively good yields of the complex.



Chemical analysis

The elemental analysis found is in good agreement with the calculated composition of the complex.

Vibrational spectra

FT-IR spectrum

The vibration bands of the FT-IR spectrum (in cm⁻¹) (Fig. 1) and their assignments are the following: 1622(m) δ_{HOH}, 1400(m) δ_{NH4⁺}, 1190(w), 1136(w) and 1045(w) ν_{3(SO4)}, 968(s) and 936(m) ν_{as(Mo-O_t)}, 856(m), 802(vs), 729(vs)

$\nu_{as}(Mo-O_{br}-Mo)$, 571(s) and 474(m) $\delta(Mo-O_{br}-Mo)$, where O_t , O_{br} are terminal oxygen atoms and bridged oxygen atoms, respectively.

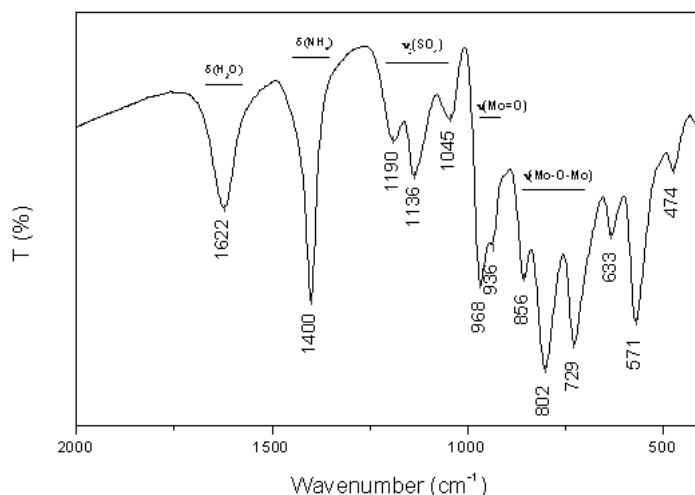


Figure 1. FT-IR spectrum of $\{Mo_{132}-U^{IV}\}$ cluster.

The five anti-symmetric stretching vibrations $\nu_{as}(Mo-O_t)$ and $\nu_{as}(Mo-O_{br}-Mo)$ characteristic to Mo-O bonds are recorded in the range of 700-1000 cm^{-1} [11]. The spectroscopic data indicate the polyoxometalate nature of the $\{Mo_{132}-U^{IV}\}$ cluster, and the binding of uranium cations to the SO_4^{2-} ligands, because the frequency values of the coordinated sulfate group in the infrared spectrum are similar to the spectrum of the $\{Mo_{132}\}$ type spherical clusters [9].

Raman spectrum

The vibration bands of Raman spectrum (Fig. 2) (in cm^{-1}) are: 974(m) $\nu_s(SO_4)$, 946(m) $\nu_s(M=O)$, 876(vs) and 838(vs) $\nu_s(Mo-O_{br}-Mo)$, 378(w), 312(w).

The three characteristic medium, strong and very strong bands, registered at 946, 876 and 838 cm^{-1} , are assigned to the $\nu_s(Mo-O_t)$, $\nu_{as}(Mo-O_t)$, and $\nu_s(Mo-O_{br}-Mo)$ vibrations, respectively. The last two bands in the Raman spectrum of $\{Mo_{132}-U^{IV}\}$ compound are due to the splitting process of the band from 878 cm^{-1} of the $\{Mo_{132}-sulphate\}$ cluster. This splitting is due to the distortions in the MoO_6 octahedra upon coordination of the uranium(IV) ions [12].

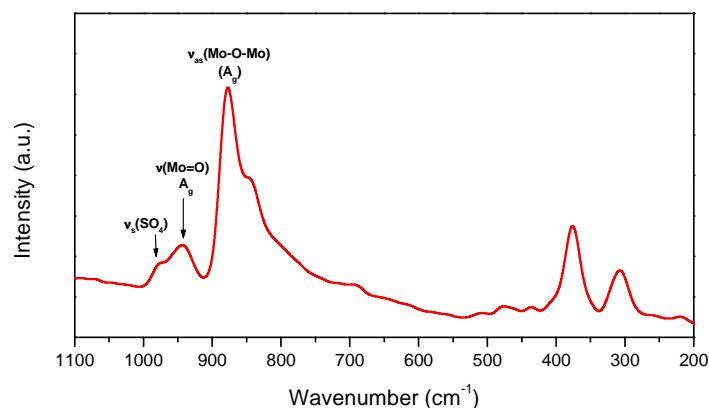


Figure 2. Raman spectrum of the $\{\text{Mo}_{132}\text{-U}^{\text{IV}}\}$ cluster.

Electronic spectra

UV spectrum

The absorption bands (in nm/cm⁻¹) and their assignments are: ν_1 between 229.5/43572 (sh) and 267/37453 (sh) (CT) Mo-O_{br}-Mo and ν_2 at 208.5 / 47961 (CT) Mo-O_t.

The UV spectra of polyoxometallate clusters generally exhibit two charge-transfer (CT) bands, characteristic to the polyoxoanionic framework and assigned to oxygen-to-metal-transitions [13, 14].

In the UV spectrum of the $\{\text{Mo}_{132}\text{-U}^{\text{IV}}\}$ cluster, the broad ν_1 CT band is reduced to two shoulders at 229.5/43572 (sh) and 267/37453 (sh), due to the $d_{\Pi}\text{-p}_{\Pi}\text{-d}_{\Pi}$ transitions from the three center Mo-O_{br}-Mo modes. Due to the $d_{\Pi}\text{-p}_{\Pi}$ transitions of the Mo-O_t bonds, the sharper ν_2 CT band has the maximum value positioned at 208.5 nm (47961 cm⁻¹). The in-spectrum presence of the two shoulders indicates that the cluster anion has nonequivalent Mo-O_{br}-Mo bonds, caused by the U^{IV} ion coordination.

Vis-NIR spectrum

In polyoxometallates with reduced addenda, new intervalence charge-transfer (IVCT) bands arise in the visible and NIR domains. In most cases, three IVCT bands are observed, marked by A, B and C [15, 16]. For the $\{\text{Mo}_{132}\text{-U}^{\text{IV}}\}$ cluster, the reduced addendum is the Mo^V metal centre, which yields in the presence of the homo-nuclear IVCT Mo^V→Mo^{VI} C band. The recorded spectrum shows a strong absorption over the entire visible domain, which extends in NIR and accounts for the dark brown color of the substance, in both solid state and solution.

The absorption bands (in nm/cm⁻¹) and their assignments are: 457/21881 homo-nuclear IVCT band C $Mo^V \rightarrow Mo^{VI}$ (Fig. 3a) (this band is present also in Mo_{132} -sulphate at 455/21978), 795.5/12570 and 1143/8748 (hetero-nuclear IVCT bands A and B, $U^{IV} \rightarrow Mo^{VI}$) (Fig. 3 b).

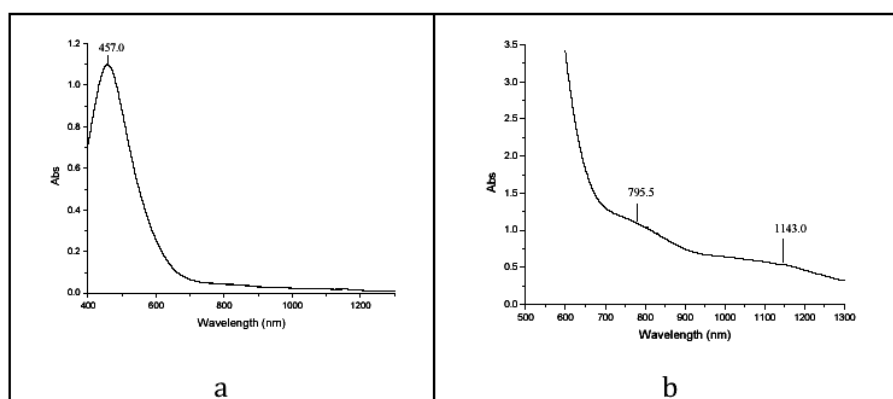


Figure 3. Vis-NIR absorption electronic spectrum of $\{Mo_{132}-U^{IV}\}$ in aqueous solution ($c=5 \cdot 10^{-4}$ mol L⁻¹). a-homo-nuclear IVCT band,C; b-hetero-nuclear IVCT bands A, B.

The heteronuclear broad A IVCT band, located in NIR at 1143 nm (8748 cm⁻¹), as well as the B IVCT band, recorded at 795.5 nm (12570 cm⁻¹) and the intense homo-nuclear C IVCT band cover the f-f electron transfer (ET) bands, characteristic to the U^{4+} ion (of f^2 electron configuration) in cubic field. These ET bands, specific to the ${}^3H_4 \rightarrow {}^3P_2$, ${}^3H_4 \rightarrow {}^1I_6$, ${}^3H_4 \rightarrow {}^3P_1$, ${}^3H_4 \rightarrow {}^1D_2$ (1G_4) and ${}^3H_4 \rightarrow {}^3P_0$ transitions, would have been expected at approximately 423, 496, 565, 647 and 689.6 nm (23600, 20160, 17670, 15440 and 14500 cm⁻¹). [17]

Magnetic susceptibility measurements

The monomeric character of the $\{Mo_{132}-U^{IV}\}$ cluster is confirmed by the magnetic susceptibility measurements. In the temperature range of 135÷290 K, the values of the magnetic susceptibility corresponds to a Curie-Weiss behavior. The magnetic susceptibility data were corrected for diamagnetic and temperature-independent paramagnetic (TIP) contributions, both calculated from the tabulated values from the diamagnetic cluster ($\chi_0=2.73 \cdot 10^{-3}$ emu/mol). Figure 4 shows the dependence of the reverse of the molar susceptibility ($\chi-\chi_0$) vs temperature.

The experimental data were fitted using the following equation [18]:

$$\chi_m = \frac{N\mu_B^2\mu_{eff}^2}{3kT} + \chi_0 \quad (1)$$

The obtained effective magnetic moment is $\mu_{eff} = 2.83 \mu_B$ and indicates that the uranium ion is in the oxidation state +4 [19]. Such low value is obtained when the uranium(IV) ion is in a high symmetry environment, particularly in a local cubic symmetry, with 3H_4 ground state. [20]

At relatively low temperatures, the uranium ions are well separated and do not interact. The nine-fold degenerated ground state 3H_4 of the uranium $5f^2$ electrons split into Γ_1 , Γ_3 , Γ_4 and Γ_5 levels by the eightfold cubic crystal field of oxygen ions around the uranium ion. The temperature-independent para-magnetism is big enough ($\chi_0 = 2.73 \cdot 10^{-3}$ emu/mol). This value suggests that Γ_1 is the lowest level [18]. This is in accordance with the fact that for this uranium(IV) complex we have not obtained any electron paramagnetic spectrum at room temperature and liquid nitrogen temperature.

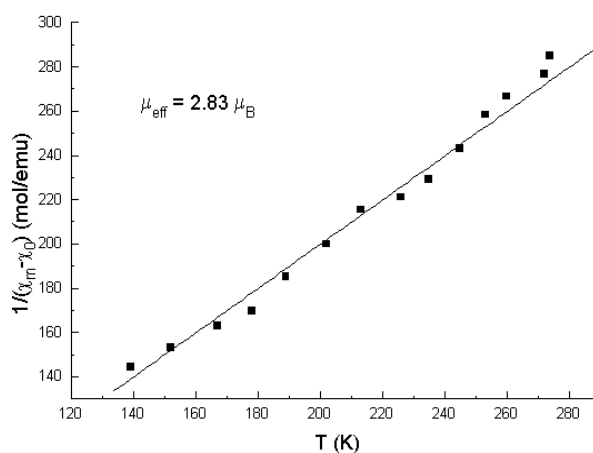


Figure 4. The $1/\chi$ vs T curve for $\{Mo_{132}-U^{IV}\}$ cluster.

EPR spectrum

The powder EPR spectrum of the compound $\{Mo_{132}-U^{IV}\}$ obtained in X band at room temperature (Fig. 5) exhibits the most intense signals in the 3250–3400 G region.

The main values of the gyro-magnetic tensor, slightly decreased below the free electron $g_0 = 2.0023$ value, indicate that the obtained spectrum is the contribution both of U^{IV} and Mo^V ions. [21]. The fine structure of the EPR spectrum can be interpreted by considering one $S_{eff} = 1$ effective spin for the uranium(IV) ion and a Γ_5 sublevel of the 3H_4 multiplet as ground state [22, 23].

The shape of the ESR spectrum can be interpreted by considering one $S_{eff} = 1$ effective spin state of the uranium (IV) non-Kramers ion. In a cubic crystalline field, the degeneracy of the ground state 3H_4 is partially removed to $\Gamma_1(1)$, $\Gamma_4(3)$, $\Gamma_3(2)$, $\Gamma_5(3)$ levels. The lowest level is either Γ_5 or Γ_1 , but only the first of them is EPR active [24].

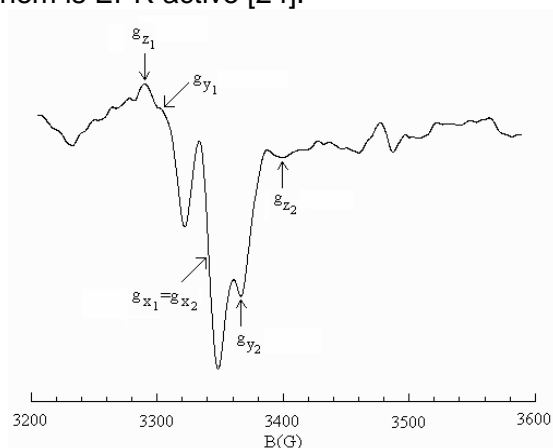


Figure 5. EPR spectrum of the $\{M_{132}-U^{IV}\}$ cluster at room temperature.

Owing to the fact that we have obtained an EPR spectrum even at room temperature, we conclude that the Γ_5 multiplet is energetically the lowest and may be described by an effective $S_{eff} = 1$ spin.

The resonance B values of the fine structure signals ($B_{z1} = 3284$ G, $B_{y1} = 3306$ G, $B_{x1} = B_{x2} = 3342$ G, $B_{y2} = 3366$ G, $B_{z2} = 3408$ G) indicate a small orthorhombic distortion from the cubic symmetry. The main values of the gyromagnetic tensor g ($g_x = 1.922$, $g_y = 1.940$, $g_z = 2.005$) and the zero-field splitting parameters ($D = 18.31 \cdot 10^{-4} \text{ cm}^{-1}$, $E = 5.99 \cdot 10^{-4} \text{ cm}^{-1}$) were calculated with the usual procedure for $S = 1$ systems. [24] This result confirms that every U^{IV} ion is surrounded by eight oxygen ions, arranged like a basis for anti-prismatic configurations. The orthorhombic EPR spectrum proves that the 5f electrons are trapped at the uranium sites, indicating the dominance of the spin-orbit coupling.

CONCLUSIONS

The paper reports the synthesis and structural investigation of the new $(NH_4)_{60}\{U_3\{Mo^{VI}\}Mo_5^{VI}O_{21}(H_2O)_6\}_{12}\{Mo_2^{VO_4}(SO_4)\}_{30}\} \cdot 308H_2O$ nano-sized inorganic cluster.

The vibration bands of the FT-IR and Raman spectra are characteristic to the $\{Mo_{132}\}$ spherical clusters framework.

The UV spectrum shows two charge-transfer (CT) bands recorded at 229.5 - 267 and 208.5 nm, specific to the polyoxometalate edifice.

The Vis-NIR spectrum exhibits three inter-valence charge-transfer (IVCT) bands, owing to the presence of the Mo^V metal centre, as a reduced addendum. The Mo^V - Mo^{VI} homo-nuclear IVCT band and U^{IV} - Mo^{VI} hetero-nuclear IVC bands are recorded at 457, 795.5 and 1143 nm. These bands were superposed over the f - f electron transfer bands characteristic to the U^{4+} ions.

Magnetic susceptibility measurements demonstrate that the uranium ions are well separated and display no interaction. The obtained effective magnetic moment is $\mu_{eff} = 2.83 \mu_B$ and it indicates that the uranium ion is in the oxidation state +4 in a high symmetry environment, particularly in a cubic local symmetry, with 3H_4 ground state.

The EPR spectral data indicate a small orthorhombic distortion from the cubic symmetry for U^{IV} ions and confirms that every U^{IV} ion is surrounded by eight oxygen ions, arranged like the basis for anti-prismatic configurations.

Based on these results, we propose in Fig. 6 a schematic representation of the uranium ions coordination to the ligand, similar to the one related to Ce^{III} ions, as shown in the literature [9].

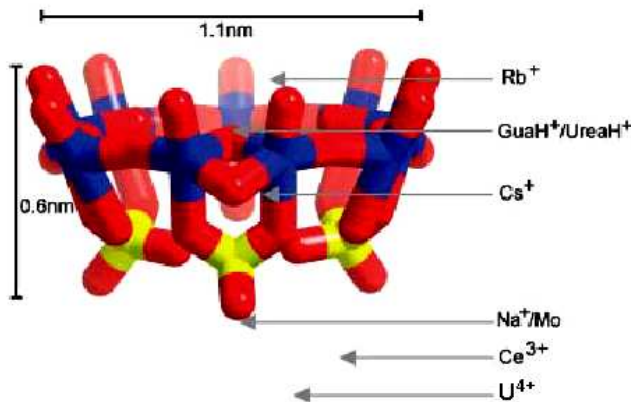


Figure 6. The relative positions of all the fixed substrates in one of the 20 channels [9], color code: Mo blue, O red, S yellow, other respective substrates/cations in different color.

Three U^{IV} cations are disordered over 30 equivalent positions forming an icosidodecahedron, where each underoccupied uranium center is coordinated symmetrically in a bidentate fashion to two O atoms of a SO_4^{2-} bidentate ligand and by four O atoms of the $\{H_2O\}_{60}$ - type shell, as well as two O atoms of the $\{H_2O\}_{20}$ - type shell as ligands, thus forming an anti-prismatic - type coordination [10].

EXPERIMENTAL SECTION

Materials

Reagent grade chemicals were used and all syntheses and studies were carried out in distilled water.

Syntheses

The ammonium salt of the novel uranium(IV) cluster {Mo₁₃₂-U^{IV}} was prepared in two steps, as follows:

Synthesis of (NH₄)₄₂[Mo^{VI}₇₂Mo^V₆₀O₃₇₂(CH₃COO)₃₀(H₂O)₇₂] · 300 H₂O abbreviated as {Mo₁₃₂-acetate}

The substance was prepared according to the procedure described in the literature [1] and was characterized by FT-IR spectrum.

Synthesis of (NH₄)₆₀{U₃{(Mo^{VI})Mo^V₅O₂₁(H₂O)₆}₁₂{Mo^V₂O₄(SO₄)₃₀} · 308H₂O abbreviated as {Mo₁₃₂-U^{IV}}

A sample of U(SO₄)₂ (10.0 g, 23.2 mmol) was added after 1.5 hours to a refluxing solution of {Mo₁₃₂-acetate} (5.0 g., 0.18 mmol) and ammonium sulphate (15 g, 113.5 mmol) in H₂O (400 mL). The resulting solution was refluxed for 30 minutes and filtered hot. After three days, dark brown crystals of {Mo₁₃₂-U^{IV}} appeared, which were collected by filtration over a sinterized glass frit, washed with ice-cold 2-propanol, and dried in air. Yield: 4.40 g (0.146 mmol) 78% based on {Mo₁₃₂-acetate}.

Elemental analyses (%) calcd: U 2.37, N 2.78, S 3.18, Mo 42.02; found: U 2.12, N 2.90, S 3.26, Mo 42.00.

Methods and instrumentation

ICP-AES (Inductive Coupled Plasma Atom Emission Spectroscopy) was used for the elemental analysis of uranium and molybdenum. The nitrogen and sulphur were analyzed with a Vario EL device. The crystallization water content was determined by means of the difference between the initial sample and the weight of sample after being heated for 30 minutes at 120°C.

A FTIR-JASCO 610 spectrophotometer was used to record IR spectra for samples pelleted in KBr.

Raman spectra were performed on a Bruker FTIR IFS 66 with a Raman FRA 106 unit spectrophotometer ($\lambda_e=1064$ nm), using solid compound powders.

UV-Vis spectra were recorded on a JASCO V-670 spectrophotometer in aqueous solutions having concentrations of 10⁻⁵ M and 10⁻³ M.

EPR spectra were performed on powder of the compound, at room temperature, at 9.4 GHz (X band) using a standard JOEL-JES-3B equipment.

Magnetic susceptibility measurements were performed in the 135-290 K temperature range with a Faraday balance.

REFERENCES

1. A. Müller, E. Krickemeyer, H. Bögge, M. Schmidtman, F. Petres, *Angew. Chem. Int. Ed.*, **1998**, *37*, 3360.
2. De-L. Long, L. Cronin, *Chem. Eur. J.*, **2006**, *12*, 3698.
3. A. Müller, P. Peters, M.T. Pope, D. Gatteschi, *Chem Rev.*, **1998**, *98*, 239.
4. M.T. Pope, A. Müller, *Angew. Chem. Int. Ed. Engl.*, **1991**, *30*, 34.
5. M.T. Pope, A. Müller, "Polyoxometalates. From Platonic Solids to Anti-Retroviral Activity", Kluwer Academic Publishers, Dordrecht, The Netherlands, **1994**, pp. 1, 109.
6. A. Müller, P. Kögerler, C. Kuhlmann, *Chem. Comm.*, **1999**, 1347-1358.
7. A. Müller, *Science*, **2003**, *300*, 749-750.
8. A. Müller, E. Krickemeyer, H. Bögge, M. Schmidtman, S. Roy, A. Berkle, *Angew. Chem. Int. Ed.*, **2002**, *41*, 3604.
9. A. Müller, S.K. Das, S. Talismanov, S. Roy, E. Beckmann, H. Bögge, M. Schmidtman, A. Merca, A. Berkle, L. Allouche, Y. Zhou, L. Zhang, *Angew. Chem. Int. Ed.*, **2003**, *42*, 5039.
10. A. Müller, Y. Zhou, L. Zhang, H. Bögge, M. Schmidtman, M. Dressel, J. van Slageren, *Chem. Commun.*, **2004**, 2038.
11. C. Rocchiccioli-Deltcheff, R. Thouvenot, *Spectrochim. Acta*, **1976**, *32A*, 587.
12. C. Rocchiccioli-Deltcheff, C. Fournier, M. Franck, R. Thouvenot, *Inorg. Chem.*, **1983**, *22*, 46.
13. S. Hyunsoo, M.T. Pope, *Inorg. Chem.* **1972**, *11*, 1441.
14. X. Zhang, G. Chen, D.C. Duncan, R.J. Lachicotte, C.L. Hill, *Inorg. Chem.*, **1997**, *36*, 4381.
15. J.M. Fruchart, G. Hervé, J.P. Launay, R. Massart, *J. Inorg. Nucl. Chem.*, **1976**, *38*, 1627.
16. G.M. Varga, E. Papaconstantinou, M.T. Pope, *Inorg. Chem.*, **1970**, *9*, 662.
17. P. Gans, B.J. Hathway, B.C. Smith, *Spectrochim. Acta*, **1965**, *21*, 1589.
18. O. Vogt, K. Mattenberger, J. Löhle, J. Rebizant, *J. of Alloys and Comp.*, **1998**, *271-273*, 508.
19. C. A. Hutchison Jr., G. A. Candela, *J. Chem. Phys.*, **1957**, *27*, 707.
20. B. Jezowska-Tezebiatowska, *J. Chem. Phys.*, **1963**, *60*, 48.
21. Jing - Yang Niu, Xiao - Zeng You, Chun -Ying Duan, *Inorg. Chem.*, **1996**, *35*, 4211.
22. A. Abragam and B. Bleaney, *Electron Paramagnetic Resonance of Transition Metal Ions*, Clarendon Press, Oxford, **1980**, p. 354.
23. I. Ursu, *Magnetical Resonance of uranium compounds*, Acad. RSR, Bucuresti, **1979**, pp. 189.
24. D. Gourier, D. Caurant, T. Arliguie, M. Ephritikhine, *J. Am. Chem.Soc.*, **1998**, *120*, 6084.

BIOSORPTION OF Cd²⁺ IONS BY IMMOBILIZED CELLS OF *SACCHAROMYCES CEREVISIAE*. ADSORPTION EQUILIBRIUM AND KINETIC STUDIES

TONK SZENDE^a, CERASELLA INDOLEAN^b, SILVIA BURCĂ^b,
ANDRADA MĂICĂNEANU^{b,*}, KOCSIS BELA^c, CORNELIA MAJDIK^b

ABSTRACT. Biosorption of cadmium (II) ions from aqueous solution onto immobilized cells of *Saccharomyces cerevisiae* was investigated. Equilibrium and kinetic studies were conducted taking into consideration the effect of initial cadmium (II) concentration. The obtained results showed that the uptake of heavy metal increases with an increase of initial cadmium (II) concentration. Langmuir and Freundlich isotherm models were used to analyze the equilibrium data. Based on correlation coefficients, it has been concluded that the Langmuir isotherm is more suitable to describe the cadmium biosorption equilibrium data. First and pseudo-second order kinetic models were applied to describe the biosorption process. It was found that the kinetics data fitted well the pseudo second order model.

Keywords: biosorption, cadmium, *Saccharomyces cerevisiae* cells, adsorption isotherm, kinetics

INTRODUCTION

The presence of industrial effluent containing heavy metals into freshwater poses serious problems to the ecological system including humans as they are toxic even at low concentrations [1,2]. One of the most common toxic metals found in industrial effluents is cadmium. It may come from various industrial sources such as electroplating, fertilizers, mineral processing and battery manufacturing [3,4].

The removal of this metal from waters and industrial wastewaters has become a challenge for researchers. Many studies confirm that various biological materials including fungi, algae, bacteria and yeast could be used in

^a Sapientia University, Faculty of Sciences and Arts, 4, Matei Corvin Str., RO-400112 Cluj-Napoca, Romania, tonk.szende@sapientia.ro

^b Babeş-Bolyai University, Faculty of Chemistry and Chemical Engineering, 11, Arany Janos Str., RO-400028 Cluj-Napoca, Romania, andrada@chem.ubbcluj.ro

^c Pécsi Tudományegyetem, Általános Orvostudományi Kar, Szigeti út 12, HU - 7624 Pécs, Magyarország, Bela.Kocsis@aok.pte.hu

biosorption process to remove metal ions in wastewater [5,6.] The biosorption process is a passive uptake that utilizes cell wall of biomass to sequester the metal ions from aqueous solutions [7,8]. The presence of functional groups on biomass cell wall such as carboxyl, hydroxyl, ketones and amino groups will involve a physical-chemical interaction between the metal ions during the biosorption processes [9]. Metal uptake is dependent not only on the type of species of microorganism, but also on growth conditions. Growth conditions considerably influence the composition of all yeast and thereby the binding abilities of cells for metal ions also. Since cell wall structure and the metabolic state of the cell depend on substrate composition, the growth in different media should influence the capacity and selectivity of metal uptake by creating other binding sites or diverse enzymatic system within the cell [10,11].

Cell immobilization is one of the methods used to overcome the incorporating free suspended cell in industrial operations. It offers several advantages including minimal clogging in continuous systems, is easy to separate from the reaction system and can be regenerated and reused the immobilized cells for a few cycles [3]. Natural polymers mostly used, as the matrix for the immobilization of cells is the alginate.

This study was carried out in order to determine the potential of immobilized living cells of *Saccharomyces cerevisiae* (DSM 1333) to adsorb cadmium (II) ions. Langmuir and Freundlich adsorption isotherms were used to correlate the equilibrium adsorption data, while first and pseudo-second order kinetic models were applied to describe the biosorption process.

RESULTS AND DISCUSSION

Cadmium biosorption

The biosorption of cadmium ions on the pure *Saccharomyces cerevisiae* strain (DSM 1333) in immobilized form was investigated in biosorption equilibrium experiments. The effect of initial cadmium ions concentration on the biosorption capacity of Cd^{2+} onto immobilized cells was studied.

Initial cadmium concentration influence over the equilibrium adsorption capacities (maximum adsorption capacity for specific working conditions) obtained during Cd^{2+} adsorption experiments is presented in Figure 1. Equilibrium adsorption capacities increase from 0.2197 mg Cd^{2+} /g for the initial 4.82 mg Cd^{2+} /L to 3.7825 mg Cd^{2+} /g for the initial 99.75 mg Cd^{2+} /L. These results suggest that the *Saccharomyces cerevisiae* cells we used as biosorbent have high capacity for heavy metal biosorption.

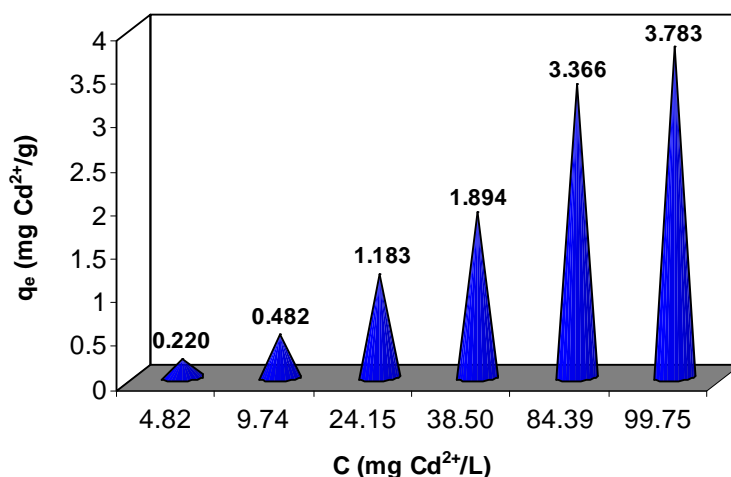


Figure 1. Initial cadmium concentration influence over the equilibrium adsorption capacities obtained during Cd²⁺ adsorption experiments.

Equilibrium isotherm models

Langmuir and Freundlich models were used to determine the sorption equilibrium between the biosorbent and metal ions.

The Langmuir model assumes that a monomolecular layer is formed when biosorption takes place without any interaction between the adsorbed molecules [12]. Freundlich isotherm is an empirical equation based on a heterogeneous adsorption due to the diversity of adsorption sites or diverse nature of the adsorbed metal ions, free or hydrolyzed species [13].

The Langmuir isotherm equation has a hyperbolic form:

$$q_e = \frac{q_{\max} \cdot b \cdot C_e}{1 + b \cdot C_e} \quad (2)$$

where, q_e is the solid-phase adsorbate concentration at equilibrium (mg/g), q_{\max} is the maximum adsorption capacity corresponding to the monolayer adsorption capacity (mg/g),

C_e is the concentration of Cd²⁺ solution at equilibrium (mg/L), and b is related to the strength of adsorbent-adsorbate affinity.

The linear form of the Langmuir isotherm, eq. (2), is expressed as:

$$\frac{1}{q_e} = \frac{1}{q_{\max} \cdot b} \cdot \frac{1}{C_e} + \frac{1}{q_{\max}} \quad (3)$$

From the $1/q_e$ vs. $1/C_e$ plot, Figure 2, $q_{\max} = 2.713$ mg Cd²⁺/g and $b = 1.936$ L/mg were calculated. Langmuir isotherm model describes well the experimental values (q_e and C_e), Figure 3.

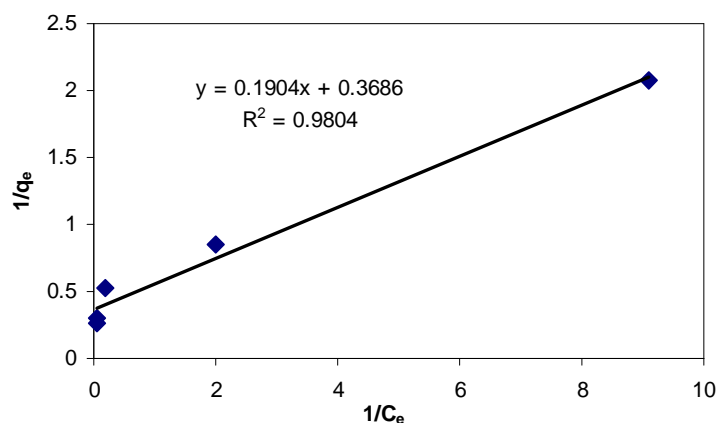


Figure 2. Langmuir adsorption model for cadmium biosorption on immobilized biomass.

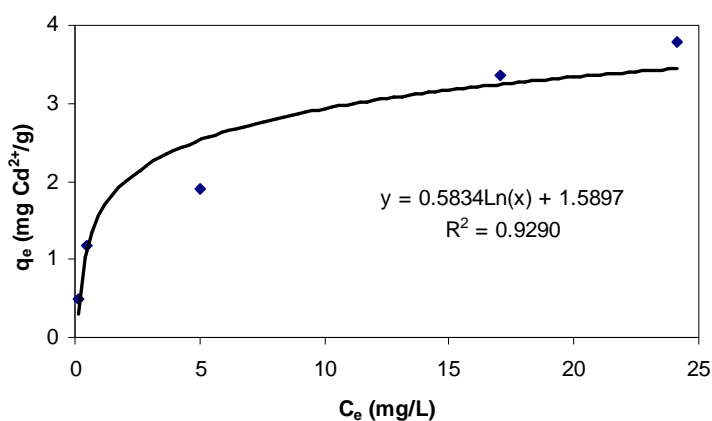


Figure 3. Langmuir adsorption isotherm for cadmium biosorption on immobilized biomass.

The empirical Freundlich isotherm equation given by eq. (4), while its logarithmic form (linear) is given by eq. (5):

$$q_e = k \cdot C_e^{(1/n)} \quad (4)$$

$$\log q_e = \log k + \frac{1}{n} \cdot \log C_e \quad (5)$$

where, k is related to adsorption capacity, and n is related to intensity of adsorption.

From the $\log q_e$ vs. $\log C_e$ linear plot, (figure not shown), we determined a correlation coefficient of 0.9600, which is smaller than that obtained for the Langmuir model, 0.9804. Therefore we concluded that cadmium biosorption on immobilized biomass is better described by the Langmuir isotherm.

Kinetic models

The kinetic of heavy metal ions biosorption is usually described by two different kinetic models, i.e. the first- and second order [14,15].

The first-order rate equation may be represented as follows:

$$\frac{dq_t}{dt} = k_1(q_e - q_t) \quad (6)$$

Integrating eq. (6) from the boundary conditions $t = 0$ to $t = t$ and $q_t = 0$ to $q_t = q_t$, gives:

$$\ln(q_e - q_t) = \ln q_e - k_1 t \quad (7)$$

where q_e and q_t are the amounts of cadmium adsorbed (mg/g) at equilibrium and time t , respectively, and

k_1 is the rate constant of first order adsorption (1/min).

In order to determine the rate constant and equilibrium cadmium uptake, the straight line plots of $\ln(q_e - q_t)$ against t , eq. (7), were made at five different initial cadmium concentrations. Correlation coefficients obtained in this case were under 0.9 (figure not shown).

The pseudo second order kinetic model may be expressed as:

$$\frac{dq_t}{dt} = k_2(q_e - q_t)^2 \quad (8)$$

Integrating eq. (8) from the boundary conditions $t = 0$ to $t = t$ and $q_t = 0$ to $q_t = q_t$, gives:

$$\frac{1}{(q_e - q_t)} = \frac{1}{q_e} + k_2 t \quad (9)$$

where, q_e and q_t as above, and

k_2 is the rate constant of pseudo second order adsorption (g/mg·min).

Equation (9) can be rearranged in a linear form, as follows:

$$\frac{t}{q_t} = \frac{1}{k_2 q_e^2} + \frac{t}{q_e} \quad (10)$$

In order to determine the rate constant and equilibrium cadmium uptake, the straight line plots of t/q_t against t , eq. (10), were made at five different initial cadmium concentrations. Correlation coefficients between 0.9941 and 0.9998 were obtained (Figure 5 and Table 1).

If we compare correlation coefficient for the first and pseudo second order models, we can conclude that cadmium biosorption on immobilized biomass can be classified as pseudo second order, fact confirmed by the literature data [16].

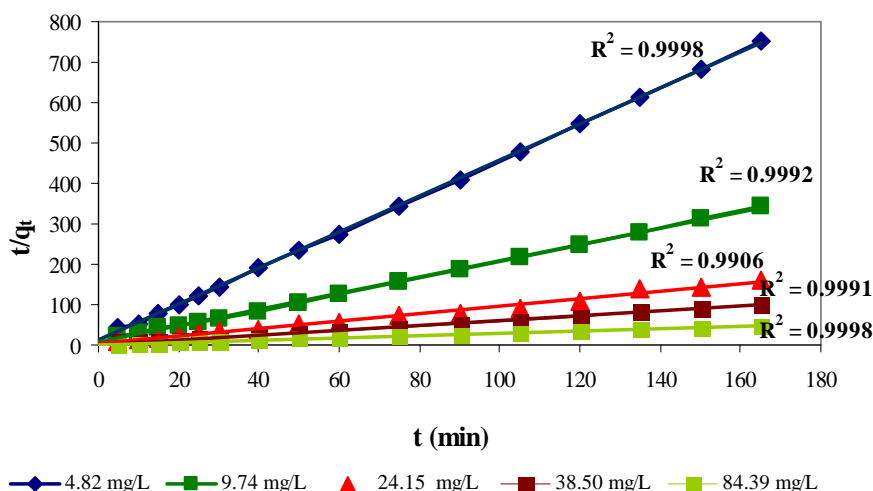


Figure 4. Correlation of the experimental data using the pseudo second order model for cadmium biosorption on immobilized biomass.

Table 1. Second order adsorption kinetic parameters.

C_0 , (mg Cd ²⁺ /L)	q_e (exp), (mg Cd ²⁺ /g)	q_e (calc), (mg Cd ²⁺ /g)	k_2 , (g/mg·min)	R^2
4.82	0.220	0.224	1.80	0.9998
9.74	0.482	0.496	0.59	0.9992
24.15	1.183	1.084	0.23	0.9906
38.50	1.894	1.720	0.17	0.9991
84.39	3.366	3.433	0.11	0.9998

CONCLUSIONS

The ability of immobilized cells (DSM 1333) to adsorb cadmium (II) ions from aqueous solution was investigated. The obtained results showed that the uptake of heavy metal increases with an increase of initial cadmium (II) concentration. Cadmium adsorption capacity increases with an increase of the initial cadmium (II) concentration suggesting that the *Saccharomyces cerevisiae* cells we used have high capacity for heavy metal biosorption. The biosorption of metal ions studied is a rapid process and often reaches equilibrium within three hours; the maximum biosorption capacity was calculated to be 3.7825 mg Cd²⁺/g yeast.

Langmuir and Freundlich adsorption isotherms were used to correlate the equilibrium adsorption data. The cadmium ions biosorption by immobilized *Saccharomyces cerevisiae* cells is well described by the Langmuir isotherm model.

Also, first and pseudo-second order kinetic models were applied to describe the biosorption process. Based on mathematical calculations carried out, it was found that the kinetics data fitted well the pseudo-second order model and the parameters for this kinetic were determined.

EXPERIMENTAL SECTION

Microorganism, media and culture conditions

Saccharomyces cerevisiae (DSM 1333) yeast was used in this study. The yeast was provided by University of Pécs Medical School, Department of Medical Microbiology and Immunology (Hungary), in the lyophilized form. The composition of growth medium was Müller-Hinton substrate (3% glucose, pepton, yeast-extra, NaCl, pH=7). The medium was sterilized by autoclaving at a pressure of 1.5 atm and temperature of 121°C for 20 minutes. The pure yeast culture grown in an incubator at 30°C, 200 rpm for 48 hours (New Brunswick Scientific). During the process the growth of yeast was controlled by measuring the absorbance of the culture. After completion of the yeast production the suspension was centrifuged 4500 rpm for 30 minutes, and two times washed with steril PBS (phosphate-buffer solution). Cells were then lyophilized and used in this form for all trials [17,18].

Biosorbent immobilization

The cross-linking procedure with calcium alginate that we used, is the current method for immobilization of biomass [19].

The immobilization of yeast was carried out as follows: 2 g of lyophilized biosorbent was suspended in 50 ml distilled water. This suspension was next blended with a mixture formed from 1g sodium-alginate and 2 ml ethanol. The mixture was then dropped with a peristaltic pump into a solution containing 0.2 M CaCl₂. During this process, the drops of alginate-biomass mixture were gelled into beads with a diameter of 4.0±0.2 mm. The Ca-alginate immobilized yeast beads were stored in 0.2 M CaCl₂ solution at 4°C for 1 hour to cure and to form the cross-linking bonds. The beads were rinsed with distilled water to remove the excess of calcium ions and stored at 4°C prior to use.

Cadmium solution preparation

The stock cadmium solution was prepared by dissolving Cd(NO₃)₂×4H₂O of analytical grade reagent in an appropriate amount of distilled water. Cadmium solutions of different concentration (4.82, 9.74, 24.15, 38.5, 84.39 and 99.75 mg/L) were obtained by diluting the stock solution. The concentration of Cd²⁺ ions from different samples was determined using a flame atomic absorption spectrophotometer (SensAA Dual GBS Scientific Equipment, Australia).

Biosorption studies

The immobilized pure yeast biomass was contacted with 100 ml of initial cadmium solution. The reaction mixture was agitated at 875 rpm on a magnetic stirrer at room temperature (20°C) in isothermal conditions, pH 6.8-7.2, for 3 hours.

Kinetics studies were performed using different concentrations of cadmium solutions (4.82, 9.74, 24.15, 38.50, 84.39, 99.75 mg/L).

In order to determine the exact concentration of cadmium ions and establish the evolution of the removal process, samples of 100 µL from the supernatant were collected at different time intervals.

The amount of cadmium (II) ions bound by biosorbent was calculated using the following equation:

$$q_t = \frac{(C_0 - C_t)}{w} \cdot \frac{V}{1000} \quad (1)$$

where, q_t is time t adsorption capacity (mg/g),

C_0 is the initial cadmium concentration (mg/L),

C_t is time t cadmium concentration (mg/L),

$V = 100$ ml, and

w is the quantity of the adsorbent (g).

ACKNOWLEDGMENTS

The authors would like to thank to Hungarian Academy of Science for financial support of this study.

REFERENCES

1. M. D. Mashitah, Y. Yus Azila, S. Bhatia, *Bioresource Technology*, **2008**, 99, 4742.
2. E. Malkoc, Y. Nuhoglu, *Journal of Hazardous Materials*, **2005**, B 127, 120.
3. M. Y. Arica, Y. Kacar, O. Genc, *Bioresource Technology*, **2001**, 80, 121.
4. J. Wase, C. Forster, *Biosorbents for Metal Ions*, Taylor&Francis Ltd., **1997**, 4, 67.
5. C. C. V. Cruz, A.C.A. Da Costa - Henriques, C. A. Luna, *Bioresource Technology*, **2004**, 91, 249.
6. A. Kapoor, T. Viraraghavan, D. R. Cullimore, *Bioresource Technology*, **1999**, 70, 95.
7. T. Viraraghavan, J. Jegan, K. Palanivelu, M. Velan, *Chemosphere*, **2005**, 60, 419.
8. A. Y. Dursun, A. Y., *Biochemical Engineering Journal*, **2006**, 28, 187.
9. G. M. Gadd, *Microbes in Extreme Environments*. Academic Press, London, **1987**, 84.
10. G. Bayramoglu, S. Bektas, M. Y. Arica, *Journal of Hazardous Materials*, **2003**, B 101, 285.

BIOSORPTION OF Cd²⁺ IONS BY IMMOBILIZED CELLS OF SACCHAROMYCES CEREVISIAE

11. P. Dostalek, M. Patzak, P. Matejka, *International Biodeterioration & Biodegradation*, **2004**, 54, 203.
12. Z. Asku, *Process Biochemistry*, **2002**, 38, 89.
13. C. Namasivayam, D. Sangeetha, *Adsorption*, **2006**, 12, 103.
14. V. Padmavathy, *Bioresource Technology*, **2008**, 99, 3100.
15. Y. Azila, M.M. Don, S. Bhatia, *Journal of Hazardous Materials*, **2009**, 161, 189.
16. P. Vasudevan, V. Padmavathy, S. C. Dhingra, *Bioresource Technology*, **2003**, 89, 281.
17. P. Dostalek, M. Patzak, P. Matejka, *International Biodeterioration & Biodegradation*, **2004**, 54, 203.
18. N. Goyal, S.C. Jain, U.C. Banerjee, *Advances in Environmental Research*, **2003**, 7, 311.
19. S. Schiewer, E. Fourest, K. H. Chong, B. Volesky, *Biohydrometallurgical Processing*, **1995**, 2, 219.

THE TESTING AND CALIBRATION OF A ROTATING RHEOMETER

NICU BORȘ^a, ANDRA TĂMAȘ^b

ABSTRACT. The testing and calibration of the rotating viscometer were done by direct measurement of some standard liquids viscosity - aqueous glycerol or ethylene glycol solutions- and comparison with data measured on a standard viscometer (Rheotest). Formulas are presented for physical data that define the liquids rheological behavior: shear rate $\dot{\gamma}$, shear stress τ and viscosity η , particularized for this rheometer. Also, it was established the correction factor for the rotor end effect.

Keywords: gap, rotating viscometer, shear rate, shear stress, viscosity

INTRODUCTION

The rheometer (modified Couette type) subject to testing and calibration, consists of two coaxial glass cylinders. The inner cylinder is rotated and the fluid of whose rheological behavior is to be studied is placed in the ring-shaped space (gap) between the two cylinders. This will produce a certain torsional motion of the outer cylinder (Figure 1a, b and Figure 2) [1-4].

The functioning of the device is based on the following scheme (Figure 1b):

- the inner cylinder is rotated by means of an external drive with rotation speed n and angular velocity Ω , respectively;
- the outer cylinder, fixed to an elastic joint through a rubber muff, can be rotated by driving the liquid placed in the gap with a central angle $\Delta\theta$;
- the correlation between the shear stress τ and the torsion moment M , is done by using a calibration chart, $\Delta\theta = f(M)$;
- the prescribed variable is angular velocity Ω or revolution n ;
- the measured variable is central angle $\Delta\theta$ proportional to shear stress τ .

In the calculations, instead of angular velocity Ω revolution n is used and central angle $\Delta\theta$ is expressed by the corresponding circle arc.

^a Dinkelberg Analytics GmbH, Germany, nicu.bors@online.de

^b Polytechnic University of Timisoara, Faculty of Chemical and Environmental Engineering, P-ța Victoriei Nr. 2, RO-300006 Timisoara, Romania, andra.tamas@chim.upt.ro

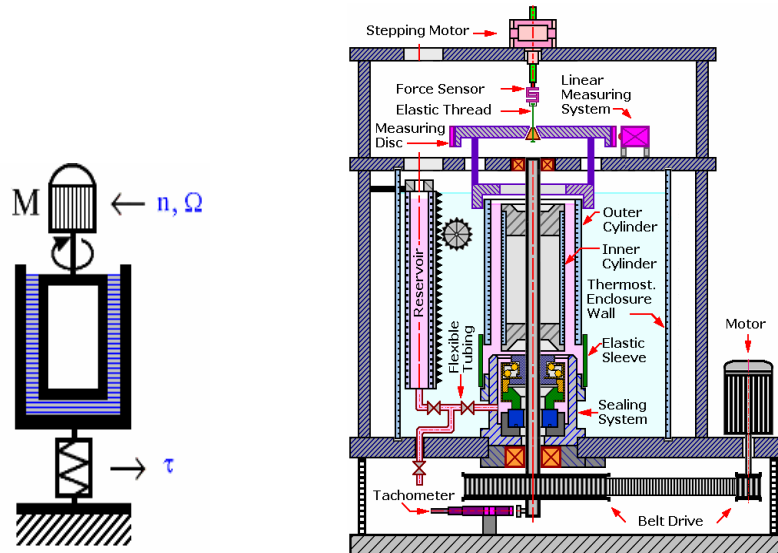


Figure 1 a,b. The Couette modified rheometer.

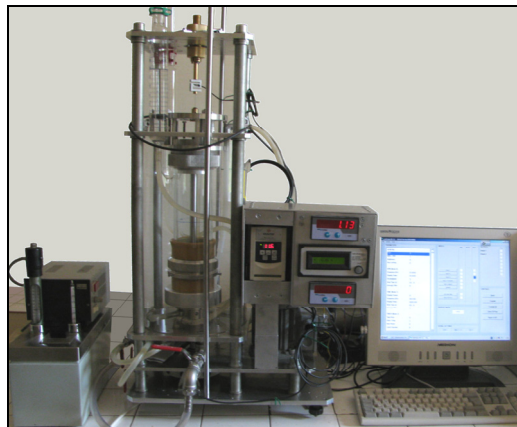


Figure 2. The achieved and tested experimental device.

RESULTS AND DISCUSSION

The calibration of the rheometer was done by comparing the rheometrical data obtained (measured or calculated) for aqueous glycerol solution (87%) or ethylene glycol with those measured for the same liquids, using a reference device (Rheotest-2), at different temperatures [5,6]. The rotation speeds at which measurements were made are within the range of $5 \div 50 \text{ rpm}$, which corresponds to the laminar flow regime of $0.86 \leq Ta_{Re} \leq 8.58$ [4].

THE TESTING AND CALIBRATION OF A ROTATING RHEOMETER

The main constructive sizes of the rheometer's cylinders: height $H = 290 \text{ mm}$; inner radius $r_i = 40 \text{ mm}$; outer radius $r_o = 42 \text{ mm}$; ratio of the radii $\delta = r_o/r_i = 1.05$; gap thickness $\Delta r = r_o - r_i = 2 \text{ mm}$ [4].

The measuring and calculation of some functional data are presented in Table 1.

Table 1. The measure and calculation route

Crt.No.	The measured/calculated data	The obtained method/relation
1	Revolution, n	Experimentally measured, [min^{-1}]
2	Shear rate, $\dot{\gamma}$	$\dot{\gamma} = 2.1467 \cdot n$, [s^{-1}]
3	Torsion circle arc, α	Experimentally measured, [div.]
4	Central angle, $\Delta\theta$	$\Delta\theta = 0.028 \cdot \alpha$, [rad]
5	Moment, M	$M = 16.78 \cdot (\Delta\theta - 0.056)$, [$\text{N} \cdot \text{m}$]
6	Shear stress, τ	$\tau = 343.18 \cdot M$, [Pa]
7	Viscosity, η	$\eta = \frac{\tau}{\dot{\gamma}} = \frac{159.86 \cdot M}{n}$, [$\text{Pa} \cdot \text{s}$]

The values of these functional parameters for different measured rotation speeds are presented in Table 2.

Table 2. Functional data for Couette modified rheometer in the case of glycerol aqueous solution (87%), at 298K and different revolution values

Revolution n	Shear rate $\dot{\gamma} = 2.1467 \cdot n$	Cylinder torsion		Torsion moment, M	Shear stress $\tau = 343.18 \cdot M$
		Motion value, α	Central angle, $\Delta\theta = 0.028 \cdot \alpha$		
min^{-1}	s^{-1}	$\text{div} \times 10^2$	$\text{rad} \times 10^3$	$[\text{N} \cdot \text{m}] \times 10^3$	Pa
0	0	0	0	0	0
5	10.73	1.00	0.28	4.0	1.37
10	21.47	1.50	0.42	6.5	2.23
15	32.20	2.25	0.63	10.0	3.43
20	42.93	2.75	0.77	12.0	4.12
25	53.67	3.25	0.91	15.0	5.15
30	64.40	4.00	1.12	18.5	6.35
35	75.13	4.50	1.26	20.5	7.03
40	85.87	5.00	1.40	23.5	8.06
45	96.60	5.75	1.61	27.0	9.26
50	107.33	6.00	1.68	27.5	9.44

By graphically representing the relation of $\tau = f(\dot{\gamma})$ a linear variation is obtained, which is mathematically expressed by equation (1), its slope being the dynamic viscosity:

$$\tau = 0.0948 \cdot \dot{\gamma} + 0.0395; \quad r^2 = 0.9986 \quad (1)$$

Thus, the dynamic viscosity obtained from the data measured with the modified Couette rheometer is $94.8 \text{ mPa} \cdot \text{s}$.

Also, through the rheological characterization of the same solution (standard) using the viscometer Rheotest-2, the relations were obtained: $\tau = f(\dot{\gamma})$ (as shown in Figure 3a) at different temperatures and $\ln \eta = f(1/T)$ (Figure 3b), respectively [6].

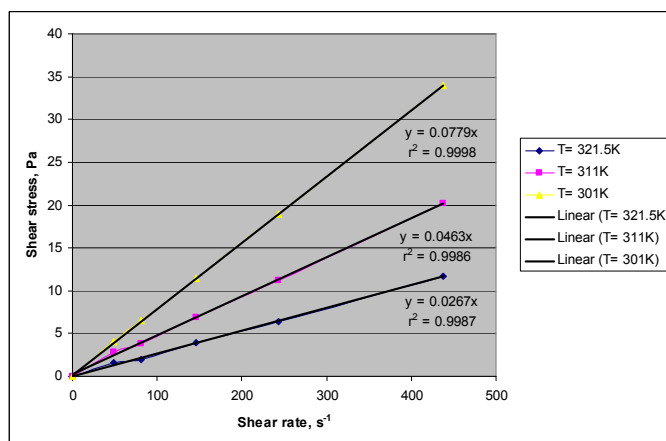


Figure 3a. $\tau = f(\dot{\gamma})$ for standard glycerol solution at different temperatures.

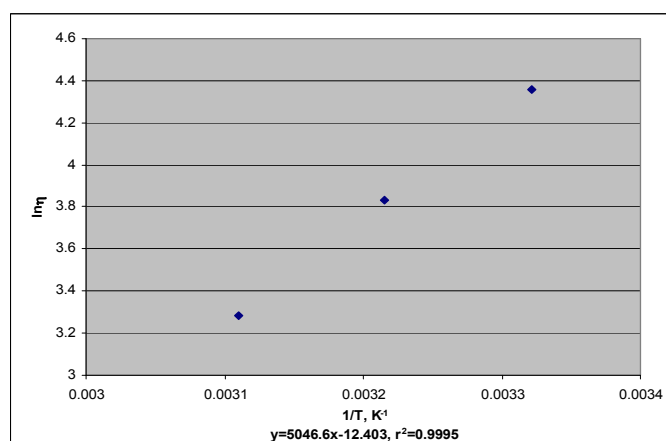


Figure 3b. $\ln \eta = f(1/T)$ for standard glycerol solution.

These relations allowed to establish rheological relations for different temperatures, as well as the general relationship between viscosity and temperature (Arrhenius type relation) [4,6]:

$$\eta = A \cdot e^{E_a/R \cdot T} = 4.106 \cdot 10^{-6} \cdot e^{5046/T} \quad (2a)$$

Particularizing this for glycerol at operating temperature (T=298K), the value was obtained of standard solution dynamic viscosity $\eta_R = 92.93 \text{ mPa} \cdot \text{s}$ and the activation energy of viscous flow $E_a = 41.94 \text{ kJ} \cdot \text{mol}^{-1}$.

Similar results were obtained also for ethylene glycol (activation energy $E_a = 25.35 \text{ kJ} \cdot \text{mol}^{-1}$).

$$\eta = A \cdot e^{E_a/R \cdot T} = 4.98 \cdot 10^{-4} \cdot e^{3050/T} \quad (2b)$$

The calculations did not take into account the additional effect introduced by the rotor rheometer terminal part (end effect). By correlating the values obtained experimentally with this device η_C , and the reference value η_R (standard), the correction coefficient was defined for the end effect:

$$CI = \frac{\eta_C}{\eta_R} = \frac{94.8}{92.93} = 1.02 \quad (3)$$

The correction of viscosity calculated value η_C is done by multiplying it by the factor $f = 1/CI$.

CONCLUSIONS

A modified Couette-type rotating viscometer was made in which the measurement part consists of glass cylinders. It gives the advantage of viewing the hydraulic phenomena that occur, especially in the field of transitional flow regime;

The methodology for measurement (revolution, torsion angle) was established and verified, as well as for the calculation of functional parameters (torsion moment, shear rate, shear stress) so that the rheological characterization and calculation of liquids viscosity can be realized;

Comparing the obtained viscosity value with the standard liquids viscosity, the end effect and the adequate correction factor were calculated. This coefficient is not significantly different from 1.

EXPERIMENTAL SECTION

The torsion of the measuring disk (Figure 1b) by which the central angle $\Delta\theta$ is assessed, was experimentally determined by calibration [6]. To a complete rotation, ($2 \cdot \pi$, rad.) 224.41 divisions correspond, and to a division

correspond 0.028 rad., respectively.

The measurement of the dependence between central angle $\Delta\theta$ and the torsion moment M was experimentally done using a torsion balance. The torsion force was applied to the upper side of the outer cylinder on the measuring disk, the force arm being $b = 72.5 \text{ mm}$. The calibration chart was made for the muff thickness 1.5 mm , at room temperature (298K) and is plotted in Figure 4a, b. For work domain, the dependence is practically linear, with a slope of $0.06 \text{ rad}/N \cdot m$ (Figure 4a), but for the start domain ($M < 50 \cdot 10^{-3} N \cdot m$) it shows a slight hysteresis phenomenon (Figure 4b).

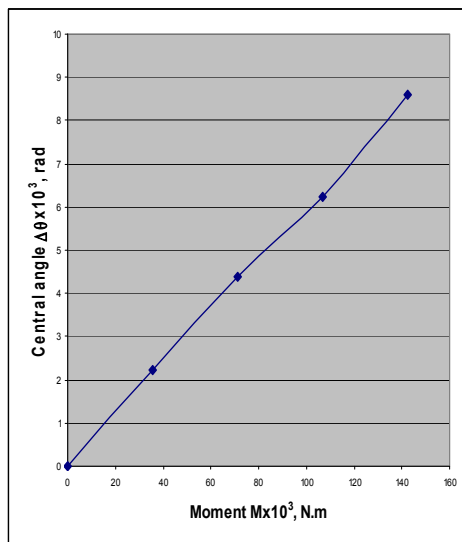


Figure 4a. Calibration chart $\Delta\theta = f(M)$.

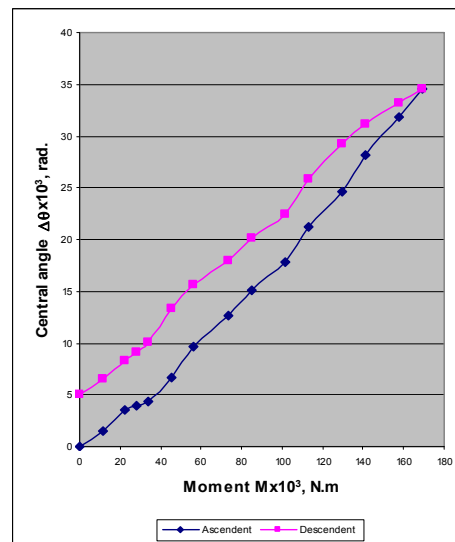


Figure 4b. Hysteresis curve $\Delta\theta = f(M)$.

REFERENCES

1. G. Schramm, "Einführung in Rheologie und Rheometrie", Thermo Haake GmbH, Karlsruhe, **2002**.
2. N. Latrache, A. Ezersky, I. Mutabazi, Proceedings of 13th International Couette-Taylor Workshop, Barcelona, July 3-5, **2003**, 89.
3. G.S. Lewis, H.L. Swinney, *Phys.Rev.E.*, **1999**, 59, 5457
4. N. Bors, A.Tamas, *Scientific Bull. of the "Politehnica" Univ. of Timisoara, Transactions on Mechanics*, **2010**, in press.
5. N. Bors, A. Tamas, Z. Gropsian, *Studia Universitatis Babeș-Bolyai, Chemia, Cluj-Napoca*, **2009**, LIV, 4(I), 55.
6. N. Bors, A. Tamas, Z. Gropsian, *Chem. Bull. "Politehnica" Univ. Timisoara*, **2008**, 53(67), 1-2, 16.

STARCH HYDROLYSIS WITH COMMERCIAL ENZYME PREPARATES

LACRIMIOARA SENILA^a, MIRELA MICLEAN^a, MARIUS ROMAN^a,
MIRCEA CHINTOANU^a, GABRIEL KATONA^b, CECILIA ROMAN^a,
CORNELIA MAJDIK^{*b}

ABSTRACT. There has been a growing interest in the use of starch containing wastewaters in bioprocessing technologies with various commercial available amyolytic enzyme preparates. In this paper for the enzymatic hydrolysis of residual starch in waste waters is described.

Keywords: *Amylase, starch hydrolysis, bioprocessing*

INTRODUCTION

Starch is the most abundant storage polysaccharide in plants. Hence, its application is very important in the food industries such as in the production of oligosaccharides and glucose by starch hydrolysis. Acid splitting is the traditional method for the production of glucose syrup. However, the procedures are not suitable for industrial mass production since the products are rather complicated and require high purification costs. And since the cost of using starch-hydrolyzed enzymes is lower and its procedures are much simpler, it has become the main method in starch hydrolysis [1,2]. A number of enzymes are used in starch hydrolysis. Glucoamylase is one of the key enzymes used for starch processing which has extensive uses in the manufacture of crystalline glucose or glucose syrup, either as soluble or immobilized enzymes. The enzyme hydrolyzes α -1,4- and α -1,6-glycosidic linkages of starch to produce glucose [3].

Microbial communities can be found in the most diverse conditions, including extremes of temperature, pressure, salinity and pH. These microorganisms, called extremophiles, produce biocatalysts that are functional under extreme conditions. The biocatalysts obtained from these microorganisms could be applicable in similarly diverse conditions [4].

^a INCDO-INOE 2000, Research Institute for Analytical Instrumentation, Donáth 67, 400293, Cluj-Napoca, Romania; E-mail: icia@icia.ro

^b "Babes-Bolyai" University, Faculty of Chemistry and Chemical Engineering, Arany János 11, 400028, Cluj-Napoca, Romania

Thermophilic extremophiles have attracted most attention. In particular extremophilic proteases, lipases and polymer-degrading enzymes, such as cellulases, chitinases and amylases have found their way into industrial applications.

The reasons to exploit enzymes that are stable and active at elevated temperatures are obvious. At elevated temperatures the solubility of many reaction components, in particular polymeric substrates, is significantly improved. Moreover, the risk of contamination, leading to undesired complications, is reduced at higher temperatures. Enzymes from microorganisms that can survive under extreme pH could be particularly useful for applications under highly acidic or highly alkaline reaction conditions, for example in the production of detergents and starch hydrolysis. Several enzymes used for starch-hydrolysis (e.g. amylases, pullulanases, glucoamylases and glucosidases that are active at low pH) have been isolated [5].

In this work, with the aim to develop an efficient process for the enzymatic hydrolysis of residual starch in wastewaters, the use of several commercial available amylolytic preparates was tested. The optimal conditions were determined in each case.

RESULTS AND DISCUSSION

The enzymatic activity of commercial available amylolytic preparates was first determined in a prescreening test by measuring the concentration of starch solution before and after 10 min. enzymatic treatment, using the colorimetric method (see experimental part).

One international unit (IU) of amylolytic preparate is defined as that amount of enzyme which hydrolyse 1 μmol of starch per min under the specified conditions.

Table 1. Enzymatic activity of commercial available preparates at pH 7 and 25 °C

Enzyme preparate	Absorbance at 580 nm		Enzymatic activity (IU)
	0 min	10 min	
Fungamyl 800L	0,965	0,604	4,5
DextrozymeDX1.5X	0,416	0,385	0,9
Finizym W	2,867	1,885	4,1
Dextrozyme GA	0,392	0,333	1,8
Shearzyme	2,984	2,737	1,0
Termamyl	2,673	2,643	0,1
Liquizyme	1,072	0,976	1,1

The most efficient catalyst for enzymatic hydrolysis of starch proved to be Fungamyl 800L (4.5 IU) and Finizym W (4.1 IU).

STARCH HYDROLYSIS WITH COMMERCIAL ENZYME PREPARATES

1. The influence of enzyme-substrate ration

Using 3 mL of starch solution and the two best enzyme preparates, the evolution of enzymatic hydrolysis was monitored by measuring the starch concentration after 10 min. as described, using the calibration curve.

Table 2. The influence of enzyme-substrate ratio at pH 7 and 25 °C

Entry	Enzyme preparate	Volume enzyme preparate (µL)	Enzymatic activity (IU)
1	Finizym W	100	0,1
2		200	7,9
3		300	4,9
4		400	3,0
5	Fungamyl 800L	1	1,7
6		2	3,0
7		3	7,3
8		4	10,4
9		5	8,4
10		6	9,1
11		7	9,8
12		8	9,9
13		9	9,7

As observed in Table 2, Fungamyl 800L is more active as Finizym W. The best results were obtained when 200 µL of Finizym W (Table 2, entry 2) or 4 µL of Fungamyl 800L (Table 2, entry 8) were used for hydrolysis 3 ml 4% starch solution at pH 7 and 25 °C.

In these cases, the concentration of starch was monitored for 2 hours (Figure 1) measuring the absorbance as described earlier.

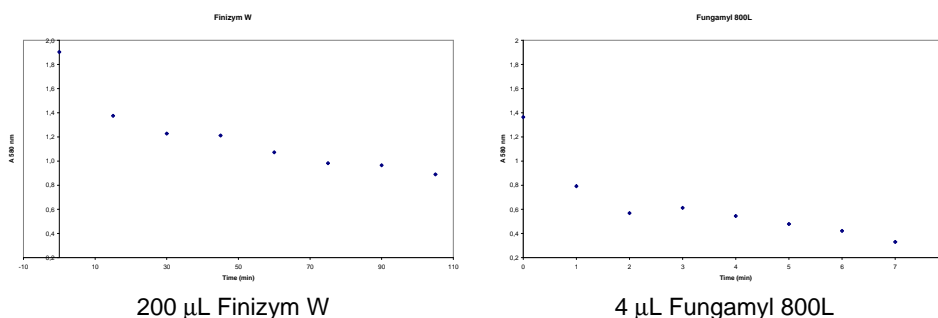


Figure 1. Decreasing of starch concentration in time

2. The influence of temperature on the enzymatic hydrolysis of starch

The temperature dependence of the hydrolytic activity of tested enzyme preparates is shown in Figure 2. The optimum reaction temperature was at 60 °C for both cases.

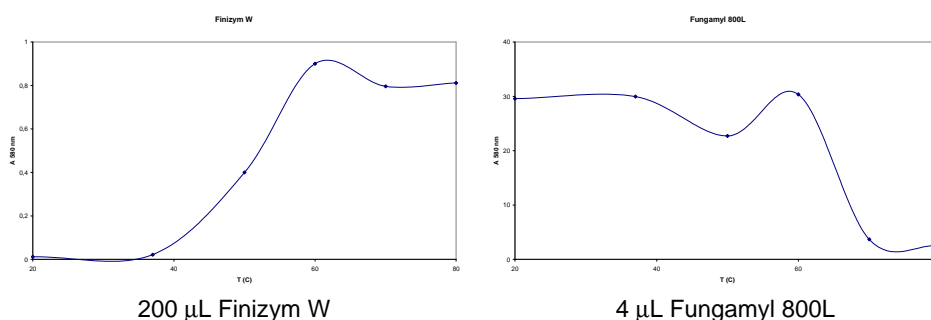


Figure 2. The influence of temperature on the enzymatic hydrolysis of starch

3. The influence of pH on the enzymatic hydrolysis of starch

The effect of pH on the enzymatic activity of tested enzyme preparates was studied by varying the pH of the reaction medium from 3 to 9 at an interval of 1 units and the pH profile is shown in Figure 3.

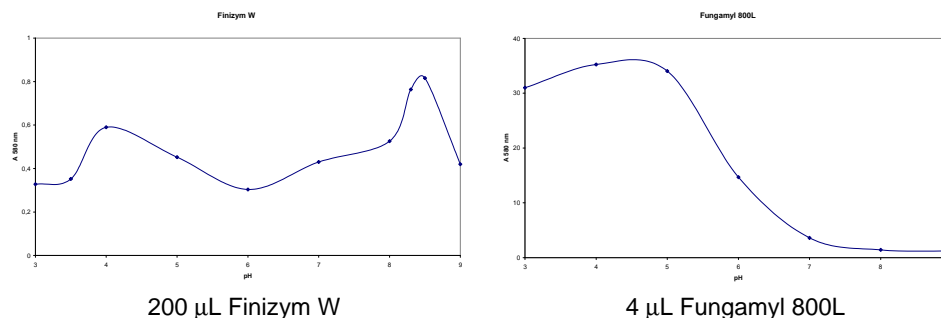


Figure 3. The influence of pH on the enzymatic hydrolysis of starch

CONCLUSIONS

Some commercial available amyolytic enzyme preparates were tested for the hydrolysis of residual starch in waste waters from the food industry. For the two best preparates, the optimum conditions (substrate-enzyme ratio, temperature and pH) were experimental determined.

STARCH HYDROLYSIS WITH COMMERCIAL ENZYME PREPARATES

Table 3. The optimum conditions for enzymatic hydrolysis of starch

Enzyme prepareate	Substrate [*] -prepareate ratio (V/V)	Temperature (°C)	pH
Finizym W	15	60	8.5
Fngamyl 800L	750	60	4

^{*} 4% starch solution

EXPERIMENTAL SECTION

Materials and methods

The next enzyme prepares, commercial available by Novozym, Denmark, were used: Fungamyl 800 L (a fungic α -amylase from *Aspergillus oryzae*), Dextrozyme GA and Dextrozyme DX 1.5X (α -amylases), Finizym W (a fungic β -D-glucanase with residual phospholipase activity), Thermamyl (an α -amylase from *Bacillus licheniformis*), Shearzyme 500 L (an endo-1,4-xylanase from *Aspergillus oryzae*) and Liquizyme Supra.

Stoc solutions

- 4% starch solution in tested buffer
- 6% acetic acid
- 0.0005 N iodine solution

Methods

The amounts of unhydrolyzed starch was determined spectrophotometrically in presence of iodine, measuring the absorbance of the blue inclusion complexe at 580 nm [6].

The hydrolysis experiments were performed at controlled temperature and pH using starch solutions (4%, 10 mL) in the corresponding buffer. After adding the enzyme, samples (3 mL) were taken at 0 and 10 min and 6% acetic acid solution (1 mL) was added for stopping the hydrolysis. In each sample, iodine solution (0.0005N, 1 mL) was added and the absorbance of formed blue complex was measured at 580 nm.

ACKNOWLEDGEMENTS

The financial support from the Romanian Ministry of Education and Research (PNCD II Project Nr. 51001/2007, Valorificarea soluțiilor reziduale de amidon în scopul modernizării producției alimentare REZAMIDO) is gratefully acknowledged.

REFERENCES

1. H. Tatsumi, H. Katano, T. Ikeda, *Biosci. Biotechnol. Biochem.*, **2007**, *71*, 946-950; W. J. Wang, A. D. Powell, C. G. Oates, *Bioresour. Technol.*, **1996**, *55*, 55–61.
2. S.-C. Wu, Y.-K. Lia, *J. Mol. Catal. B: Enzymatic*, **2008**, *54*, 103–108; P. Nigam, D. Singh, *Enzym. Microb. Technol.*, **1995**, *17*, 770–778.
3. G. D. Haki, S. K. Rakshit, *Bioresource Technology*, **2003**, *89*, 17–34.
4. C. Bertoldo, G. Antranikian, *Curr. Opin. Chem. Biol.*, **2002**, *6*, 151-160.
5. B. van den Burg, *Curr. Opin. Microbiol.*, **2003**, *6*, 213–218.
6. M.R. Dhawale, J.J. Wilson, G.G. Khachatourians, W.M. Ingledew, *Appl. Environm. Microbiol.*, **1982**, *4*, 747-750.

THE CELLULAR BIODEGRADATION OF DI- AND TRIHYDROXYBENZENES

GABRIEL KATONA^a, MIRELA MICLEAN^b, MIRCEA CHINTOANU^b,
MARIUS ROMAN^b, EMIL LUCA^c, LACRIMIOARA SENILA^b,
CORNELIA MAJDIK^a, CECILIA ROMAN^{*,b}

ABSTRACT. The enzymatic transformation of di- and trihydroxybenzenes with water-suspended mixed *Pelobacter acidigallici* and *Pseudomonas putida* cells was investigated.

Key words: *Pelobacter acidigallici*, *Pseudomonas putida*, enzymatic hydroxylation, cellular biodegradation, dihydroxy benzene

INTRODUCTION

Phenols widely exists in many industry wastewaters and effluents. Their derivatives like chlorophenol, especially 4-chlorophenol and di- and trihydroxy benzenes are been detected in several industries (wood preservation, agriculture by using pesticides, fungicides and herbicides, byproducts formed during bleaching of pulp with chlorine or chlorination of drinking water [1-3]. Subsequently they have widely contaminated soil and groundwater, and their toxicity seriously affects living organisms. Even low concentration of these phenols could seriously damage the environment.

The efficient removal of these compounds from industrial aqueous effluents is of great practical significance for environmental protection. Many environment protection problems caused by phenols can be solved by employing the ability of microorganisms to degrade these compounds [4-11].

Pelobacter acidigallici have the ability to metabolise gallic acid into acetate via trihydroxybenzenes. As reported by us this bacterial strain can be used succesfully for the biodegradation of several kind of trihydroxibenzenes. In the present work we describe the interaction of mixed *Pelobacter acidigallici* and *Pseudomonas putida* cells with dihydroxybenzenes.

^a Babeş-Bolyai University, Faculty of Chemistry and Chemical Engineering, Str. M. Kogălniceanu, No. 1, RO-400084 Cluj-Napoca, Romania

^b INCDO-INOE Research Institute for Analytical Instrumentation - ICIA, 67 Donath-67 400293 Cluj-Napoca, Romania, * cicj_roman@yahoo.com

^c University of Agricultural Sciences and Veterinary Medicine Cluj-Napoca, Faculty of Horticulture, 3 Calea Manastur St., 400372 Cluj-Napoca, Romania

RESULTS AND DISCUSSION

First we investigated the interaction of the dihydroxybenzenes (catechol, resorcinol, hydroquinone) with *Pseudomonas putida* cells. It was shown that this microorganism has the ability to introduce in *ortho* position a hydroxylic group when the substrate is a substituted or not substituted phenol. Using HPLC-MS (UV) first the chromatographic separation of the commercially available dihydroxybenzenes and their possible reaction products, pirogallol for the hydroxylation of catechol and rezorcinol and 1,2,4-trihydroxy benzene for the transformation of hydroquinone was set up. As we expected all the three dihydroxy benzenes were ben transformed into the corresponding products as it is shown in Figure 1.

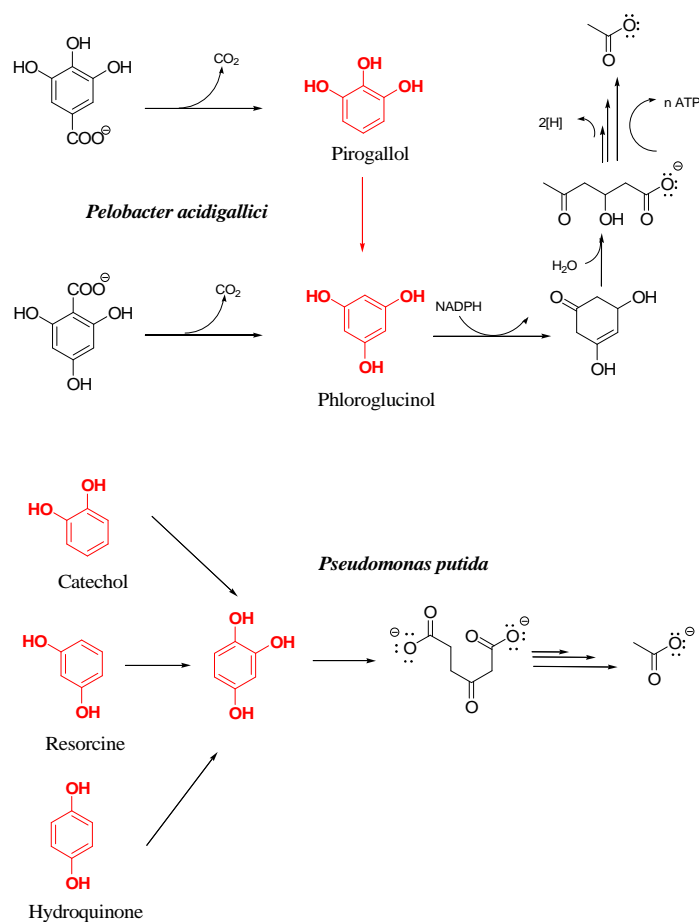


Figure 1. The enzymatic transformation of the dihydroxybenzenes followed by the metabolism of the formed trihydroxybenzenes

THE CELLULAR BIODEGRADATION OF DI- AND TRIHYDROXYBENZENES

For all of the cases kinetic data shown an approximative 25 μ mol/min/mg enzyme activity.

As it was demonstrated by us using *Pelobacter acidigallici* cells pirogallol can be converted into phloroglucinol. The latter compound will be further transformed by the cells into acetic acid.

In contrast to the metabolism of pirogallol, 1,2,4 trihydroxybenzene will be enzymatically converted into succinyl acetate, which will be further transformed in the Krebs cycle into acetyl-CoA.

In this way we demonstrated that enzymes presents in *Pelobacter acidigallici* are able to transform di- and trihydroxybenzenes. Further we investigated the interaction of the above mentioned compounds with *Pelobacter acidigallici* harvested cells.

As reference we used the kinetic data for the biodegradation of gallic acid, a natural substrate of *Pelobacter acidigallici*. Using solution with variable concentrations of the natural substrate first the specific activity of the cells was determined. For this, after the incubation of the gallic acid with *Pelobacter acidigallici* cells periodically samples were taken which were centrifugated and subjected to HPLC-UV analysis.

Further all the three dihydroxybenzenes were incubated in the same manner with the *Pseudomonas putida* cells. In Table 1 it is shown the values for the specific activity of the cells for the transformation of gallic acid in *Pelobacter acidigallici* compared with the degradation of resorcinol in *Pseudomonas putida*.

Table 1. Specific activity for the cellular degradation of gallic acid and resorcinol.

Entry	$C_{\text{substrate}}$ [mM]	Specific activity [U/g cell] Gallic acid	Specific activity [U/g cell] resorcinol
1.	0.05	3.61	-
2.	0.1	3.53	0.59
3.	0.25	7.23	0.88
4.	0.5	7.44	1.37
5.	0.75	7.53	1.76
6.	1	7.78	1.84
7.	1.5	8.39	2.13
8.	2	8.29	2.27
9.	2.5	8.39	2.45
10.	3	8.61	-

Using the Lineweaver-Burke linearization method it was demonstrated that the global rate of the transformation of the polyhydroxybenzenes is governed by enzymes. Further it was calculated the k_M and the v_{max} for the biodegradation of all the mentioned compounds.

Table 2. The Michaelis constant and the relative rate of the cellular transformation of polihydroxybenzenes.

Substrate	K_M [μ M]	$V_{max}/V_{max \text{ gallic acid}}$
Gallic acid	0.032	1
catechol	0.076	0.34
pirogallol	0.134	1.00
phloroglucinol	0.048	1.00
resorcine	0.032	0.29
hydrochinone	0.048	0.49

After that we studied the kinetic parameters for the transformation of the natural substrate of the cells in presence of di- and trihydroxybenzenes. For this we suspended the *Pellobacter acidigallici* and *Pseudomonas putida* cells in solution of gallic acid and we add different amount of polihydroxy benzenes into the suspension. The working-up and analytical procedures were the same as used for activity measurement. It was shown that all of the used phenols are weak competitive inhibitors for the biodegradation of the gallic acid as shown in Table 3.

Table 3. V_{max} , K_M and competitive inhibition constants for the biodegradation of gallic acid in presence of various phenols

Compound	K_M [mM]	V_{max} [U/mg]	K_i [μ M]
catechol		25.76884	18 \pm 2
pirogallol		23.16081	33 \pm 5
phloroglucinol	15.72	24.14445	41 \pm 10
resorcine		23.20162	25 \pm 5
hydrochinone		22.76602	39 \pm 2

Finally we investigated the biodegradation of the mixture of all of the studied compounds using an initial concentration of 10mM for each compound. Due to their weak inhibitory effect the global biodegradation rate of each compound was poorly affected, the individually decreasing of the reaction rate for each compound was not higher than 10%. After 24 hours no phenolic compound was detected using HPLC-UV analysis. It is known that the detection limit for these compounds is around 1 μ M. To detect lower concentration of untransformed phenols, the cellular suspension was centrifuged and the supernatant was filtered on a small size C18 cartridge. The cartridge was eluted with a mixture of acetonitrile-water (50:50, v/v). From the obtained concentrated solution was determined a residual untransformed mixture of phenols with 0.1-0.15 μ M concentration calculated for the volume of the initial cellular suspension.

CONCLUSIONS

It can be concluded that the mixture of *Pelobacter acidigallici* and *Pseudomonas putida* cells in water suspension can be successfully used for the biodegradation of polihydroxy phenols. The biochemical path of these biotransformation was demonstrated and kinetic measurement were performed for each individual compound. Activity measurements using a two component mixture of the natural substrate and a poliphenol demonstrated that the global rate for the transformation of gallic acid was weakly affected. Moreover the biodegradation of the complex mixture of phenols undergoes with good rate, the untransformed phenol concentration was not higher than 0.15 μM .

EXPERIMENTAL SECTION

Pelobacter acidigallici and *Pseudomonas putida* cells were grown and isolated as described in standard methods. The enzyme assay was carried out at 30 °C in a discontinuous fashion by HPLC analysis of the products.

Their concentrations in the assay mixture were as follows: 100 mM potassium phosphate buffer, (pH 7.2), 10 mmol dihydroxybenzene, and 1 U of enzyme in 1 mL. Samples (20 μL) were withdrawn with a unimetric-pipet and the reaction was terminated by adding 0.1 M H_3PO_4 (5 μL) and diluted 10 times with double distilled water followed by the centrifugation before injection. The withdrawals occurred soon after start of the reaction and then at regular intervals. The conditions for the HPLC analyses were: on a C18 ec column using as eluent 20 mM HCl in water: acetonitrile (95: 5, v/v) in an isocratic manner at a 1 mL \times min⁻¹ flow rate.

For the cellular biodegradation a concentration of 1g harvested cell in 1 mL of buffer was used. The substrate concentration was varied in 10-50 mM range. Before injection cells were centrifugated and the supernatant was filtered. The HPLC analysis was performed as previously described.

ACKNOWLEDGMENTS

The financial support from the Romanian Ministry of Education and Research (No. 31016/2007, within the PNCD2 Program) is gratefully acknowledged.

REFERENCES

1. A.R. Bielefeldt, H. D. Stensel. *Biodegradation*, **1999**, 10:1.
2. V. Kavitha, K. Palanivelu. *Chemosphere* **2004**, 55:1235.
3. S.H. Yuan, X. H. Lu. *Journal of Hazardous Materials*, **2005**, 118:85.
4. V.V. Vel'kov, *Biotekhnologiya*, **1995**, 3-4:20.

G. KATONA, M. MICLEAN, M. CHINTOANU, M. ROMAN, E. LUCA, L. SENILA, C. MAJDIK, C. ROMAN

5. F.M. Khabibulina, A.A. Shubakov, I.B. Arhegova, G.G. Romanov. *Biotekhnologiya*, **2002**, 6:57.
6. T.O. Anokhina, V.V. Kochetkov, N.F. Zelenkova, V.V. Balakshina, A.M. Boronin. *Prikladnaia Biokhimiia Mikrobiolgiya*, **2004**, 40:654.
7. F. Bux, B. Akkinson, K. Kasan. *Water ScienceTechnology*, **1999**, 39:127.
8. A. Zumriye, A. Derya, R. Elif. *Process Biochemistry*, **1999**, 35:301.
9. A. Fialova, E. Boschke, T. Bley. *Biodegradation*, **2007**, 18:719.
10. Z. Ai, P. Yang, X. H. Lu. *Journal of Hazardous Materials*, **2005**, 124:147.
11. Z. Aleksieva, D. Ivanova, T. Godjevargova. *Process Biochemistry*, **2007**, 37:1215.

SYNTHESIS, STRUCTURE AND REACTIVITY INVESTIGATIONS OF SOME NEW MONO- AND BIS(5,5-DIBROMOMETHYL-1,3-DIOXAN-2-YL) DERIVATIVES

ALIN MIHIȘ, LIGIA MIRABELA GOLBAN, ELENA BOGDAN,
ANAMARIA TERC AND ION GROSU*

ABSTRACT. The good yielding synthesis of some new mono and bis(5,5-dibromomethyl-1,3-dioxan-2-yl) derivatives and their NMR structural investigations are reported. Substitution of bromine in bromomethyl groups with thioacetate units in some of these compounds was also investigated.

Keywords: 1,3-dioxanes, dimercapto derivatives, NMR, conformational analysis

INTRODUCTION

The stereochemistry of saturated six-membered rings were extensively investigated using as model compounds a plethora of differently substituted 1,3-dioxane derivatives [1-5]. The last ones are easily investigated using NMR methods [6], available in good yields by different acetalization reactions [7] and manifest remarkable stability in non-acidic media [8].

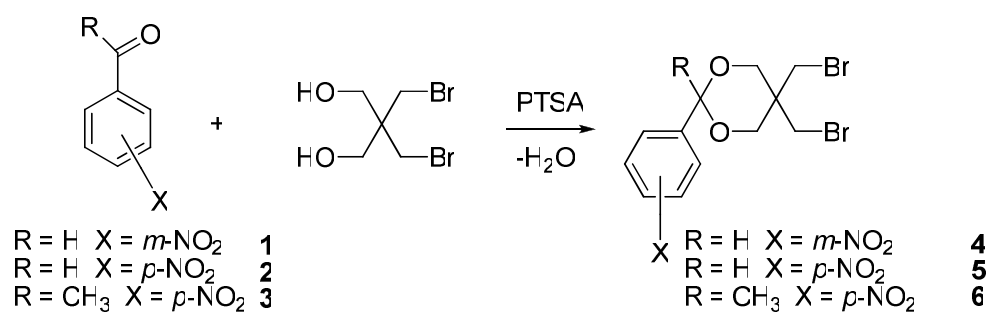
In previous works, we investigated either compounds with one, two or even three 1,3-dioxane units connected to the same substrate [9-14] and we found out flexible, semiflexible or anancomeric (rigid) structures. These investigations revealed the high conformation enthalpies (A-values) of the substituents located at position 2 and the preference of these groups for the equatorial orientation [9-14]. If several 1,3-dioxane rings are connected to the same substrate, in the more stable conformation the reference (main) unit occupies similar orientations for all 1,3-dioxane rings. These orientations are similar to those observed in the corresponding mono-1,3-dioxane derivative.

Thus, using the acetalization of 2,2-dibromomethyl-1,3-propanediol with different monocarbonyl and dicarbonyl compounds, we considered of interest to prepare new anancomeric 1,3-dioxanes bearing a "holding group" at position 2 and geminal bromomethyl groups at position 5.

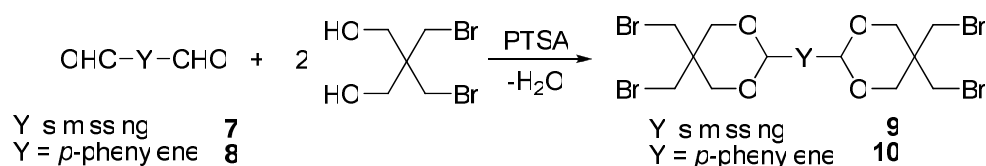
* Babeș-Bolyai University, Faculty of Chemistry and Chemical Engineering, 11 Arany Janos str., RO-400028 Cluj-Napoca, Roumania, igrosu@chem.ubbcluj.ro

RESULTS AND DISCUSSION

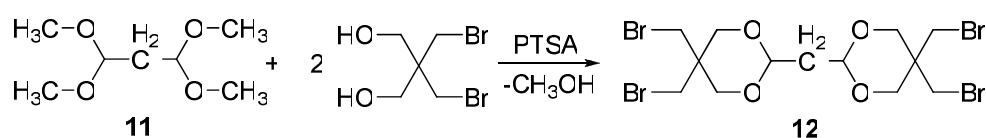
New 1,3-dioxane derivatives (**4-6**, **9**, **10** and **12**) were synthesized in good yields (Table 1) by the acetalization of monocarbonyl derivatives **1-3**, dialdehydes **7**, **8** and by the transacetalization of 1,1,3,3-tetramethoxypropane **11** with 2,2-dibromomethyl-1,3-propanediol (Schemes 1-3).



Scheme 1



Scheme 2



Scheme 3

Table 1. Results of the syntheses of compounds **4-6**, **9**, **10** and **12**

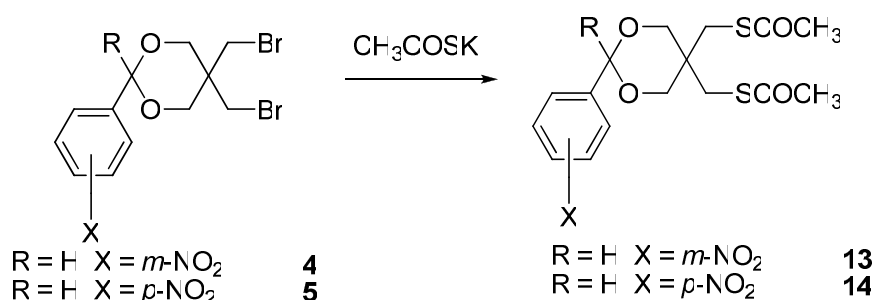
Compd.	4	5	6	9	10	12
Yields (%)	71	83	70	57	64	49

The yields in mono 1,3-dioxane derivatives (**4-6**) were higher than those of bis(1,3-dioxan-2-yl) compounds (**9**, **10** and **12**). The yield for the acetalization of *p*-nitrobenzaldehyde (**2**) was higher than that carried out with *p*-nitroacetophenone **3**.

In order to develop the chemistry of these brominated compounds, we investigated the nucleophilic replacement of the bromine atoms with protected mercapto groups. In this purpose, compounds **4** and **5** were used

as references substrates by applying similar procedures previously described in the literature[15].

Thus, the reaction of **4** and **5** with freshly prepared CH_3COSK in different solvents (CH_2Cl_2 , CH_3CN) at room temperature afforded compounds **13** and **14** in poor yields (10-15%, Scheme 4).



Scheme 4

That is, the raw products were contaminated with important amounts of monomethylthioacetate derivatives and different disulfides as side products.

Compounds **13** and **14** were obtained in good yields by a different approach using as starting material $\text{HOCH}_2\text{-C}(\text{CH}_2\text{-SCOCH}_3)_2\text{-CH}_2\text{OH}$ [16, 17].

All investigated brominated compounds were anancomeric structures as their conformational equilibria (Scheme 5) were shifted towards the conformer (I) in which the larger group (R^1) had an equatorial orientation [R^1 = nitrophenyl (**4** and **5**), CH_3 (**6**), 5,5-dibromomethyl-1,3-dioxan-2-yl (**9**), (*para*-5,5-dibromomethyl-1,3-dioxan-2-yl)phenyl (**10**) and (5,5-dibromomethyl-1,3-dioxan-2-yl)methyl (**12**)].



Scheme 5

The anancomeric behavior of compounds **4-6**, **9**, **10** and **12** was deduced from the NMR spectra which exhibit different signals for the axial and equatorial protons of the 1,3-dioxane ring and for the protons and carbon atoms of the axial and equatorial bromomethyl groups located at position 5 (Table 2).

Table 2. Selected NMR data (δ , ppm) for compounds **4-6**, **9**, **10** and **12**

Compd.	^1H				^{13}C	
	4-H, 6-H		5-CH ₂ Br		5-CH ₂ Br	
	ax	eq	ax	eq	ax	eq
4	3.90	4.29	3.94	3.32	35.7	34.1
5	3.89	4.29	3.94	3.32	35.6	34.1
6	3.52	3.92	3.95	3.11	35.6	34.3
9	3.70	4.20	3.88	3.25	35.5	33.9
10	3.84	4.08	3.96	3.31	36.0	34.4
12	3.62	4.08	3.88	3.23	36.0	34.3

Positions 4 and 6 of the 1,3-dioxane units and the protons of the CH₂Br groups were not diastereotopic. This NMR equivalence, also observed for compound **4** bearing a dissymmetrical aromatic group, suggests the free rotation, at room temperature, of the equatorial *meta*-nitrophenyl group located at position 2.

CONCLUSIONS

New compounds with one or two 1,3-dioxane units were obtained in good yields by acetalization or transacetalization of 2,2-dibromomethyl-1,3-propanediol. The NMR spectra of the new compounds exhibit different signals for the 1,3-dioxanic axial and equatorial protons and for the protons and carbon atoms of the axial and equatorial bromomethyl groups reveal the anancomeric structure of all derivatives. The procedure for the substitution of the bromine atoms of the bromomethyl groups with nucleophiles of type thioacetate was investigated and revealed poor yields for this reaction.

EXPERIMENTAL SECTION

^1H NMR (300 or 250 MHz) and ^{13}C NMR (75 or 62.9 MHz) spectra were recorded in CDCl₃ on Bruker spectrometers. ESI MS were recorded on Agilent 6320 ion trap spectrometer in positive mode. Melting points are uncorrected. Thin layer chromatography (TLC) was carried out on aluminium sheets coated with silica gel 60 F₂₅₄ using UV and KMnO₄ visualization.

General procedure for synthesis of derivatives 4-6, 9, 10 and 12

A catalytic amount of *para*-toluenesulfonic acid (PTSA, 0.1 g) was solved in 100 ml toluene. To this solution, 5 (**4-6**) or 10 (**9**, **10** and **12**) mmol of 2,2-dibromomethyl-1,3-propanediol and 5 mmol of (di)carbonyl compound or of the tetracetal **11** (synthesis of **12**) were added. The reaction mixture was heated to reflux and the resulting water from the reaction was removed using a Dean-Stark trap (a simple reflux was used in the synthesis of **12**).

When 80% of the theoretical amount of water has been separated (6 - 10 h) the mixture was cooled at room temperature and the PTSA was neutralized with sodium acetate in excess (0.2 g), under stirring (over one hour). The reaction mixture was washed twice with 50 ml water. The organic phase was dried with anhydrous sodium sulphate, and then the toluene was removed in vacuo. The crude solid product was purified by crystallization from ethanol.

5,5-dibromomethyl-2-(3'-nitrophenyl)-1,3-dioxane 4. White solid, m.p. = 79-80 °C, yield 71%. Calculated for $C_{12}H_{13}Br_2NO_4$ (395.04): C, 36.48; H, 3.32; N, 3.55; Br, 40.45. Found: C, 36.69; H, 3.51; N, 3.43; Br, 40.18. 1H NMR (300 MHz, $CDCl_3$, δ ppm): 3.32 [2H, s, 5- CH_2Br (eq)], 3.90 (2H, d, $J = 12.0$ Hz, 4- H_{ax} , 6- H_{ax}), 3.94 [2H, s, 5- CH_2Br (ax)], 4.29 (2H, d, $J = 12.0$ Hz, 4- H_{eq} , 6- H_{eq}), 5.49 (H, s, 2- H_{ax}), 7.56 [H, t (overlapped dd), $J = J' = 8.0$ Hz, 5'-H], 7.81 (H, d, $J = 7.7$ Hz, 6'-H), 8.22 (H, d, $J = 8.2$ Hz, 4'-H), 8.34 (H, s, 2'-H). ^{13}C NMR (75 MHz, $CDCl_3$, δ ppm): 34.1 [5- CH_2Br (eq)], 35.7 [5- CH_2Br (ax)], 37.3 (C^5), 71.8 ($C^{4,6}$), 100.3 (C^2), 121.4 (C^2), 123.9 (C^4), 129.31 (C^5), 132.2 (C^6), 139.1 (C^1), 148.0 (C^3).

5,5-dibromomethyl-2-(4'-nitrophenyl)-1,3-dioxane 5. White solid, m.p. = 128-129 °C, yield 83%. Calculated for $C_{12}H_{13}Br_2NO_4$ (395.04): C, 36.48; H, 3.32; N, 3.55; Br, 40.45. Found: C, 36.33; H, 3.47; N, 3.69; Br, 40.61. 1H NMR (250 MHz, $CDCl_3$, δ ppm): 3.32 [2H, s, 5- CH_2Br (eq)], 3.89 (2H, d, $J = 11.9$ Hz, 4- H_{ax} , 6- H_{ax}), 3.94 [2H, s, 5- CH_2Br (ax)], 4.29 (2H, d, $J = 11.9$ Hz, 4- H_{eq} , 6- H_{eq}), 5.49 (H, s, 2- H_{ax}), 7.66 (H, d, $J = 8.7$ Hz, 2',6'-H), 8.24 (H, d, $J = 8.7$ Hz, 3',5'-H). ^{13}C NMR (62.9 MHz, $CDCl_3$, δ ppm): 34.1 [5- CH_2Br (eq)], 35.6 [5- CH_2Br (ax)], 37.4 (C^5), 72.0 ($C^{4,6}$), 100.5 (C^2), 123.5 ($C^{3,5}$), 127.2 ($C^{2',6'}$), 143.6 (C^1), 148.3 (C^4).

5,5-dibromomethyl-2-methyl-2-(4'-nitrophenyl)-1,3-dioxane 6. White solid, m.p. = 176-177°C, yield 70 %. Calculated for $C_{13}H_{15}Br_2NO_4$ (409.07): C, 38.17; H, 3.70; N, 3.42; Br, 39.07. Found: C, 38.42; H, 3.51; N, 3.26; Br, 38.89. 1H NMR (300 MHz, $CDCl_3$, δ ppm): 1.56 (3H, s, 2- CH_3), 3.11 [2H, s, 5- CH_2Br (eq)], 3.52 (2H, d, $J = 11.8$ Hz, 4- H_{ax} , 6- H_{ax}), 3.92 (2H, d, $J = 11.8$ Hz, 4- H_{eq} , 6- H_{eq}), 3.95 [2H, s, 5- CH_2Br (ax)], 7.60 (H, d, $J = 8.9$ Hz, 2',6'-H), 8.27 (H, d, $J = 8.9$ Hz, 3',5'-H). ^{13}C NMR (62.9 MHz, $CDCl_3$, δ ppm): 30.9 (2- CH_3), 34.3 [5- CH_2Br (eq)], 35.6 [5- CH_2Br (ax)], 37.5 (C^5), 66.3 ($C^{4,6}$), 100.7 (C^2), 124.3 ppm ($C^{3',5'}$), 127.6 ($C^{2',6'}$), 147.2 (C^1), 148.0 (C^4).

bi(5,5-dibromomethyl-1,3-dioxan-2-yl) 9. White solid, m.p. = 199.2°C, yield 57 %. Calculated for $C_{12}H_{18}Br_4O_4$ (545.88): C, 26.40; H, 3.32; Br, 58.55. Found: C, 26.58; H, 3.44; Br, 58.32. 1H NMR (300 MHz, $CDCl_3$, δ ppm): 3.25 [4H, s, 5(5')- CH_2Br (eq)], 3.70 [4H, d, $J = 11.8$ Hz, 4(4')- H_{ax} , 6(6')- H_{ax}], 3.88 [4H, s, 5(5')- CH_2Br (ax)], 4.20 [4H, d, $J = 11.8$ Hz, 4(4')- H_{eq} , 6(6')- H_{eq}], 4.43 (H, s, 2- H_{ax}). ^{13}C NMR (62.9 MHz, $CDCl_3$, δ ppm): 33.9 [5- CH_2Br (eq)], 35.5 [5- CH_2Br (ax)], 37.7 (C^5), 71.5 ($C^{4,6}$), 100.0 (C^2).

1,4-Bis(5',5'-dibromomethyl)-1',3'-dioxan-2'-yl)benzene 10. White solid, m.p.=204-205°C, yield 64%. Calculated for C₁₈H₂₂Br₄O₄ (621.98): C, 34.76; H, 3.57; Br, 51.39. Found: C, 34.92; H, 3.40; Br, 51.25. ¹H NMR (300 MHz, CDCl₃, δ ppm): 3.31 [4H, s, 5'(5'')-CH₂Br (eq)], 3.84 [4H, d, J = 10.8 Hz, 4'(4'')-H_{ax}, 6'(6'')-H_{ax}], 3.96 (4H, s, 5'(5'')-CH₂Br(ax)], 4.24 [4H, d, J = 10.8 Hz, 4'(4'')-H_{eq}, 6'(6'')-H_{eq}], 5.41 [2H, s, 2'(2'')-H], 7.49 (4H, s, 2-H, 3-H, 5-H, 6-H). ¹³C NMR (75 MHz, CDCl₃, δ ppm): 34.4 [5'(5'')-CH₂Br(eq)], 36.0 [5'(5'')-CH₂Br(ax)], 37.4 (C^{5',5''}), 71.8 (C^{4',4'',6',6''}), 101.8 (C^{2',2''}), 126.0 (C^{2,3,5,6}), 138.2 (C^{1,4}).

Bis(5,5-dibromomethyl-1,3-dioxan-2-yl)methane 12. White solid, m.p.= 151.5 °C, yield 49%. Calculated for C₁₃H₂₀Br₄O₄ (559.91): C, 27.89; H, 3.60; Br, 57.08. ¹H NMR (300 MHz, CDCl₃, δ ppm): 2.03 (2H, t, J = 5.5 Hz, 2(2')-CH₂-), 3.23 [4H, s, 5(5')-CH₂Br (eq)], 3.62 (4H, d, J = 11.8 Hz, 4(4')-H_{ax}, 6(6')-H_{ax}), 3.88 [4H, s, 5(5')-CH₂Br (ax)], 4.08 (4H, d, J = 11.8 Hz, 4(4')-H_{eq}, 6(6')-H_{eq}), 4.59 [2H, t, J = 5.4 Hz, 2(2')-H_{ax}]. ¹³C NMR (75 MHz, CDCl₃, δ ppm): 34.3 [5(5')-CH₂Br (eq)], 36.0 [5(5')-CH₂Br (ax)], 37.3 (C^{5,5'}), 39.5 (CH₂), 71.4 (C^{4,4',6,6'}), 99.6 (C^{2,2'}).

ACKNOWLEDGMENTS

We acknowledge the financial support of this work by PNCDI II program (UEFISCSU; projects IDEAS 515, 2278).

REFERENCES

- [1]. M. J. O. Anteunis, D. Tavernier, F. Borremans, *Heterocycles*, **1976**, 4, 293.
- [2]. E. Kleinpeter, *Advances in Heterocyclic Chemistry*, **1998**, 69, 217.
- [3]. E. Kleinpeter, *Advances in Heterocyclic Chemistry*, **2004**, 86, 41.
- [4]. E.L. Eliel, S.H. Wilen, *Stereochemistry of Organic Compounds*, Wiley & Sons, New York, **1994**, p 696.
- [5]. F.G. Riddell, *The Conformational Analysis of Heterocyclic Compounds*, Academic Press, London, **1980**, p 114.
- [6]. G. Plé, I. Grosu, S. Mager, M. Darabanțu, *Résonance Magnétique Nucléaire Appliquée à l'Analyse Structurale de Composés Organiques*, Publications de l'Université de Rouen, **1999**, pp 145-190.
- [7]. F.A.J. Meskens, *Synthesis*, **1981**, 501.
- [8]. N. Bogdan, I. Grosu, E. Condamine, L. Toupet, Y. Ramondenc, I. Silaghi-Dumitrescu, G. Plé, E. Bogdan, *Eur. J. Org. Chem.*, **2007**, 4674.
- [9]. S. Mager, I. Hopartean, M. Horn, I. Grosu, *Stud. Univ. Babeș-Bolyai, Chem.*, **1979**, 24, 32.
- [10]. S. Mager, I. Grosu, *Stud. Univ. Babeș-Bolyai, Chem.*, **1988**, 33, 47.
- [11]. I. Grosu, S. Mager, G. Plé, N. Plé, A. Toscano, E. Mesaros, R. Martinez, *Liebigs Annalen/Recueil*, **1997**, 2371.

SYNTHESIS, STRUCTURE AND REACTIVITY INVESTIGATIONS OF SOME DERIVATIVES...

- [12]. I. Grosu, S. Mager, L. Toupet, G. Plé, E. Mesaros, A. Mihis, *Acta Chem. Scand.*, **1998**, *52*, 366.
- [13]. I. Grosu, S. Mager, E. Mesaros, G. Plé, *Heterocycl. Commun.*, **1998**, *4*, 53.
- [14]. M.C. Florian, M. Cîrcu, L. Toupet, A. Terec, I. Grosu, Y. Ramondenc, N. Dincă, G. Plé, *Centr. Eur. J. Chem.*, **2006**, *4*, 808.
- [15]. R. Turdean, E. Bogdan, A. Terec, A. Petran, L. Vlase, I. Turcu, I. Grosu, *Centr. Eur. J. Chem.*, **2009**, *7*, 111.
- [16]. A. Mihiş, L. M. Golban, C. Raţ, E. Bogdan, A. Terec, C. Cismaş, I. Grosu, submitted.
- [17]. A. Mihiş, PhD Thesis, Babes-Bolyai University, Cluj-Napoca, Romania, 2010.

STACKING INTERACTIONS BETWEEN PYRIDINE FRAGMENTS IN CRYSTAL STRUCTURES OF TERPYRIDYL COMPLEXES

GORAN JANJIĆ^a, PREDRAG PETROVIĆ^b, DRAGAN NINKOVIĆ^b,
DUŠAN VELJKOVIĆ^a, AGNEŠ KAPOR^b AND SNEŽANA D. ZARIĆ^c

ABSTRACT. In the crystal structures of terpyridyl complexes from the Cambridge Structural Database (CSD) stacking interaction between the pyridine fragments were studied. Square-planar complexes where the distance between the centers of two pyridine fragments was below 4.6 Å were retrieved from CSD. With this search 68 crystal structures with 167 interactions were found. In the interactions one, two or three pyridine fragments of one complex can be involved in overlapping with pyridine fragments of the other complex.

Keywords: *Transition metal complexes, Crystal structures, stacking interaction, Cambridge Structural Database, terpyridyl*

INTRODUCTION

The noncovalent interactions of π -systems have been extensively studied in recent years. These interactions are important in many areas of chemistry and biochemistry [1–9]. The importance of noncovalent interactions of π -systems, cation– π [1-3], XH/ π hydrogen bonds (X = O,N,C) [4-7], and stacking interactions [4,8,9], have motivated studies of the noncovalent interactions in transition-metal complexes [10-14].

Several studies of chelate rings with delocalized π -bonds, which can be involved in noncovalent interactions [12-21] in ways similar to aromatic organic molecules [22], were published. Chelate rings can be involved in CH/ π interactions as hydrogen acceptors with organic moieties and in stacking interactions with aryl rings. The delocalized π -system of chelate rings can be considered as a soft base, similar to double, triple bonds or aromatic rings. These observations could be connected with an assumption that planar chelate rings with delocalized π -bonds can have aromatic character [23]. Several studies about interactions where the π -systems of chelate rings

^a ICTM, University of Belgrade, Njegoševa 12, 11000 Belgrade, Serbia

^b Department of Physics, Faculty of Natural Sciences and Mathematics, University of Novi Sad, Serbia

^c Department of Chemistry, University of Belgrade, Studentski trg 16, 11000 Belgrade, Serbia, szaric@chem.bg.ac.rs

interact with C–H groups, belonging to an organic moiety, were published [15–18]. CH/ π interactions with chelate rings of coordinated porphyrin in transition metal porphyrinato complexes and in porphyrin containing proteins were also observed [16, 18]. The results showed that these interactions contribute to the stability of porphyrin containing proteins and may play some role in the function of these proteins [18].

We have analyzed CH/ π interactions between π -systems of coordinated acetylacetonato ligand and phenyl rings. Quantum chemical calculations on a few model systems show that the energies of the CH/ π interactions where the acetylacetonato ligand is the hydrogen atom donor (metal ligand CH/ π (MLCH/ π) interactions) are in the range of 0.6–2.4 kcal/mol, while the energies of the CH/ π interaction where phenyl group is the hydrogen atom donor are in the range of 1.5–2.7 kcal/mol [13].

Our previous results show that there are stacking interactions between chelate rings with delocalized π -bonds, and aryl rings containing six carbon atoms (C6-aryl), in crystal structures of square-planar transition-metal complexes [19, 20]. These interactions were first characterized in square-planar complexes of Cu(II). Further investigations show that interactions between chelate and phenyl rings exist in square-planar complexes of different transition metals. In these crystal structures, the geometry of the stacking interaction, between C6-aryl rings and chelate rings, is similar to the geometry of the stacking interaction of two benzene rings [22].

Here we present the results on stacking interactions between pyridine fragments in crystal structures of square planar terpyridyl complexes from the Cambridge Structural Database (CSD). We analyzed types of overlapping and mode of the packing in the crystal structures.

RESULTS AND DISCUSSION

A survey of crystal structures from CSD that contain square-planar terpyridyl complexes where the intermolecular distances between centroids of the two pyridine fragments are below 4.6 Å revealed 68 structures with 167 interactions. In order to describe these interactions, several geometrical parameters of the interactions were analyzed.

In Figure 1 a histogram presenting centroid-centroid distance (**D_{pp}**) of the two interacting pyridine fragments in the studied structures is shown. The distribution of the centroid-centroid distances has a peak from 3.6 to 3.9 Å, and for the substantial number of interactions the distance is above 4.0 Å.

The angle between planes P_1 and P_2 of the two pyridine fragments for almost all interactions is less than 10 degrees, indicating parallel or almost parallel orientation of the two rings. Normal distances (**R**) between the planes P_1 and P_2 are in the range of 3.0 to 3.8 Å, while the peak of the distribution is from 3.3 to 3.5 Å (Fig. 2). These normal distances are in agreement with the distances in stacking interactions [8a].

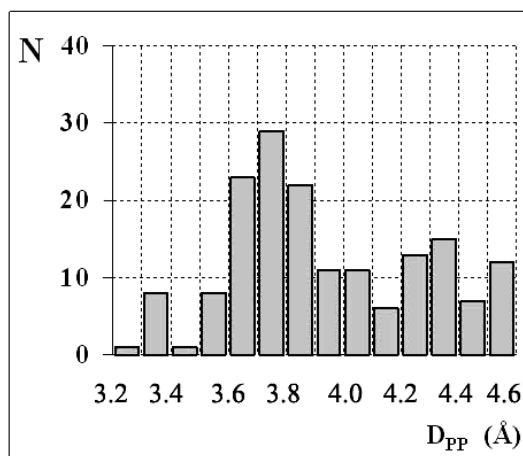


Figure 1. Histogram presenting centroid-centroid distance (**D_{pp}**) of the two interacting pyridine fragments.

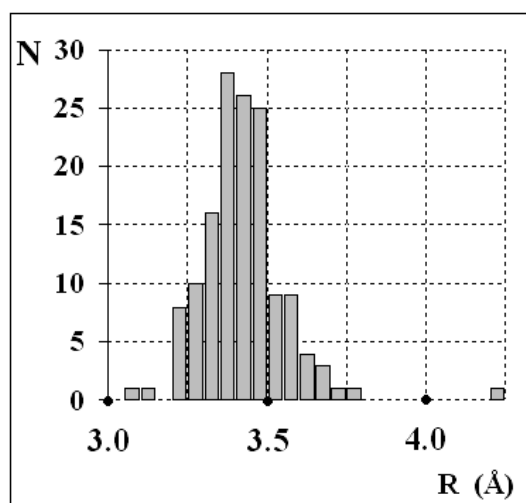


Figure 2. Histogram presenting normal distances (**R**) between the planes P_1 and P_2 of the two interacting pyridine fragments

The parallel orientations and normal distances of the pyridine fragments planes indicate the stacking interactions. In the terpyridyl ligand there are three pyridine fragments and there are possibilities that one, two or all three fragments are involved in the intermolecular stacking interactions. The analysis shows that only in three structures overlapping includes the whole ligand (and all three pyridine fragments) (Fig. 3). In these structures M...M distances are quite short. In the ABAXIL structure the metal ion is Ni^{2+} , and M...M distances

are 3.205, 3.142 and 3.204 Å. In the FECFOJ structure the metal ion is Ag^+ , with an M...M distance of 3.550 Å, while in the NEDVIC structure the metal ion is Pt^{2+} , with an M...M distance of 3.988 Å.

There are 9 interactions with very short Dpp distances, below 3.4 Å (Fig. 1). All these interactions are in ABAXIL structure where the two terpyridyl ligands of two complexes are overlapping with the whole surface.

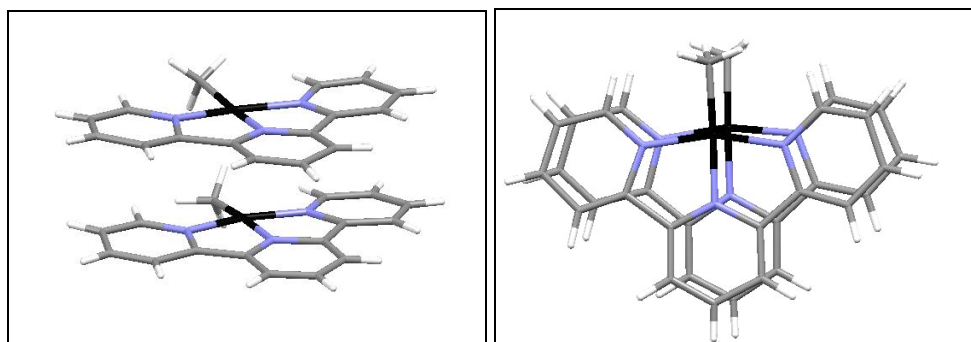


Figure 3. Overlap of square-planar complexes in crystal structure ABAXIL

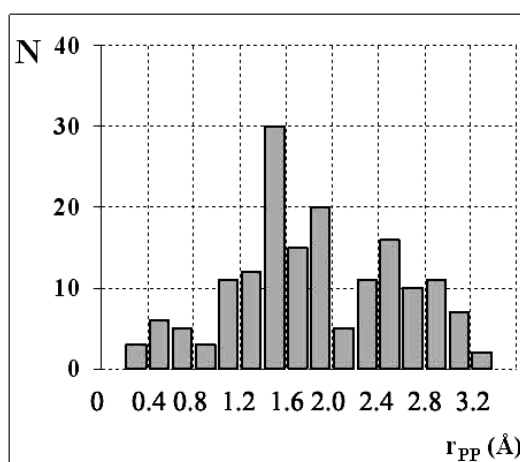
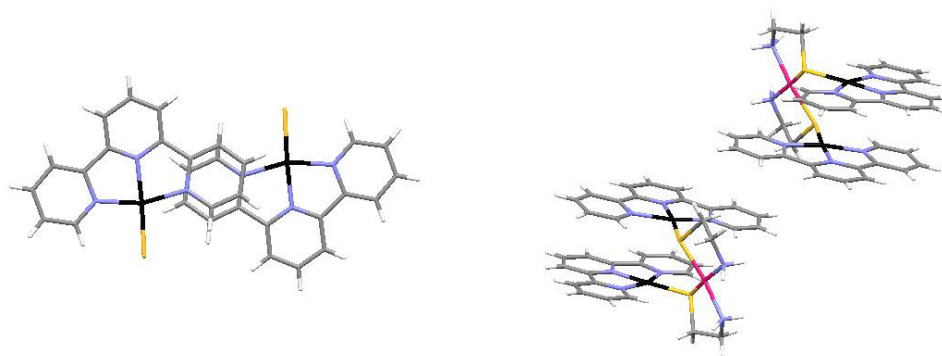


Figure 4. Histogram presenting horizontal displacement r of two interacting pyridine fragments

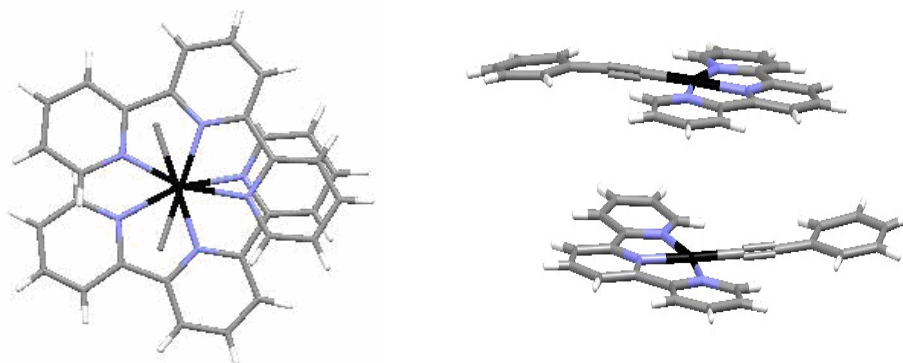
A histogram presenting the horizontal displacement r of two interacting pyridine fragments is shown in Fig. 4. In the ABAXIL structure there are very short **Dpp** distances, and also very short displacements r (Fig. 3). The other interactions with the displacement r smaller than 1.0 Å are in four structures where one ring overlaps and in two structures where two rings overlap. Two examples of structures where one ring is involved in overlap

are shown in Figure 5, structures GUMPUZ and PUWJIA. In both structures terminal pyridine fragments overlap, however, the orientations of the whole complexes are very different. In the structure PUWJIA metal-metal distance is very short (the Pt...Pt distance is 3.375 Å).

Two structures with overlap of two pyridine fragments are shown in Figure 6. In the structure LAJYUQ two terminal pyridine fragments overlap and so do both chelate rings; hence, a large part of the molecule is involved in the overlap, including also the metal atoms. In the structure NEVTAK, only the terminal and central pyridine fragment overlap, while the rest of the molecule is not involved in the overlap.

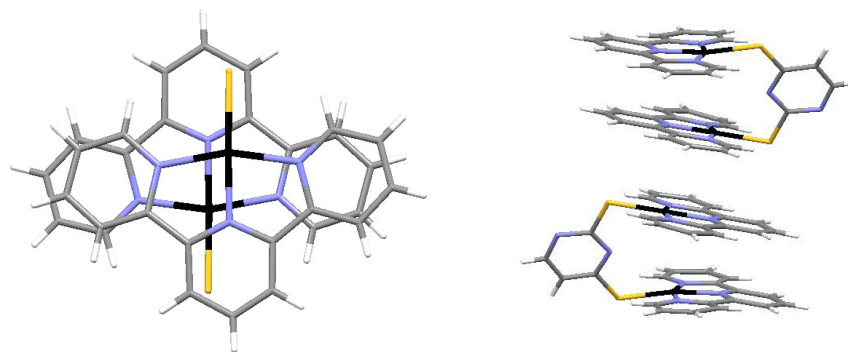


Structure GUMPUZ

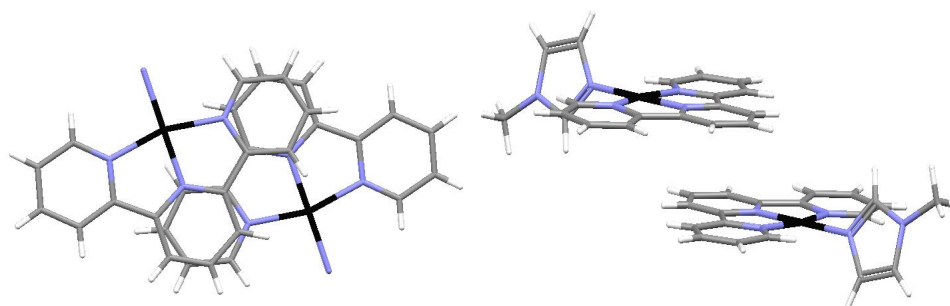


Structure PUWJIA

Figure 5. Overlap of terminal pyridine fragments in crystal structures GUMPUZ and PUWJIA



Structure LAJYUQ



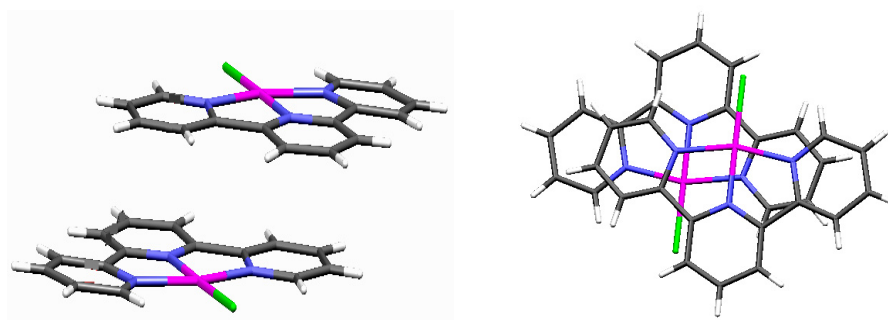
Structure NEVTAK

Figure 6. Overlapping of two pyridine fragments in crystal structures LAJYUQ and NEVTAK

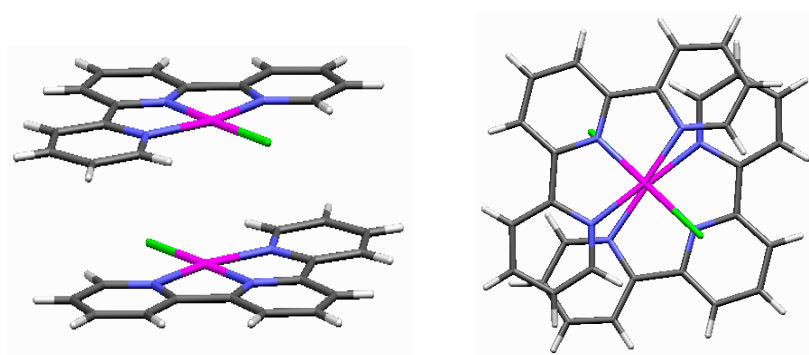
The distribution of horizontal displacement r values shows that in large number for the structures r is from 1.4 to 2.0 Å (Fig. 4). However, a substantial number of structures have r value above 2.4 Å. When offset r is close to 3.0 Å, the overlap of the rings is quite small. The examples of the structures with the horizontal displacement r values in the range of 1.4 to 2.0 Å are given in the Fig. 7, 8, and 9.

In some of these structures, not only the pyridine fragment but also a large part of the complex is involved in the overlap (structures SASRUA01 and HAYNAX, Fig. 7). In these two structures the mutual orientations of the complexes are very different. In some complexes two pairs of pyridine fragments, terminal and central, can overlap, without involving the rest of the complex. The example is shown in Figure 8.

STACKING INTERACTIONS BETWEEN PYRIDINE FRAGMENTS IN CRYSTAL STRUCTURES ...



Structure SASRUA01



Structure HAYNAX

Figure 7. Example of the crystal structures in which large part of the complex is involved in the overlap

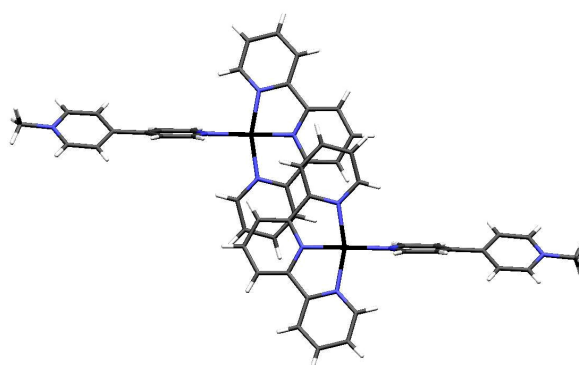


Figure 8. Example of crystal a structure (KAGQUF) with overlap of terminal and central pyridine fragments.

There are also examples where only one pyridine fragment is involved in the overlap. The example is structure NIKHIY with overlap of terminal pyridine fragments (Figure 9).

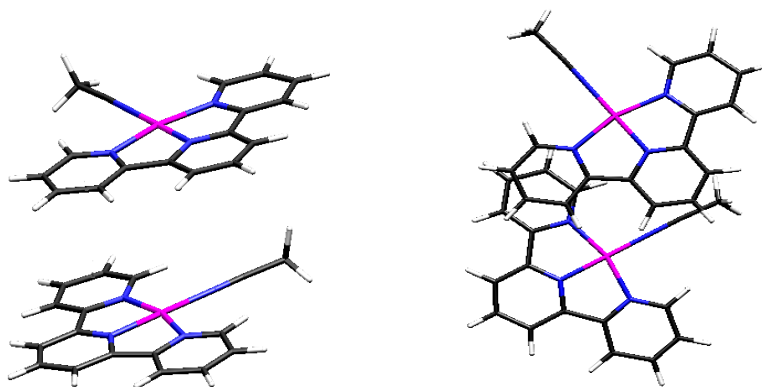
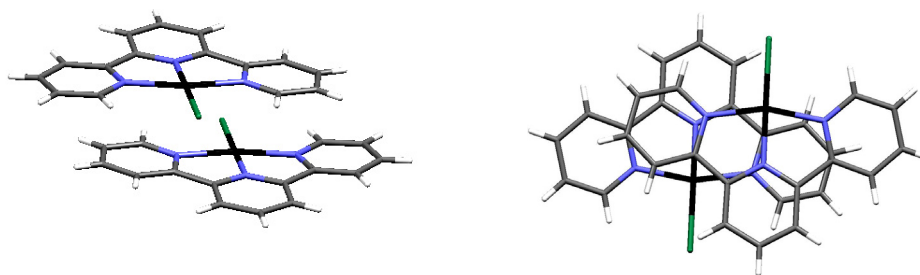


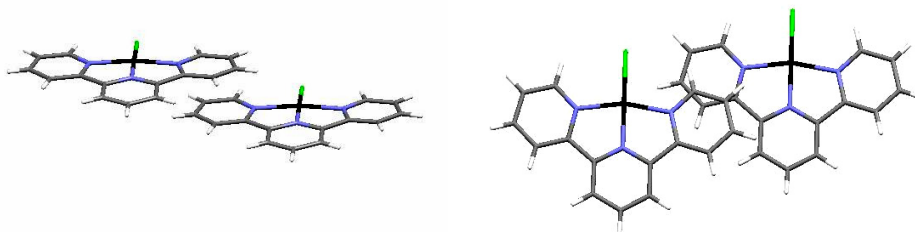
Figure 9. Overlap of terminal pyridine fragments in crystal structure NIKHIY

The examples of the structures with very small overlap area, and the horizontal displacement r larger of 2.5 Å are shown in Figures 10 and 11. The small overlap of pyridine fragments can occur in the structures where pyridine fragments overlap with chelate ring, structure AXEROK, Figure 10. Also small overlap can occur in structures where only terminal pyridine is involved, like in the structure BUYMOX.



Structure AXEROK

Figure 10. Example of the crystal structure with small overlap of pyridine fragments.



Structure BUYMOX

Figure 11. Example of the crystal structure with small overlap of pyridine fragments.

CONCLUSIONS

In the crystal structures of terpyridyl complexes from Cambridge Structural Database (CSD) stacking interactions between the pyridine fragments were studied. Square-planar complexes where the distance between the centers of two pyridine fragments was below 4.6 Å were retrieved from CSD. With this search 68 crystal structures with 167 interactions were found. In the interactions one, two or three pyridine fragments of one complex can be involved in overlapping with pyridine fragments of the other complex. The normal distances are in the range of 3.0 to 3.8 Å, in agreement with the typical distances in stacking interactions. The horizontal displacements of the two pyridine fragments are in large range, from values below 1.0 Å, up to 3.2 Å, indicating very different area of the overlap of the rings. In a small number of the structures whole area of the pyridine fragments overlap. In most of the structures the horizontal displacement is from 1.4 to 2.0 Å. Visual inspections of the structures revealed that various orientations of the pyridine fragments and the complexes are possible, with overlap of only one pyridine fragment of the complex, to overlap of the large area of the complex.

METHODOLOGY SECTION

The study is based on the crystal structures archived in the Cambridge Structural Database. The crystal structures of square-planar terpyridyl complexes were screened for intermolecular contacts. The CSD search program ConQuest 1.10 was used to retrieve structures satisfying the following criteria: a) the crystallographic R factor < 10% b) the error-free coordinates according to the

criteria used in the CSD c) the H-atom positions were normalized using the CSD default X-H bond lengths (O-H = 0.983 Å; C-H = 1.083 Å and N-H = 1.009 Å) d) no polymer structures.

In order to find intermolecular stacking interactions between terpyridyl ligands we searched for the structures with the distance between centroids of pyridine fragments below 4.6 Å. The same criteria were used before [8a]. This search separated 68 crystal structures with a total of 167 interactions. In the terpyridyl ligand there are two types of pyridine fragments: terminal (T) and central fragments (C) (Figure 12).

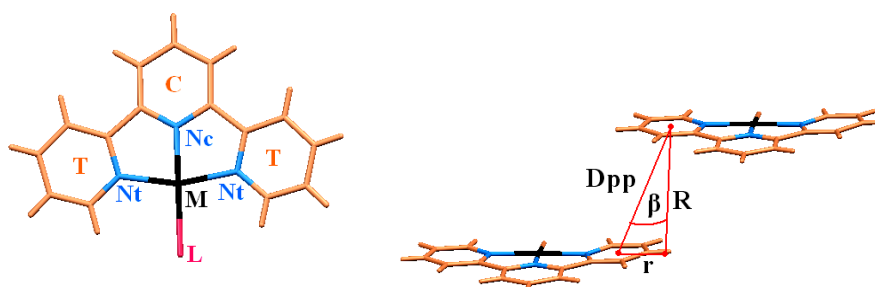


Figure 12. Atom labeling scheme and geometric parameters used for stacking interactions analysis

The geometric parameters used for analyzing geometries of the interactions and the atom labeling scheme are given in Figure 12. The distances between centroids of the rings are Dpp (two pyridine fragments). The angle β is defined as the angle between the vector connecting the centers of pyridine rings (Dpp) and the normal to the plane of one of the rings. The normal distance between the planes of interacting rings is R. The distance of the projection of the center of the first pyridine ring onto the plane of the second ring from the center of the second ring is the horizontal displacement r (Figure 12).

T₁

T₂

ACKNOWLEDGMENTS

Financial support was provided by the Foundation of Serbian Ministry of Science (Grant No. 142037).

REFERENCES

1. J.C. Ma, D.A. Dougherty, *Chemical Reviews*, **1997**, 97,1303.
2. (a) K.K. Laali, S. Hupertz, A.G. Temu, S.E. Galembeck, *Organic & Biomolecular Chemistry*, **2005**, 3, 2319; (b) Y. Li, C.M. Yang, *Journal of the American Chemical Society*, **2005**, 127, 3527; (c) W.L. Zhu, X.J. Tan, J.H. Shen, X.M. Luo, F. Cheng, P.C. Mok, R.Y. Ji, K.X. Chen, H.L. Jiang, *The Journal of Physical Chemistry A*, **2003**, 107, 2296; (d) X.L. Yuan, X.L. Cheng, X.F. Su, *International Journal of Quantum Chemistry*, **2009**, 109, 972. (e) D.Q. Zhu, B.E. Herbert, M.A. Schlautman, E.R. Carraway, *Journal of Environmental Quality*, **2004**, 33, 276.
3. (a) E.V. Pletneva, A.T. Laederach, D.B. Fulton, N.M. Kostic, *Journal of the American Chemical Society*, **2001**, 123, 6232; (b) T.P. Burghardt, N. Juranic, S. Macura, K. Ajtai, *Biopolymers*, **2002**, 63, 261; (c) K.A. McMenimen, E.J. Petersson, H.A. Lester, D.A. Dougherty, *ACS Chemical Biology*, **2006**, 1, 227.
4. (a) E.A. Meyer, R.K. Castellano, F. Diederich, *Angewandte Chemie Int. Ed.*, **2003**, 42, 1210; (b) P. Hobza, R. Zahradnik, K. Muller-Dethlefs, *Collect. Czech. Chemical Communications*, **2006**, 71, 443.
5. (a) T. Steiner, *Angewandte Chemie, Int. Ed.*, **2002**, 41, 48; (b) M. Nishio, *CrystEngComm*, **2004**, 6, 130. (c) S. Anand, A. Anbarasu, R. Sethumadhavan, *International Journal of Biological Macromolecules*, **2008**, 43, 468.
6. (a) S. Tsuzuki, K. Honda, T. Uchimarui, M. Mikami and A. Fujii, *The Journal of Physical Chemistry A*, **2006**, 110, 10163; (b) K. Shibasaki, A. Fujii, N. Mikami and S. Tsuzuki, *The Journal of Physical Chemistry A*, **2006**, 110, 4397.
7. (a) T. Steiner, G. Koellner, *Journal of Molecular Biology*, **2001**, 305, 535; (b) M. Brandl, M.S. Weiss, A. Jabs, J. Suhnel, R. Hilgenfeld, *Journal of Molecular Biology*, **2001**, 307, 357.
8. (a) C. Janiak, *Journal of the Chemical Society Dalton Transactions*, **2000**, 3885; (b) S.L. Cockroft, C.A. Hunter, K.R. Lawson, J. Perkins, C.J. Urch, *Journal of the American Chemical Society*, **2005**, 127, 8594.
9. (a) C.E. Crespo-Hernandez, B. Cohen, B. Kohler, *Nature*, **2005**, 436, 1141; (b) C.F. Matta, N. Castillo, R.J. Boyd, *The Journal of Physical Chemistry B*, **2006**, 110, 563.
10. (a) W. Schmitt, C.E. Anson, J.P. Hill, A.K. Powell, *Journal of the American Chemical Society*, **2003**, 125, 11142; (b) O. Yamauchi, A. Odani, M. Takani, *Journal of the Chemical Society, Dalton Transactions*, **2002**, 3411; (c) S. Novokmet, F.W. Heinemann, A. Zahl, R. Alsfasser, *Inorganic Chemistry*, **2005**, 44, 4796; (d) A. Tamayo, L. Escriche, J. Casabo, B. Covelo, C. Lodeiro, *European Journal of Inorganic Chemistry*, **2006**, 15, 2997; (e) C.F. Wang, Z.Y. Zhu, Z.X. Zhang, Z.X. Chen, X.G. Zhou, *CrystEngComm*, **2007**, 9, 35; (f) J. Zokerman-Schpector, I. Haiduc, *CrystEngComm*, **2002**, 33, 178; (g) A. Fernandez-Botello, A. Holy, V. Moreno, B.P. Operschall, H. Sigel, *Inorganica Chimica Acta*, **2009**, 28, 433.
11. (a) S.D. Zarić, *Chemical Physics Letters*, **1999**, 311, 77; (b) S.D. Zarić, D. Popović, E.W. Knapp, *Chemistry - A European Journal*, **2000**, 6, 3935; (c) M.K. Milčić, S.D. Zarić, *European Journal of Inorganic Chemistry*, **2001**, 8, 2143; (d) M.K. Milčić, Z.D. Tomić, S.D. Zarić, *Inorganica Chimica Acta*, **2004**, 357, 4327. (e) G.V. Janjić, M.K. Milčić, S.D. Zarić, *Chemical Papers*, **2009**, 63, 298.

12. S.D. Zarić, *European Journal of Inorganic Chemistry*, **2003**, 2197.
13. M.K. Milčić, V.B. Medaković, D.N. Sredojević, N.O. Juranić, S.D. Zarić, *Inorganic Chemistry*, **2006**, *45*, 4755.
14. (a) H. Suezawa, T. Yoshida, Y. Umezawa, S. Tsuboyama and M. Nishio, *European Journal of Inorganic Chemistry*, **2002**, 3148; (b) H. Kumita, T. Kato, K. Jitsukawa, H. Einaga and H. Masuda, *Inorganic Chemistry*, **2001**, *40*, 3936; (c) H. Tsubaki, S. Tohyama, K. Koike, H. Saitoh, O. Ishitani, *Dalton Transactions*, **2005**, 385.
15. (a) G.A. Bogdanović, A. Spasojević-de Bire and S.D. Zarić, *European Journal of Inorganic Chemistry*, **2002**, *7*, 1599; (b) M.K. Milčić, V.B. Medaković, S.D. Zarić, *Inorganica Chimica Acta*, **2006**, *359*, 4427.
16. (a) G.A. Bogdanović, V.B. Medaković, M.K. Milčić, S.D. Zarić, *International Journal of Molecular Sciences*, **2004**, *5*, 174; (b) V.B. Medaković, M.K. Milčić, G.A. Bogdanović, S.D. Zarić, *Journal of Inorganic Biochemistry*, **2004**, *98*, 1867; (c) P.D.W. Boyd, A. Hosseini, *Acta Crystallographica, Sect. E*, **2006**, *E62*, o2081.
17. (a) Y.F. Jiang, C.J. Xi, Y.Z. Liu, J. Niclos-Gutierrez and D. Choquesillo-Lazarte, *European Journal of Inorganic Chemistry*, **2005**, 1585; (b) V. Philip, V. Suni, M.R.P. Kurup, M. Nethaji, *Polyhedron*, **2004**, *23*, 1225; (c) H. Tsubaki, S. Tohyama, K. Koike, H. Saitoh, O. Ishitani, *Dalton Transactions*, **2005**, 385; (d) U. Abram, A. Castineiras, I. Garcia-Santos, R. Rodriguez- Riobo, *European Journal of Inorganic Chemistry*, **2006**, 3079.
18. S.D. Stojanović, V.B. Medaković, G. Predović, M. Beljanski, S.D. Zarić, *The Journal of Biological Inorganic Chemistry*, **2007**, *12*, 1063.
19. (a) Z.D. Tomić, S.B. Novaković, S.D. Zarić, *European Journal of Inorganic Chemistry*, **2004**, 2215; (b) D.N. Sredojević, Z.D. Tomić, S.D. Zarić, *Central European Journal of Chemistry*, **2007**, *5*, 20.
20. (a) Z.D. Tomić, D.N. Sredojević, S.D. Zarić, *Crystal Growth & Design*, **2006**, *6*, 29; (b) D. Sredojević, G.A. Bogdanović, Z.D. Tomić, S.D. Zarić, *CrystEngComm.*, **2007**, *9*, 793; (c) D.N. Sredojević, Z.D. Tomić, S.D. Zarić, *Crystal Growth&Design*, **2010**, *10*, 3901.
21. (a) A. Castineiras, A.G. Sicilia-Zafra, J.M. Gonzales-Perez, D. Choquesillo-Lazarte and J. Niclos-Gutierrez, *Inorgic Chemistry*, **2002**, *41*, 6956; (b) E. Craven, C. Zhang, C. Janiak, G. Rheinwald, H. Lang, *Z. Anorg. Allg. Chem.*, **2003**, 629, 2282; (c) U. Mukhopadhyay, D. Choquesillo-Lazarte, J. Niclos-Gutierrez, I. Bernal, *CrystEngComm*, **2004**, *6*, 627.
22. (a) S. Tsuzuki, K. Honda, T. Uchimaru, M. Mikami, K. Tanabe, *Journal of American Chemical Society*, **2002**, *124*, 104; (b) M.O. Sinnokrot, E.F. Valeev, C.D. Sherrill, *Journal of American Chemical Society*, **2002**, *124*, 10887. (c) M.O. Sinnokrot, C.D. Sherrill, *The Journal of Physical Chemistry A*, **2006**, *110*, 10656 (d) R. Podeszwa, R. Bukowski, K. Szalewicz, *The Journal of Physical Chemistry A*, **2006**, *110*, 10345 (e) M. Pitonak, P. Neogrady, J. Rezac, P. Jurecka, M. Urban, P. Hobza, *Journal of Chemical Theory and Computation*, **2008**, *4*, 1829.
23. H. Masui, *Coordination Chemistry Rewievs*, **2001**, 957, 219.

TRI-ARMED PODANDS AS EFFICIENT PRECURSORS FOR SUPRAMOLECULAR SYSTEMS

CORNELIA OPREA, VLAD PAȘCANU, CRINA CISMAȘ*,
ANAMARIA TEREĆ, RICHARD ATILA VARGA AND ION GROSU

ABSTRACT. The synthesis and structure of podands with isocyanurate core are described. The tosyl and azide terminal groups can ensure further functionalization towards supramolecular architectures. The tritosylated derivative was subjected to strong basic treatment to yield an *N*-tosyloxazolidin-2-one, thus providing a new route to *N*-substituted oxazolidinones. X-ray crystal structure of the triazide podand is discussed.

Keywords: *tripodands, isocyanurate, azides, x-ray diffraction, hydrogen bonding*

INTRODUCTION

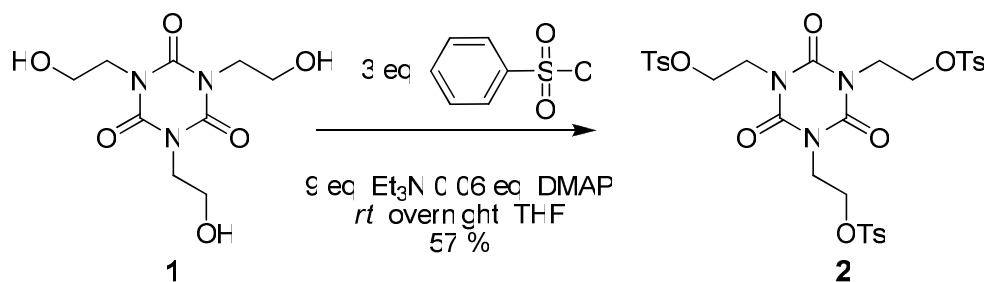
In the last decades, supramolecular chemistry [1] is one of the most dynamic areas in the chemical research. Its development requires rapid access to large molecules with well defined architectures. Tripodal structures represent smaller molecules which can be used as building blocks for macro- and supramolecular constructions. The elaboration of simple and efficient procedures for their synthesis is a continuous challenge for most of the researchers interested in this field. In this context, substrates with C_3 symmetry are of high interest, many studies being focused on the synthesis of derivatives with 1,3,5-trisubstituted benzene, [2] tertiary amines [3] or phosphines [4], cyclotrimertrilene [5] and 1,3,5-triazine[6] units. Transformation of C_3 symmetrical tripodal molecules into efficient hosts requires reactive terminal functional groups at the ends of the pendant arms. These peripheral groups have to exhibit: i) either the ability to participate in ring closure reactions with the formation of the corresponding cryptands; ii) or to allow reactions in which different units with high affinity for supramolecular interactions (*e.g.* by hydrogen bonding) can be attached to the pendant arms in order to promote the construction of supramolecular entities based on acyclic hosts. Recent developments in organic synthesis, *i.e.* click chemistry [7], suggest azide and tosylate as efficient terminal group candidates towards versatile tripodal intermediates.

* *Organic Chemistry Department, Faculty of Chemistry and Chemical Engineering, Babes-Bolyai University Cluj-Napoca, 11 Arany Janos str., RO-400028 Cluj-Napoca, Romania, csocaci@chem.ubbcluj.ro*

In our ongoing studies on the synthesis of various cryptand molecules we became interested in the synthesis of podands with isocyanuric platform. This central core may participate in hydrogen bonding interactions for highly functionalized supramolecular systems. We report hereafter the synthesis of two preorganized podands, as well as the solid state structure of one of them exhibiting already its supramolecular organization in the crystal.

RESULTS AND DISCUSSION

The synthesis of the tri-tosylated derivative **2** started from the commercially available 1,3,5-tris(hydroxyethyl) cyanuric acid **1** (Scheme 1). The substitution with tosyl chloride proceeded in the presence of triethylamine and *N,N*-dimethyl-aminopyridine (DMAP) as bases. The role of DMAP as an additional base is still obscure, however we observed a significant yield decrease (from 56 to 15 %) when the reaction was performed with the assistance of triethylamine only.



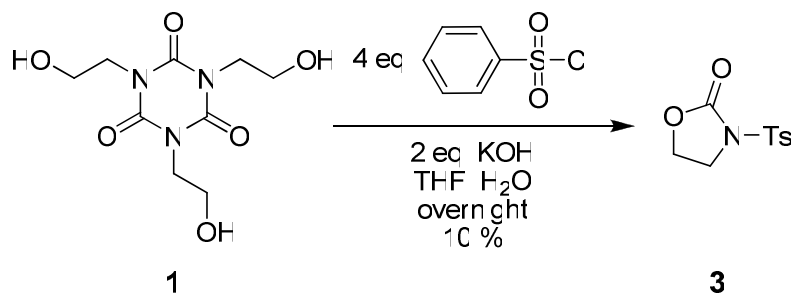
Scheme 1

The structure of tri-tosylate **2** has been proven by NMR Spectroscopy, meanwhile the ESI Mass Spectrum showed, besides the $[M+H]^+$ peak also the potassium adduct $[M+K]^+$ as well.

Even though the yield of **2** was not very high (57 %), this new podand represents, by its peripheral triple functionalities, an interesting precursor for various applications in the synthesis of supramolecular systems. Indeed, the ability of the tosylate fragment to be one of the best leaving group in the S_N substitutions is already a classic concept in organic synthesis.

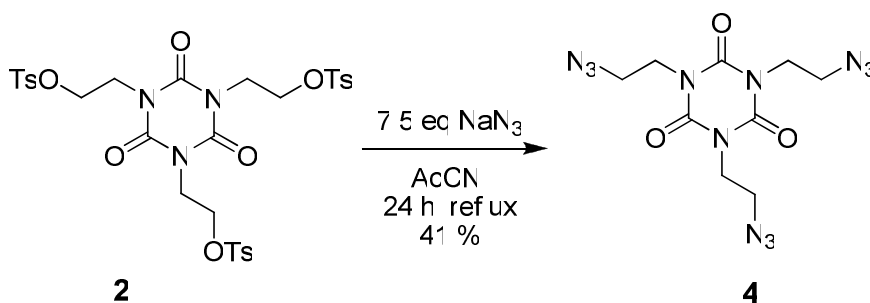
Next, using sodium hydroxide as base in aqueous tetrahydrofuran, a typical approach applied to **1** yielded the *N*-tosyl-oxazolidin-2-one **3** (Scheme 2). We have observed a similar behaviour of the commercially available compound **1** when propargylbromide, in strong basic protic media was employed.[8] Although compound **3** has been previously reported starting from dimethylenecyclourethane,[9] we considered our approach more facile in terms of synthetic methodology and

availability of the starting material. Nevertheless, the formation of derivative **3** can also be seen as a new route towards different *N*-substituted oxazolidinone derivatives, after optimizing the reaction.



Scheme 2

Finally, the synthesis of the triazide **4** was accomplished by nucleophilic displacement of tosyl groups of **2**, carried out with sodium azide, in acetonitrile (*Scheme 3*). The NMR spectra **4** are in accordance with the previously published ones by Sato *et al.*[10] In this case we were able to grow single crystals suitable for X-ray diffraction from an ethyl acetate/pentane (2/1) mixture.



Scheme 3

X-ray crystallographic analysis revealed the disposition of two of the pendant arms on one side of the isocyanuric plane, while the third one is facing the opposite direction, the last one showing unresolved nitrogen atoms of the azide group (**Figure 1**). The well resolved azide groups show a longer N(3)-N(4) [1.218 Å] and a shorter N(4)-N(5) [1.125 Å] bonds and the angle N(3)N(4)N(5) is slightly smaller (171.34°). The crystal packing presents an antiparallel arrangement of the azide groups, with a long intermolecular distance (3.607 Å). This is in accordance with the previously observed data showing that specific intermolecular contacts in the polyazides crystals are either absent or very weak.[11] We also observe another type of intermolecular contacts, namely hydrogen bonds between the isocyanurate oxygen atom and the methylene protons (2.409 Å).

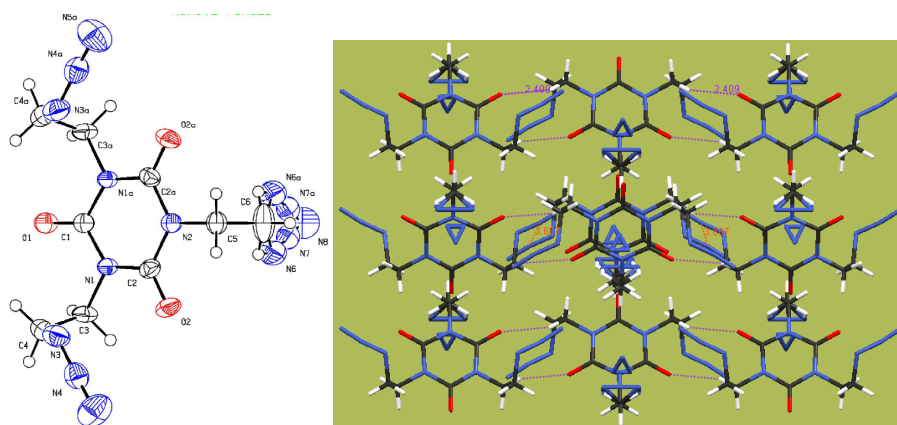


Figure 1. ORTEP diagram (left) and Mercury representation of the lattice (right) for compound **4**

Starting from the commercially available 1,3,5-tris(hydroxyethyl) cyanuric acid, two new podands with isocyanuric core were successfully obtained. The X-ray structure investigation of a triazide type tri-armed podand revealed the disposition of the pendant arms on both faces of the heterocyclic unit and the formation in the lattice of supermolecular aggregates by hydrogen bonding.

EXPERIMENTAL SECTION

^1H and ^{13}C NMR spectra were recorded on a Bruker Avance 300 spectrometer operating at 300 MHz (^1H) and 75 MHz (^{13}C) relative to TMS. MS were recorded on an ESI ion trap mass spectrometer (Agilent 6320) in positive mode. Solvents were dried and distilled under argon using standard procedures prior to use. Chemicals of commercial grade were used without further purification. Melting points are uncorrected. Column chromatography was carried out on Merck silica gel Si 60 (40–63 mm). TLC was carried out on aluminium plates coated with silica gel 60 F254 using UV lamp (254 nm) and KMnO_4 visualization.

The experimental conditions for the X-ray structure determination of compound **4** are as follows. The sample was studied on a Bruker SMART APEX with graphite monochromatized Mo $K\alpha$ radiation. The structure was solved with SHELXS [12] which reveals the non hydrogen atoms of the molecule. The whole structure was refined with SHELXL-97 [12] by the full-matrix least-square techniques. Atomic scattering factors from International Tables for X-ray Crystallography (1992) [13]. ORTEP view was realized with ORTEP3 [14]. The structural data is deposited at the Cambridge Crystallographic Data Center.

2,2',2''-(2,4,6-Trioxo-1,3,5-triazinane-1,3,5-triyl)tris(ethane-2,1-diyl)tris(4-methylbenzenesulfonate) (2)

A solution of compound **1** (2.000 g, 7.600 mmol), triethylamine (4.000 ml, 28.000 mmol) and *N,N*-dimethylaminopyridine (0.049 g, 0.400 mmol) in THF (50 ml) was cooled at 0-3 °C. After stirring for 90 minutes, a solution of tosyl chloride (4.130 g, 22.000 mmol) in THF (40 ml) was added dropwise with a push-syringe (rate: 0.5 ml/h). The resulting mixture was stirred overnight at room temperature, then extracted twice with ethyl acetate (2x35 ml). The organic phase was washed with water (2x50 ml), dried over sodium sulfate and concentrated in vacuo. The resulting powder was subjected to column chromatography using petroleum ether/ethyl acetate 1/1 as a mobile phase ($R_f = 0.6$). Compound (**2**) was obtained as white solid (m.p. = 125°C) in 57 % yield.

¹H-NMR: (300MHz, CDCl₃) δ ppm: 2.43 (s, 9H, CH₃), 4.13 (t, 6H, $J = 5.3$ Hz, N-CH₂), 4.26 (t, 6H, $J = 5.3$ Hz, CH₂-OTs), 7.32 (d, 6H, $J = 8.3$ Hz, CH-aromatic), 7.75 (d, 6H, $J = 8.3$ Hz, CH-aromatic)

¹³C-NMR: (75 MHz, CDCl₃) δ ppm: 21.7 (CH₃), 41.6 (O-CH₂), 65.8 (CH₂-OTs), 127.9 (2 x CH-aromatic), 129.9 (2 x CH-aromatic), 132.6 (C-S), 145.1 (C-CH₃), 148.3 (C=O)

ESI-MS: $m/z = 724$ ([M+H]⁺), 746 ([M+Na]⁺), 762 ([M+K]⁺)

***N*-Tosyl-oxazolidin-2-one (3)**

To a solution of 1,3,5-tris(hydroxyethyl)cyanuric acid **1** (2.00 g, 7.60 mmol) in THF (50 ml) a KOH solution (0.89 g, 16 mmol in 15 ml H₂O) was added. The mixture was cooled to 0° C and a solution of tosyl chloride (5.56 g, 30.00 mmol) in THF (20 ml) was added dropwise. The mixture was extracted with ethyl acetate (2x50 ml) and the organic phase washed with water (2x70 ml) and aqueous solution of NaHCO₃ (50 ml), concentrated and the crude product subjected to column chromatography using petroleum ether/ethyl acetate 2/1 as a mobile phase ($R_f = 0.23$). Compound (**3**) was obtained as a white solid (m.p. = 183°C (dec.)) 10% yield (for a 50% conversion).

¹H-NMR (300 MHz, CDCl₃) δ ppm: 2.46 (s, 3H, CH₃), 4.05 (t, $J = 7.8$ Hz, 2H, N-CH₂), 4.37 (t, $J = 7.8$ Hz, 2H, O-CH₂), 7.37 (d, $J = 8.2$ Hz, 2H, CH-aromatic), 7.95 (d, $J = 8.2$ Hz, 2H, CH-aromatic)

¹³C-NMR (75 MHz, CDCl₃) δ ppm: 21.7 (CH₃), 44.6 (N-CH₂), 62.2 (O-CH₂), 128.3 (CH-aromatic), 129.9 (CH-aromatic), 133.7 (C-S), 145.8 (C-CH₃), 152.0 (C=O)

1,3,5-Tris(2-azidoethyl)-1,3,5-triazinane-2,4,6-trione (4)

A mixture of compound **2** (1.00 g, 1.61 mmol), sodium azide (0.80 g, 12.00 mmol) in acetonitrile (25 ml) was refluxed for 24 hours under vigorous stirring. The reaction mixture was evaporated and the residue was dissolved in ethyl acetate (50 ml). The insoluble impurities were removed by filtration. The crude mixture was subjected to column chromatography pentane/ethyl acetate 2/1 ($R_f = 0.64$). The white solid was obtained in 41% yield (m.p. = 84 °C).

¹H-NMR (300MHz, CDCl₃) δ ppm: 3.58 (t, *J* = 6.0 Hz, 6H, N-CH₂), 4.16 (t, *J* = 6.0 Hz, 6H, CH₂-N₃)
¹³C-NMR (75MHz, CDCl₃) δ ppm: 41.7 (N-CH₂), 48.4 (CH₂-N₃), 148.6 (C=O)

ACKNOWLEDGMENTS

This work was supported by CNCSIS –UEFISCSU, project number PNII – IDEI 2358/2008. VP thanks Babes-Bolyai University for the Performance Scholarship.

REFERENCES

1. J. L. Atwood, J. W. Steed, *Encyclopedia of Supramolecular Chemistry*, Marcel Dekker, Inc., 2004.
2. a) B. Gomez-Lor, G. Hennrich, B. Alonso, A. Monge, E. Gutierrez-Puebla, A.M. Echavarren, *Angew. Chem. Int. Ed.* **2006**, *45*, 4491. b) K. Kumazawa, Y. Yamanoi, M. Yoshizawa, T. Kusukawa, M. Fujita, *Angew. Chem. Int. Ed.*, **2004**, *43*, 5936-5940; c) S. Kotha, D. Kashinath, K. Lahiri, R.B. Sunoj, *Eur. J. Org. Chem.*, **2004**, 4003.
3. C. Seel, F. Vogtle, *Angew. Chem. Int. Ed.*, **1992**, *31*, 528.
4. K.H. Lee, D.H. Lee, S. Hwang, O.S. Lee, D.S. Chung, J.I. Hong, *Org. Lett.*, **2003**, *5*, 1431.
5. a) C. Carruthers, T.K. Ronson, C. Sumbly, A. Westcott, L.P. Harding, T.J. Prior, P. Rizkallah, M.L. Hardie, *Chem. Eur. J.* **2008**, *14*, 10286. b) R. Ahmad, M.J. Hardie *Supramol. Chem.*, **2006**, *18*, 29.
6. a) P.L. Anelli, L. Lunazzi, F. Montanari, S. Quici, *J. Org. Chem.*, **1984**, *49*, 4197; b) G. Sandford, *Chem. Eur. J.*, **2003**, *9*, 1465.
7. H.C. Kolb, M.G. Finn, K.B. Sharpless, *Angew. Chem. Int. Ed.*, **2001**, *40*, 2004.
8. F. Piron, C. Oprea, C. Cismaș, A. Terec, J. Roncali, I. Grosu *Synthesis*, **2010**, *10*, 1639.
9. J.E. Herweh, W.J. Kauffmann, *Journal of Heterocyclic Chemistry*, **1971**, *8*, 983.
10. T. Nabeshima, S. Masubuchi, N. Taguchi, S. Akine, T. Saiki, S. Sato, *Tetrahedron Lett.*, **2007**, *48*, 1595.
11. K.A. Lyssenko, Y.V. Nelubina, D.V. Safronov, O.I. Haustova, R.G. Kostyanovsky, D.A. Lenev, M.Y. Antipin, *Mendeleev Commun.*, **2005**, *15*, 232.
12. G.M. Sheldrick, *Acta Cryst.*, *A64*, **2008**, 112.
13. A.J.C. Wilson (Ed.) *International Tables for X-ray Crystallography* Vol. C, Kluwer Academic Publisher, Dordrecht, **1992**.
14. L.J. Farrugia, *J. Appl. Crystallogr.*, **1997**, *30*, 565.

**SYNTHESIS, SEPARATION AND X-RAY DIFFRACTOMETRY
INVESTIGATIONS OF *TRANS, TRANS* 1,4-BIS(5'-HYDROXYMETHYL-
2',5'-DIMETHYL-1',3'-DIOXAN-2'-YL)BENZENE**

**MONICA CÎRCU, VLAD NISTE, RICHARD ATTILA VARGA,
EMESE DÉNES, ELENA BOGDAN, CRINA CISMAȘ
AND ION GROSU**

ABSTRACT. The isolation of pure *trans - trans* isomer of 1,4-(2,5,5-trimethyl-5,5-dihydroxymethyl-1,3-dioxan-2-yl)benzene *via* O-protection, column chromatography then deprotection followed by determination of its structure by solid state X-ray diffractometry are reported.

Keywords: 1,3-dioxanes, X-ray structure, supramolecular C-H- π interactions

INTRODUCTION

The stereochemistry of compounds bearing two or even three 1,3-dioxane rings attached to the same aromatic group was largely investigated by our group and the preference of the aromatic substituent either for the equatorial or axial orientation was observed [1-7].

The derivatives in which the aromatic unit is the unique substituent at the position 2 of the 1,3-dioxane ring (*i.e.* in compounds obtained by the acetalization of aromatic dialdehydes) exhibited the aromatic ligand in equatorial positions. In contrast, the simultaneous presence of methyl and aryl groups at the position 2 of the 1,3-dioxane units (in compounds obtained by the acetalization of 1,4-diacetylarenes) determines the axial orientation of the aromatic substituent (Chart 1).

These results were in agreement with literature data which predict, at the position 2 of the 1,3-dioxane ring, higher A-values for alkyl groups than for the aromatic ones [8-12].

Compounds possessing identical groups at position 5 of the 1,3-dioxane rings do not exhibit diastereomerism, whereas in the case of the derivatives having different groups at position 5, *cis-cis*, *trans-cis* and *cis-cis* steric relationships are possible (Chart 2).

* Babeș-Bolyai University, Faculty of Chemistry and Chemical Engineering, 11 Arany Janos str., RO-400028 Cluj-Napoca, Roumania, igrosu@chem.ubbcluj.ro

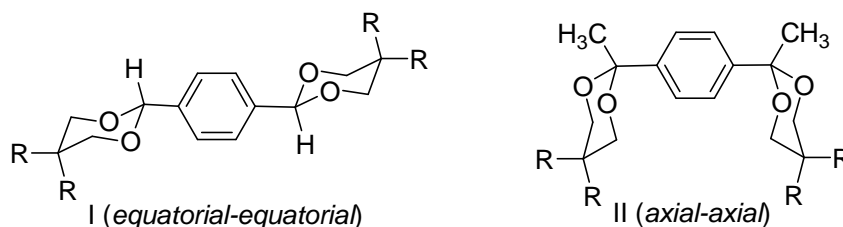
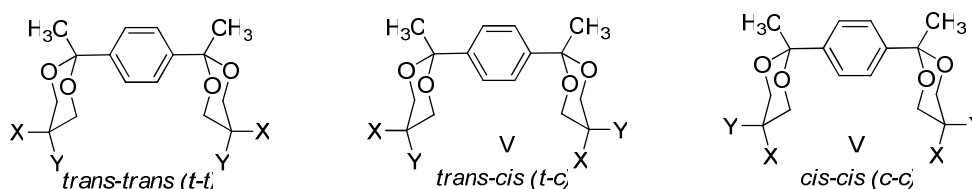


Chart 1. Bis(1,3-dioxan-2-yl)arenes with equatorial-equatorial (I) and axial-axial (II) orientations of the aromatic groups (see above).



CIP rank $X > Y$ and 1,4-phenylene $> Me$ for the descriptors *c* (*cis*) and *t* (*trans*)

Chart 2. *Trans-trans* (III), *trans-cis* (IV) and *cis-cis* (V) diastereomers of 1,4-bis(2-methyl-5-X-5-Y-1,3-dioxan-2-yl)benzene

Recently, *cis-cis* stereoisomers of some bis(1,3-dioxan-2-yl)arenes bearing equatorial hydroxymethyl functionalities at position 5 were isolated, then successfully used in the syntheses of molecular machines with cyclophane motifs [13,14].

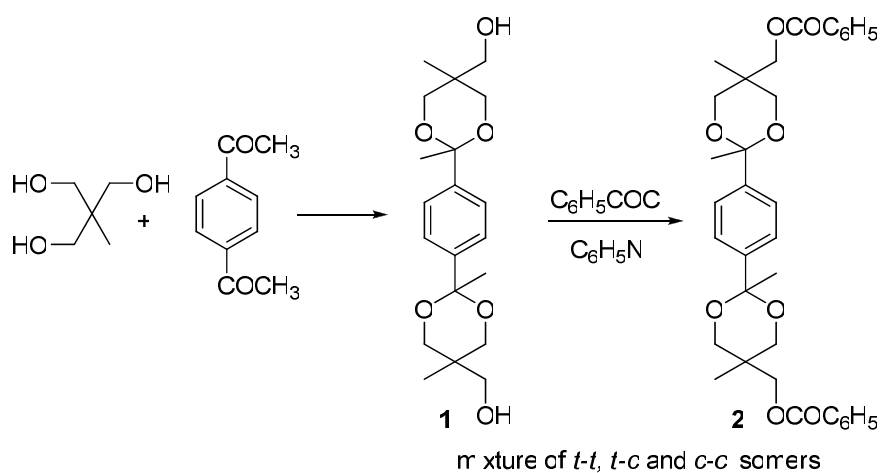
Hence, we considered of outstanding interest to also separate the *trans-trans* isomer of 1,4-(2,5,5-trimethyl-5,5-dihydroxymethyl-1,3-dioxan-2-yl)benzene of type III (*t-t*) ($X = CH_2OH$, $Y = Me$), to investigate its structure and to predict the possibilities to use this diastereomer as building block in cyclophanes synthesis.

RESULTS AND DISCUSSION

The synthesis of the diastereomeric mixture of 1,4-(2,5,5-trimethyl-5,5-dihydroxymethyl-1,3-dioxan-2-yl)benzenes **1** (Scheme 1) was carried out following a previously described procedure [5, 15]. Thus, in agreement with literature data [5,15] the *trans-trans* isomer of **1** was indeed the major component (60%) of the above mixture as the *cis-trans* and *cis-cis* analogous were obtained in smaller amounts.

The spatial disposal of the *cis-cis* isomer of **1** was previously considered the most appropriate to be used for further macrocyclization.

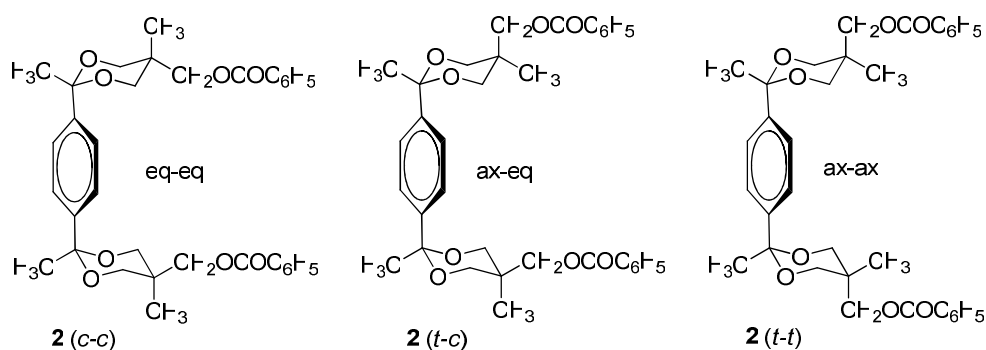
However, the separation of **1** (*c-c*) could not be carried out neither by crystallization nor by column chromatography since the solubility of these diols in usual solvents was low. In addition, not only that the NMR spectra of the mixture **1** (*c-c*), **1** (*c-t*) and **1** (*t-t*) exhibited many non-separable signals but also their individual appearance was very similar.



Scheme 1

In order to avoid these problems, the mixture of stereoisomers of diol **1** was converted into the corresponding mixture of diesters upon benzylation with benzoyl chloride. The ^1H NMR signals of the new mixture of diastereomeric diesters were well separated allowing easily the individual assignment of **1** (*c-c*), **1** (*c-t*) and **1** (*t-t*) [13,15].

Next, the *cis-cis* diastereomer of **2**, **2** (*c-c*) (Scheme 2) could be isolated simply as pure compound by repetitive crystallizations from diethylether. Then, its LiOH hydrolysis gave the *cis-cis* diol **2** (*c-c*) as unique isomer in good yields [13, 15].

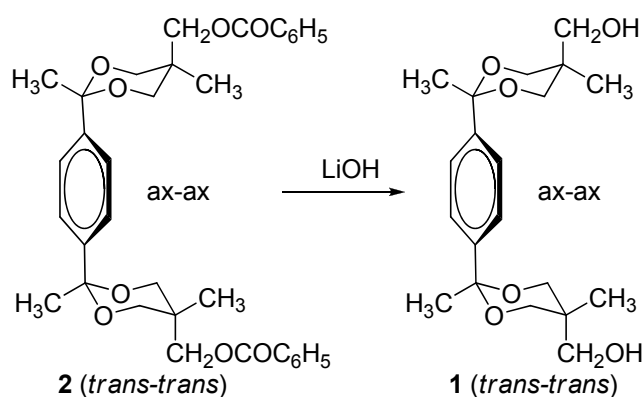


Scheme 2

In contrast, the *axial-axial* diester **2** (*t-t*) could not be isolated as single compound during the work-up described above [15].

Therefore, in the present study, we carried out the isolation of the *trans-trans* diester **2** (*t-t*) (Scheme 2) by column chromatography (eluent ethyl acetate: petroleum ether 1:1) and we investigated it as unique structure.

Then, as above, by LiOH deprotection (Scheme 3) we did succeed the obtention of the *trans-trans* diol **1** (*t-t*) as a single compound. Its structure was fully confirmed by NMR and its molecular structure provided by X-ray diffractometry.



Scheme 3

As expected, the later X-ray diffractometry molecular structure (Figure 1) revealed, the axial orientation of the phenylene and hydroxymethyl groups together with the opposite orientation of the 1,3-dioxane rings with respect to the plane of the aromatic linker.

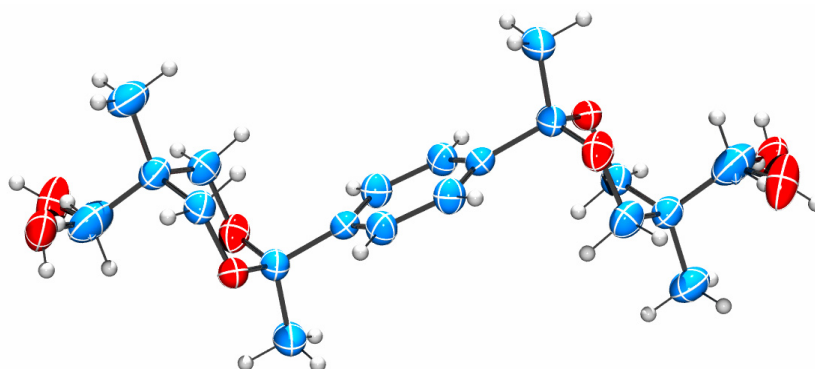


Figure 1. ORTEP diagram for the *trans-trans* diastereomer of **1**.

The phenylene ring exhibited an expected twice orthogonal rotameric orientation (the torsion angle $\text{CH}_3\text{-C}^{2'}\text{-C}_{\text{ar}}\text{-C}_{\text{ortho}} = 87.37^\circ$). The hydroxymethyl groups displayed a "hydrogen inside" conformation and this arrangement generated two diastereomeric arrangements, namely *syn* and *anti*.

One must observe that, due to the opposite sense of the 1,4-phenylene connection, the *syn* isomer is chiral, exhibiting both its OH groups on the same part of the plane containing the carbon atoms at the 1,3-dioxanic positions 2 and 5 being perpendicular on the aromatic ring. Conversely, the *anti* isomer is centrosymmetric, hence achiral, and disclosed the hydroxy groups on opposite sides of considered plane (Chart 3).

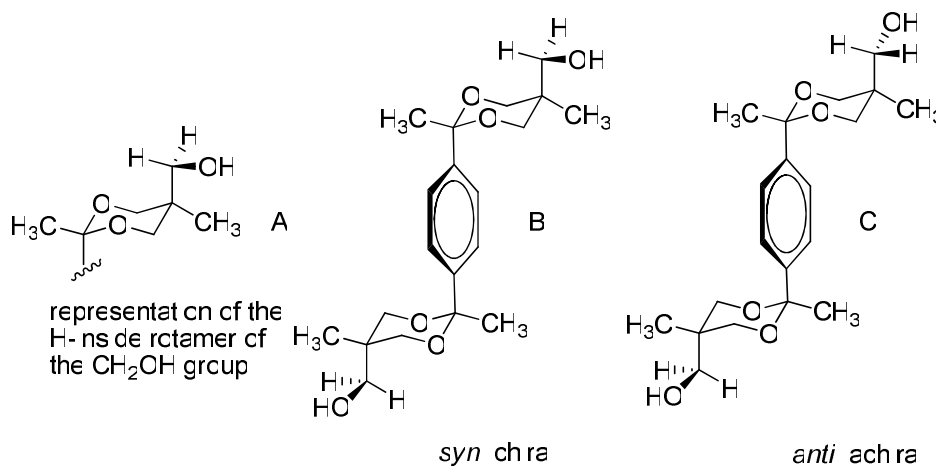


Chart 3. Representations of the H-inside rotamer (A) of the axial CH_2OH group and of the *syn* (B) and *anti* (C) isomers of **1** (*trans-trans*).

In the crystal, all stereoisomers, (\pm)*syn* and *anti*, were present and, as a consequence, when the structure of the compound was solved at each position, both orientations of the OH group exhibited the same probability, 50 % (Figure 1).

In the lattice (Figure 2), the formation of linear polymers along the *c* axis by C-H \cdots π interactions involving the hydrogen atoms of the methyl groups at 1,3-dioxanic positions 2 and the aromatic rings were observed (Figure 2). Each aromatic unit is connected on both sides with the methyl groups of the neighbouring molecules. The distances from the H atoms of the methyl group of one molecule to the centroid of the aromatic ring of the partner molecule are $d = 3.253, 3.648$ and 3.714 \AA .

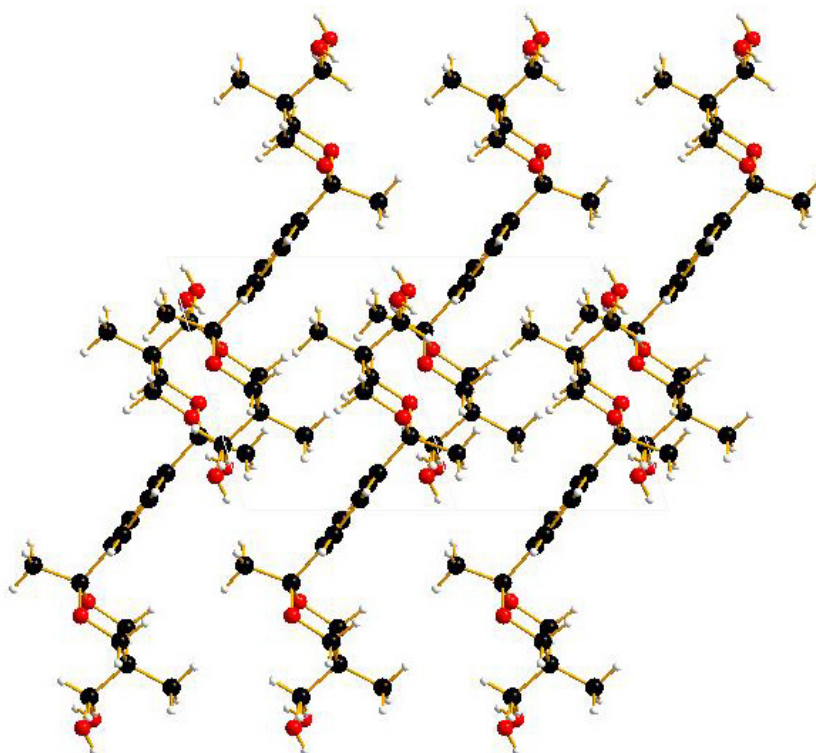


Figure 2. View (along the axis c) of the lattice of **1** (*trans-trans*)

CONCLUSIONS

The *trans-trans* isomer of 1,4-(2,5,5-trimethyl-5,5-dihydroxymethyl-1,3-dioxan-2-yl)benzene **1**, was isolated by column chromatography *via* its dibenzoyl derivative and its structure was determined by X-ray diffractometry. The solid state molecular structure revealed the axial orientation of the aromatic and of the hydroxymethyl groups. In the lattice, all aromatic rings were parallel and the formation of a linear polymer by C-H - π interactions involving the protons of the equatorial methyl groups at positions 2', 2'' and the aromatic rings was observed.

EXPERIMENTAL SECTION

^1H NMR (300 MHz) and ^{13}C NMR (75 MHz) spectra were recorded in CDCl_3 . APCI MS were recorded on ion trap spectrometer in positive mode. Melting points are uncorrected. Thin layer chromatography (TLC) was carried out on aluminium sheets coated with silica gel 60 F_{254} using UV and KMnO_4 visualization.

X-Ray data were collected at room temperature (297 K) using graphite-monochromated MoK α radiation. The structures were refined with anisotropic thermal parameters. The hydrogen atoms were refined with a riding model and a mutual isotropic thermal parameter. For structure solving and refinement the software package SHELX-97 was used.^{16,17} The drawings were created with Ortep¹⁸ and Diamond programs.¹⁹

1,4-(2',5',5'-trimethyl-5',5'-dihydroxymethyl-1',3'-dioxan-2'-yl)benzene (1)

The benzoylated ester **2** (2 mmol, 1.15 g) was dissolved in a mixture of THF (400 ml), MeOH (40 ml) and H₂O (20 ml) and cooled to 0 °C. LiOH (5 mmol, 0.210 g LiOHxH₂O) was added and the mixture was stirred at 0 °C until the complete saponification of the ester occurred (TLC monitoring). The solvents were evaporated and the crude product was dissolved in 50 ml diethyl ether and washed with brine. The organic phase was dried over anhydrous sodium sulphate and concentrated to dryness afford the desired product in 98% yield.

The desired *trans-trans* isomer was obtained as white solid, m.p.= 232-233^oC. *Calculated for C₂₀H₃₀O₆ (366.45): C, 65.55; H, 8.25; Found: C, 65.72; H, 8.40.*

¹H-NMR: (300 MHz, CDCl₃) δ ppm: 0.61 [s, 6H, 5'-CH_{3(eq)}], 1.53 (s, 6H, 2'-CH₃), 1.68 (t, *J* = 5.2 Hz, 2H, 5'-CH₂-OH), 3.47 (d, *J* = 11.6 Hz, 4H, 4'-H_{ax}, 6'-H_{ax}), 3.68 (d, *J* = 11.6 Hz, 4H, 4'-H_{eq}, 6'-H_{eq}), 3.91 (d, *J* = 5.2 Hz, 4H, 5'-CH₂), 7.43 (s, 4H, 2-H, 3-H, 5-H, 6-H, 1,4-phenylene).

¹³C-NMR: (75 MHz, CDCl₃) δ ppm: 17.0 (5'-CH₃), 32.1 (2'-CH₃), 34.6 (5'-C), 65.7 (5'-CH₂), 67.4 (4'-C, 6'-C), 100.4 (2'-C), 127.1 (2-C, 3-C, 5-C, 6-C), 140.0 (1-C, 4-C).

APCI-MS: *m/z* = 367 ([M+H]⁺).

1,4-(2',5',5'-trimethyl-5',5'-benzoyloxymethyl-1',3'-dioxan-2'-yl)benzene (2)

To a solution of C₆H₅COCl (20 ml) in dry pyridine (100ml) 1,4-(2,5,5-trimethyl-5,5-dihydroxymethyl-1,3-dioxan-2-yl)benzene **1** (10 mmol, 3,66 g) was added. The reaction mixture was stirred for 24 hours at room temperature. After removing the solvent, the crude product was dissolved in dichloromethane (100 ml), washed with aq. 10% NaOH (10%), H₂O (100 ml) and HCl solution (2%), then concentrated to dryness. The crude product was subjected to column chromatography using petroleum ether/ethyl acetate 2/1 as a mobile phase. The desired isomer, *trans-trans* (*R_f* = 0.32) was obtained as white solid (m.p. = 235-236^oC) in 30% yield.

Calculated for C₃₄H₃₈O₈ (574.66): C, 71.06; H, 6.67; Found: C, 70.89; H, 6.95.

¹H-NMR: (300MHz, CDCl₃) δ ppm: 0.70 [s, 6H, 5'-CH_{3(eq)}], 1.54 (s, 6H, 2'-CH₃), 3.53 (d, *J* = 11.0 Hz, 4H, 4'-H_{ax}, 6'-H_{ax}), 3.78 (d, *J* = 11.0 Hz, 4H, 4'-H_{eq}, 6'-H_{eq}), 4.62 (s, 4H, 5'-CH₂), 7.41-7.49 (overlaped signals, 8H, 2-H, 3-H, 5-H, 6-H, *m*-H), 7.54 (multiplet, 2H, *p*-H), 8.04 (d, *J* = 7.1 Hz, 4H, *o*-H).

¹³C-NMR: (75 MHz, CDCl₃) δ ppm: 17.7 (5'-CH₃), 32.4 (2'-CH₃), 34.1 (5'-C), 67.4 (5'-CH₂), 67.8 (4'-C, 6'-C), 101.0 (2'-C), 127.5 (2-C, 3-C, 5-C, 6-C), 128.73 (*m*-C), 129.9 (*o*-C), 130.6 (C quaternary aromatic), 133.3 (*p*-C), 140.3 (1-C, 4-C), 166.9 (5'-CH₂-O-C=O).

ACKNOWLEDGMENTS

We acknowledge the financial support of this work by PNCDI II program (UEFISCSU; project IDEAS 2278/2008) and we are grateful to Babes-Bolyai University for the performance research fellowship provided to V. Niste.

REFERENCES

- [1]. I. Grosu, S. Mager, G. Plé, N. Plé, A. Toscano, E. Mesaros, R. Martinez, *Liebigs Annalen / Recueil*, **1997**, 2371
- [2]. I. Grosu, S. Mager, L. Toupet, G. Plé, E. Mesaros, A. Mihis, *Acta Chem. Scand*, **1998**, 52, 366
- [3]. I. Grosu, S. Mager, E. Mesaros, G. Plé, *Heterocycl. Commun.*, **1998**, 4, 53
- [4]. M. C. Florian, M. Cîrcu, L. Toupet, A. Terec, I. Grosu, Y. Ramondenc, N. Dincă, G. Plé, *Centr. Eur. J. Chem.*, **2006**, 4, 808
- [5]. I. Grosu, L. Muntean, L. Toupet, G. Plé, M. Pop, M. Balog, S. Mager, E. Bogdan, *Monatsh. Chem.*, **2002**, 133, 631
- [6]. N. Bogdan, F. Pop, A. Gaz, E. Bogdan, A. Terec, L. David, I. Grosu, *Studia Univ. Babes-Bolyai, Chem.*, **2006**, LI, 3
- [7]. N. Bogdan, F. Pop, E. Bogdan, A. Gaz, A. Terec, L. David, I. Grosu, *Studia Univ. Babes-Bolyai, Chem.*, **2006**, LI, 13
- [8]. M.J.O. Anteunis, D. Tavernier, F. Borremans, *Heterocycles*, **1976**, 4, 293
- [9]. E. Kleinpeter, *Adv. Heterocycl. Chem.*, **1998**, 69, 217
- [10]. E. Kleinpeter, *Adv. Heterocycl. Chem.*, **2004**, 86, 41
- [11]. E.L. Eliel, S.H.Wilen, *Stereochemistry of Organic Compounds*, Wiley&Sons, New York, **1994**, p. 696
- [12]. F.G. Riddell, *The Conformational Analysis of Heterocyclic Compounds*, Academic Press, London, **1980**, p. 114
- [13]. M. Balog, I. Grosu, G. Plé, Y. Ramondenc, E. Condamine, R. Varga, *J. Org. Chem.* **2004**, 69, 1337
- [14]. N. Bogdan, I. Grosu, G. Benoît, L. Toupet, Y. Ramondenc, E. Condamine, I. Silaghi Dumitrescu, G. Plé, *Org. Lett.*, **2006**, 8, 2619
- [15]. M. Balog, PhD Thesis, Babes-Bolyai University and Université de Rouen, Cluj-Napoca, **2004**
- [16]. Sheldrick, G. M., *SHELX-97*, Universität Göttingen, Germany, **1997**
- [17] (a) Bruker (**1999**). SMART (Version 5.611), SAINT (Version 6.02a), SHELXTL, (Version 5.10) and SADABS. Bruker AXS Inc., Madison, Wisconsin, USA. (b) Claridge, J.B.; Layland, R.C.; Loye, H.-C. *Acta Cryst.*, **1997**, C53, 1740
- [18]. Farrugia, L.J., *J. Appl. Cryst.*, **1997**, 30, 565
- [19] *DIAMOND* - Visual Crystal Structure Information System; CRYSTAL IMPACT: P.O.B. 1251, D-53002 Bonn, Germany

PRELIMINARY INVESTIGATION OF MOCS METEORITE BY LEAD ISOTOPIC RATIO USING QUADRUPOLE INDUCTIVELY COUPLED PLASMA MASS SPECTROMETRY

CLAUDIU TĂNĂSELIA^a, STANKO ILIK-POPOV^b, DANA POP^c,
BELA ABRAHAM^a, CECILIA ROMAN^a, TRAJČE STAFILOV^b,
LEONTIN DAVID^d, MARIANA UDRESCU^d

ABSTRACT. Lead isotopic ratios ($^{207}\text{Pb}/^{206}\text{Pb}$ and $^{208}\text{Pb}/^{206}\text{Pb}$) were measured on a sample of Mocs L5-6 chondritic meteorite (from the collection of meteorites of the Museum of Mineralogy of the Babeş-Bolyai University, Cluj-Napoca, Romania), using a inductively coupled plasma quadrupole mass spectrometry method. A NIST 981 standard reference material was used for calibration and control. The obtained data for the standard reference material were within the certified range; the isotopic ratio values measured for Mocs meteorite were 0.8656 ± 0.0084 for $^{207}\text{Pb}/^{206}\text{Pb}$ and 2.1011 ± 0.0036 for $^{208}\text{Pb}/^{206}\text{Pb}$ and they were compared with other chondritic meteorites. The measured total Pb content was 0.888 ± 0.005 mg/kg. Due to isobaric interferences with ^{204}Hg , ^{204}Pb was excluded, but further method improvement is planned to include all lead stable isotopes due to their importance to geochronology dating.

Keywords: Pb isotopes, ICP-MS, Mocs meteorite, L5-6 chondrite

INTRODUCTION

Mocs meteorite, classified as L5-6 chondrite [1] fell as a shower of stones on 3rd February 1882, in Transylvania region over an area of several dozen squared kilometers near Mocs village (now Mociu, Cluj County, Romania, coordinates 46°48' N, 24°2' E). The number of recovered fragments was estimated at 3000, with a total weight of about 300 kg [2]. According to the Meteoritical Bulletin Database, Mocs is one of the 31 approved meteorites classified as L5-6. The exact fall location of the investigated Mocs meteorite sample (inv. no. I.34B) is Chesău village (Keszú, in the official catalogues of meteorites, e.g. [2]), Mociu Commune, Cluj County). Due to the large amount

^a INCDO-INOE2000 Research Institute for Analytical Instrumentation (ICIA), Donath 67, 400293 Cluj-Napoca, Romania, claudiu.tanaselia@icia.ro

^b Institute of Chemistry, Faculty of Science, POB 162, 1000, Skopje, Republic of Macedonia

^c Museum of Mineralogy, Babeş-Bolyai University, Kogălniceanu 1, 400084 Cluj-Napoca, Romania

^d Faculty of Physics, Babeş-Bolyai University, Kogălniceanu 1, 400084, Cluj-Napoca, Romania

of material present in more than 30 museums worldwide [2], Mocs meteorite has been intensely studied before; however, no lead isotopes measurements have been done so far. Our experiments concerned whole rock fragments.

With a wide spreading among analytical laboratories, ICP-MS technique has become an important tool for trace elements determination; the same technique allows isotopic ratio measurements, since the core of the instrument is represented by a quadrupole that can differentiate between different isotopes.

SAMPLE PREPARATION

A meteorite sample was provided for this study by Museum of Mineralogy, Babeş-Bolyai University, Cluj-Napoca, Romania. Prior to the measurements, the samples were well wash using ultrapure water and were carefully manipulated afterwards, avoiding any lead contamination. The samples had the fusion crust removed and then the fragment was precisely weighted and divided into three sub-samples with various mass. The sample was not fragmented by using a saw, in order to avoid contamination during processing into fine powder. The powder mass was weighted (0.2 grams each) and compared with the original mass of the bulk sample. Every sub-samples was digested separately and the dissociation was performed in a Teflon beaker on a sand box. The Teflon device was cleaned with *aqua regia* before measurements. Temperature of the sand box was kept constant ($T = 90^{\circ}\text{C}$). Every step uses a combination of strong acids as each step destroyed a part of the complex compound matrix. Following the dissociation, the solution was filtered into a 25 ml flask. The purpose of the procedure was to obtain enough concentrated solution that could be precisely measured with the ICP-MS. The steps are listed in Table 1.

Table 1. Four-step mineralization method for Mocs meteorite

Step 1	Step 2	Step 3	Step 4
2x5 ml HNO ₃ heat until 2ml left	5 ml HF 1.5 ml HClO ₄ heat until 2ml left	No heating 1 ml HCl 5 ml HNO ₃ ultrapure water	5 ml HNO ₃ 6.5 ml HF 5 ml HCl 1 ml H ₂ SO ₄ heat until 2ml left

For calibration and mass bias correction, a solution of NIST 981 standard reference material (natural lead standard, $^{204}\text{Pb}/^{206}\text{Pb} = 0.059042 \pm 0.000037$, $^{207}\text{Pb}/^{206}\text{Pb} = 0.91464 \pm 0.00033$, $^{208}\text{Pb}/^{206}\text{Pb} = 2.1681 \pm 0.0008$) was used. From the initial solid, wire-shaped material, a 20 ppb solution was prepared for daily use, by dissolving a weighted fragment of the reference material in nitric acid. The NIST 981 SRM sample was purchased directly from the National

Institute for Standards and Technology, NIST (USA). All other reagents were supplied by Merck. 18 M Ω cm⁻¹ DI water was prepared in the laboratory, using a Millipore- Milli-Q® ultrapure water purification system.

INSTRUMENTATION

SCIEX Perkin Elmer Elan DRC II (Canada) inductively coupled plasma mass spectrometer (with quadrupole and single detector setup) was used for this study. The operating parameters are listed in Table 2. The instrument's running parameters were checked and adjusted each analysis day, using a solution with 1 ppb In, 1 ppb Ce, 10 ppb Ba and 1 ppb Th and Mg. Oxides levels and double ionized levels were kept under 3%, backgrounds for both low and high mass were below 1 cps and all the other parameters were chosen considering the best signal/noise ratio. The detector was used in pulse mode, for better sensitivity. The dynamic reaction chamber (DRC) was used in rf-only mode (no gas); its parameters optimization procedure has been described elsewhere [3].

Table 2. Elan DRC II running parameters.

Parameter	Value
Plasma	
Power / W	1350
Plasma gas flow /min ⁻¹	12.00
Auxiliary gas flow /min ⁻¹	1.20
Nebuliser gas flow /min ⁻¹	1.05
Sample/Skimmer cone	Platinum
Quadrupole	
Quadruple rod offset (QRO) / V	0.00
Cell rod offset (CRO) / V	- 8.00
Cell path voltage (CPV) / V	- 20.00
Measurement mode	Peak hopping
Dwell time / ms	100 (²⁰⁶ Pb, ²⁰⁷ Pb), 70 (²⁰⁸ Pb)
Integration time / ms	5000 (²⁰⁶ Pb, ²⁰⁷ Pb), 3500 (²⁰⁸ Pb)
Reading per point	300
Reading per replicate	1
Replicate measurements	4
DRC	
Reaction Gas	None
Lens voltage / V	11.00

RESULTS AND DISCUSSION

For this study, ^{206}Pb , ^{207}Pb and ^{208}Pb were selected for measurement. Due to isobaric interferences, the quadrupole cannot differentiate between ^{204}Pb and ^{204}Hg isotopes and mercury was found at a level of 1.047 mg/kg (other studies [4] found 1.120 mg/kg), which is impossible to ignore in our lead measurements. For terrestrial samples with known Hg isotopic ratio, mathematical correction can be performed for subtracting ^{204}Hg counts from the total counts at mass 204. Since no data about Hg isotopic ratio in Mocs meteorite are yet provided, no such mathematical correction could be applied; interferences from Hg would have caused a false signal on mass 204 that would have rendered correct ^{204}Pb determination to be impossible with current method. Isotopic ratio determination for Hg by hydride generation would be able to improve ^{204}Pb measurements.

No internal standard was used during the measurements, but after every two sample, the NIST 981 SRM calibration solution was read, to correct for any mass bias effect. Correction factor was automatically calculated by the instrument's software.

The obtained solutions for Mocs sample and NIST 981 SRM were measured in three consecutive days. Settings for dwell time distribution were chosen according to previous studies [5] thus tuned for maximizing the sensibility - in this case, without using ^{204}Pb isotope but keeping the same ratio, meaning: 37% ^{206}Pb , 37% ^{207}Pb and 26% ^{208}Pb .

Table 3. Measured averages (\pm Standard Deviation)

		$^{207}\text{Pb}/^{206}\text{Pb}$	$^{208}\text{Pb}/^{206}\text{Pb}$
NIST 981	<i>Measured</i>	0.9142 ± 0.0005	2.1683 ± 0.0015
	<i>Certified</i>	0.9146 ± 0.0003	2.1681 ± 0.0008
Mocs (L5-6)		0.8656 ± 0.0084	2.1011 ± 0.0036
Sharps (H3.7)*		1.0918 ± 0.0021	3.1029 ± 0.0005
Mező-Madaras (L3.7)*		1.0985 ± 0.0014	3.1317 ± 0.0003

* average corrected ratios, according to [9].

Quantitative analysis revealed 0.888 ± 0.005 mg/kg concentration of Pb in Mocs sample (which is in good agreement with the results from literature [4]). The average values for the measured Pb isotopic ratios in NIST SRM and Mocs meteorite are reported in Table 3, together with comparative data on two other chondrites from references [9]. Other works on lead isotopic ratio on soils revealed $^{207}\text{Pb}/^{206}\text{Pb}$ ratio between 1.187 – 1.199 and $^{206}\text{Pb}/^{206}\text{Pb}$ ratio between 2.476 – 2.530 [14].

Lead isotopes in meteoritic materials are used for studying and dating early events in the solar system. "Initial" Pb isotope ratios obtained on troilite (FeS) in the least-radiogenic Canyon Diablo iron meteorite were used either as complementary reference for terrestrial ore Pb values, or as the assumed initial composition of Earth Pb ("primordial lead") that further evolved into all the other Pb-containing terrestrial phases [7]. There are no significant differences between the initial Pb ratios in Canyon Diablo troilite as compared to some chondritic meteorites selected for their low degree of early planetary metamorphism [9].

The oldest recorded Pb-Pb meteoritic age, obtained on Ca-Al-rich inclusions in Allende (CV3) carbonaceous chondritic meteorite [6] and the Angra dos Reis achondrite (angrite) [12], is of about 4.56 Ga (1 Ga = 10^9 years) [9]. When calculating internal $^{207}\text{Pb}/^{206}\text{Pb}$ ages for chondrites, caution should be taken in order to exclude pre-analysis contamination with terrestrial lead. This can be done by comparing isotope correlations between the acid-washes of analyzed samples, which basically would contain all the contamination lead induced by some type of fluid transport, and the residual washed samples [9].

Mocs is an ordinary chondrite with a relatively high degree of thermal metamorphism (petrologic type L5-6) and heterogeneous degrees of shock metamorphism, from S3 to S5 [1]. Extreme crushing and distortion of all mineral components was found on Mocs meteorite [11]. By taking these into consideration, as expected, the average lead concentration in Mocs sample (0.888 ± 0.005 mg/kg) is much lower than that in less metamorphosed whole rock chondrites, e.g. 5.44 mg/kg in Mezö-Madaras (L3.7) or 1.93 mg/kg in Sharps (H3.7) [9] due to the greater amounts of volatile elements in type 3 chondrites [13]. The same is true for the values of the $^{207}\text{Pb}/^{206}\text{Pb}$ and $^{208}\text{Pb}/^{206}\text{Pb}$ ratios (Table 3).

CONCLUSIONS

An inductively plasma mass spectrometer with single detector and a quadrupole for mass discrimination was used for lead isotopic ratio measurements on Mocs meteoritic sample. The proposed method was tested using a NIST 981 standard reference material and it offered good results for lead determination. Even if the calculation of radiometric ages is not possible by using the current results, they may provide some comparative grounds for Pb isotope compositions on other chondritic meteorites. Further method improvements for including determination of ^{204}Pb isotope is currently underway.

REFERENCES

1. Miura Y., Iancu G. Iancu G., Yanai K., Haramura H. *Proceedings NIPR Symposium of Antarctic Meteorites*, **1995**, 8, 153.
2. Grady, M.M., Hutchinson, R., Graham, A.L., 2000. "Catalogue of Meteorites; with special reference to those represented in the collection of the British Museum (Natural History)", 5th ed., British Museum (Natural History), UK, **2000**, 689.
3. Tănăselia C., Miclean M., Roman C., Cordoş E. and David L., *Studia Universitatis Babeş-Bolyai Chemia*, **2008**, LIII, 4, 123.
4. Hintenberger H., Jochum K.P., Seufert M., *Earth and Planetary Science Letters*, **1973**, 20, 391.
5. Monna F., Loizeau, J.L., Thomas B.A., Gueguen C. and Favarger P.Y., *Spectrochimica Acta Part B*, **1998**, 53, 1317.
6. Chen, J.H., Wasserburg, G.J., *Earth and Planetary Science Letters*, **1981** 52, 1.
7. Cumming, G.L., Richards, J.R., *Earth and Planetary Science Letters*, **1975**, 28, 155.
8. Dodd, R.T., "Meteorites, a petrological-chemical synthesis" Cambridge University Press, UK, **1981**, 368.
9. Hanan, B.B., Tilton, G.R., *Earth and Planetary Science Letters*, **1985**, 74, 209-219.
10. Ikramuddin, M., Lipschutz, M.E., Van Schmus, W.R., *Nature*, **1975**, 253, 703.
11. Urey, H.C., Mayeda, T., *Geochimica et Cosmochimica Acta*, **1959**, 17, 113.
12. Wasserburg, G.J., Tera, F., Papanastassiou, D.A., Huneke, J.C., *Earth and Planetary Science Letters*, **1977**, 352, 94.
13. Wasson, J.T., 1974. "Meteorites", Springer Verlag, New York, **1974**, 188.
14. C. Tănăselia, M. Miclean, C. Roman, E. Cordoş, L. David, *Optoelectronics and advanced materials – Rapid Communications*, **2008**, 2, 5, 299.

SEASONAL VARIATIONS IN THE BIOCHEMICAL COMPOSITION OF BUFFALO MILK

MARIAN MIHAIU^a, CONSTANTIN BELE^a, ALEXANDRA LAPUSAN^a,
ROMOLICA MIHAIU^b, SORIN DANIEL DAN^a, CARMEN TAULESCU^a,
CRISTIAN MATEA^a

ABSTRACT. In this study the seasonal variations of buffalo milks' composition and fatty acids profile with emphasis on the percentage of Saturated Fatty Acids (SFA), Mono Unsaturated Fatty Acids (MUFA) and Poly Unsaturated Fatty Acids (PUFA) was investigated. In each season we gathered 30 samples of milk from the same farm located in North Transylvania. The mean data from the 120 samples gathered in all four season (September 2009 – August 2010) were compared using the ANOVA test. There were no significant differences in the amount of lactose, but the protein percent differed in a noticeable manner from winter to spring season. The significant differences were found also at the average percent of milk fat that ranged between 6.69% - 12% with a peak in the months of winter. The content of PUFA varied very little, the main fatty acid being the linoleic acid (C18:2). Our data show that the season influences the buffalo milk's biochemical composition and the fatty acids profile probably via the type and quality of forages consumed and of course the amount of supplementation used in the buffaloes' diet.

Keywords: buffalo, fatty acids, season, protein, fat, lactose.

INTRODUCTION

Although buffaloes hold the greatest promise and potential for milk production [1] and the Food and Agriculture Organization has rightly termed it „an asset under evaluated”, little attention has been paid to buffaloes' milk biochemical composition. The buffalo breeds are widely spread, but because of their wild behavior they are considered rogue animals, and no concerted efforts were made to grade them according to their productivity. Our study was conducted on the Murrah buffalo which is the most popular breed with a minimum milk yield of no less than 1,360 kg in 300 days [2]. Knowing the variation of the main biochemical parameters in the milk composition of this

^a University of Agricultural Sciences and Veterinary Medicine, Faculty of Veterinary Medicine, 3-5 Mănăştur str., 400372, Cluj-Napoca, Romania, email: m.mihaiufmv@yahoo.com

^b Babes-Bolyai University, Faculty of Economics and Business Administration, Cluj-Napoca, Romania

particular breed contributes to the development of the scientific data base necessary for the impact evaluation of the quality markers established in the traditional primary milk chain. The nutritional value of buffalo milk was analyzed by investigating the most common parameters like milk fat, protein, lactose, focusing mostly on the fatty acids composition, as they are the most important quality markers of a milk product.

Dairy fat is one of the most complex dietary fat and more than 400 different fatty acids have been detected in it. On account of higher content of saturated fatty acid, trans fatty acids, butyric acid and conjugated linoleic acid, the milk fat has been associated with human health, adversely or positively. Even though the milk fat content is high in saturated fatty acids, which have been claimed to contribute to heart disease [3], other components of milk are considered to be beneficial for human health [4]. Unsaturated fatty acids (UFA) particularly omega 3 – polyunsaturated fatty acids (PUFA), have been shown to have potential health effects, for example the prevention of mammary gland in skin tumors [5]. The variation of milk fatty acids has been shown to be influenced at bovines by the forage and concentrate ratio [6] and level of intake of saturated fatty acids, especially the ones high in oleic acid [7]. The numbers of studies concerning the seasonal influence on the biochemical composition of buffalo milk are too few to form an accurate statement that is why our study focuses on this matter.

RESULTS AND DISCUSSION

The results obtained after analyzing the main biochemical parameters investigated (fat, protein, lactose) are presented in figure 1.

Regarding the fat percent, the statistical analysis revealed that there were significant changes between the average value recorded in spring (8.88%) and the one recorded in winter (9.5%) ($P < 0,05$), but no significant changes among the rest of them (autumn: 8.34%, summer: 8.20%) ($P > 0.05$). This difference in the fat content is probably due to the feeding frequency of low fiber, high grain diets which increase milk fat levels during the winter and autumn period and the lack of herbage which was not available, only in the spring and summer seasons. The same results were obtained by Anderson and Pollak (1980) who have reported that the percentage of fat in bovine milk raised in countries with the same climate conditions has been influenced by the seasonal variations.

This seasonal effect was also significant in regard to the average protein content of milk (winter: 5.16 g%, spring: 4.05 g%, summer: 4.06 g%, autumn: 4.30 g%) ($P < 0.05$). In the spring and summer season, again probably due to the diet based mainly on green forages, the protein content decreased, showing a slightly increase in autumn and then reaching the peak in winter months.

SEASONAL VARIATIONS IN THE BIOCHEMICAL COMPOSITION OF BUFFALO MILK

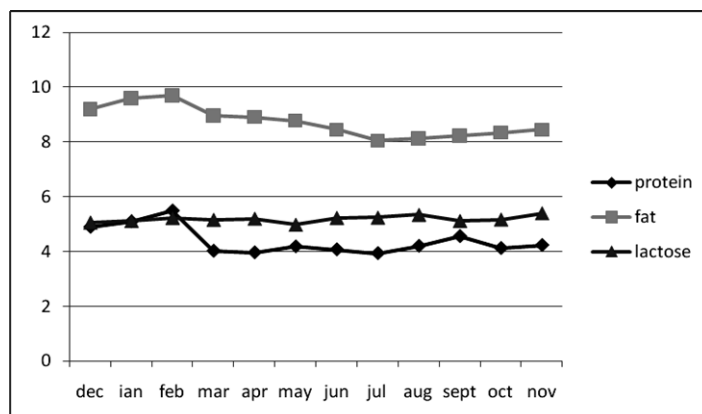


Figure 1. The average percent of the biochemical parameters in the months studied

The lactose average percentage during the period studied did not show significant changes ($P > 0.05$), varying very little from one season to another (autumn: 5.4 g%, winter: 5.13 g%, spring: 5.11 g%, summer: 4.85 g%).

The composition of fatty acids (FAs) in buffalo milk throughout the four seasons of the year is presented in table 1. The FA composition was eminently influenced as the function of sampling season. The five most important fatty acids in quantitative terms (C10:0, C14:0, C16:0, C18:0 and C18:1) accounted for more than 80% of the total fatty acids in all the samples studied, no matter the season in which they were collected. Overall the concentration of short chain fatty acids (<14:0) in milk were highest in the winter season and the lowest in the spring season.

The content of palmitic acid (C16:0) was significantly higher in the autumn season compared with the summer season, and varied by 5 – 6 % throughout the year. In a study made by Talpur et al. (2008) the percent of palmitic acid in the milk of various ruminants (cow, ewe, goat, buffalo) was found to be the highest during the summer season, and varied very much 16 – 25% throughout the year. These changes can contribute to human health, as it is well known that only C12:0, C14:0 and C16:0 affect the plasma cholesterol levels LDL [10,11]. The C18:0 content varies along the entire year and being significantly lower in the summer period, a fact possible due to the changes in the food supplement of polyunsaturated fatty acids (PUFAs). The main poly unsaturated fatty acid was the linoleic acid which hasn't shown real differences in the values of each season.

Figure 1 and 2 illustrates the chromatograms of the most representative samples collected in autumn (September), respectively summer (August), in which the fatty acids are registered in the form of peaks separated from each other by increasing the length chain, and at the same length chain by increasing of unsaturated degree.

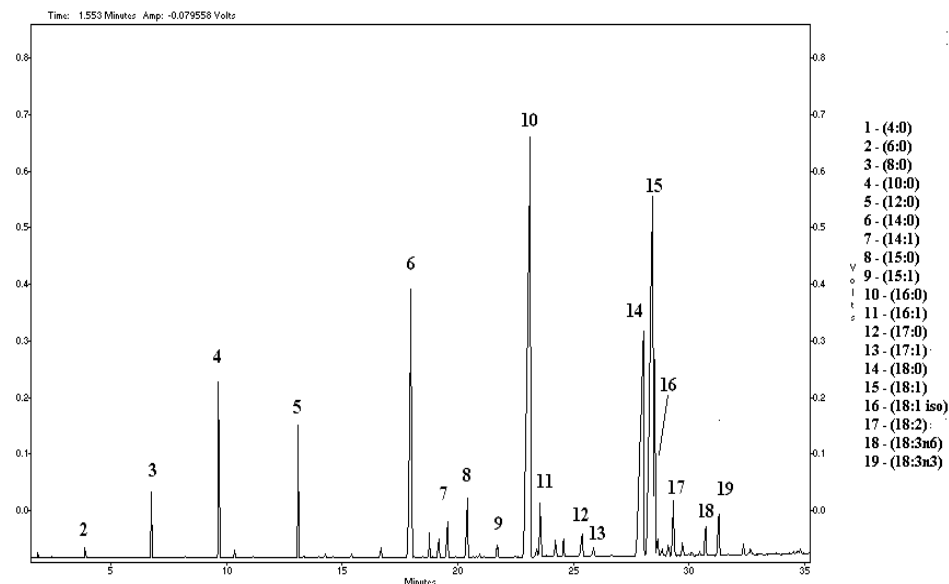


Figure 2. The cromatogram of a milk representative sample collected in autumn (September)

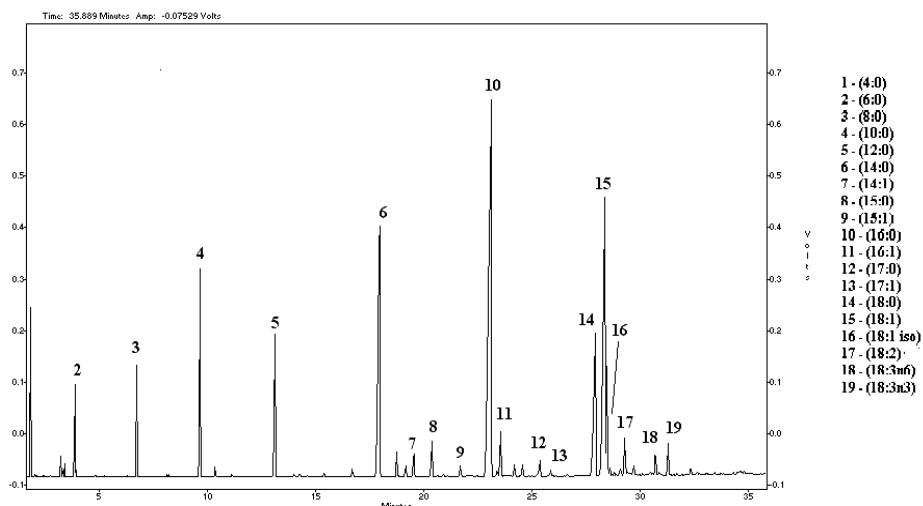


Figure 3. The cromatogram of a representative sample collected in summer (August)

Table 1. Seasonal changes in the fatty acid profile of buffalo milk taken from the semi-subsistence dairy farm

Fatty acid	Winter	Spring	Summer	Autumn	Average	SEM	ANOVA
Butyric	C4:0 n.d	n.d	n.d	n.d			
Caproic	C6:0 1.28	1.47	1.35	1.86	1.48	0.25	***
Caprylic	C8:0 1.16	1.82	1.13	1.17	1.32	0.33	***
Capric	C10:0 2.36	4.06	2.21	2.50	2.78	0.85	***
Undecanoic	C11:0 n.d	n.d	n.d	n.d	N.D		
Lauric	C12:0 5.30	2.74	4.49	2.69	3.80	1.30	***
Tridecanoic	C13:0 n.d	n.d	n.d	n.d	N.D		
Miristic	C14:0 13.36	9.46	9.43	11.62	10.96	1.89	***
Miristoleic	C14:1 0.55	0.77	0.98	0.44	0.68	0.23	**
Pentadecanoic	C15:0 1.21	1.22	1.13	1.54	1.27	0.18	*
Cis -10 -Pentadecanoic	C15:1 0.30	0.27	0.30	0.34	0.30	0.02	NS
Palmitic	C16:0 25.38	23.65	22.79	26.71	24.63	1.75	***
Palmitoleic	C16:1 1.42	1.36	1.60	1.41	1.44	0.10	NS
Heptadecanoic	C17:0 0.64	0.82	0.86	1.02	0.83	0.15	**
Cis-10-Heptadecanoic	C17:1 0.28	0.35	0.27	0.30	0.30	0.03	NS
Stearic	C18:0 14.91	14.18	12.09	15.02	14.05	1.35	***
Oleic	C18:1 22.80	26.78	24.99	23.35	24.48	1.79	***
Elidic	C18:1iso 4.90	2.77	3.50	4.71	3.97	1.01	***
Linoleic	C18:2 1.59	1.90	2.13	1.71	1.83	0.23	**
Linolenic	C18:3n3 0.75	1.21	0.93	0.84	0.93	0.19	**
γ - linolenic	C18:3n6 1.10	1.23	1.68	0.90	1.22	0.33	*

Significance, NS, not significant P>0.5; * P< 0.5; ** P<0.01; *** P<0.001;
Data is presented as least square mean.SEM, standard error of the mean.

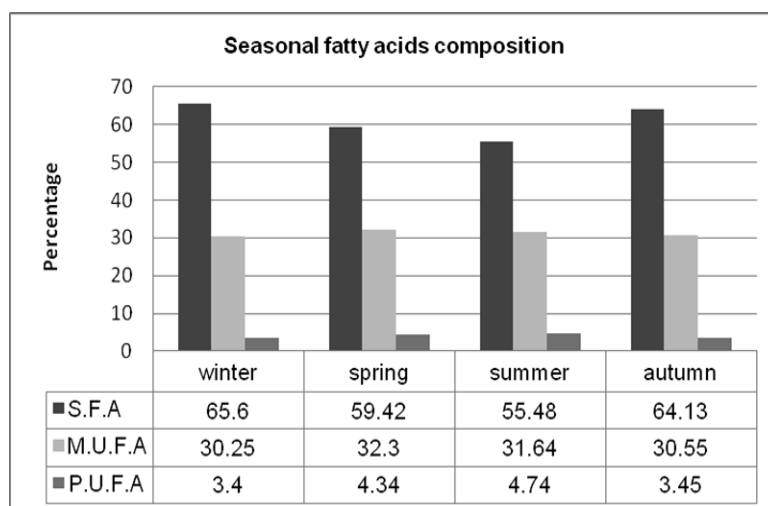


Figure 4. The seasonal average fatty acids composition in the buffalo milk samples studied

The FA composition was eminently influenced as the function of sampling season. As it is presented in figure 4 the seasonal average of the fatty acids composition varied in the year studied. In general the saturated fatty acids (SFA) were higher in winter and lowest during the summer, there being 5–10% less SFAs present in milk fat in summer compared with winter. The mono saturated fatty acids (MUFA) showed a lower discrepancy in comparison to the SFAs, varying only with 1 -3% throughout the year. The lowest percentage of MUFA was registered in winter (30.25%) and the highest in spring (32.3%) but then again the differences were not significant. A high concentration of PUFA (polyunsaturated fatty acids) was noticed during the summer season reaching an average of 4.75% in comparison to the autumn season when the lowest value was registered (4.34%).

CONCLUSIONS

The main biochemical parameters evaluated in the milk samples gathered from Murrah buffaloes are strongly influenced by the season variations. The average fat and protein percent recorded at the samples collected in the warm seasons (spring, summer) is lower than the one registered in the cold ones (winter and autumn). The lactose percent varied very little according to the seasonal changes. The five most important fatty acids in quantitative terms in the buffalo milk are C10:0, C14:0, C16:0, C18:0 and C18:1 which counted for more than 80% in all the seasons in which the samples were taken and analyzed. The hypercholesterolemic average values

(C12:0, C14:0 and C16:0) obtained in this study, varied from 35.85% in spring to 45.59% in winter. This shows a significant increase due to the feeding particularities of these seasons. The highest amount of monounsaturated fatty acids was found in the samples collected in spring season (32.3%) and the polyunsaturated fatty acids average percent (4.74%) was the highest in summer, in this respect the milk's nutritional quality being the highest during the warm seasons. The quantification of the seasonal variations in the main biochemical parameters with an emphasis on the fatty acids profile from milk certifies them as quality and traceability markers at the Murrah buffaloes' milk primary production.

EXPERIMENTAL SECTION

Samples

The samples were gathered from a semi-subsistence buffalo dairy farm situated in north Transylvania, monthly starting from September 2009 and finishing in August 2010. Each month 30 samples were collected from buffaloes fed on the same dietary regimen throughout the year, including green forages (constitutes 70% of dietary intake during spring and summer) and a mixture of crop residues.

The analysis of the main biochemical parameters

During milk collection and preparation, concerted efforts were made to avoid microbial contamination. The raw, unpreserved samples were stored overnight at +4°C and analyzed on the following day. Milk was analyzed for protein, lactose and fat content on a Milkoscan 134 (Foss-Electric A/C, Hillord, Denmark) (IDF standard 141 B:1996) which applies the well-known infrared spectrophotometry, providing a simple, rapid and accurate analysis of the key control parameters.

Milk fat extraction

Milk fat was extracted by using the following protocol: About 2ml of milk samples were mixed with 0,6 ml ammonia 25%, 2ml EtOH, 4ml Ethyl ether and 4 ml hexane and then agitated for 2-3min. After this process the lower layer (the ammonia layer) was discarded. Following this step the mixture was passed through a cellulose filter with Na₂SO₄ and then brought to dryness.

Transesterification

Fatty acids were converted to methyl esters by reaction with boron trifluoride/methanol at 80°C for two hours in a closed Pyrex glass tube. The content was transferred into a separatory funnel.

The methyl ester extraction

The extraction was made using 10 ml hexane. The hexanic fractions collected were dried using anhydrous sodium sulfate, filtered, concentrated under a nitrogen stream and finally re-eluted in 1 mL hexane. Fatty acids were analyzed by gas chromatography (GC) with flame ionization detection (FID). A 1 μ L sample was injected into the Shimadzu GC-17A series gas-chromatograph, equipped with a 30m polyethylene glycol coated column (Alltech AT-WAX, 0.25mm I.D., 0.25 μ m film thickness). Helium was used as the carrier gas at a pressure of 147 kPa. The injector and detector temperatures were set at 260°C. For the oven temperature the following program was used: 70°C for 2 min. then raised to 150°C at 10°C/ min. rate and held at 150°C for 3min., then further raised up to 235°C at a 4°C/min.

ACKNOWLEDGMENTS

This study has been financed by the National Council of Scientific Research of Higher Education, Romania, Ideas Project no.1083/2009.

REFERENCES

1. W.R. Cockrill, "Present and future of buffalo production in the world", *Proceedings of the Fifth World Buffalo Congress*, 27 - 30 June, **1994**, Sao Paolo, Brazil.
2. M.M. Appannavar, S. Kumar, T. Shashidara, "Note on production traits in a herd of Surti buffaloes", *Indian J.Dairy Sci.*, **1995**, *48*:480-481.
3. A. Chisholm, J. Mann, D.W. Sutherland, A. Duncan, M. Skeaff, C. Frampton, "Effect on lipoprotein profile of replacing butter with margarine in a low-fat diet: randomised cross-over study with hypercholesterolaemic subjects", *Medical British Journal*, **1996**, *312*, 931-934.
4. P.W. Parodi, "Milk fat in human nutrition", *Dairy Technology Journal*, **2004**, *59*, 3-59.
5. M.A. Belury, "Dietary conjugated linoleic acid in health: Physiological effects and mechanism of action", *Annual Reviewing Nutrition*, **2002**, *22*, 505 - 531.
6. J.M. Griinari, D.A. Dwyer, M.A. McGuire, D.E. Bauman, D.L. Palmquist, K.V.V. Nurmela, "Trans-octadecenoic acids and milk fat depression in lactating dairy cows", *Journal of Dairy Science*, **1998**, *81*, 1251 - 1261.
7. T.R. Dhiman, G.R. Anand, L.D. Satter, M.W. Pariza, "Conjugated linoleic acid content of milk from cows fed different diets", *Journal of Dairy Science*, **1999**, *82*, 2146 - 2156.
8. G. Anderson, M. Pollack, "Genetic variation in the yields and contents of milk constituents", *International Bulletin Dairy Federation*, **1980**, *125*, 73 - 82.

SEASONAL VARIATIONS IN THE BIOCHEMICAL COMPOSITION OF BUFFALO MILK

9. F.N. Talpur, M.I. Bhangar, A.A. Khooharo, G. Zuhra Memon, "Seasonal variation in fatty acid composition of milk from ruminants reared under the traditional feeding system of Sindh, Pakistan", *Livestock Science*, Elsevier, **2008**, *118*, 166 - 172.
10. E.H. Maniapan, A.M. Salter, Diet, Lipoproteins and Coronary Heart Disease: A Biochemical Prospective. Nottingham University Press, Nottingham, **1999**.
11. K. Majjala, "Cow milk and human development and well being", *Livestock Production Science*, **2000**, *65*, 1 -18.
12. C.G. Harfoot, G.P. Hazlewood, "Lipid metabolism in the rumen", *The Rumenmicrobial Ecosystem*, Blackie Pp. London, **1997**, 382 - 426.
13. M. Doreau, Y. Chilliard, "Digestion and utilization of fatty acids by ruminants", *Animal Feed Science and Technology*, **1997**, *45*, 379 - 396.

ASSAYS FOR PEROXIDASE ACTIVITY: THE HRP CASE

RADU SILAGHI-DUMITRESCU^a

ABSTRACT. Horseradish peroxidase (HRP) is a versatile oxidative enzyme with multiple practical applications. Furthermore, peroxidase activity is common in many other proteins, extending far beyond the class of peroxidases. As such, methods for assaying peroxidase activity have been sought for various applications. Here, a review of these methods is given, showing an inventory of almost 200 compounds employed as substrates in such assays, and with methods ranging from chronometric to colorimetric, fluorescent, polarography, or electron paramagnetic resonance (EPR) spectroscopy.

Keywords: *peroxidase, assay, phenols, HRP*

Horseradish peroxidase (HRP) is the archetypal heme peroxidase.[1-3] It is a globular glycoprotein with a mass of 42000, of which the protein moiety is approximately 34000, the rest of the molecular weight being accounted for by the prosthetic group (b-type heme), two calcium ions and some surface bound glycans.[4] The HRP structure (including a view of the active site) is shown in Figure 1. There are two similar, well-defined, domains within the apoprotein. Each domain contains one calcium ion, which provides structural stability and implicitly controls the enzyme's activity. The two domains provide a hydrophobic crevice in which the heme lies. A histidine occupies the fifth coordination position of the iron. This situation is very similar to that encountered in hemoglobin and myoglobin, so that the histidine is termed proximal histidine, and the protein domain providing this ligand is termed the proximal domain. The other domain is analogously named the distal domain and contains one relevant non-coordinated histidine, which is termed the distal histidine.[4]

The HRP general mechanism (Figure 2)[2,5,6] is initiated from the pentacoordinated ferric heme, binding peroxide. One of the H₂O₂ oxygen atoms then leaves as water, while the other is retained as a ferryl group to generate Compound I, featuring an Fe(IV) center coupled to a porphyrin cation radical.[7] Compound I then accepts one electron from a substrate molecule (typically an aromatic compound – phenolic or aminic), yielding Compound II, which still contains a ferryl group, but no porphyrin radical cation.[7]

^a *Universitatea Babeş-Bolyai, Facultatea de Chimie și Inginerie Chimică, Str. Kogălniceanu, Nr. 1, RO-400084 Cluj-Napoca, Romania, rsilaghi@chem.ubbcluj.ro*

Compound II then accepts one electron from a second substrate molecule, yielding the enzyme native state (ferric). As to the fate of the substrate, loss of one electron, usually accompanied by loss of a proton, leads to the formation of a radical. The high reactivity and low selectivity usually associated with organic radicals make the chemistry of the peroxidase products particularly complicated.[4]

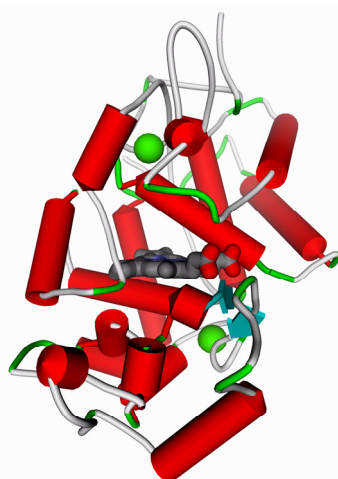


Figure 1. The HRP structure. The heme and the essential calcium ions are shown as sticks and spheres, respectively.

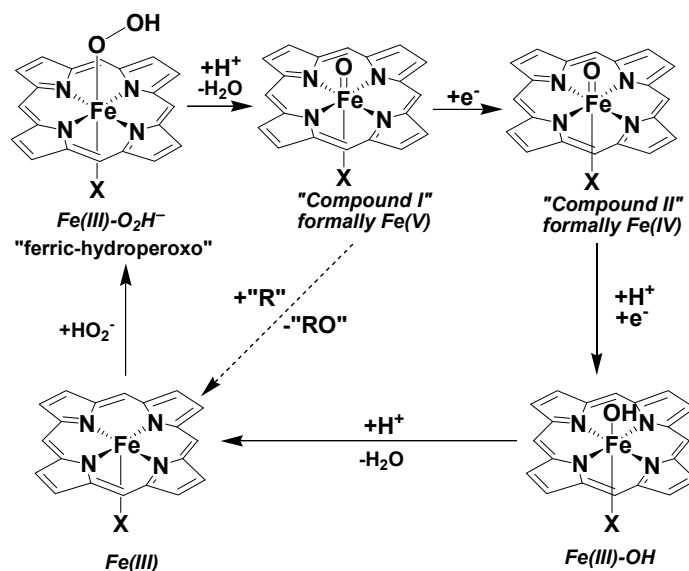


Figure 2. HRP general mechanism. Shown with a dashed arrow is the alternative peroxygenase reaction (R is typically an organic molecule).

ASSAYS FOR PEROXIDASE ACTIVITY: THE HRP CASE

Some substrates are oxidized by HRP in a single two-electron step: guaiacol (can be oxidized in either mono- or bi-electronic fashion), iodide, thiocyanate, and thioanisoles. There are also some (very few) instances where HRP acts as a peroxygenase, transferring an oxygen atom from the peroxide to the substrate (e.g., thioanisoles, hydroxylamine derivatives).[4,8]

One of the easiest ways to evaluate the HRP content of a preparation is by examination of its UV-VIS spectrum and determining the value of RZ (A_{403}/A_{280} , with 403 nm specific for heme and 280 nm specific for general protein material). For activity determinations, over 200 substrates, listed in Table 1, together with the type of method employed) have been used. These substances span most of the classes of substrates used by HRP, and employ several instrumental techniques – with UV-vis spectroscopy being the most widely-applied, as expected since many peroxidase substrates and products are colored.[4]

Table 1. Substrates and methods for HRP activity determination

Substrate	Method	Observations
ABTS (2,2'-azino-di[3-ethyl-benzothiazolin-(6)-sulfonate])	UV-vis[9-24]	the method of choice, also used in ELISA
pyrogallol	UV-vis[25-47]	(the result is also known as P.Z.-Purpurogallinzahl)
	fluorimetric[47-49]	
	polarographic[25]	
	titrimetric[25]	
	gasometric[25,50]	
guaiacol	UV-vis[9, 17, 18, 51-64]	
	chronometric[65]	
	titrimetric[25]	
hydroquinone	polarographic[25,52,66-68]	the residual H ₂ O ₂ or substrate concentration are determined
	fluorimetric[69]	the residual hydroquinone is detected with silver halides
	chronometric[70]	together with ascorbate
o-tolidine	UV-vis[23]	also in ELISA
5-aminosalicylic acid	UV-vis[15,23,64]	also in ELISA
o-phenylenediamine	UV-vis[15,22,23,25, 52,71-75]	also in ELISA; reducing agents such as sulfite stabilize the system by reacting with excess H ₂ O ₂ after the enzymatic reaction has been terminated
	UV-vis[76,77]	in reversed micelles
	pH changes are measured[78]	
p-hydroxy-benzensulfonate	UV-vis[79]	coupled to 4-aminoantipyrine

Substrate	Method	Observations
4-aminoantipyrine	UV-vis[79]	coupled to p-hydroxybenzenesulfonate
	UV-vis[80]	coupled to N-ethyl-N-(2-hydroxy-3-sulfopropyl)-m-toluidine
	UV-vis[21,23,57,81-85]	coupled to phenol; also in EIA (Trinder reagent) and also applied for model systems
	UV-vis[86]	coupled to N,N-diethyl-aniline
	UV-vis[87]	coupled to 2,4-dichlorophenol
3,3',5,5'-tetramethyl-benzidine	UV-vis[12,15,23,52,75,88-95]	also in ELISA; surfactants, cyclodextrin, penicillin (or derivatives thereof) may be used as additives after electrophoresis[96]
phenol	EPR[97]	
	UV-vis[21,23,85]	coupled to 4-aminoantipyrine, in EIA (Trinder reagent)
	UV-vis[52]	
5-phenyl-4-pentenyl-hydroperoxide (PPHP)	UV-vis[98]	selective peroxidase reagent, used together with a reducing substrate
fluorescein	fluorimetric[99,100]	
p-anisidine	UV-vis[46]	
3-methyl-2-benzothiazolinon hydrazone (MBTH)	UV-vis[79]	yields an indamine when reacting with m-dimethylaminobenzoic acid
	UV-vis[15]	ELISA
m-dimethyl-aminobenzoic acid	UV-vis[79]	yields an indamine when reacting with MBTH
luminol	fluorimetric[61,101-103]	in EIA; an impressive number of substances may be used as activators
L012 (luminol analog)	fluorimetric[104]	same as above
N-ethyl-N-(2-hydroxy-3-sulfopropyl)-m-toluidine	UV-vis[105]	coupled to 4-aminoantipyrine
3,3'-diamino-benzidine	UV-vis[82,106-109]	
p-phenylene-diamine	UV-vis[51,52,88,110]	
m-phenylene-diamine	UV-vis[52]	
pyrocatechin	UV-vis[25,52]	
	polarographic[25]	
	iodometric[12]	enzymatically produced quinone is titrated with iodine
o-dianisidine	UV-vis[88,110-116]	free or dextrane-bound
caffeic acid	fluorimetric[17]	
ferulic acid	fluorimetric[17]	
p-coumaric acid	fluorimetric[17]	
coniferyl alcohol	fluorimetric[17]	

ASSAYS FOR PEROXIDASE ACTIVITY: THE HRP CASE

Substrate	Method	Observations
5-(5'-azoluciferinyl)-2,3-dihydro-1,4-phtalazindione (ALPDO)	fluorimetric[117]	
p-hydroxy-phenylpropionic acid	fluorimetric[17,77,118-122]	also in ELISA; alone or together with a surfactant (CTAB or CTAC)
homovanillic acid	fluorimetric[123,124]	o-dianisidine may be used as activator
N,N-diethylaniline	UV-vis[77,86]	also coupled to 4-aminoantipyrine; also used for model systems
3-amino-9-ethylcarbazole	UV-vis[15]	ELISA
mesidine	UV-vis[9,25,125-128]	
ferrocyanide	[9]	
malachite green	UV-vis[25,41,52,129]	
guaiac resin	chronometric[65]	
	UV-vis[25]	guiaiaconic acid is the main product
benzidine	chronometric[45]	ascorbate is also needed
	UV-vis[25,52,58,62,130-135]	
2,6-dichlorophenol-indophenol	UV-vis[25,29,62,136,137]	
2,3',6-trichlorophenol-indophenol	UV-vis[25,138]	
pyrogalllic acid	UV-vis[64,139]	yields galloporpurin
phenolphthalein	UV-vis[25,52,64,140]	
o-toluidine	UV-vis[25,77,141]	
	chronometric[25,41]	ascorbate is also needed
guaiaconic acid	UV-vis[25]	
p-toluidine	UV-vis[25,77,141]	
acetylguaiacol	UV-vis[25]	
o-cresol	UV-vis[25,77,141]	
p-cresol	UV-vis[25,77,141]	
m-cresol	UV-vis[25,77,141]	
α-naphtol	UV-vis[25,142,143]	also coupled with dimethyl-phenylendiamine (NADI reagent) or with p-phenylendiamine (Guthrie reagent) to yield indophenols
aniline	UV-vis[52,77,144]	
ascorbate	UV-vis[25]	
	chronometric[25]	iodide, o-toluidine, or benzidine are used as second substrates
	polarographic[25]	
iodide	chronometric[25,145]	ascorbate is used as a second substrate
	chronometric[146]	starch, thiosulfate and iodide are also needed

Substrate	Method	Observations
	UV-vis or titrimetric[25]	
2,7-diaminofluorene	UV-vis[25]	
p-aminobenzoic acid	UV-vis[25,52]	
brilliant green	UV-vis[25]	
N,N-dimethyl-p-phenylene-diamine	UV-vis[52,147]	
thymol	UV-vis[52]	
resorcin	UV-vis[52]	
orcin	UV-vis[52]	
fluoroglucine	UV-vis[52]	
benzoic acid	UV-vis[52]	
salicylic acid	UV-vis[52]	
pyrocatechuic acid	UV-vis[52]	
galic acid	UV-vis[52]	
adrenaline	UV-vis[52]	
tyrosine	UV-vis[52]	
tryptophane	UV-vis[52]	
flavones	UV-vis[52]	
2-methyl-6-(p-methoxyphenyl)-3,7-dihydroimidazo-[1,2-a]-pirazin-3-one	chemiluminescence[148]	luciferin analog
acetaminophen and its derivatives	fluorescence[120]	fluorescent 5,5'-diacetamido-2,2'-bisphenol formation
p-phenyl-phenol, p-cresol, 1-naphtol or aniline	fluorescence[149]	a second compound is used to trap HRP-generated substrate radicals
2,4-dichlorophenol	UV-vis[77,150]	also in ELISA
Lumigen PS-3	chemiluminescence[151]	western, southern
2-methyl-1-propenol	chemiluminescence[152]	coupled to a lipase
acridan-9-carboxylic derivatives	chemiluminescence[152]	
tyramide derivatives	fluorescence[153]	
homogentisic acid γ -lactone	chemiluminescence[154]	ELISA
3-(10-phenothiazinyl)-propanesulfone		employed together with luminol[155]
4-(4-hydroxy-phenylcarbonyl)-butanoate	fluorimetric[156]	ELISA
acetanilide and its derivatives	fluorimetric[157]	
p-hydroxy-benzoic acid /terbium	chemiluminescence[158]	
alloxantin	chronometric[41]	ascorbate is also needed
1-amino-2-naphtol azo-derivatives	UV-vis[159]	

ASSAYS FOR PEROXIDASE ACTIVITY: THE HRP CASE

Substrate	Method	Observations
6-hydroxy-dopamine	UV-vis[160]	O ₂ may oxidize the substrate, to yield H ₂ O ₂ ; peroxidase accelerates the oxidation
eosine	chemiluminescence[161]	
4-methoxy-1-naphtol	UV-vis[162]	
4-and 5-substituted o-phenylendiamine derivatives	UV-vis[162]	
4-chloro-1-naphtol	UV-vis[162]	
2-hydroxy-2,4,6-cyclohepta-trienone (tropolone)	UV-vis[163]	coupled to 3-methyl-2-benzothiazolinone hydrazone (MBTH) or its derivatives
7 amino-indazole	UV-vis[164]	
5 amino-indole	UV-vis[164]	
7 amino-indole	UV-vis[164]	
5 amino-benzimidazole	UV-vis[164]	
7 amino-benzimidazole	UV-vis[164]	
5 amino-benzothiazole	UV-vis[164]	
7 amino-benzothiazole	UV-vis[164]	
5 amino-benzoxazole	UV-vis[164]	
7 amino-benzoxazole	UV-vis[164]	
5 amino-indazole	UV-vis[164]	
7-dimethylamino-naphtalen-1,2-dicarboxylic acid hydrazide	UV-vis[165]	
2-phenylamino-5-amino-pyridine	UV-vis[166]	
2-(4-hydroxy-3,5-dimethoxyphenyl)-4,5-bis(4-methoxyphenyl)imidazole,	UV-vis[167]	a phenolic derivative is used as mediator
2-(3,5-dibromo-4-hydroxyphenyl)-4,5-diphenylimidazole	UV-vis[167]	a phenolic derivative is used as mediator
2-(3-bromo-5-methoxy-4-hydroxyphenyl)-4,5-bis(4-methoxyphenyl)imidazole	UV-vis[167]	a phenolic derivative is used as mediator
4,5-bis(4-dimethylaminophenyl)-2-(4-hydroxyphenyl)imidazole	UV-vis[167]	a phenolic derivative is used as mediator
4,5-bis(4-dimethylaminophenyl)-2-(4-hydroxy-3-methoxyphenyl)imidazole	UV-vis[167]	a phenolic derivative is used as mediator
2-(4-hydroxyphenyl)-4,5-bis(4-methoxyphenyl)imidazole	UV-vis[167]	a phenolic derivative is used as mediator

Substrate	Method	Observations
4,5-bis(4-dimethylaminophenyl)-2-(4-hydroxy-3,5-dimethoxyphenyl)imidazole	UV-vis[167]	a phenolic derivative is used as mediator
m-aminosalicylic acid	UV-vis[168]	
6-carboxy-3-methylbenzothiazolone-hydrazone	UV-vis[169]	coupled to aniline derivatives: N,N-(biscarboxymethyl)aniline; N,N-(biscarboxymethyl)-4-methoxyaniline; N,N-(bis-beta-carboxyethyl)aniline; coupled to aniline derivatives: N,N-(biscarboxymethyl)aniline; N,N-(biscarboxymethyl)-4-methoxyaniline; N,N-(bis-beta-carboxyethyl)aniline; N-ethyl-N-phenylglycine; N-ethyl-N-carboxyethylaniline; N-phenylpiperidinyl succinate; N-ethylanilinopropanamine; N-methylanilinopropanamine; N-methyl-N-carboxyethylaniline; N,N-(bis-beta-carboxyethyl)2,5-dimethylaniline; N-β-carboxyethylaminobenzoate
N,N-disubstituted aniline derivatives; 4-aminoantipyrine, 4-(dimethylamino)antipyrine, 4-(ethylamino)antipyrine, 4-(methylamino)antipyrine, 4-(sulfonato-methylamino)antipyrine, 4-(sulfonomethyl)(isobutyl)aminoantipyrine, 4-(sulfonomethyl)(methyl)aminoantipyrine, 4-(isopropyl)aminoantipyrine	UV-vis[170]	coupled to 3-methyl-2-benzotiazolinon hidrazone, 1-methyl-2-quinolin hidrazone, N-methyl-pyridon-4-hidrazone, N-methyl-pyridon-2-hidrazone, N-methyl-quinolin-2-hidrazone, N-methyl-quinolin-4-hidrazone, N-methyl-2-benzotiazolinon hidrazone, N-methyl-thiazolinon-2-hidrazone, N-methyl-thiazolinon-2-hidrazone, N-methyl-4-phenylthiazolinon-2-hidrazone, N-methyl-oxazolinon-2-hidrazone, N-methyl-benzoxazolinon-2-hidrazone, 1,3-dimethyl-benzimidazolinon-2-hidrazone, 3-(C1-4 alkyl)-2-benzotiazolinon hidrazone
methylen-bis (N-ethyl-N-sulfopropyl-3,5-dimethylaniline)	UV-vis[171]	
p-phenylenediamine derivatives	UV-vis[172]	
dicyanoethylaryl derivatives	UV-vis[173]	

ASSAYS FOR PEROXIDASE ACTIVITY: THE HRP CASE

Substrate	Method	Observations
3,3'-di-carboxyloxy- or sulfonyloxy-benzidine	UV-vis[174]	
3-amino-pyrazole derivatives	UV-vis[175]	
p-chlor-phenol	UV-vis[77]	
2,4-dibromophenol	UV-vis[77]	
p-bromophenol	UV-vis[77]	
2,3-dichlorophenol	UV-vis[77]	
2-nitrophenol	UV-vis[77]	
3-nitrophenol	UV-vis[77]	
2-aminophenol	UV-vis[77]	
m-aminophenol	UV-vis[77]	
2-bromoaniline	UV-vis[77]	
3-bromoaniline	UV-vis[77]	
2-chloroaniline	UV-vis[77]	
3-chloroaniline	UV-vis[77]	
m-toluidine	UV-vis[77]	
dimethylaniline	UV-vis[77]	
o-anisidine	UV-vis[77]	
m-anisidine	UV-vis[77]	
2-methyl-2,6-dinitrophenol	UV-vis[77]	
2-methoxy-5-nitroaniline	UV-vis[77]	
2-methyl-5-nitroaniline	UV-vis[77]	
3,5-dihydroxytoluene	UV-vis[77]	
3-methoxyphenol	UV-vis[77]	
2-amino-5-methylphenol	UV-vis[77]	
2-hydroxy-3-methylbenzoate	UV-vis[77]	
2-hydroxyphenylacetate	UV-vis[77]	
2,3-dimethylphenol	UV-vis[77]	
2,5-dimethylphenol	UV-vis[77]	
2-ethylphenol	UV-vis[77]	
3-ethylphenol	UV-vis[77]	
2-methoxymethylphenol	UV-vis[77]	
2,3-dimethylaniline	UV-vis[77]	
2,5-dimethylaniline	UV-vis[77]	
3,5-diethylaniline	UV-vis[77]	
3-(dimethylamino)-phenol	UV-vis[77]	
3-methoxy-N,N-dimethylaniline	UV-vis[77]	
N,N-diethyl-1,3-phenyldiamine	UV-vis[77]	
3,5-dimethyl-1,2-phenyldiamine	UV-vis[77]	
N-ethyl-N-(3-methylphenyl)-N'-acetylenyldiamine	UV-vis[77]	

Substrate	Method	Observations
fluorophenols	[176]	the liberated fluoride is quantitated
aromatic urea derivatives	UV-vis[177]	
2,4-dichloro-1-naphtol	UV-vis[178]	
phenoxazine derivatives	UV-vis[179]	
2-(2-phenyl-3-indolyl)-4,5-di[4-(dimethylamino)-phenyl]imidazole and similar imidazoles	UV-vis[180]	
4-methoxyphenol	UV-vis[181]	
4-ethoxyphenol	UV-vis[181]	
4-iodophenol	UV-vis[181]	
4-hydroxyphenyl-acetic acid	UV-vis[181]	
4-hydroxyhippuric acid	UV-vis[181]	
tyramine	UV-vis[181]	
chlorpromazine	UV-vis[182]	
(3-acylamino benzo (b)furan-2(3H)one)	fluorimetric[183]	
hydroxycoumarines	fluorimetric[184]	
nitroxides	EPR[97]	hydroxylamines are formed
MeOOH	UV-vis[185]	in vivo estimation
H ₂ O ₂	polarographic[25]	excess H ₂ O ₂ is determined
	manometric[186]	

Besides the mentioned substrates, a very large number of compounds have been reported to be useful in the respective reaction mixtures (either as activators or stabilizers).[4]

ACKNOWLEDGMENTS

Funding from the Romanian Ministry of Education and Research, (grant PCCE 140/2008) is gratefully acknowledged.

REFERENCES

1. S.P. de Visser, S. Shaik, P.K. Sharma, D. Kumar, W. Thiel. *J Am Chem Soc*, **2003**, *125*, 15779-88
2. R. Davydov, R.L. Osborne, S.H. Kim, J.H. Dawson, B.M. Hoffman. *Biochemistry*, **2008**, *47*, 5147-5155
3. G.I. Berglund, G.H. Carlsson, A.T. Smith, H. Szoke, A. Henriksen, J. Hajdu. *Nature*, **2002**, *417*, 463-468

4. R. Silaghi-Dumitrescu. *Horseradish peroxidase - a versatile catalyst. Research Signpost, India*, **2006**
5. R. Silaghi-Dumitrescu. *Eur. J. Inorg. Chem.*, **2008**, 5404-5407
6. H.P. Hersleth, U. Ryde, P. Rydberg, C.H. Gorbitz, K.K. Andersson. *J Inorg Biochem*, **2006**, *100*, 460-76
7. R. Silaghi-Dumitrescu. *J. Biol. Inorg. Chem.*, **2004**, *9*, 471-476
8. R. Silaghi-Dumitrescu, F.D. Irimie, C. Paizs, C. Majdik, M. Tosa, P. Moldovan, A. Sas, L. Tamas. *Studia Univ. Babes-Bolyai, Chemia*, **2003**, *48*, 177-182
9. Y.X. Ci, F. Wang. *Mikrochim. Acta*, **1990**, *1*, 63-68
10. A.R. Pokora. US1989000305311, IPC Class: C12N 009/08
11. G.R. Schonbaum, S. Lo. *J. Biol. Chem.*, **1972**, *247*, 3353-3360
12. H.U. Bergmeyer, M. Grassl, H.E. Walter. "Methods of Enzymatic Analysis", 3rd edn., vol. 2, pp. 267-268, Verlag Chemie, Weinheim, **1983**
13. M.C. Shin, H.C. Yoon, H.S. Kim. *Anal. Chim. Acta*, **1996**, *329*, 223-230
14. C.V. Kumar, G.L. Mclendon. *Chem. Mater.*, **1997**, *9*, 863-870
15. E.I. Tawn, M.I. Savenkova, D.I. Metelitz. *Biokhim.*, **1995**, *60*, 1062-72
16. R.A. Marinelli, J.M. Pellegrino, M.C. Larocca. *Can. J. Physiol. Pharmacol.*, **1996**, *74*, 89-96
17. M. Urrutigoity, M. Baboulene, A. Lattes, J. Soupe, J.L. Seris. *Biochim. Biophys. Acta*, **1991**, *1079*, 209-13
18. O. Ryan. *Enzyme Microb. Technol.*, **1994**, *16*, 501-5
19. I. Weinryb. *Arch. Biochem. Biophys.*, **1968**, *124*, 285-091
20. W. Tischer, et al. US1986000930871, IPC Class: C12Q 001/28; C12N 011/02; C12N 011/06; C12N 009/96
21. N.N. Ugarova, I.V. Berezin, B.M. Kershengolts, I.D. Artamonov. *Biokhim.*, **1976**, *41*, 1829
22. T.M. Radhakrishnan, E. Raghupathy, P.S. Sarma. *Indian J. Chem. Sect. B*, **1963**, *1*, 40-4
23. D.G. Wilkinson. *Curr. Opinion in Biotechnology*, **1995**, *6*, 20-23
24. B. Rihn, et al. *J. Biochem. Biophys. Methods*, **1995**, *30*, 91-102
25. U. Spohn, D. Narasaiah, L. Gorton. *J. Prakt. Chem. / Chem.-Ztg.*, **1997**, *339*, 607-614
26. A. Katayama, T. Kamidate, H. Watanabe. *Bull. Chem. Soc. Jpn.*, **1992**, *65*, 2501-2504
27. S. Chao, R. Simon, T. Mallouk, M. Wrighton. *J. Am. Chem. Soc.*, **1988**, *110*, 2270-2276
28. A. Krause, E. Nowakowski. *Z. Naturforsch.*, **1965**, *20b*, 718-9
29. C.J. Cairns, et al. *J.Chem.Soc., Dalton Trans.*, **1987**, 2505-2510
30. R. Willstatter, A. Stoll. *Ann.*, **1918**, *416*, 21-64
31. J. Szamos, A. Hoeschke. *Acta Alim.*, **1992**, *21*, 253-60
32. Y. Tokita, H. Nakatsuji. *J. Phys. Chem. B*, **1997**, *101*, 3281-3289
33. T. de Lumley-Woodyear, D.J. Caruana, C.N. Campbell, A. Heller. *Anal. Chem.*, **1999**, *71*, 394-398

34. H. Drahovska. *Biologia (Bratislava)*, **1994**, *49*, 333-7
35. M. Shiga, et al. *Anal. Sci.*, **1995**, *11*, 591-5
36. B. Harvey, J. Durrant, M. Cunningham. *Methods Mol. Biol. (Totova N.)* 1996, *58* (Basic DNA and RNA protocols), 67-75,
37. R.P.M. Vangijlswijk, et al. *Cytogenetics And Cell Genetics*, **1996**, *75*, 258-262
38. H.C. Warren, F.T. Oakes. US1993000058723 IPC Class: C12N 009/96; C12N 009/04; C12N 009/06; C12N 009/08.
39. M.P. van de Corput, R.W. Dirks, R.P. van Gijlswijk, F.M. van de Rijke, A.K. Raap. *Histochem. Cell Biol.*, **1998**, *110*, 431-7
40. H. Akhavani-Tafti, et al. PCT Int Appl WO 96 07,912 (Cl C01N33/535), 14 Mar 1996, US Appl 300,462, 2Sep1994
41. H. Yamazaki, C.S. Boyd. U.S. US5,512,448 (Cl.435-7.9;GO1N33/53), 30Apr 1996, Appl 234,925, 28Apr1994
42. S.A. Weston, B. Crossett, D.S. Tuckwell, M.J. Humphries. *Anal. Biochem.*, **1995**, *225*, 28-33
43. J.P. Banga, P. Penfold, I.M. Roitt. *Biochem. J.*, **1981**, *198*, 421-423
44. M.M. Mesulam, et al. *J. Histochem. Cytochem.*, **1980**, *28*, 1255-1259
45. M.L. Schmidt, J.Q. Trojanowski. *Anal. Biochem.*, **1986**, *155*, 371-5
46. S. Avrameas, N. Gonatas, B. Guilbert. "*Methodologie de la structure et du metabolisme des glycoconjugues (glycoproteines et glycolipides)*", Vol 2. Paris, Centre National de la Recherche Scientifique, **1974**, pp. 733-9
47. M. Kressel. *J. Histochem. Cytochem.*, **1998**, *46*, 527-34
48. B.J. Appelmelk, et al. *Anal. Biochem.*, **1992**, *207*, 311-316
49. G. Degand, A. Bernes-Duyckaerts. *Anal. Chim. Acta.* **1993**, *275(1-2)*, 241-247
50. P. Skladal, T. Kalab. *Anal. Chim. Acta.*, **1995**, *316*, 73-78
51. B.C. Saunders. in Eichhorn G.L., "*Inorganic Biochemistry*", Elsevier, Amsterdam, **1973**, pp 955-1024
52. B.C. Saunders. "*Peroxidase-Action and Use in Organic Synthesis*", Butterworths, London **1957**
53. R. Song, A. Sorokin, J. Bernadou, B. Meunier. *J. Org.Chem.*, **1997**, *62*, 673-678
54. H. Sugimoto, D.T. Sawyer. *J. Am. Chem. Soc.*, **1984**, *106*, 4283-4285
55. P.M. Cooper, J.F. Largier. *Process Biochem.*, **1968**, *3*, 22-5
56. A.R. Pokora, et al. US1987000070594 IPC Class: C08G 065/38; C12P 007/32
57. T.C. Hall, et al. *Phytochemistry*, **1969**, *8*, 385-91
58. R.E. Bartovek. *J. Biotechnol.*, **1994**, *37*, 133-42
59. I.G. Gazarian, et al. *FEBS Lett.*, **1994**, *354*, 248-50
60. M. Lasagna, V. Vargas, D.M. Jameson, J.E. Brunet. *Biochemistry*, **1996**, *35*, 973-9
61. L. Piras, M. Adami, S. Fenu, M. Dosis, C. Nicolini. *Anal. Chim. Acta.*, **1996**, *335*, 127-135
62. G. Giraudi, C. Baggiani, C. Giovannoli. *Anal. Chim. Acta.*, **1997**, *337*, 93-97
63. H. Hosoda, et al. *Chem. Pharm. Bull.*, **1985**, *33*, 249-255

ASSAYS FOR PEROXIDASE ACTIVITY: THE HRP CASE

64. G.W. Koszalka, H.E. Swaisgood, H.R. Horton. *Biochim. Biophys. Acta*, **1987**, 915, 321-9
65. V.N. Denisov, D.I. Metelitsa. *Biokhim.*, **1987**, 52, 1248-1257
66. D.C. Gowda. *Bioconjug. Chem.*, **1996**, 7, 265-270
67. E.I. Karaseva, A.N. Eremin, D. I. Metelitsa. *Bioorg. Khim.*, **1992**, 18, 498-508
68. E.F. Panarin, V.E. Baikov, O.G. Paskhina. *J. Appl. Chem. USSR*, **1992**, 65, 987-988
69. M. Iwata, et. al. Jpn Kokai Tokkyo Koho JP0805, 560 [96 05, 560] (Cl. GO1N21/78), 12ian1996, Appl 94/137, 058, 20iun1994
70. H. Nygren, H.A. Hansson. *J. Hisrochem. Cytochem.*, **1981**, 29, 266-270
71. A. Sakai, et al. *Chem. Pharm. Bull.*, **1991**, 39, 2984-2989
72. W.C. Shen, H.J. Ryser. *Proc. Natl. Acad. Sci. USA.*, **1978**, 75, 1872-6
73. A.N. Eremin. *Prikl. Biokhim. Mikrobiol.*, **1990**, 26, 764-70
74. S. Birnbaum, L. Bulow, H. Kimber, B. Danielsson, K. Mosbach. *Anal. Biochem.*, **1986**, 158, 12-19
75. F. Dittrich, et al. Ger (East) DD 279, 586 (Cl C12N9/02), 13 Jun 1990, Appl 283, 126
76. S.D. Mangru, D.J. Harrison. *Electrophoresis*, **1998**, 19, 2301-7
77. J. Everse. *Free Radic, Biol. Med.*, **1998**, 24, 1338-46
78. G.E. Griesmann. *J. Immunol Methods*, **1991**, 138, 25-9
79. N.P. Danilova. *Bioorg. Khim.*, **1995**, 21, 632-635
80. W.D. Ellis, H.B. Dunford. *Can. J. Biochem.*, **1968**, 46, 1231-5
81. J. Everse, K. Everse, B.M. Grisham. *"Peroxidases in Chemistry and Biology"*, CRC Press, Boca Raton, **1991**,
82. H. Hosoda, et. al. *Chem. Pharm. Bull.*, **1986**, 34, 4177-4182
83. J.R. Lindsay-Smith, R.J. Lower. *J. Chem. Soc., Perkin Trans.*, **1992**, 2187
84. V.F. Sukhikh. *Problemy Endokrinologii*, **1982**, 28, 80-4
85. R.H. Haschke, J.M. Ordronneau, A.H. Bunt. *J. Neurochem.*, **1980**, 35, 1431-5
86. T. Porstmann, et al. *Biomed. Biochim. Acta*, **1987**, 46, 867-75
87. N. Colclough, J.R. Lindsay-Smith. *J. Chem. Soc., Perkin Trans.*, **1994**, 6, 1139
88. H. Gallati. *J. Clin Chem. Clin Biochem.*, **1979**, 17, 1
89. C. Somfay, et al. Hung Teljes HU 49, 151 (Cl C07K13/100), 28 Aug 1989, Appl 88/4, 932, 07 Mar 1986
90. C.B. Rasmussen, A.K. Abelskov, R.B. Jensen, K.G. Welinder. *Phys. Plant.*, **1997**, 100, 102-110
91. A. Szutowicz, R.D. Kobes, P. Orsulak. *J., Anal. Biochem.*, **1984**, 138, 86-94
92. E. Lodemann, Z.H.M. El-Kirdassy, A. Wacker. *Arzneim. Forsch.*, **1980**, 30, 395-397
93. N.P. Groome. *J. Clin. Chem. Clin. Biochem.*, **1980**, 18, 345-9
94. G.A.W. Rook. *Leprosy Review*, **1981**, 52, 281-283
95. A.P. Bogoyavlensky, I.E. Digel, V.E. Berezin. *Biochemistry (Mosc)*, **1997**, 62, 870-1
96. M. Miyamoto. *MHC - Major Histopathol. Complex*, **1994**, 1, 130-132
97. K.G. Paul. *Acta Chem. Scand.*, **1958**, 12, 1312-18
98. V.G. Gorbunova. *Radiobiologiya*, **1967**, 7, 167-70

99. R. Kuhn, D.B. Hand, M. Florkin. *Z. Physiol. Chem.*, **1931**, 201, 255-66
100. J. Eukama. *Suomen Kemistiehti*, **1946**, 19b, 32-4
101. J. Bielefeld. *Z. Vitaminforsch.*, **1943**, 13, 286-94
102. A. Bach. *Ber.*, **1904**, 37, 3785
103. J.B. Sumner, E.C. Gjessing. *Arch. Biochem. Biophys.*, **1943**, 2, 291-3
104. A.V. Zherdev, N.A. Bizova. *Proc. Intl. Symp. Plant Perox.*, 5th, Columbus Ohio, 5th, Columbus, Ohio 1999,
105. L. Barta. *Biochem. Z.*, **1937**, 293
106. L. Jin. *Anal. Biochem.*, **1995**, 229, 54-60
107. B. Ghislaine. *Arch. Intern. Physiol. Biochim.*, **1937**, 44, 212-15
108. H. Theorell. in Sumner B.J., "*The Enzymes. Chemistry and Mechanism of Action*" Academic Press New York, 1951 pp 397-426
109. A. Bach. *Ber.*, **1914**, 47, 2125
110. K. Wallenfels, A. Gauhe. *Ber.*, **1942**, 75, 413
111. R. Willstatter, H. Weber. *Ann.*, **1926**, 449, 156-174
112. G. Pineiro-Avila, A. Salvador, M. de la Guardia. *Analyst*, **1998**, 123, 999-1003
113. G. Ahnstrom, et al. *Acta Chem. Scand.*, **1961**, 15, 1417
114. R. Nilsson. *Acta Chem. Scand.*, **1964**, 18, 389-401
115. G. Ahnstrom, R. Nilsson. *Acta Chem. Scand.*, **1965**, 19, 313-16
116. J. Etori. *Biochem. J.*, **1949**, 44, 35-8
117. L. Rozental. *Roczniki Pnsh. Zakl. Hig.*, **1951**, 2, 319-54
118. R. Puchades. *Analisis*, **1994**, 22, 76-81
119. F.D. Snell, C.T. Snell. '*Spectrofotometric Methods of Analysis*', Vol 4, D. Van Nostrand Comp Inc, 3rd edn, New York 1954
120. D.R. Doerge, R.L. Divi, M.I. Churchwell. *Anal. Biochem.*, **1997**, 250, 10-17
121. N. Parij, J. Neve. *Eur. J. Pharmacol.*, **1996**, 311, 259-264
122. W.M. Hunting, et al. *Anal. Chem.*, **1959**, 31, 143-144
123. A. Pollinger. *Z. Anal. Chem.*, **1941**, 357
124. B.B. Dey. *J. Indian Chem. Soc.*, **1936**, 13, 390-8
125. M.V. Sithamaran, S. Rengachan. *J. Indian Chem. Soc.*, **1937**, 14, 278-90
126. H. Theorell. *Enzymologia*, **1942**, 10, 250-2
127. D.M. Aronbaev, S.D. Varfolomeev, V.I. Krivoruchko, M.V. Simonova. *Meditinskaja Tekhnika*, **1990**, 39-40
128. H.G. Deux. *Proc. Nederlanden Akad. Wetensch.*, **1942**, 45, 844-9
129. F. Caillaud, P. du Pasquier. *Annales de Virologie*, **1983**, 134, 267-276
130. E. Kogme, et. al. Ger Offen DE 3, 641, 489 (CI C12Q1/28), 11iun 1987, JP Appl 851272, 426, 05 Dec 1985
131. A. Krause, E. Nowakowski. *Z. Naturforsch.*, **1965**, 20b, 498-90
132. H. Sugimoto, L. Spencer, D.T. Sawyer. *Proc. Natl. Acad. Sci. USA*, **1987**, 84, 1731-1733

ASSAYS FOR PEROXIDASE ACTIVITY: THE HRP CASE

133. B. Unterhalt, G. Baudner, C. Gerke. *Pharmazie*, **1994**, 49, 829-33
134. D.I. Metelitzka, et al. *Biokhim.*, **1995**, 60, 1659-68
135. X. Dou, T. Takama, Y. Yamaguchi, H. Yamamoto. *Anal. Chem.*, **1997**, 69, 1492-1495
136. H. Akhavan-Tafti, et al. *J. Org. Chem.*, **1998**, 63, 930-937
137. F. Cui. *Bioorg. Med. Chem.*, **1995**, 3, 471-7
138. M. li, et al. *Biochem. Biophys. Res. Commun.*, **1993**, 193, 540-5
139. H. Gallati, H. Brodbeck. *J. Clin. Chem. Clin. Biochem.*, **1982**, 20, 221-5
140. S. Nakamura, T. Mashino, M. Hirobe. *Tetrahedron. Lett.*, **1992**, 33, 5409-5412
141. T. Porstmann, et al. *J. Clin. Chem. Clin. Biochem.*, **1985**, 23, 41-44
142. H.M. Salem. *Pakistan J. Sci. Ind. Res.*, **1968**, 11, 35-8
143. B. Porstmann, U. Evers, E. Nugel, H. Schmechta. *Z. Med. Lab. Diagn.*, **1991**, 32, 38
144. L. Klemens, et al. *Anal. Biochem.*, **1997**, 244, 96-102
145. M. Jayle. *Compt. Rend. Soc. Biol.*, **1938**, 128, 1074-6
146. S.M. Khonyutov, A.N. Resheltilov. *J. Anal. Chem. (Transl of Zh Anal. Khim)*, **1995**, 50, 599-602
147. K. Asano, et. al. *Hiroshima Journal of Medical Sciences*, **1992**, 41, 1-5
148. B.S. Karon, T.M. Daly, M.G. Scotta. *Clin. Chem.*, **1998**, 44, 155-160
149. K. Myauchi, A. Muke. Jpn Kokai Tokkyo Koho JP 07, 39, 394 [95 39, 394] (Cl. C12Q1/28), 10feb1995, Appl 93/188, 329, 29iul1993
150. H. Gallati. *J. Clin. Chem. Clin. Biochem.*, **1977**, 15, 699-703
151. O. Mosato. Jpn Kokai Tokkyo Koho JP 06, 33, 33, 797 [94, 133, 797] (Cl C12Q, 152), 17 mai 1994 Appl 92/292, 956, 30oct 1992
152. H. Pauly, et al. Ger Offen D.E. DE 3, 541, 978 (Cl. C12Q1/28), 04 iun 1987, Appl 28 Nov 1985
153. T. Hiraoka. *Acta Histochem. Cytochem.*, **1997**, 30, 545-550
154. G. Volpe, D. Compagnone, G. Palleschi. *Analyst*, **1998**, 123, 1303-1307
155. K. Kamakatsu, Y. Amano. Jpn Kokai Tokkyo Koho JP0889, 291 [96 89, 291] (Cl. C12Q1/28), 9Apr1996, Appl 94/259, 326, 28sep1994
156. M. Koyama. Jpn Kokai Tokkyo Koho JP07, 111, 899 [95 111, 899] (Cl. C12Q1/28), 02May1995, Appl 93/259, 917, 18oct1993
157. J.R. Crowther, L. Angarita, J. Anderson. *Biologicals*, **1990**, 18, 331-6
158. H. Gallati, I. Pracht. *J. Clin. Chem. Clin. Biochem.*, **1985**, 23, 453-60
159. M. Takada, S. Yoshida. Jpn Kokai Tokkyo Koho JP0880, 199 [96 80, 199] (Cl. C12Q1/28), 26 Mar1996, Appl 94/217, 433, 12sep1994
160. K.L. Moore, M.M. Moronne, R.J. Mehlhorn. *Arch. Biochem. Biophys.*, **1992**, 299, 47-56
161. P.E. Weller, C.M. Markey, L.J. Marnett. *Arch. Biochem. Biophys.*, **1985**, 243, 633-643
162. T. Segawa, A. Kakizaki, T. Kamidate, H. Watanabe. *Anal. Sci.*, **1992**, 8, 785-788
163. A.V. Lomakin, G.A. Kan, P.A. Motavkin. *Biull. Eksp. Biol. Med.*, **1990**, 109, 583-4
164. M.A. Matsenboeker, K. Kondo. *J. Biolumin Chemilumin.*, **1994**, 9, 15-20

165. A. Hinkkanen, K. Decker. *Hoppe-Seylers Z. Physiol. Chem.*, **1983**, 364, 1549-53
166. D.B. Wagner, et. al. US1988000272360 IPC Class: C12Q 001/00; C12Q 001/28; G01N 033/53
167. B. Quinn, A.M. Graybiel. *J. Histochem. Cytochem.*, **1996**, 44, 71-74
168. J.I. Morrell, L.M. Greenberger, D.W. Pfaff. *J. Histochem. Cytochem.*, **1981**, 29, 903-916
169. A.H. Hopman, S. Claessen, E.J. Speel. *Histochem. Cell Biol.*, **1997**, 108, 291-8
170. D.M. Mikhlin, Z.S. Bronovitskaya. *Biokhim.*, **1949**, 14, 379-81
171. J. Puetter, R. Struffe. *Clin. Chim. Acta*, **1967**, 15, 189-63
172. K.L. Jakobsen. *Scand. J. Chim. & Lab. Invest.*, **1960**, 12, 76-9
173. S.K.J. Clark, J.M. Conroy, P.J. Harris. *Mol. Immunol.*, **1983**, 20, 1379-84
174. H.V. Malmstadt, T.P. Hadjioannou. *Anal. Chem.*, **1963**, 35, 14-16
175. C.E. Eriksson, S.G. Svensson. *Biochim. Biophys. Acta*, **1970**, 198, 449-459
176. I.D. Karalimos, D.S. Papastathoulos. *Anal. Lett.*, **1996**, 29, 1293-1308
177. T. Sudhaharan, A. Ram Reddy. *Anal. Biochem.*, **1999**, 271, 159-167
178. Q.G. Li, et al. *Anal. Chim. Acta*, **1994**, 298, 279-84
179. Q.G. Li, J.G. Xu, X.Z. Huang, G.Z. Chen. *Talanta*, **1994**, 41, 2049-2054
180. M. Shiga, K. Yakata, K. Sasamoto, M. Takagi, K. Ueno. *Anal. Sci.*, **1995**, 11, 195-201
181. X. Peng, Q.G. Li, J. Xu, G. Chen. *Xiamen Daxue Xuebao Ziran Kexueban*, **1995**, 34, 405-9
182. Q.G. Li, et al. *Xuaxue Xuebao*, **1995**, 53, 248-53
183. A.S. Brill. in Florkin M., Stotz H.E., "Comprehensive Biochemistry", 1966, Vol 14, pp 447
184. H. Iwai, F. Ishihara, S. Akihama. *Chem. Pharm. Bull.*, **1983**, 31, 3579-3582
185. G. Guilbault, D.N. Kramer, E. Mackley. *Anal. Chem.*, **1967**, 39, 27
186. G.M.K. Hughes, B.C. Saunders. *Chem. & Ind.*, **1954**, 47, 7

STRUCTURAL STUDY OF NEW CYCLO-1, 3-DIPHOSPHABUTANES

RALUCA SEPTELEAN, PETRONELA M. PETRAR,
IULIA COMAN, GABRIELA NEMES^a

ABSTRACT: A novel cyclic 1,3-diphospha-butane was obtained starting from 9-trimethylsilyl-fluorene and PCl_3 in a one-pot procedure and investigated through spectroscopic methods. Theoretical studies were also carried out, showing that the head-to-tail isomer of 1, 3-diphosphacyclo-butane is more likely to be formed during the reaction through the dimerization of a fluorenyl-substituted phosphoalkene. This type of cyclic derivative can replace phosphoallenes as ligands in the synthesis of coordination compounds with potential biological activity.

Keywords: phosphoalkenes, diphosphacyclo-butane, DFT calculations

INTRODUCTION

Low-coordinated phosphorus centers involving multiple bonding, such as phosphoalkenes, have been recently used as ligands in the coordination chemistry of transition metals [1-3], with proof that they would have applications in catalysis [2, 3]. The synthesis of the first diphosphoallene $\text{Mes}^*\text{P}=\text{C}=\text{PMes}^*$ [4] by stabilization with bulky organic groups was stimulated by the fact that the presence of two phosphorus atoms in the molecule gives rise to several intriguing possibilities as far as the coordination ability of such systems is concerned. Following our interest in the design of transition metal compounds coordinated by phosphapropenes [5] and in the study of heteroallenes [6-9] it became apparent that the cyclic compounds containing two or more phosphorus atoms could replace diphosphoallenes without raising the same problems related to their insaturation and instability. For instance, 1,3-diphosphacyclobutanes would be the equivalent of 1,3-diphosphoallenes as ligands in the synthesis of transition metal-complexes.

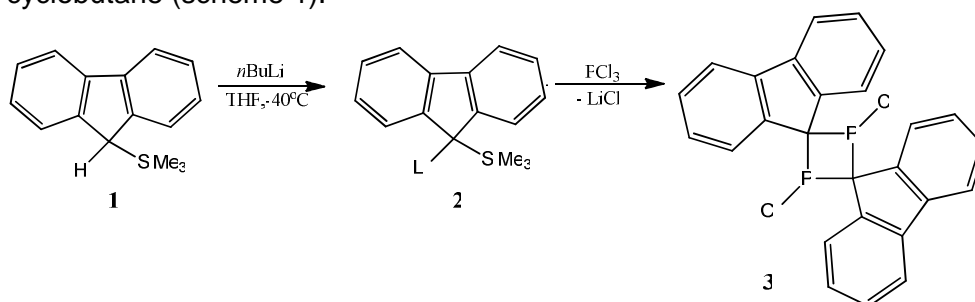
We report the synthesis of a novel 1,3-diphosphacyclobutane in a one-pot procedure, starting from the readily accessible trimethylsilylfluorenyllithium and PCl_3 . The choice of the fluorenyl group as the substituent on the carbon

^a Babes-Bolyai University, Faculty of Chemistry and Chemical Engineering, 11 Arany Janos, RO-400028, Cluj-Napoca, Romania

atoms represents a good compromise between the sterical hindrance needed and the availability of both sides of the four-member ring towards the transition metal. In addition, fluorenyl compounds are known to crystallize easily. Theoretical calculations also presented in this paper support the use of fluorenyl-derivatives in the synthesis of 1,3-diphosphacyclobutanes.

RESULTS AND DISCUSSIONS

A new derivative 1,3-diphosphacyclobutane **3** was obtained by reaction of the 9-trimethylsilylfluorenyllithium derivative **2** with PCl_3 at low temperature. This and the lack of evidence for the presence of the phosphalkene lead us to believe that dimerization readily occurs with the formation of a diphosphacyclobutane (scheme 1).



Scheme 1

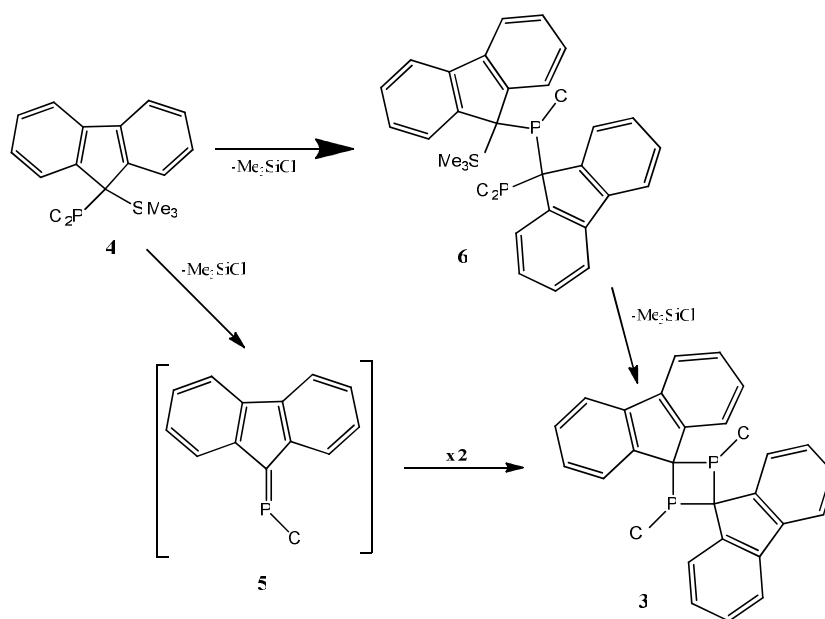
The obtained derivative **3** was characterized in solution through multinuclear NMR spectroscopy. Only one signal in ^{31}P NMR at a chemical shift of 179.47 ppm is observed, so only one of the two isomers, *cis* and *trans* (indicating the position of the chlorine atoms with respect to the four-atom ring) is obtained.

Most likely, the formation of **3** is the result of the intramolecular elimination of Me_3SiCl from the sterically-hindered **4**, followed by the dimerization of the phosphalkene **5**. The formation of **5** is the result of the more sterically favored head-to-tail dimerization. Other possible reaction routes are presented in scheme 2.

The presence of a triplet (121.47 ppm) in the ^{13}C NMR spectrum of the reaction product, indicating coupling with the phosphorus nucleus, supports our assumption for the formation of a 4 atom-cyclic derivative, in which the two carbon atoms would be equivalent. If the elimination of Me_3SiCl would occur with the formation of derivative **6**, two different signals should be observed for the carbon atoms bonded to phosphorus. Instead, only one such signal, a triplet, is observed, which could be attributed for either the *cis* or the *trans* isomer of the cyclic dimer. Lack of further experimental data stopped us

STRUCTURAL STUDY OF NEW CYCLO-1, 3-DIPHOSPHABUTANES

from attributing the signal to one of them, so a theoretical study was undertaken in order to evaluate which one of the isomers is present. We excluded from the start the possibility of obtaining the head-to-head dimer for two reasons: first, that the head-to-tail dimerization should be thermodynamically favored, leading to the formation of two C-P bonds instead of one P-P and one C-C bond, and second because even though the fluorenyl groups are planar, their position should exert some strain on the head-to-head orientation of the monomers.



However, with the available experimental proof, it was not possible to irrefutably state the presence of either one of the possible reaction products resulted from dimerization, so we turned to theoretical investigations in order to establish the outcome of the reaction.

In this study, we had to consider that elimination of Me_3SiCl during the reaction can occur via either intra- or intermolecular route, and considering the high reactivity of the monomer (due to the presence of the double bond, the chlorine substitution at a P(III) atom and the relatively low sterical hindrance) in both cases cyclic diphosphabutanes would be obtained.

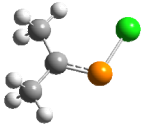
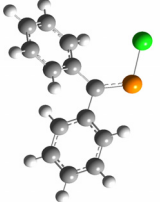
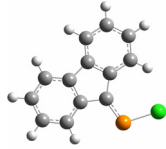
Supposing that the monomer is indeed the reaction product which readily undergoes dimerization, two different routes must be considered: "head to head" and "head to tail" dimerization.

Three model compounds were considered: $\text{Me}_2\text{C}=\text{PCI}$, $\text{Ph}_2\text{C}=\text{PCI}$ and the presumed reaction intermediate, $\text{Fl}_2\text{C}=\text{PCI}$ ($\text{Fl}_2\text{C}=\text{ fluorenyl}$). The Me and Ph groups were chosen in order to evaluate any changes when going from an alkyl to an aryl substituent on the carbon atom. Sterical hindrance is relatively low in the case of the fluorenyl group, because of the planar conformation, so the steric factor was not evaluated. Presumably, a bulkier organic group on the carbon would prevent dimerization by both protecting the double bond and increasing the strain of the four-atom ring in the dimer; these considerations, are the basis of a separate on-going theoretical investigation and will not be discussed herein. The calculated energies, optimized structures and some relevant geometrical data are given in tables 1 and 2. The numbering of the atoms and color codes are given in scheme 3.



Scheme 3

Table 1. Calculated B3LYP/6-311G(d,p) energies for $\text{R}_2\text{C}=\text{PCI}$ derivatives

Molecule			
E(HF)	-919.4957612	-1302.97658	-1301.784577

As expected, the $\text{P}=\text{C}$ distances are around 1.70 Å and do not vary too much with the nature of the group, however, the same cannot be said about the bond order. The Wiberg bond order (WBO) is 1.73 for the methyl-substituted derivative, and lower for the aryl-derivatives (Table 2).

Table 2. Calculated selected geometrical data for the monomeric species

Molecule	P-C (Å)	WBO	P-Cl (Å)	WBO	C-P-Cl (°)	C ₁ -C-P (°)	C ₂ -C-P (°)
$\text{Me}_2\text{C}=\text{PCI}$	1.68	1.73	2.12	0.89	105.3	129.6	114.5
$\text{Ph}_2\text{C}=\text{PCI}$	1.70	1.61	2.11	0.90	106.7	130.0	112.3
$\text{R}_2\text{C}=\text{PCI}$	1.70	1.56	2.10	0.92	107.2	136.9	117.5

The NBO analysis shows that charge transfer from a lone pair on the chlorine atom to the antibonding orbital of π symmetry of the P=C bond is present for all the monomers, and the values of the second order perturbation energy are 7.72 kcal for $\text{Me}_2\text{C}=\text{PCl}$, 8.14 kcal for $\text{Ph}_2\text{C}=\text{PCl}$, and 8.04 for the fluorenyl derivative. Figure 2 presents the shape of the two NB orbitals involved in the charge-transfer for $\text{Me}_2\text{C}=\text{PCl}$. In addition to this, in the case of the aryl-substituted species, other interactions occur which lead to a greater population of the antibonding orbital, with contributions from orbitals of π symmetry localized on the double C=C bonds of the aliphatic rings. These lead to a decrease of the bond order of the P=C bond.

The HOMO orbitals have bonding character, but only in the case of $\text{Me}_2\text{P}=\text{CCl}$ they are situated on the P=C bond. The LUMOs present an antibonding character and π symmetry, and they are situated for all monomers on the double bond.

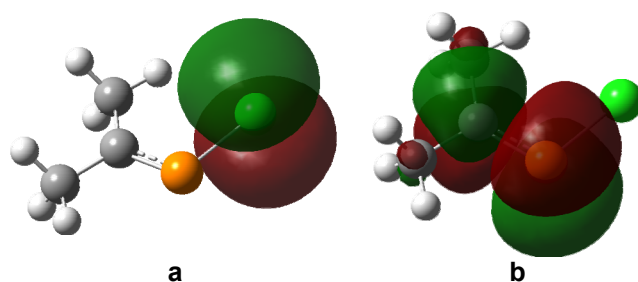
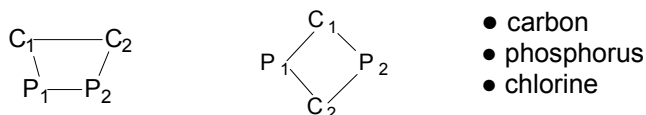


Figure 2. Shape of the NB orbitals involved in charge transfer for $\text{Me}_2\text{C}=\text{PCl}$:
(a) lone pair on the chlorine atom; (b) anti-bonding orbital of π symmetry localized on the P-C bond

In the case of dimeric species, two possible ways of dimerization for the monomers considered above, both involving the P=C double bond, and leading to either the *head-to-head* or the *head-to-tail* dimers. For each case, the chlorine atoms on the phosphorus can adopt either a *cis* or a *trans* orientation with respect to the plane of the four-atom ring. Thus, four different dimers were investigated through theoretical calculations (B3LYP/6-311G(d,p)) for each different monomer.

Table 3 contains the calculated B3LYP/6-311G(d,p) energies and relative energies (reported to the lowest-energy structure) for the dimeric species, six *head-to-head*, and six *head-to-tail* dimers. The optimized geometry is also presented. The hydrogen atoms have been omitted for clarity, and the rings are oriented so that the numbering of the atoms corresponds to that given in scheme 4.

**Scheme 4**

It can be noted that the presence of two phenyl groups on the carbon atom imposes greater strain on the four atom ring compared to the fluorenyl-substituted analogue. In the absence of any such constrain, that is, for the methyl-derivative, the energies of the four dimers are within less than 5 kcal/mol of each other. However, a slightly bigger group, like fluorenyl, significantly changes the situation, first by stabilizing the *trans head-to-head* dimer and then by increasing the energy difference to about 10 kcal/mol between the lowest-energy isomer and the *cis head-to-tail* one. This trend is not kept for the phenyl disubstituted dimers, where the *trans head-to-tail* isomer is the highest in energy. In all cases though, the difference between the *cis* and *trans* conformations of the same isomer are not significant.

Table 3. Calculated B3LYP/6-311G(d,p) energies (HF) and relative energies (kcal/mol) for the dimeric species

Dimer	<i>trans, head-to-tail</i>	<i>cis, head-to-tail</i>	<i>trans, head-to-head</i>	<i>cis, head-to-head</i>
R	Me	Me	Me	Me
E	-1839.017129	-1839.012333	-1839.019696	-1839.013043
ΔE	1.61	4.62	0.00	4.17
R	Ph	Ph	Ph	Ph
E(HF)	-2605.951626	-2605.94615	-2605.929117	-2605.928376
ΔE	0.00	3.44	14.12	11.15
R	Fluorenyl	Fluorenyl	Fluorenyl	Fluorenyl
E	-2603.579908	-2603.579908	-2603.579908	-2603.579908
ΔE	0.00	3.21	8.24	9.83

Some relevant geometrical data for the dimers are given in table 4. The optimized geometrical parameters are similar to those found in the literature [12-15].

The relatively low values for the energy barrier between the four possible dimers do not allow to state the existence of only one of them during the reaction, although the experimental evidence points to the formation of only the *trans head-to-tail* dimer for R= fluorenyl. Although thermodynamically favored, the head-to-head isomers can be kinetically less stable, due to the presence of the P-P bond in the ring. Also, a solvent-induced rearrangement to the head-to-tail dimers can not be excluded.

However, by comparing the calculated energies of the dimers to the double of the monomer's value, we can establish if the dimerization is favored. The dimerization energy can be estimated as:

$$E_{dimerization} = 2 \times E_{monomer} - E_{dimer}$$

The dimerization energies calculated with the above formula for the formation of the *trans head-to-tail* dimer are: 17.68 kcal/mol for R=Me, -15.09 kcal/mol for R=Ph and 6.75 kcal for R=Fl₂C.

A graphical representation is found in figures 3-5. It can be noticed that the calculated energies of the dimers are 17.68 kcal/mol (table 5) smaller than the double of the monomer's value which means that the dimerization is favored. Interesting is that the lowest in energy is the *trans head-to-head* dimer.

Regarding the phenyl-derivative the double of the monomer's energy is 15.09 kcal/mol (table 4) smaller than the energies of the dimers which means that the dimerization is not favored. This fact is due to the presence of the two phenyl groups which impose a greater strain on the four atom ring compared to the methyl-derivative. However the difference between the double of the monomer's energy and the *trans head-to-tail* dimer is very small (figure 4).

The head-to-tail dimers with fluorenyl have the calculated energies smaller with 6.75 kcal/mol (table 5) than the double of the monomer's energy. Instead the *head-to-head* dimers have values of the energies higher than the double of the monomer's calculated energy. This means that the dimerization is favored only for the two *head-to-tail* isomers. Although a bulkier organic group like phenyl on the carbon would prevent dimerization, the dimerization occurs in the case of the fluorenyl-derivative because of the planar conformation of the substituent and the *trans* orientation with respect to the four-atom ring.

Table 4. Calculated selected geometrical data and Wiberg bond orders for the dimeric head-to-head and head-to-tail species

Molecule	P1-C1 (Å)	WBO	P1-C11(Å)	P2-P1 (Å)	WBO	C1-C2(Å)	WBO	P-P-C(°)	P-C-C(°)	P1...C2(Å)	P-C-C-P(°)
R=Me, head-to-head, <i>trans</i>	1.92	0.87	2.09	2.30	0.93	1.59	0.96	75.2	101.4	2.60	22.2
R=Me, head-to-head, <i>cis</i>	1.94	0.86	2.11	2.24	0.96	1.58	0.96	76.1	94.0	2.59	33.1
R=Ph, head-to-head, <i>trans</i>	1.98	0.84	2.16	2.27	0.95	1.62	0.95	80.6	99.2	2.73	10.4
R=Ph, head-to-head, <i>cis</i>	1.97	0.83	2.08	2.28	0.92	1.65	0.94	81.6	100.8	2.63	21.4
R=Fl ₂ C, head-to-head, <i>trans</i>	1.95	0.83	2.12	2.30	0.94	1.61	0.94	79.7	100.1	2.74	5.2
R=Fl ₂ C, head-to-head, <i>cis</i>	1.93	0.84	2.09	2.32	0.91	1.62	0.92	81.6	102.6	2.60	20.8
Molecule	P1-C1(Å)	WBO	P1-C11(Å)	P2-C2(Å)	WBO	P2-C12(Å)	P-C-P(°)	C-P-C(°)	P...P(Å)	C...C(Å)	P-C-P-C(°)
R=Me, head-to-tail, <i>trans</i>	1.90	0.87	2.13	1.93	0.85	2.12	90.9	85.3	2.72	2.61	18.6
R=Me, head-to-tail, <i>cis</i>	1.92	0.86	2.11	1.92	0.86	2.11	95.0	84.8	2.83	2.59	4.4
R=Ph, head-to-tail, <i>trans</i>	1.92	0.84	2.11	1.94	0.82	2.10	89.1	88.1	2.71	2.66	20.5
R=Ph, head-to-tail, <i>cis</i>	1.93	0.84	2.10	1.93	0.84	2.10	94.2	84.2	2.83	2.59	13.8
R=Fl ₂ C, head-to-tail, <i>trans</i>	1.94	0.80	2.09	1.94	0.80	2.09	90.8	87.5	2.76	2.68	13.6
R=Fl ₂ C, head-to-tail, <i>cis</i>	1.93	0.80	2.10	1.93	0.80	2.10	90.9	89.1	2.75	2.71	0.0

CONCLUSIONS

A novel cyclic 1,3-diphospha-butane was obtained starting from 9-trimethylsilyl-fluorene and PCl_3 in a one-pot procedure. The derivative was characterized in solution through multinuclear NMR spectroscopy. The proposed mechanism of formation involves the presence of the phosphalkene $\text{Fl}_2\text{C}=\text{PCl}$. Theoretical investigations were carried out at the B3LYP/6-311G(d,p) level in order to gain an insight on the dimerization of the phosphalkene to the 1,3-diphospha-cyclobutane.

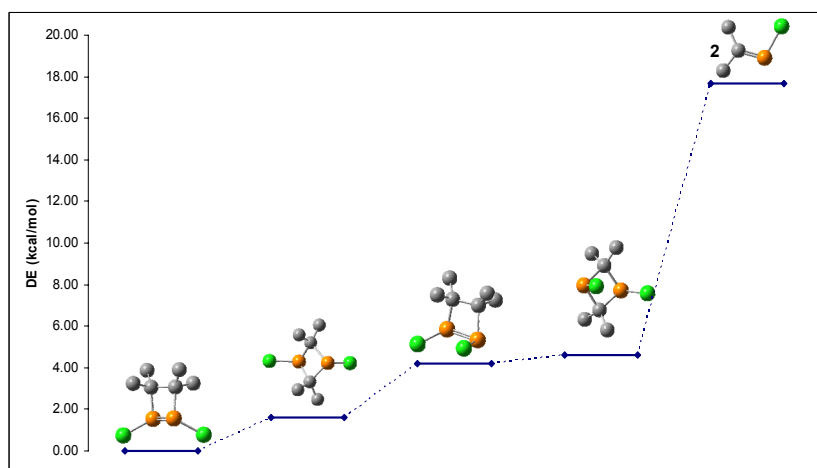


Figure 3. Energy barriers between possible dimers for $[\text{Me}_2\text{CPCl}]_2$

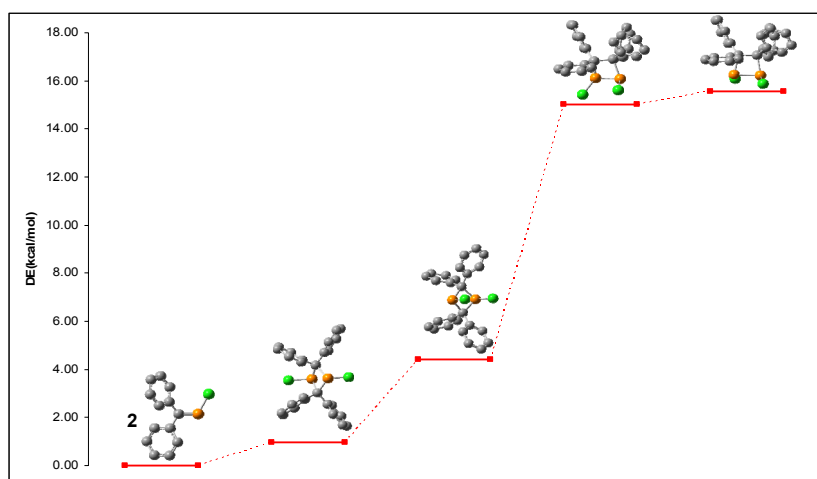


Figure 4. Energy barriers between possible dimers for $[\text{Ph}_2\text{CPCl}]_2$

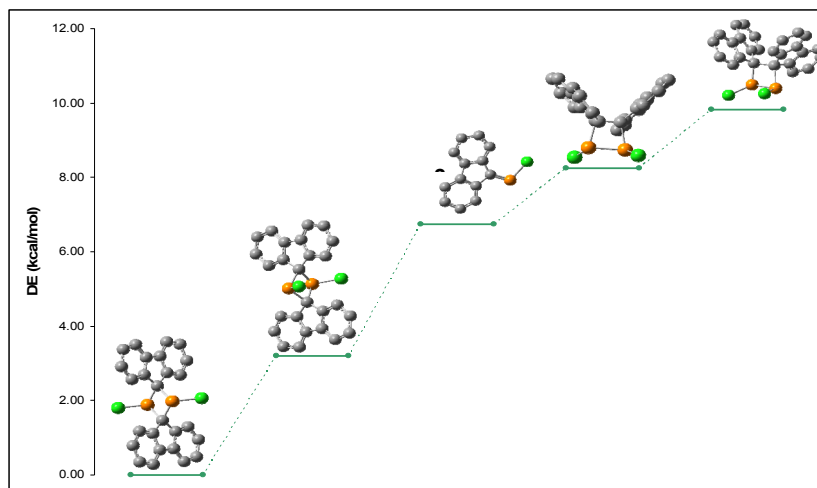


Figure 5. Energy barriers between possible dimers for $[\text{Fl}_2\text{CPCl}]_2$

Three model compounds were considered: $\text{Me}_2\text{C}=\text{PCl}$, $\text{Ph}_2\text{C}=\text{PCl}$ and the supposed reaction intermediate, $\text{Fl}_2\text{C}=\text{PCl}$ ($\text{Fl}_2\text{C}=\text{fluorenyl}$). The energies of the possible dimers were calculated and the energy barriers between them were estimated in every case. The calculated dimerization energies showed that in the case of the less hindered methyl- and fluorenyl-substituted phpsphaalkenes, dimerization should readily occur, with the formation of mainly the head-to-tail dimer.

The 1,3-diphosphacyclobutane will be employed as the equivalent of phosphaaalkenes in organometallic chemistry, with focus on the synthesis of Pt and Pd-coordinated compounds which can be tested for biological activity.

EXPERIMENTAL SECTION

Theoretical calculations were carried out on model compounds of the monomeric (R_2CPCl) and dimeric ($[\text{R}_2\text{CPCl}]_2$) species, at the B3LYP[10]/6-311G(d,p) level, using Gaussian09 [11]. Starting geometries were built with GaussView4.1, and then optimized and a frequency analysis was performed in order to confirm that the optimized structure is indeed a true minimum. In the case of the dimers, the chlorine atoms on the phosphorus can be in either *cis* or *trans* orientation with respect to each other, relatively to the plane of the 4-atom ring, so four structures were optimized for each dimer.

The starting geometries were approximated by the software user, since the built-in GaussView minimizer led to improbable structures as starting point. As in the case of phosphaaalkenes, the optimization was followed by a vibrational analysis which allowed us to establish that there are no imaginary frequencies for the diphosphacyclobutanes involved.

Due to the air and moisture sensitivity of most of phosphorus derivatives, all experiments were carried out in flame-dried glassware under an argon atmosphere using high-vacuum-line techniques.

All the employed solvents were purified using an automated solvent purifying system (MBRAUN AUTO SPS). NMR spectra were recorded in CDCl₃ on a Bruker Avance 300 spectrometer

Synthesis and characterization of 1,3-diphosphacyclobutane 3

A solution of 6 ml *n*-BuLi 1,6 M (9.6 mmol) was added at – 40° C to a solution of FSiMe₃ (2g, 8.4 mmol) in 30 ml of diethyl-ether. The reaction mixture was stirred for 20 minutes and at the same temperature, then 0.74 ml of PCl₃ (8.5 mmol) were slowly injected into the reaction mixture by a syringe. The solvent was then removed under vacuum and replaced with a mixture of 10 ml THF and 10 ml toluene. Lithium salts were removed by filtration and a white-yellow precipitate appeared.

¹H NMR (CDCl₃): 7.47-7.62 ppm, m, 4H, H_b,H_c; 7.90 ppm, d, 2H H_d (²J_{H-H} = 7.50Hz); 8.06 ppm d, 2H, H_a (²J_{H-H} = 7.80 Hz);

¹³C NMR (CDCl₃): 120.50- 122.45 ppm, t, 2C, (²J_{P-C} = 117.61 Hz);

³¹P NMR (CDCl₃): 179.47 ppm, s.

ACKNOWLEDGMENT

This work was supported by CNCSIS –UEFISCSU, project number PNII - PD 438/2010.

REFERENCES

1. S. Ito and M. Yoshifuji, *Chem. Commun.*, **2001**, 1208.
2. H. Liang, K. Nishide, S. Ito and M. Yoshifuji, *Tetrahedron Lett.*, **2003**, *44*, 8297.
3. S. Ito, K. Nishide and M. Yoshifuji, *Organometallics* **2006**, *25*, 1424.
4. M. Yoshifuji, K. Toyota and N. Inamoto, *J. Chem. Soc. Chem. Commun.*, **1984**, 689.
5. R. Septelean, G. Nemes, J. Escudié, I. Silaghi-Dumitrescu, H. Ranaivonja-tovo, P. Petrar, H. Gornitzka, L. Silaghi-Dumitrescu and N. Saffon, *Eur J Inorg Chem.*, **2009**, 628.
6. Septelean R, Ranaivonjatovo H, Nemes G, Escudié J, Silaghi-Dumitrescu I, Gornitzka H, Silaghi-Dumitrescu L, Massou S, . *Eur J Inorg Chem.*, **2006**, 4237.
7. J. Escudié and H. Ranaivonjatovo, *Organometallics*, **2007**, *26*, 1542.
8. R. Septelean, P.M. Petrar, G. Nemes, J. Escudié, I. Silaghi-Dumitrescu, *J. Mol. Mod.*, **2010**, DOI 10.1007/s00894-010-0872-8.
9. J. Escudié, G. Nemeş, *Comptes Rendus Chim*, **2010**, *13*, 954.

10. a) A.D. Becke, *J.Chem.Phys.*, **1993**, *98*, 5648; b) C. Lee, W. Yang and R.G. Parr, *Phys. Rev. B*, **1988**, *37*, 785; c) S.H. Vosko, L. Wilk and M. Nusair, *Can. J. Phys.*, **1980**, *58*, 1200; d) P.J. Stephens, F.J. Devlin, C.F. Chabalowski and M.J. Frisch, *J. Phys. Chem.*, **1994**, *98*, 11623.
11. Gaussian 09, Revision A.02, M.J. Frisch, G.W. Trucks, H.B. Schlegel, G.E. Scuseria, M.A. Robb, J.R. Cheeseman, G. Scalmani, V. Barone, B. Mennucci, G.A. Petersson, H. Nakatsuji, M. Caricato, X. Li, H.P. Hratchian, A.F. Izmaylov, J. Bloino, G. Zheng, J.L. Sonnenberg, M. Hada, M. Ehara, K. Toyota, R. Fukuda, J. Hasegawa, M. Ishida, T. Nakajima, Y. Honda, O. Kitao, H. Nakai, T. Vreven, J.A. Montgomery, Jr., J.E. Peralta, F. Ogliaro, M. Bearpark, J.J. Heyd, E. Brothers, K.N. Kudin, V.N. Staroverov, R. Kobayashi, J. Normand, K. Raghavachari, A. Rendell, J.C. Burant, S.S. Iyengar, J. Tomasi, M. Cossi, N. Rega, J.M. Millam, M. Klene, J.E. Knox, J.B. Cross, V. Bakken, C. Adamo, J. Jaramillo, R. Gomperts, R.E. Stratmann, O. Yazyev, A.J. Austin, R. Cammi, C. Pomelli, J.W. Ochterski, R.L. Martin, K. Morokuma, V.G. Zakrzewski, G.A. Voth, P. Salvador, J.J. Dannenberg, S. Dapprich, A.D. Daniels, Ö. Farkas, J.B. Foresman, J.V. Ortiz, J. Cioslowski, and D.J. Fox, Gaussian, Inc., Wallingford CT, **2009**.
12. G. Becker, W. Massa, O.Mundt, R. Schmidt, *Z. Anorg. Allg. Chem.*, **1982**, *485*, 23
13. M. Schmitz, S. Leininger, V. Bergstrasser, *Heteroat. Chem.*, **1998**, *9*, 453.
14. A.N. Chernega, G.N. Koidan, A.P. Marchenko, *J. Struct. Chem*, **1992**, *33*, 155.
15. A.V. Guton, A.N. Chernega, *Private Communication*, **2006**.

^2H NMR SPECTROSCOPY OF SOME ROMANIAN COMERCIAL WINES

**ADRIAN PÎRNĂU^a, MIRCEA BOGDAN^a,
CĂLIN G. FLOARE^a, DANA ALINA MĂGDAȘ^a**

ABSTRACT. The requirements for quality food products have been increased in recent years and the interest in the quality and purity of spirits, wines and fruit juices has grown in this connection as well. In the early 90's the EU adopted the ^2H -NMR method for wine analysis as an official method (EEC 2676/90), in order to tackle the problem of over-capitalization of wines in Europe. A deuterium natural abundance quantitative NMR method (SNIF-NMR) was developed as an efficient and powerful tool capable of characterizing the chemical origins of organic molecules and distinguishing their biological and geographical origin. Usually this type of measurements are performed with dedicated NMR equipments and computerized programs elaborated, commercialized and maintained by Eurofins Scientific (France).

Keywords: ^2H NMR, wine, isotopic ratio

INTRODUCTION

Making fraudulent profit from misrepresentation of food has been a future of society from historical times. Nowadays frauds in various consumer sectors are commonly practiced. The addition of beet or cane sugar or concentrated rectified must to grape must or wine before or during fermentation is used to increase the natural content of ethanol and therefore the value of wine, which commands higher prices on the market. Consumers are thus deceived since added sugar is not declared on the product. Another type of economic fraud is mixing high quality wines with low quality ones that often originate from other geographical regions or countries. A memorable example is the adulteration of Austrian wine and also some Italian and German wines with poisonous antifreeze ethylene glycol with intention to give the impression of a wine with a greater body. Identifying fraudulence related to fruit juices is also of great economic importance because of the large quantities of juice consumed.

The type of adulteration include diluting with water, the addition of sugar solution, citric and tartaric acid, and colorants to the pure juice, and the addition of cheaper juices originating from other fruits, mainly from grape fruit.

^a National Institute for Research and Development of Isotopic and Molecular Technologies, Donath 65-103, RO- 400293, Cluj-Napoca, Romania, apirnau@itim-cj.ro

The consumption of virgin olive oil, which is defined as oil obtained only by mechanical means is increasing due to its nutritional properties arising from the high content of unsaturated acids (oleic and linoleic acids). Natural phenolic compounds present only in virgin olive oil are responsible for its oxidation and for characteristic sensory attributes. The high sensory and nutritional quality and consequently higher commercial value of virgin olive oil has led to its adulteration with low-grade foreign oils (seed oils), esterified oils or refined olive oils, which due to the refining process and solvent extraction have lost phenolic compounds.

In order to guarantee the quality of marketed products, very drastic requirements tend to be legally imposed. To undertake necessary controls and to detect the adulteration of food products many analytical techniques are used: HPLC, GC-MS, GC-FTIR, IRMS and NMR [1]. Isotopic analyses are now official or standard methods in Europe and North America for routine use in testing the authenticity of several food products. These methods are based on the measurement of stable isotope content (^2H , ^{13}C , ^{18}O) of the product or of a specific component such as an ingredient or target molecule of the product. The determinations carried out using nuclear magnetic resonance (NMR), and/or Isotopic Ratio Mass Spectrometry (IRMS), provide information on the botanical and geographical origin of the food product.

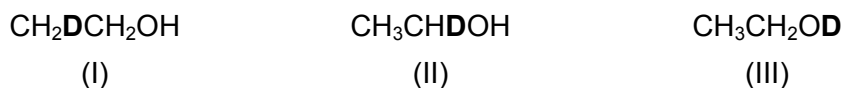
In the early 1990`s the EU adopted the ^2H -NMR method for wine analysis as an official method (EEC/2676/90), in order to tackle the problem of over-chapitalization or over-enrichment of wines in Europe [2]. This was followed by the official publication of a method for the determination of $^{18}\text{O}/^{16}\text{O}$ isotopic ratios of water from wine by IRMS (EEC/822/97) [3]. The measurement of $^{13}\text{C}/^{12}\text{C}$ isotopic ratios of ethanol from wine has been accepted as an OIV Resolution [4].

The main idea behind these authorized methods is that each plant has its own unique pattern of naturally occurring stable isotopes of carbon (^{12}C , ^{13}C), nitrogen (^{14}N , ^{15}N), hydrogen (^1H , ^2H), and oxygen (^{16}O , ^{18}O) whose distribution has been influenced by a number of physical and/or biochemical properties and geoclimatic conditions. The isotope content of natural products depends on their botanic and geographical origin. The most sophisticated and most specific method for detecting adulteration is SNIF - NMR (Site -specific Natural Isotope Fractionation - NMR). This method is based on the measurement of deuterium / hydrogen (D/H) ratios at the specific sites of the ethanol molecule [5]. In the case of European wines, it was decided in 1991 to build an isotopic data bank concerning wines of all Member States producing wine. At this time, the official laboratories of these States supply the data bank that is maintained in the Joint Research Centre of Ispra (Italy) [6].

RESULTS AND DISCUSSION

The purpose of this paper is to implement the SNIF-NMR technique on the BRUKER Avance III 500 UltraShield NMR spectrometer equipped with a special probehead (SEX 500 MHz S2 10 mm) for recording ²H RMN spectra, proton decoupling and lock on ¹⁹F.

The SNIF method is based on the measurement of deuterium / hydrogen (D/H) ratios at the specific sites of the ethanol. In ethanol, deuterium may be located in the sites:



Scheme 1

The (D/H)_i ratios are determined at the methyl (D/H)_i and methylene (D/H)_{ii} sites of the ethanol molecule.

(D/H)_i mainly characterizes the vegetable species which synthesized the sugar and to a lesser extent the geographical location of the place of harvest (type of water used during photosynthesis).

(D/H)_{ii} represents the climatology of the place of production of the grapes (type of rain water and weather conditions) and to a lesser extent the sugar concentration of the original must.

$R = \frac{2(D/H)_{ii}}{(D/H)_i}$ expresses the relative enrichment or depletion of the methylene site, the methyl site being arbitrary given the statistical weight 3. A random distribution of deuterium within the ethyl fragment would therefore be characterized by a value of $R = 2$. Since the area of an NMR signal is proportional to the number of nuclei resonating at the considered frequency, the isotope parameters are directly accessible from peak area measurements. Thus, if S_i and S_{ii} denote the areas of the methyl and methylene signals in the deuterium spectrum of a distillate, $R = 3 \frac{S_{ii}}{S_i}$. The

value of R varies according to the fermentation process and the sugar used.

Using this method we present the obtained results for a series of Romanian wines:

- sample 1, semi-sweet white wine;
- sample 2, semi-dry red wine;
- sample 3, semi-dry white wine;
- sample 4, semi-dry white wine.

Figure 1 represents a ^2H NMR spectrum, recorded on a sample of ethanol obtained from wine by distillation. In this spectrum, we can see the signals for the three sites of ethanol.

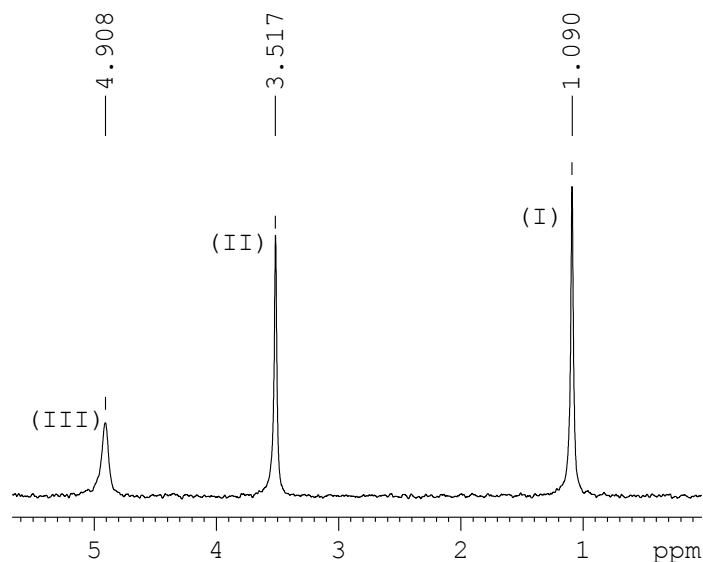


Figure 1. ^2H NMR spectrum of ethanol distilled from wine

Table 1. The R values and their standard deviations for each studied samples

Sample	R	$\bar{R} \pm SD$
1	2.37548	2.403±0.026
	2.41916	
	2.38682	
	2.42974	
2	2.31089	2.357± 0.044
	2.35831	
	2.41488	
	2.34192	
3	2.47975	2.408±0.057
	2.33918	
	2.43982	
	2.42170	
4	2.36202	2.404±0.057
	2.46609	
	2.47893	
	2.34082	
	2.36295	
	2.40770	
	2.36967	

The obtained values of R and their standard deviations are given in Table 1. The number of experiments / sample was 4. In order to obtain more quantitative data, mainly (D/H)_{II}, (D/H)_I and R, we need a reference substance with very well defined D/H ratio. SNIF NMR recommends that tetramethylurea (TMU) supplied by IRMM, Geel Belgium to be used. In order to decide if a certain wine was modified or not, the producer must supply an original wine sample which will be considered as reference one. Detailed results will be published in a forthcoming paper.

CONCLUSIONS

In this paper, were performed ²H NMR measurements on ethanol distilled from wine by distillation. For each sample four measurements were made and the R average value and standard deviation for each sample were obtained separately.

Our results prove that R value can be obtained with a standard deviation of maximum ± 0.06 .

EXPERIMENTAL SECTION

NMR measurements were performed on the BRUKER Avance III 500 UltraShield NMR spectrometer equipped with a special probehead (SEX 500 MHz S2 10 mm) for recording ²H RMN spectra, proton decoupling and lock on ¹⁹F.

All measurements were performed using the following acquisition parameters:

Spectral width	10 ppm
Data points	8 K
Pulse width	23.5 μ s
Frequency	76.77 MHz
Number of scans	256
FID resolution	0.093 Hz
Acquisition time	5.33 s
Relaxation delay	5 s
Temperature	302 K

ACKNOWLEDGMENTS

This work was supported by CNCSIS-UEFISCSU, project number: PN II-RU PD_130/2010.

REFERENCES

1. C. Cordela, I. Moussa, A.C. Martel, N. Sbirrazzuoli, L. Lizzani-Cuvelier, *J. Agric. Food Chem.*, **2002**, *50*, 1751.
2. EC Regulation No. 2676/90, *Off. J. Eur. Commun.*, **1990**, *L272*, 64.
3. EC Regulation No. 822/97, *Off. J. Eur. Commun.*, **1997**, *L117*, 10.
4. Office International de la Vigne et du Vin (OIV), *Resolution OENO/SCMA/00/177*, **2001**.
5. G.G. Martin, R. Wood, G.J. Martin, *JAOAC Int.*, **1996**, *79*, 917.
6. EC Regulation No. 2348/91, *Off. J. Eur. Commun.*, **1991**, *L214*, 39.

INORGANIC RINGS: EIGHT-MEMBERED Pd₄S₄ RING IN [Pd₄Cl₄{1-S-2-SCH₂COOMe-C₆H₄-κ²S,S'}₄]

IOANA GEORGETA GROSU^{a,b}, SANTIAGO GOMÉZ-RUIZ^{b,c},
LUMINIȚA SILAGHI-DUMITRESCU^{a,*} AND EVAMARIE HEY-HAWKINS^{b,*}

ABSTRACT. Under solvothermal conditions in methanol the mononuclear complex *cis-rac*-[PdCl₂{1,2-(HOOCCH₂S)₂C₆H₄-κ²S,S'}] (2) reacted to give the tetranuclear palladium(II) complex [Pd₄Cl₄{1-S-2-SCH₂COOMe-C₆H₄-κ²S,S'}₄] (3). The molecular structure of 3 was investigated by single-crystal X-ray structure analysis.

Keywords: palladium(II) complex, solvothermal, S-dealkylation, X-ray crystallography, inorganic ring

INTRODUCTION

A topic of current interest in recent years has been the chemistry of coordination polymers due to their fascinating architectures and applications in many fields like catalysis, gas storage, magnetism, ion exchange, and nonlinear optics [1-5]. One of the most widely used methods to synthesize coordination polymers is molecular self-assembly [6, 7], but the controlling factors and experimental conditions for the preparation of such polymers are not yet completely understood [8, 9]. Therefore, in recent years rational synthetic approaches for the assembly of target structures from molecular building blocks have been considered. The key step in the rational approach is the design of suitable molecular building blocks which can direct the formation of the desired architecture and functionality of the target compound. In this context, we have previously reported several mononuclear transition metal complexes of 1,2-phenylenebis(thio)diacetic acid as potential building blocks for the rational synthesis of coordination polymers [10]. Here we present the unexpected formation of tetranuclear palladium(II) complex [Pd₄Cl₄{1-S-2-SCH₂COOMe-C₆H₄-κ²S,S'}₄] (3) under solvothermal conditions from mononuclear *cis-rac*-[PdCl₂{1,2-(HOOCCH₂S)₂C₆H₄-κ²S,S'}] (2) under solvothermal conditions in methanol.

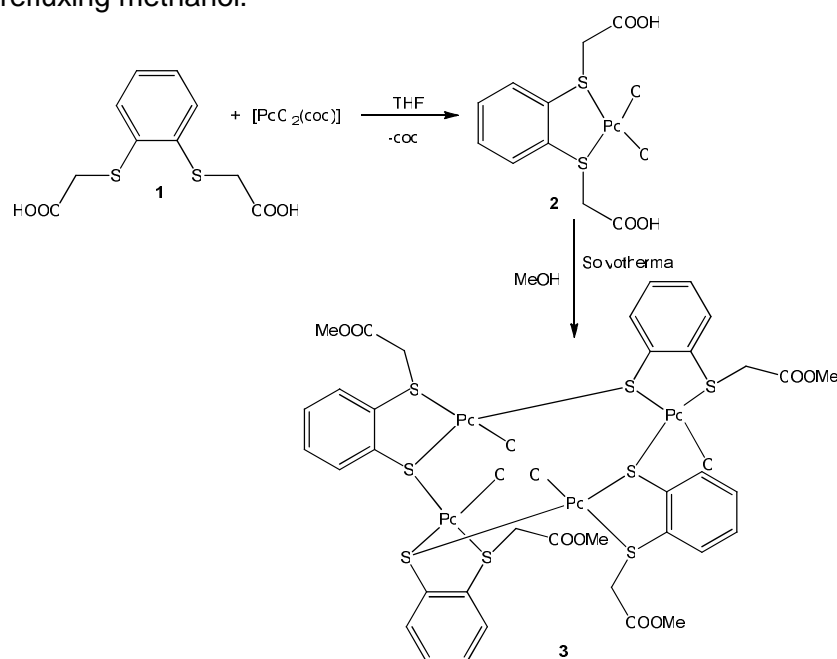
^a Babeş-Bolyai University, Faculty of Chemistry and Chemical Engineering, 11 Arany Janos str., RO-400028 Cluj-Napoca, Romania

^b Universität Leipzig, Institut für Anorganische Chemie, Johannisallee 29, D-04103 Leipzig, Germany

^c new address: Departamento de Química Inorgánica y Analítica, Universidad Rey Juan Carlos, C/ Tulipán s/n, E-28933. Móstoles (Madrid), Spain

RESULTS AND DISCUSSION

Complex **2** was obtained according to a previously published method [10] from 1,2-phenylene phenylenebis(thio)diacetic acid [11] and $[\text{PdCl}_2(\text{cod})]$ (cod = 1,5-cyclooctadiene). Heating a highly diluted methanol solution of **2** under solvothermal conditions at 120 °C for 12 hours and then slowly cooling to room temperature gave dark orange crystals of tetranuclear complex **3** (Scheme 1). Unfortunately, complex **3** could not be reproduced under solvothermal conditions or in refluxing methanol.



Scheme 1

The formation of tetranuclear sulfido-bridged palladium(II) complex **3** may have occurred by methylation of the carboxylato groups followed by elimination of chloromethyl acetate. Similar *S*-dealkylation of some palladium(II) complexes was observed for the series $[\text{MX}_2(1\text{-AsMe}_2\text{-2-MeSC}_6\text{H}_4\text{-}\kappa\text{S})_2]$ ($\text{M} = \text{Pt, Pd}$; $\text{X} = \text{Cl, Br, I}$; $\text{R} = \text{CH}_3$). The reaction gave metal complexes $[\text{M}(1\text{-AsMe}_2\text{-2-SC}_6\text{H}_4\text{-}\kappa^2\text{As, S})_2]$ in which the ligand is strongly bonded to the metal center through the sulfur and arsenic atoms [12].

Complex **3** crystallizes in the monoclinic space group $P2_1/c$ with four molecules in the unit cell. Each palladium atom is fourfold-coordinated in a square-planar fashion by three sulfur atoms, two of which belong to the same ligand and the third to a ligand of another palladium complex unit (Figure 1).

The coordination sphere is completed by one chloro ligand. The four 1-S-2-SCH₂COOMeC₆H₄ ligand molecules differ from each other in that the four pendant arms (CH₂COOMe) exhibit different conformations with C_{aromatic}-S-CH₂-COOMe torsion angles of 58.68(1), 48.46(1), 65.80(7), and 43.32(2)°, respectively.

The four palladium atoms alternate with four bridging thiolato groups and together form an inorganic eight-membered ring in a boat–boat conformation due to short Pd(1)···Pd(2) (3.1589(8) Å) and Pd(3)···Pd(4) (3.2401(8) Å) contacts (Figure 2). These contacts suggest interactions between the palladium atoms, but they are significantly longer than the Pd–Pd bonds observed in related compounds, e.g., 2.581(3) Å in {[Pd(μ-SC₆F₅)(μ-dppm)Pd}(μ-SC₆F₅)₄2O(C₂H₅)₂ (dppm = diphenylphosphinomethane) [13] and 2.7247(5) Å in [Pd₂(dtp)₄] (dtp = dithiopropionate, C₂H₅CS₂⁻), which exhibits one-dimensional metal-dimer chains of [Pd₂(dtp)₄] with moderate interdimer contacts (3.428(2) Å) [14]. Shorter Pd···Pd contacts (2.942(2) Å) were observed in [Pd₂(μ-N-S-pyS-κ²N,S)₂Cl₂(PMe₃)₂] (pyS = μ-pyridine-2-thiolate) [15].

The Pd–S bond lengths (2.244(2) Å to 2.313(2) Å) are longer than the Pd–S bonds in complex **2** but are similar to Pd–S bonds observed in related compounds [13–15].

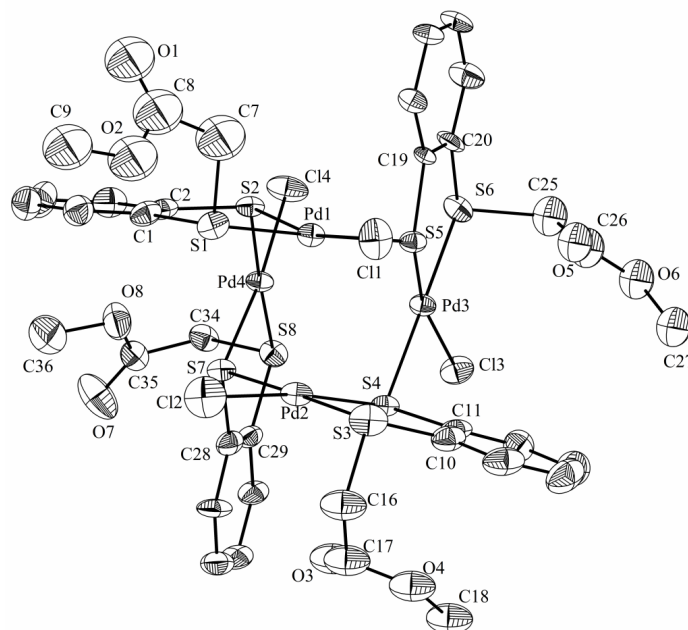


Figure 1. Molecular structure of **3** with atom labeling (thermal ellipsoids at 50% probability; hydrogen atoms omitted for clarity).

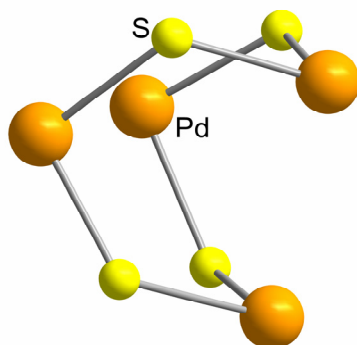


Figure 2. Central Pd₄S₄ ring showing boat–boat conformation.

Table 1. Selected bond lengths (Å) and angles (°) in **3**

Pd(1)-S(1)	2.285(2)	S(1)-Pd(1)-S(2)	89.64(7)
Pd(1)-S(2)	2.248(2)	S(2)-Pd(1)-S(5)	92.41(7)
Pd(1)-S(5)	2.311(2)	S(1)-Pd(1)-S(5)	177.14(7)
Pd(1)-Cl(1)	2.341(2)	S(2)-Pd(1)-Cl(1)	167.69(8)
Pd(2)-S(3)	2.282(2)	S(3)-Pd(2)-S(4)	89.76(8)
Pd(2)-S(4)	2.245(2)	S(4)-Pd(2)-S(7)	90.99(7)
Pd(2)-S(7)	2.329(2)	S(4)-Pd(2)-Cl(2)	172.75(8)
Pd(2)-Cl(2)	2.327(2)	S(7)-Pd(2)-Cl(2)	91.29(7)
Pd(3)-S(4)	2.321(2)	S(5)-Pd(3)-S(6)	89.25(7)
Pd(3)-S(5)	2.253(2)	S(4)-Pd(3)-S(5)	93.70(7)
Pd(3)-S(6)	2.284(2)	S(4)-Pd(3)-S(6)	176.85(7)
Pd(3)-Cl(3)	2.334(2)	S(5)-Pd(3)-Cl(3)	168.31(7)
Pd(4)-S(2)	2.313(2)	S(2)-Pd(4)-S(7)	91.38(7)
Pd(4)-S(7)	2.248(2)	S(2)-Pd(4)-S(8)	177.69(7)
Pd(4)-S(8)	2.275(2)	S(2)-Pd(4)-Cl(4)	89.73(7)
Pd(4)-Cl(4)	2.335(2)	S(8)-Pd(4)-Cl(4)	88.99(7)

In the network, the molecules of **3** have an edge-to-face arrangement (Figure 3). Moreover, there are π - π stacking interactions between two phenyl rings belonging to two different molecules of **3** even though the phenyl rings are not strictly parallel to each other. The rings have an offset face-to-face arrangement with a distance between the centroids defined by the phenyl rings of 4.285 Å and an offset of 2.55.

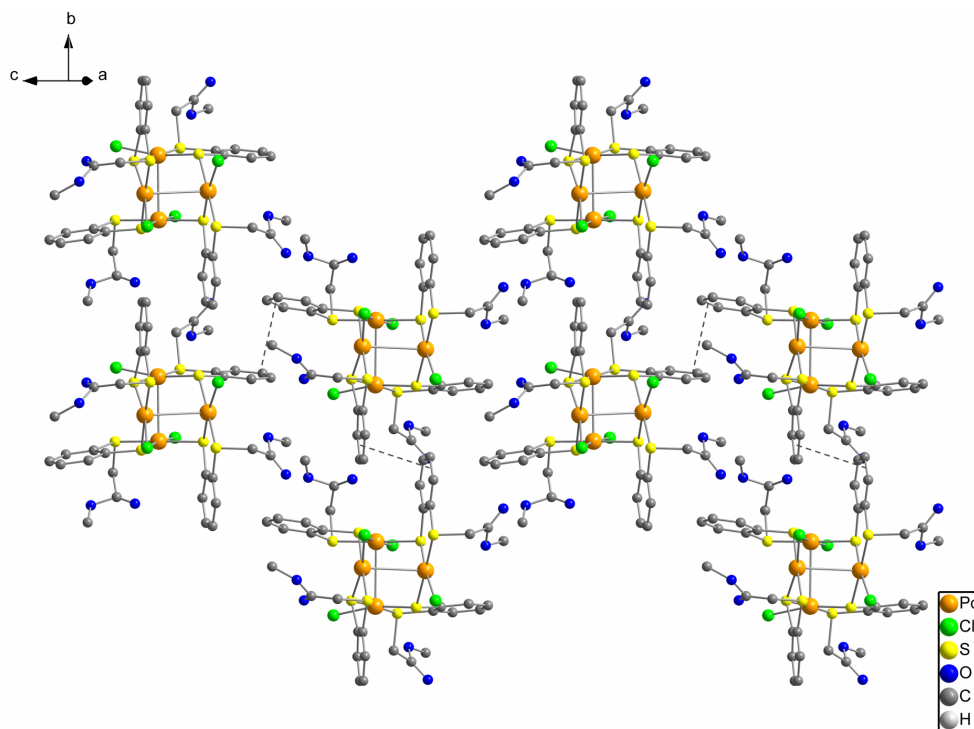


Figure 3. Edge-to-face arrangement and π - π stacking interactions of phenylene rings in **3** (view along the *a*-axis, hydrogen atoms omitted for clarity).

CONCLUSIONS

Under solvothermal conditions the mononuclear palladium(II) complex **2** eliminates chloro acetic acid (or chloromethyl acetic acid after esterification) to give a tetranuclear palladium(II) complex. The structure of the tetranuclear complex was determined by X-ray crystallography.

EXPERIMENTAL SECTION

The data of **3** were collected on a CCD Oxford Xcalibur S ($\lambda(\text{MoK}\alpha) = 0.71073 \text{ \AA}$) in ω and Φ scan modes with $\text{MoK}\alpha$ radiation ($\lambda 0.71073 \text{ \AA}$). Data reduction was performed with CrysAlis Pro including the program SCALE3 ABSPACK for empirical absorption correction [16]. All structures were solved by direct methods [17] and the refinement of all atoms was performed with SHELXL-97 [17]. Structure figures were generated with DIAMOND-3 [18]. Some fragments of the ester moieties are disordered and were refined over split positions with constrained geometry and fixed atomic displacement parameters (SADI and EADP instructions).

A summary of the data collection, structure solution, and refinement details for compound **3** is given in Table 2. CCDC 805586 (**3**) contains the supplementary crystallographic data for this paper. These data can be obtained free of charge from The Cambridge Crystallographic Data Centre via www.ccdc.cam.ac.uk/data_request/cif.

Table 2. Crystal Data and Structure Refinement for **3**

Empirical formula	C ₃₆ H ₃₆ Cl ₄ O ₈ Pd ₄ S ₈
<i>M</i>	1420.53
<i>T</i> /K	130(2)
Crystal system	Monoclinic
Space group	<i>P</i> 2 ₁ / <i>c</i>
<i>a</i> /Å	20.4269(8)
<i>b</i> /Å	10.8202(4)
<i>c</i> /Å	21.6073(9)
β /°	109.804(4)
<i>V</i> /Å ³	4493.3(3)
<i>Z</i>	4
<i>D</i> _{calcd} /Mg m ⁻³	2.100
μ /mm ⁻¹	2.235
<i>F</i> (000)	2784
Reflections collected	65370
Independent reflections	8189 [R(int) = 0.1104]
Restraints/parameters	19/501
Goodness of fit on <i>F</i> ²	0.896
Final <i>R</i> indices	<i>R</i> 1 = 0.0464,
[<i>I</i> > 2σ(<i>I</i>)]	<i>wR</i> 2 = 0.0697
<i>R</i> indices (all data)	<i>R</i> 1 = 0.1053,
	<i>wR</i> 2 = 0.0808
Largest diff. peak and hole/e Å ⁻³	1.477 and -1.343

Synthesis of [Pd₄Cl₄{1-*S*-2-*S*-CH₂COOMe-C₆H₄-κ²S,S'}₄] (**3**)

A solution of complex **2** (0.004 g, 0.009 mmol) in MeOH (4 mL) was placed in a stainless steel container, which was heated gradually over 12 hours to 120 °C, maintained at this temperature for a further 12 hours, and slowly cooled to room temperature over 12 hours. Dark orange crystals of **3** were obtained directly from the reaction mixture.

ACKNOWLEDGMENTS

We gratefully acknowledge financial support from the Deutscher Akademischer Austausch Dienst (DAAD, sandwich-PhD scholarship and SOE programme) (I.G.G.) and the Alexander von Humboldt-Stiftung for a Humboldt-Fellowship (S.G.-R.).

REFERENCES

1. A.Y. Robin, K.M. Fromm, *Coord. Chem. Rev.*, **2006**, *250*, 2127; S. Kitagawa, K. Uemura, *Chem. Soc. Rev.*, **2005**, *34*, 109; S. Bureekaev, S. Shimomuram, S. Kitagawa, *Sci. Technol. Adv. Mater.*, **2008**, *9*, 014108.
2. B. Moulton, M.J. Zawarotko, *Chem. Rev.*, **2001**, *101*, 1629; S. Noro, S. Kitagawa, T. Akutagawa, T. Nakamura, *Progress in Polymer Science*, **2009**, *34*, 240.
3. M.J. Rosseinsky, *Microporous and Mesoporous Materials*, **2004**, *73*, 15; J.L.C. Rowsell, O.M. Yaghi, *Microporous and Mesoporous Materials*, **2004**, *73*, 3.
4. A.K. Cheetham, C.N.R. Rao, R.K. Feller, *Chem. Commun.*, **2006**, 4780.
5. B.F. Abrahams, B.F. Hoskins, R. Robson, *J. Chem. Soc., Chem. Commun.*, **1990**, 762.
6. D. Braga, F. Grepioni, G.R. Desiraju, *Chem. Rev.*, **1998**, *98*, 1375.
7. A.M. Spokoyny, D. Kim, A. Sumrein, C.A. Mirkin, *Chem. Soc. Rev.*, **2009**, *38*, 1218.
8. S.L. James, *Chem. Soc. Rev.*, **2003**, *32*, 276.
9. D.J. Tranchemontagne, J.L. Mendoza-Cortes, M. O'Keeffe, O.M. Yaghi, *Chem. Soc. Rev.*, **2009**, *38*, 1257.
10. C. Berghof, I.G. Grosu, P. Lönnecke, S. Gómez-Ruiz, L. Silaghi-Dumitrescu, E. Hey-Hawkins, *Inorg. Chim. Acta*, in press, **2011**, doi: 10.1016/j.ica.2010.12.004.
11. A.B. Kyte, K.A. Owens, I.O. Sutherland, R.F. Newton, *J. Chem. Soc. Perkin Trans.*, **1987**, *1*, 1921; T. Wei, J. Chen, X. Wang, Y. Zhang, L. Wang, *Syn. Comm.*, **1996**, *26*, 1447.
12. J.P. Beale, N.C. Stephenson, *Acta Cryst.*, **1971**, *B27*, 73; L.F. Lindoy, S.E. Livingstone, T.N. Lockyer, *Inorg. Chem.*, **1967**, *8*, 652; J.P. Beale, N.C. Stephenson, *Acta Cryst.*, **1970**, *B26*, 1655.
13. R. Usón, J. Forniés, L.R. Falvello, M.A. Usón, I. Usón, S. Herrero, *Inorg. Chem.*, **1993**, *32*, 1066.
14. A. Kobayashi, T. Kojima, R. Ikeda, H. Kitawaga, *Inorg. Chem.*, **2006**, *45*, 322.
15. J.H. Yamamoto, W. Yoshida, C.M. Jensen, *Inorg. Chem.*, **1991**, *30*, 1353.
16. CrysAlisPro: Data collection and data reduction software package, Varian, Inc. including SCALE3 ABSPACK: Empirical absorption correction using spherical harmonics.
17. SHELX97: Includes SHELXS97, SHELXL97; G.M. Sheldrick, (1997). SHELX97. Programs for Crystal Structure Analysis (Release 97-2), University of Göttingen, Germany.
18. DIAMOND 3: K. Brandenburg, Crystal Impact GbR, Bonn, Germany.

SYNTHESIS AND CHARACTERIZATION OF NEW PHENOTHIAZINYL-DIPHENYL-PHOSPHINES

TAMAS LOVASZ^{*}, EMESE GAL, LUIZA GĂINĂ, IOANA SAS, CASTELIA CRISTEA AND LUMINIȚA SILAGHI-DUMITRESCU

ABSTRACT. New phenothiazinyl-diphenyl-phosphine derivatives were prepared based on a synthetic strategy which imply two reaction steps: a lithiation of phenothiazine derivative followed by the reaction of the C-lithiated intermediate with 1 equivalent of chlorodiphenylphosphine. Sulfonation with chlorosulfonic acid or sulfuric acid gave water soluble phenothiazinyl-phosphine ligands. Structural characterization of the new compounds is based on high resolution ¹H-, ¹³C-, ³¹P-NMR spectroscopy, FT-IR spectroscopy and mass spectrometry.

Keywords: *Phenothiazine, triphenylphosphine (TPP), arylsulfonic acid*

INTRODUCTION

Organometallic catalysis proved to be a powerful tool for increasing the stereoselective conversion of many organic substrates during important synthetic reactions. Triphenylphosphine ligands appear as parts of consecrated organometallic catalysts highly efficient in different synthetic reactions such as: carbon-carbon coupling (Heck, Suzuki), hydrogenation, hydroformylation. A green chemistry survey recognizes the use of amphiphilic triphenylphosphine ligands in aqueous-phase organometallic catalysis or biphasic catalysis, as promising developments towards more environmentally friendly chemical processes.

Amphiphilic triphenylphosphine ligands may possess in the same molecular structure both functions of a ligand and a surfactant, thus enabling the catalytic effect, as well as the easy recovery of a water soluble catalyst from the organic reaction mass. Sulfonated triarylphosphines obtained by the direct sulfonation of the aromatic rings, are frequently used as such amphiphilic ligands for aqueous and aqueous-organic two-phase catalysis.

Trisulfonated triphenylphosphine (TPPTS) was employed as a ligand in Rh complexes used in hydroformylation of olefins and hydrosoluble substrates [1] Sulfonation of Wilkinson's catalyst (tris(triphenylphosphine)rhodium

^{*} Babeş-Bolyai University, Faculty of Chemistry and Chemical Engineering, 11, Arany Janos Str., RO-400028 Cluj-Napoca, Romania, tlovasz@chem.ubbcluj.ro

chloride), was performed by a two-step method in which the synthesis of triphenylphosphine monosulfonate was followed by the formation of a complex with rhodium chloride, or, by the direct sulfonation of tris(triphenylphosphine) rhodium chloride with 20% sulfuric acid at 45°C for 8h, in sealed reaction flask and generated the trisulfonated triphenylphosphine (TPPTS) rhodium catalyst [2].

Due to the fact that the hydrophilic character of the sulfonated triarylphosphine ligand may be correlated with the number of sulfonic groups introduced in its molecular structure, different attempts to design new triarylphosphine substrates for selective sulfonation were described in the literature.

Trisulfonated triphenylphosphine (TPPTS) was prepared by the direct sulfonation of triphenylphosphine [3]. The reaction requires fuming sulfuric acid and relatively long reaction time, conditions which favors different degrees of sulfonation of the substrate and formation of phosphine oxide derivatives as well. Selective preparation of disulfonated triphenylphosphine (TPPDS), is based on careful control of reaction conditions and work-up procedure which provides TPPDS·2H₂O in 60% yield [4]. In order to avoid oversulfonation in the preparation of monosulfonated triphenylphosphine (TPPMS), the reaction needs to be interrupted at moderate conversions, thus generating low yields (29%) of TPPMS [5].

By introducing activating groups into the appropriate positions of certain phenyl-rings, the corresponding sulfonated triphenylphosphine were obtained selectively. Methyl or methoxy activating groups have been introduced into the *ortho*- and *para*-positions of the phenyl rings and the selective substitution occurred in relatively mild conditions and short reaction times without secondary oxidation reactions [6].

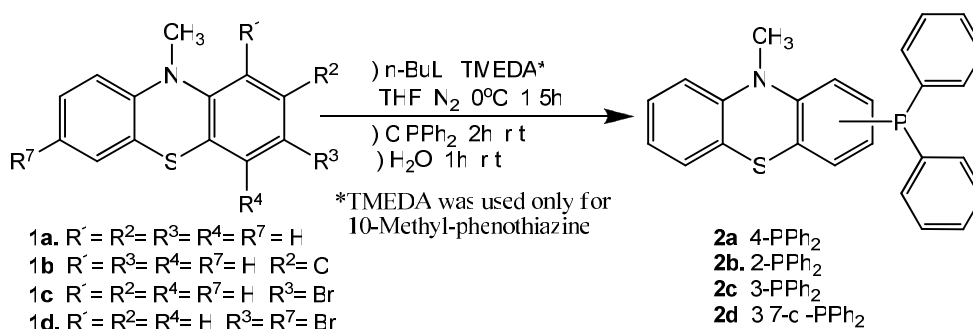
Sulfonation of dibenzofurane-aryl-phosphines occurred under mild reaction conditions, with complete selectivity and high yields, due to the presence of the π electron- rich aromatic ring [7].

Taking into consideration the facts described above, here we wish to report the preparation of some new phenothiazine containing triphenylphosphine analogues, which were transformed in water soluble sulfonates.

RESULTS AND DISCUSSION

N-alkyl-phenothiazine derivatives, are activated substrates for regioselective preparation of C-substituted phenothiazine derivatives by using direct aromatic electrophilic substitution, as well as organometallic intermediates. Halogenated N-alkyl-phenothiazine derivatives are also easily available substrates by direct halogenation of N-alkyl-phenothiazine or ring closure reactions of halogenated diphenylamines or diphenylthioethers [8]. The characteristic reactivity of the phenothiazine derivatives enabled us to develop a synthetic strategy for the preparation of phenothiazine containing arylphosphines based on

two reaction steps: i) lithiation of phenothiazine derivative followed by ii) reaction of the C-lithiated intermediate with one equivalent of chlorodiphenylphosphine. Scheme 1 shows the transformation of 10-methyl-10*H*-phenothiazine derivatives **1a-d** into the corresponding phenothiazinyl-diphenylphosphines **2a-d**.



Scheme 1

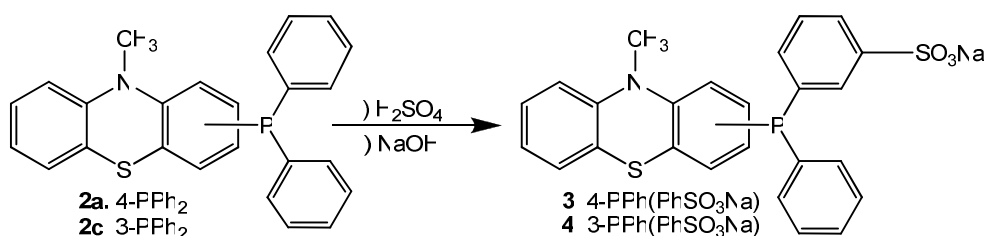
When 10-methyl-10*H*-phenothiazine **1a** was treated with *n*-butyllithium a dark red slurry was obtained, which was then treated with one equivalent of chlorodiphenylphosphine and gave 4-(diphenylphosphino)-10-methyl-10*H*-phenothiazine **2a** in 32% yields. Lithium-Halogen exchange reactions were performed starting with 2-chloro-10-methyl-10*H*-phenothiazine **1b** and 3-bromo-10-methyl-10*H*-phenothiazine **1c** respectively and thus 2-(diphenylphosphino)-10-methyl-10*H*-phenothiazine **2b** was obtained in 58% yields, while 3-(diphenylphosphino)-10-methyl-10*H*-phenothiazine **2c** was obtained in 52% yields after purification by column chromatography. 3,7-dibromo-10-methyl-10*H*-phenothiazine **1d** was also subjected to the same reactions pattern and 3,7-bis(diphenylphosphino)-10-methyl-10*H*-phenothiazine **2d** was obtained in 48% yield.

In the mass spectrometric analysis, the new 2-, 3- and 4-diphenylphosphino-10-methyl-10*H*-phenothiazine **2a-c** generate the molecular ion observable at the same value ($m/z=397$ *a.m.u.*) in high abundance. The characteristic substitution was confirmed in each case by the coupling pattern between the protons attached to the substituted phenothiazine ring, which show the signals of the protons situated in position *ortho* to the phosphorus substituent as the most shielded signals in the aromatic region ($\delta=6.4\text{-}6.7$ ppm). Even though the reactions were carried out under inert atmosphere in order to prevent the oxidation processes, small amounts of phosphinoyl analogues of **2a-b** were identified by mass spectrometry (M^+ $m/z=413$ *a.m.u.*).

The sulfonation of 10*H*-phenothiazine ring by direct electrophilic aromatic substitution appears to be difficult because of easy polysubstitution and facile oxidation of the sulfur atom. Literature data indicate the fail in the sulfonation of phenothiazine with chlorosulfonic acid [9]. Sulfonation of *N*-alkyl-phenothiazine

derivatives was reported to take place in position 3 (*para* to the nitrogen atom) [10], while sulfonation of N-acyl-phenothiazine derivatives appears with regioselectivity for position 2 (*para* to the sulfur atom in the heterocycle) [11]. We tested the reactivity of 3,7-dibromo-10-methyl-phenothiazine in the reaction with chlorosulfonic acid and we observed the formation of a water soluble adduct, but according to the coupling pattern in the recorded proton NMR spectrum, no supplementary C-substitution occurred in the aromatic rings.

The new phenothiazinyl-diphenylphosphines **2a,c** were treated with concentrated sulfuric acid and mono-sulfonation product **3** was obtained in high yields, while **4** was obtained only in small amounts (scheme 2).



Scheme 2

Assignment of the recorded proton NMR spectra of sulfonates **3**, **4** indicate that the sulfonation by a direct electrophilic aromatic substitution appeared in the *meta* position of the phenyl ring, in accordance with the directing effect of the phosphorus, which appears protonated in the strong acidic reaction medium. We can suppose that the formation of adducts with sulfuric acid considerably lowered the reactivity of the phenothiazine unit in the substrate, thus preventing the electrophilic substitution of the heterocycle. The sulfonic acids intermediates were transformed without isolation into water soluble sodium salts upon treatment with NaOH. Low amounts of phosphinoyl analogue was formed, a fact which was clearly observed in the ³¹P-NMR spectrum of **3**, where two signals situated at $\delta = -13.3$ ppm and 30.6 ppm appear in 1:6 ratio.

CONCLUSIONS

New phenothiazine containing triphenylphosphine analogues, were conveniently prepared in two reaction steps involving the lithiation of a N-acyl-phenothiazine derivative, followed by the reaction of the C-lithiated intermediate with one equivalent of chlorodiphenylphosphine. Upon treatment of the new compounds with sulfuric acid, sulfonation occurred in the *meta* position of the phenyl ring. Sulfonic acid derivatives were transformed without isolation into their water soluble sodium salts.

EXPERIMENTAL SECTION

All chemicals and solvents were dried and purified by usual methods. Compounds **1a-d** were prepared according to described procedures [12-14].

All reactions as well as column chromatography were followed by TLC analysis using Merck pre-coated silica gel 60 F₂₅₄ aluminium sheets. Column chromatography was performed using Merck silica gel 60 (63- 200 mesh). Melting points were determined with an Electrothermal IA 9200 digital melting point apparatus and are uncorrected. The mass spectra were obtained by a GC-MS (EI, CI) Shimadzu mass spectrometer. IR spectra were recorded on a Bruker Vector 22 FT-IR spectrometer fitted with a Golden Gate ATR accessory. ¹H and ¹³C-NMR spectra were recorded in CDCl₃ in 5 mm tubes at r.t., on Bruker Avance 300 MHz. The spectral data are listed below.

4-(diphenylphosphino)-10-methyl-10H-phenothiazine (2a)

To a stirred solution of 10-methyl-10H-phenothiazine (**1a**) (2.0 g, 9.4 mmol) in dry THF (40 cm³) was added TMEDA (3.0 mL, 20 mmol), followed by dropwise *n*-BuLi (20 mmol, 12.5 cm³ of a 1.6 M solution in hexane) at 0 °C under N₂. The mixture was stirred at 0 °C for 1.5 h and Ph₂PCI (4.41 g, 20 mmol) was then added. After 3 h stirring at r.t., the reaction mixture was treated with 5 mL of H₂O. The organic phase was separated and the aqueous phase was extracted with EtOAc (3x25 mL). The combined organic phase was dried over Na₂SO₄. After removal of the solvent *in vacuo*, the residue was separated by column chromatography on silica gel with toluene/Et₃N (100:1) as eluent and then recrystallized from Et₂O to give white crystals m.p.: 189-191 °C (1.2 g, 32%). **IR** (ATR) ν [cm⁻¹]: 693, 723, 744, 780, 880, 1140, 1254, 1327, 1404, 1439, 1476, 1553, 1587, 2811, 2882, 2957, 3055. **³¹P NMR** (121.5 MHz, CDCl₃) δ (ppm): -13.40. **¹H NMR** (300 MHz, CDCl₃) δ (ppm): 3.42 (s, 3H, *N*-CH₃), 6.45 (dd, 1H, ³J_{HH}= 7.5 Hz, ³J_{PH}=3.6 Hz, H₃), 6.84 (d, 2H, ³J_{HH}= 8.1 Hz, H_{1,9}), 6.93 (t, 1H, ³J_{HH}= 7.5 Hz, H₂), 7.10 (t, 1H, ³J_{HH}= 7.8 Hz, H₇), 7.16 (d, 1H, ³J_{HH}= 7.8 Hz, H₆); 7.20 (1H, t, ³J_{HH}= 8.1 Hz, H₈), 7.31-7.41 (10H, m, H_{Ph}). **¹³C NMR** (75 MHz, CDCl₃): 35.7, 113.9, 114.1, 114.4, 122.5, 123.5, 127.2, 127.5, 128.3, 128.6, 128.9, 134.0, 134.2, 135.8, 135.9, 136.1, 146.1 **MS** (EI⁺) *m/z*: 397 (M⁺, 100%), 382, 286, 273, 242, 212, 183, 77. The phosphine oxide was also detected MS (EI⁺) *m/z*: 413 (M⁺), 398, 336, 201.

2-(diphenylphosphino)-10-methyl-10H-phenothiazine (2b)

To a stirred solution of 2-chloro-10-methyl-10H-phenothiazine (**1b**) (2.47 g, 10 mmol) in dry THF (40 cm³) *n*-BuLi (20 mmol, 12.5 cm³ of a 1.6 M solution in hexane) was added drop wise at 0 °C under N₂ and the stirring was continued for 1 h. To the resulting yellow-red solution, Ph₂PCI (20 mmol, 4.41 g) was slowly added and the mixture was allowed to warm to r.t. and stirred overnight. The reaction mixture was treated with 10 cm³ H₂O. The organic phase was separated and the aqueous phase was extracted with EtOAc (3x25 cm³). The combined organic phase was dried over Na₂SO₄. After removal of the

solvent *in vacuo*, the residue was separated by column chromatography on silica gel with toluene/Et₃N (100:1) as eluent to give a yellow liquid (2.3 g, 58%). ³¹P NMR (121.5 MHz, CDCl₃) δ (ppm): - 16.02. ¹H NMR (300 MHz, CDCl₃) δ (ppm): 3.42 (s, 3H, N-CH₃), 6.69 (s, 1H, ⁴J_{HH}= 1.5 Hz, H1), 6.82 (dd, 1H, ³J_{HH}= 7.8 Hz, ⁴J_{HH}= 1.5 Hz, H3), 6.86 (d, 1H, ³J_{HH}= 8.1 Hz, H9), 6.97 (m, 2H, ⁴J_{HH}= 1.2 Hz, H6,8), 7.10 (d, 1H, ³J_{HH}= 7.8 Hz, H4); 7.20 (4H, d, ³J_{HH}= 6.3 Hz, H_{Ph}) 7.22 (1H, t, ³J_{HH}= 8.1 Hz, H7), 7.37-7.41 (6H, m, H_{Ph}). ¹³C NMR (75 MHz, CDCl₃) δ (ppm): 35.7, 114.1, 114.5, 122.4, 122.5, 123.7, 126.9, 127.2, 127.3, 127.5, 128.3, 128.5, 129.1, 132.6, 132.9, 145.8, 146.0. MS (EI⁺) m/z: 397 (M⁺, 100%), 382.

3-(diphenylphosphino)-10-methyl-10H-phenothiazine (2c)

To a stirred solution of 3-bromo-10-methyl-10H-phenothiazine (**1c**) (10 mmol, 2.92 g) in dry THF (120 cm³) *s*-BuLi (20.3 mmol, 15.6 cm³ of a 1.3 M solution in cyclohexane) was added drop wise at -78 °C under N₂ and the stirring was continued for 0.5 h. To the resulting yellow solution, Ph₂PCl (20.3 mmol, 4.48 g) was slowly added and the mixture was stirred for an additional 1h at -78 °C and then allowed to warm to r.t. overnight. The reaction mixture was treated with HCl solution (30 ml, 5%) and stirred at 0 °C for 0.5 h. The organic phase was separated and the aqueous phase was extracted with CH₂Cl₂ (3x25 cm³). The combined organic phase was dried over Na₂SO₄. After removal of the solvent *in vacuo*, the residue was separated by column chromatography on silicagel with hexane/Et₂O (19:1) as eluent to give yellow-white crystals (2.07 g, 52%) m.p.: 112.5 °C.

IR (ATR) ν [cm⁻¹]: 696, 748, 796, 818, 970, 1067, 1096, 1141, 1207, 1261, 1331, 1395, 1432, 1459, 1541, 1567, 2878, 2970, 3010, 3052. ³¹P NMR (121.5 MHz, CDCl₃) δ (ppm): - 6.92. ¹H NMR (400 MHz, CDCl₃) δ (ppm): 3.42 (s, 3H, N-CH₃), 6.78 (d, 1H, ³J_{HH}= 8.0 Hz, H₉), 6.80 (d, 1H, ³J_{HH}= 8.4 Hz, H1), 6.92 (t, 1H, ³J_{HH}= 7.6 Hz, H7), 7.06 (dd, 1H, ³J_{HH}= Hz, ³J_{HH}= Hz, H6), 7.10 (dd, 1H, ³J_{HH}= 1.2 Hz, H2); 7.14 (1H, s, H4), 7.17 (td, 1H, ³J_{HH}= 8.0 Hz, H8), 7.26-7.33 (10H, m, H_{Ph}). ¹³C NMR (75 MHz, CDCl₃) δ (ppm): 35.4, 114.2, 122.8, 123.1, 123.9, 127.3, 127.6, 128.7, 130.1, 132.2, 132.4, 133.6, 133.7, 133.9, 137.3, 145.4, 146.6. Anal. Calcd. For C₂₅H₂₀NPS (%): C, 75.54; H, 5.07; N, 3.52; S, 8.07. Found (%): C, 75.47; H, 5.04; N, 3.25; S, 8.07. MS (EI⁺) m/z: 397 (M⁺, 100%), 382, 320, 304, 289, 274, 212. The phosphine oxide was also detected MS (EI⁺) m/z: 413 (M⁺), 336, 201, 183.

3,7-bis(diphenylphosphino)-10-methyl-10H-phenothiazine (2d)

To a stirred solution of 3,7-dibromo-10-methyl-10H-phenothiazine (**1d**) (1.86 g, 5 mmol) in dry Et₂O (120 cm³) *n*-BuLi (20.4 mmol, 12.8 cm³ of a 1.6 M solution in hexane) was added drop wise at 0 °C under N₂ and the stirring was continued for 1 h. To the resulting yellow solution, Ph₂PCl (20.4 mmol, 4.5 g) was slowly added and the mixture was stirred for an additional 1 h at 0 °C and then allowed to warm to r.t. overnight. The reaction mixture was treated with H₂O (5 cm³). The organic phase was separated and the aqueous

phase was extracted with EtOAc (3x25 cm³). The combined organic phase was dried over Na₂SO₄. After removal of the solvent *in vacuo*, the residue was separated by column chromatography on silicagel with hexane/Et₂O (19:1) as eluent to give yellow crystals (1.3 g, 48%) m.p.: 140 °C. ³¹P NMR (121.5 MHz, CDCl₃) δ (ppm): - 6.92. ¹H NMR (400 MHz, CDCl₃) δ (ppm): 3.39 (s, 3H, N-CH₃), 7.07 (2H, dd, H2), 7.33 (2H, d, H1), 7.50 (2H, s, H4). ¹³C NMR (75 MHz, CDCl₃) δ (ppm): 35.4, 113.7, 114.95, 114.96, 116.3, 125.9, 128.3, 129.9, 130.0, 130.1, 132.2, 145.2. MS (EI⁺) m/z: 581 (M⁺, 100%), 566, 536, 506, 480, 424, 409, 381, 318.

General procedure for sulfonation of phosphine derivatives 2a and 2c.

Diphenylphosphino-10-methyl-10*H*-phenothiazine (0.2 g, 0.5 mol) was stirred with sulfuric acid (1 cm³) at rt. The solid slowly dissolved to give a red solution. After being stirred for 20 h the mixture was cooled to 0 °C and degassed water (8 mL) was added slowly. The mixture decolourised and a white precipitate was formed. The mixture was neutralised with 0.5 M aq NaOH to pH 7 and concentrated. The resulting white solid was extracted with ethyl acetate or methanol to give the product after evaporation of the solvent.

4-[(3-sodiumbenzenesulfonato)-phenyl-phosphino]-10-methyl-10*H*-phenothiazine 3.

The product was isolated after extraction with ethyl acetate and evaporation of the solvent as a green-white solid (0.2 g, 80%) m.p. 199 °C decomposition. IR (ATR) ν [cm⁻¹]: 692, 722, 744, 780, 1050, 1117, 1140, 1256, 1327, 1404, 1439, 1553, 1588, 2815, 2857, 2954, 3055. ³¹P NMR (121.5 MHz, CDCl₃) δ (ppm): - 13.38, oxidized product was also detected at 30.59. ¹H NMR (300 MHz, CDCl₃) δ (ppm): 3.40 (s, 3H, N-CH₃), 6.47 (ddd, 1H, ³J_{HH} = 7.5 Hz, ³J_{PH} = 3.3 Hz, ⁴J_{HH} = 0.9 Hz, H₃), 6.83 (d, 1H, ³J_{HH} = 8.1 Hz, H₉), 6.84 (d, 1H, ³J_{HH} = 7.5 Hz, H₁), 6.93 (td, 1H, ⁴J_{HH} = 0.9 Hz, H₂), 7.10 (t, 1H, ³J_{HH} = 7.8 Hz, H₇), 7.14-7.20 (m, 2H, H_{6,8}); 7.37-7.41 (9H, m, H_{Ph}). ¹³C NMR (75 MHz, CDCl₃): 35.7, 114.0, 114.1, 114.4, 122.6, 123.5, 126.8, 127.0, 127.2, 127.6, 128.5, 128.8, 129.0, 129.3, 132.0, 132.1, 134.0, 134.2, 135.8, 135.9, 136.0, 136.1, 146.1. MS (EI⁺) was not successful for the sodium salt due to low volatility of the compound and there were detected decomposition products with m/z: 490, 413, 397, 382, 286, 273, 242, 212, 183, 77.

3-[(3-sodiumbenzenesulfonato)-phenyl-phosphino]-10-methyl-10*H*-phenothiazine 4.

Sulfonation was performed according the general procedure presented above. The starting material 2c and the corresponding phosphine oxide were recovered by extraction with ethyl acetate. Extraction with methanol gave only traces of sulfonated product.

IR (ATR) ν [cm⁻¹]: 640, 695, 746, 814, 873, 1045, 1102, 1120, 1162, 1194, 1260, 1332, 1374, 1436, 1459, 1566, 1592, 2879, 2963, 3054.

ACKNOWLEDGEMENTS

We gratefully acknowledge financial support from Romanian Ministry of Education and Research, Grant CNCSIS PNII-RU-PD 416/2009.

REFERENCES

1. J.T. Sullivan, J. Sadula, B.E. Hanson, R.J. Rosso, *J. Molec. Catal. A: Chemical* **2004**, *214*, 213.
2. T. Katsuda, H. Ooshima, M. Azuma, J. Kato, *J Bioscience and Bioengineering*, **2006**, *102*, 3, 220.
3. T. Bartik, B. Bartik, T.E. Glass, W.R. Bebout, B.E. Hanson, *Inorg. Chem.* **1992**, *31*, 2667.
4. T. Thorpe, S.M. Brown, J. Crosby, S. Fitzjohn, J.P. Muxworthy, J.M.J. Williams, *Tetrahedron Lett.* **2000**, *41*, 4503.
5. F. Joo, J. Kovacs, A. Katho, A.C. Benyei, T. Decuir, D. J. Darensburg, In *Inorg. Synth.*; Darensbourg, M.Y., Ed., **1998**, *32*, pp. 1–8.
6. H. Gulyas, A. Szollosy, B.E. Hanson, J. Bakos, *Tetrahedron Letters* **2002**, *43*, 2543.
7. A.E. Sollewijn Gelpke, J.J.N. Veerman, M. Schreuder Goedheijt, P.C.J. Kamer, P.W.N.M. van Leeuwen, H. Hiemstra, *Tetrahedron*, **1999**, *55*, 6657.
8. I.A. Silberg, C. Bodea, "Advances in Heterocyclic Chemistry", **1968**, *9*, 430.
9. G.P. Sarmiento, G.Y. Moltrasio, A.G. Moglioni, *ARKIVOC* **2009** (vii) 33.
10. Wunderlich, H., Stark, A., *Pharmazie*, **1966**, *21*, 56.
11. M. Meneghin, US Patent, *5*, 109, 134, **1992**.
12. S. Ebdrup, *Synthesis*, **1998**, *8*, 1107.
13. S. Ebdrup, *J. Chem. Soc. Perkin Trans I.*, **1998**, 1147.
14. C. Bodea, M. Terdic, *Studii și Cercetări de Chimie București*, **1962**, *13*, 81.

MICROWAVES ASSSITED CYCLOADITION REACTIONS OF UNSATURATED PHENOTHIAZINE DERIVATIVES

EMESE GAL, LUIZA GĂINĂ, CASTELIA CRISTEA* AND LUMINIȚA SILAGHI-DUMITRESCU

ABSTRACT. Microwaves assisted azaDiels-Alder cycloaddition reactions using aromatic and heteroaromatic Schiff bases as heterodienes and 3,4-dihydro-2H-pyrene (DHP) as dienophile in the presence of iodine catalyst, afforded stable cycloaddition adducts, as well as their oxidation products. The structures of the new hexahydro-2H-pyrano[3,2-c]quinoline and 3-(3-hydroxypropyl)-quinoline derivatives were assigned based on spectroscopic methods (high resolution NMR and mass spectrometry).

Keywords: Phenothiazine, Ferrocene, aza-Diels-Alder cycloaddition, Schiff base, 3,4-dihydro-2H-pyrene.

INTRODUCTION

Many published papers, several books [1,2] and review articles [3,4] indicate the microwaves irradiation as an alternative technique for achieving almost all types of thermally induced reactions, including synthesis of heterocyclic compounds. Particularly efficient heating processes induced by the dielectric heating afford shorter reaction times and sometimes better yields or increased selectivities.

[4+2] Cycloaddition reaction is an extremely useful route to generate six-membered ring compounds with advanced stereocontrol [5,6]. The reaction proceeds under thermal conditions and application of high pressure, catalysts and solvent variation increase the reaction rate and selectivity [7,8]. Six member ring heterocycles (containing oxygen or nitrogen) may also be obtained by using the appropriate heterodienes or heterodienophiles. Tetrahydroquinoline derivatives were prepared by aza-Diels-Alder reactions based on [4+2] cycloaddition between *N*-arylimines (electron-poor azadiene) and electron-rich dienophiles. Among other catalysts employed in pyrano-quinoline derivatives preparation from imines and 3,4-dihydro-2H-pyrene, iodine was capable to reduce the reaction time and to increase the yields acting as a Lewis acid that coordinate to the nitrogen atom of the polar C=N bond [9,10].

* Babeş-Bolyai University, Faculty of Chemistry and Chemical Engineering, 11 Arany Janos str., RO-400028 Cluj-Napoca, Romania, castelia@chem.ubbcluj.ro

Our previous results regarding formal *aza*-Diels-Alder cycloaddition reactions between Schiff bases containing highly electron-donating phenothiazinyl- or ferrocenyl groups and 3,4-dihydro-2*H*-pyrane (DHP) in the presence of iodine catalyst, highlighted the formation of quinoline derivatives by a multistep reaction mechanism and a characteristic substituent-dependence for the subsequent transformation of the reaction adduct [11]. Depending on the substitution pattern of the N-phenyl group the reactions of phenothiazine-containing imines afforded 2*H*-pyrano[3,2-*c*]quinolines or 3-(3-hydroxypropyl)quinolines. Irrespectively of the electronic properties of the N-phenyl substituent the less reactive ferrocene-based imines were converted into quinoline products. The theoretical calculations allowed predicting reliable structure-reactivity relationships which must be taken into account when setting up procedures for related cycloaddition reactions.

In order to bring more experimental evidence for supporting these theoretical predictions regarding structure-reactivity relationships, three additional Schiff bases containing aryl, phenothiazinyl and respectively ferrocenyl units were employed as heterodienes in cycloaddition reactions performed under microwaves assisted conditions.

Schiff bases containing phenothiazine units can be obtained by the condensation of 10-alkyl-3-formylphenothiazine with aromatic amines [12], aromatic diamines or heteroaromatic amines [13]. Alternative precursors for such heterocyclic Schiff bases were N-alkyl-3-aminophenothiazine derivatives and benzaldehyde derivatives [14]. Schiff bases containing phenothiazine units appear as stable yellow solids with green-yellow fluorescence in solution [12].

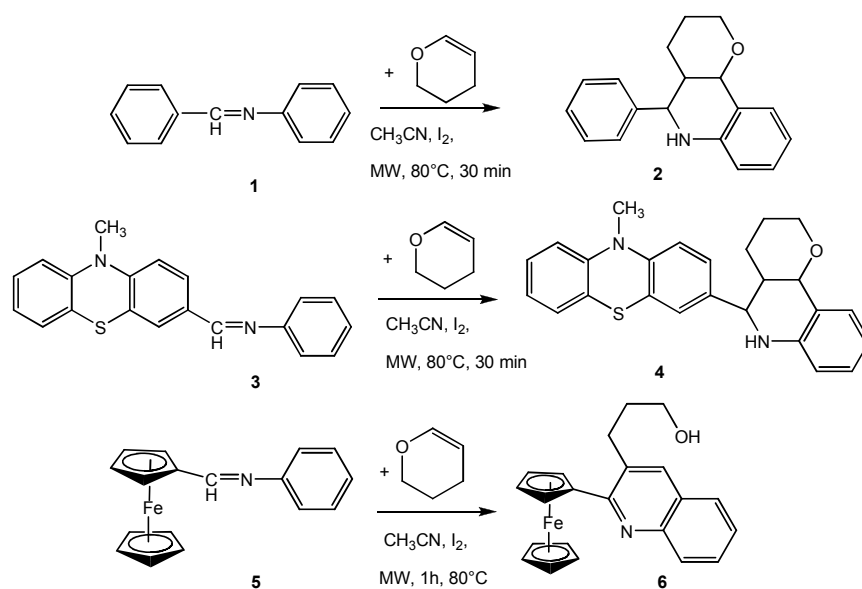
Schiff bases containing ferrocene units have been conventionally prepared by heating several hours under reflux a solution of ferrocenylcarbaldehyde and an aromatic amine in the presence of a polar solvent such as alcohol [15], a non-polar solvent such as toluene with azeotropic water removal [16] and under solvent free conditions [17] which gave the best yields. Microwave assisted synthesis in the presence of different dehydrating reagents such as zinc chloride, titanium chloride, molecular sieves, alumina [1], or using solvent free reaction conditions, greatly increased the reaction rate, prevented the formation of decomposition products and gave good reaction yields of ferrocenyl Schiff bases [18].

RESULTS AND DISCUSSION

Schiff bases **1**, **3** and **5** were prepared according to previously reported procedures by the condensation of the corresponding (hetero)aromatic aldehyde with aniline in ethanol under reflux. Thus, high yields of **1** were prepared starting with benzaldehyde, **3** was obtained from 10-methyl-10*H*phenothiazine-3-carbaldehyde [12] and **5** was obtained from ferrocenyl-carbaldehyde [17].

Schiff bases **1**, **3**, and **5** were tested as heterodienes in *aza*-Diels-Alder cycloaddition reactions. No cycloaddition adduct was obtained in reaction with cyclopentadiene dienophile, no matter what reaction conditions were employed: various catalysts (I_2 , KH_2PO_4 , $F_3C-COOH$, $pH_2N-C_6H_4-SO_3H$, or $FeCl_3$), classical heating, or microwave irradiation.

Good results were obtained when, in the presence of catalytic amounts of iodine, Schiff bases **1**, **3**, or **5** acted as electron poor azadienes in reaction with the electron rich dienophile 3,4-dihydro-2*H*-pyrane (DHP) leading to the formation of 2-phenyl-hexahydro-2*H*-pyrano[3,2-*c*]quinoline **2**, 2-(10-methyl-3-phenothiazinyl)-hexahydro-2*H*-pyrano[3,2-*c*]quinoline **4** and 2-ferrocenyl-3-(3-hydroxypropyl)quinoline **6** respectively (scheme 1).



Scheme 1

The syntheses were performed under microwaves irradiation using a CEM Discover Lab Mate microwave reactor equipped with temperature and power control. Several experimental conditions were tested in order to set up the optimal reaction parameters. The selected polar solvent was acetonitrile, which ensured an efficient dielectric heating of the reaction mixture. Unfortunately the cycloaddition reaction was accompanied by other thermally induced transformations of the sensitive Schiff base substrates and thus, the cycloaddition adducts could be isolated in 50-60% yields after 30-60 minutes reaction time (monitored by TLC). The cyclization of the less reactive ferrocenyl-Schiff base **3** required the longest reaction time. Nevertheless, the microwave assisted synthesis of these new quinoline derivatives **2**, **4** and **6** by microwave assisted

aza-Diels-Alder cycloaddition appears advantageous when taking into consideration green chemistry principles such as: atom economy, mild reaction conditions and energy saving.

Structural analysis of the cycloadducts was performed by high resolution NMR experiments which revealed the formation of stable 2-phenyl-hexahydro-2*H*-pyrano[3,2-*c*]quinoline **2** and 2-(10-methyl-3-phenothiazinyl)-hexahydro-2*H*-pyrano[3,2-*c*]quinoline **4** respectively. Analysis of the coupling pattern shown by the protons attached to the carbon atoms participating to the fused tetrahydropyran and tetrahydroquinoline rings, revealed a *cis* annelation of these heterocyclic rings. ¹H-NMR spectrum of 2-ferrocenyl-3-(3-hydroxypropyl)quinoline **6** indicate the presence of a 2,3-disubstituted quinoline unit by showing a deshielded signal (situated at 7.89 ppm) which may be assigned to the proton in position 4 of the heterocycle and of a propyl side chain indicated by the three signals situated in the aliphatic region of the spectrum (3.84, 3.25 and 2.01 ppm). Consequently, **6** was formed by the facile oxidation of the cycloaddition adduct, accompanied by the tetrahydropyran ring opening.

CONCLUSIONS

Under microwaves assisted conditions, Schiff bases containing aryl, 3-phenothiazinyl and respectively ferrocenyl units attached to the methine group, acted as heterodienes in azaDiels-Alder cycloaddition reactions in the presence of DHP filodiene and iodine catalyst, in acetonitrile solvent. The presence of rich π -electron moieties phenothiazinyl or ferrocenyl, decreases the reactivity of the Schiff bases as compared to the phenyl substituted one. Structural analysis performed by spectroscopic methods indicates the formation of stable cycloadducts containing phenyl- or phenothiazinyl substituents and the formation of highly unstable ferrocenyl substituted cycloadduct, which undergoes rapid aromatization in similar reaction conditions.

EXPERIMENTAL SECTION

FT-IR spectrometer Bruker Vector 22, 300 MHz NMR spectrometer Bruker, Shimadzu MS Spectrometer, Merck reagents were used.

General procedures for the microwaves assisted synthesis of Schiff bases

Carbalddehyde derivative (2.0 mmol) was dissolved in MeCN (4 mL) in a 10 ml microwave reaction vessel. The reaction mixture was sealed and subjected to microwave irradiation using 100 W power levels at 80°C for 30-60 min. After cooling the product was filtered and recrystallized from ethanol.

[(10-Methyl-10Hphenothiazin-3-yl)methylene]aniline (3)Dark brown oil, yield: 0.546 g, 83% IR: 2894, 1707, 1437, 1330, 1079 cm⁻¹.

¹H NMR, 300 MHz, CDCl₃: δ= 3.33 ppm (s, 3H, -CH₃); 7.60 ppm, (d, ³J= 7.8 Hz, 1H, H₂); 8.65 ppm, (s, 1H CH=N); 7.72 ppm, (s, 1H H₄); 7.21 ppm, (d, ³J= 8 Hz, 1H H₆); 6.97 ppm, (t, ³J= 8 Hz, 1H H₇); 7.26 ppm, (t, ³J= 8 Hz, 1H H₈); 6.75 ppm, (d, ³J= 8.4 Hz, 2H, H_{1,9}); 7.66 ppm, (m, 4H H_{2',3',5',6'}); 7.76 ppm, (d, ³J= 8.1 Hz, 1H); 7.73 ppm, (s, 1H); ¹³C NMR, CDCl₃ δ ppm: 35.6 (-CH₃), 126.7 (C₁), 129.4 (C₂), 130.3 (C₃), 161.3 (CH=N), δ= 129.3 (C₄), 123.7 (C_{5a}), 127.5 (C₆), 123.8 (C₇), 123.8 (C₈), 117.9 (C₉), 146.2 (C_{9a}), 148.6 (C_{10a}), 124.4 (C_{4a}) 151.4 (C_{1'}), 121.9 (C_{2',6'}), 130.8 (C_{3',5'}), 127.2 (C_{4'});

MS (EI, 70eV) m/z= 316 (100%) M⁺.**(Ferrocenylmethylene)aniline (5)**Dark brown oil yield: 0.453 g, 75% IR: 1620, 1435, 2956 cm⁻¹; ¹H

NMR 300 MHz, CDCl₃: δ=8.35 ppm (s, 1H, CH=N); 7.40 ppm (d, 2H, ³J=9 Hz H_{2,6}) 7.23 ppm (tr, 3H, J=7.5 Hz H_{3,4,5}) 4.83 ppm (s, 2H, H_{2',5'}); 4.51 ppm (s, 2H, H_{3',4'}), 4.27 ppm (s, 5H, Cp ring, Fc) ¹³C NMR δ 161.3, (CH=N), 152.7 (C₁), 129.1 (C_{3,5}), 125.1 (C₄), 120.6 (C_{2,6}), 80.3 (C_{1'}), 71.2 (C_{3',4'}), 69.2 (C_{2',5'}), MS (EI, 70eV) m/z= 302 (100%) M⁺.

General procedure for the microwaves assisted azaDiels-Alder cyclization of Schiff bases with 3,4-dihydro-2H-pyran(DHP)

To a solution of Schiff base (2.85 mmol) in 4 mL CH₃CN, 3,4-dihydro-2H-pyran (0.24 g, 2.85 mmol) and catalytic amounts of iodine were added. The resulting mixture was irradiated in the microwave reactor for 30 min. at 80°C using max. 100 W power levels. Water (15 mL) was added to the reaction mixture and then extraction with CH₂Cl₂ (3×10 mL) was performed. The organic layer was dried over anhydrous sodium sulfate and then filtered. After solvent evaporation to dryness, the crude product was obtained and it was further purified by column chromatography (using silicagel support and eluent CH₂Cl₂:MeOH 80:1) to afford the cycloadducts.

5-phenyl-3,4,4a,5,6,10b-hexahydro-2H-pyran[3,2-c]quinoline (2)Dark yellow oil; yield: 0.453 g, 60%; ¹H NMR 300 MHz, CDCl₃: δ= 4.33

ppm (s, 1H NH), 3.86 ppm (t, 1H H₂), 2.05 ppm (m, 1H, H₃), 4.57 ppm (d, 1H, J= 2.4 Hz H_{2p}), 1.65 ppm (m, 1H) H_{3a}, 6.86 ppm (1H, d, J=8.7 Hz) H₆, 6.66 ppm (1H, d, J=9.0 Hz) H₈, 7.19 ppm (1H, dd, J=9, 8.7 Hz) H₇, 7.34 ppm (3H, m) H_{2',4',6'}, 7.44 ppm (2H, m) H_{1',3'}, 3.65 ppm (1H, d, J=10 Hz, H_{2eq}), 3.47 (1H, dt, J=10, 2.1 Hz) H_{2ax}, 1.82 ppm (1H, q, J=11.2, 2.1 Hz) H_{3ax}, 1.40 ppm (1H, d, J=11.2 Hz) H_{3eq}, 1.70 ppm (1H, tt, J=11.2, 2.1 Hz) H_{4ax}, 1.55 ppm (1H, d, J=11.2 Hz) H_{4eq} ¹³C NMR δ 69.6 (C₆), 24.5 (C₅), 23.9 (C₄), 48.5 (C₃), 63.1 (C₂), 119.7 (C_{4a}), 128.1 (C₅), 120.5 (C₆), 126.3 (C₇), 110.3 (C₈), 144.9 (C_{8a}), 141 (C_{5'}), 129.8 (C_{6',4'}), 128.6 (C_{1',3'}), 126.5 (C_{2'}) MS (EI 70eV) m/z= 206 (100%), 265 (35%) M⁺.

5-(10-methyl-10Hphenothiazin-3-yl)-3,4,4a,5,6,10b-hexahydro-2H-pyrano[3,2-c]quinoline (4)

Dark brown oil; yield: 0.570 g, 50%; IR: 3376, 2932, 1546, 1464, 1331, 1256, 1083 cm^{-1} ; $^1\text{H NMR}$ 300 MHz, CDCl_3 : δ = 1.55 ppm (m, 1H, J =10.5 Hz, $\text{H}_{5\text{ax}}$), 1.65 ppm (m, 1H, J =10.6 Hz, $\text{H}_{4\text{ax}}$), 1.76 ppm (m, 1H, J =10.6 Hz) $\text{H}_{4\text{eq}}$, 1.90 ppm (m, 1H, J =10.5 Hz $\text{H}_{5\text{eq}}$), 2.59 ppm (m, 1H, J =2.5 Hz $\text{H}_{3\text{ax}}$), 3.40 ppm (s, 3H, N- CH_3), 3.65 ppm (d, 1H, J =11.5 Hz $\text{H}_{6\text{ax}}$), 3.89 ppm (d, 1H, J =2.5 Hz $\text{H}_{2\text{axp}}$); 4.10 ppm (d, 1H, J =11.5 Hz, $\text{H}_{6\text{eq}}$), 4.40 ppm (s, 1H NH), 6.84 ppm (d, 2H, J =8.5 Hz, $\text{H}_{1,9}$), 6.97 ppm (t, 1H, J =7.5 Hz H_7), 7.10 ppm (m, 4H $\text{H}_{5,6,7,8\text{Q}}$) 7.21 ppm (t, 1H, J =8.5 Hz), H_8 , 7.23 ppm (t, 1H, J =7.5 Hz H_6), 8.03 ppm (s, 1H H_4), 7.86 ppm (d, 1H, J =8.5 Hz, H_2), 7.99 ppm (dd, 1H, J =7.0 Hz, H_7), $^{13}\text{C NMR}$ δ 35.4 (CH_3), 113.7 ($\text{C}1'$), 114 ($\text{C}9'$), 127.2, 127.5, 126.5 ($\text{C}2'$, $\text{C}4'$, $\text{C}6'$), 122.5 ($\text{C}7'$), 128.3 ($\text{C}8'$), 125.3 ($\text{C}4'\text{a}$), 123.2 ($\text{C}5'\text{a}$), 61.9 ($\text{C}2\text{ch}$), 37.8 ($\text{C}3\text{ch}$), 69.6 ($\text{C}2\text{p}$), 119.7 ($\text{C}4\text{ach}$), 124.4 ($\text{C}5\text{ch}$), 126.7 ($\text{C}6\text{ch}$), 123.5 ($\text{C}7\text{ch}$), 114.5 ($\text{C}8$), 119.8 ($\text{C}8\text{a}$), 69.2 ($\text{C}2\text{p}$), 24.2 ($\text{C}5$), 69.05 ($\text{C}6$), 24.1 ($\text{C}4$), 38.7 ($\text{C}3$); MS (EI 70eV) m/z = 400 (100%) M^+ .

2-Ferrocenyl-3-(3-hydroxypropyl)quinoline (6)

Dark brown oil, 0.553 g, 58%; IR: 3139, 2998, 2935, 2832, 1721, 1291, 1038 cm^{-1} ; $^1\text{H NMR}$, 300 MHz, CDCl_3 δ = 2.01 (2H, t, J =7.2 Hz, - CH_2 -); 3.25 (2H, t, J =7.2 Hz, CH_2), 3.84 (2H, t, J =7.2 Hz, CH_2), 4.13 (5H, s, Cp ring, Fc), 4.43 (2H, s, $\text{H}3',4'$), 5.01 (2H, s, $\text{H}2',5'$), 7.46 (1H, d, J =7.5 Hz, H_7), 7.63 (1H, d, J =7.5 Hz, H_6), 7.72 (1H, d, J =7.5 Hz, H_5), 7.89 (1H, s, H_4), 8.05 (1H, d, J =8.4 Hz, H_8). $^{13}\text{C NMR}$ δ 158.7 ($\text{C}2$), 126.1 ($\text{C}6$), 146.9 ($\text{C}8\text{a}$), 133.7 ($\text{C}3$), 135.8 ($\text{C}4$), 129.2 ($\text{C}4\text{a}$), 129.0 ($\text{C}8$), 127.0 ($\text{C}7$), 127.2 ($\text{C}5$), 85.8 ($\text{C}1'$), 70.8 ($\text{C}3',4'$), 70.08 ($\text{C}2',5'$), 70.02 (Cp ring, Fc), 62.6 ($\text{C}11$), 34.2 ($\text{C}10$), 29.7 ($\text{C}9$); MS (EI 70eV) m/z = 371 (100%) M^+ , 340 (20%).

ACKNOWLEDGMENTS

Financial support from Romanian Ministry of Education Research and Innovation grant PN-II-ID-564 is greatly acknowledged.

REFERENCES

1. A. Loupy (Ed), "Microwaves in Organic Chemistry", Wiley-VCH Weinheim **2002**.
2. P. Lidstrom, J. P. Tierney (Eds), "Microwave-Assisted Organic Synthesis", Blackwell, Oxford, **2004**.
3. P. Lidstrom, J. Tierney, B. Wathey and J. Westman, *Tetrahedron* **2001**, *57*, 9225.
4. C. O. Kappe, *Angew. Chem.*, **2004**, *43*, 6250.

5. W. Carruters "Cycloaddition reactions in Organic Synthesis" Pergamon Press Oxford **1990**.
6. F. Fringuelli, A. Taticchi, "The Diels Alder Reaction. Selected practical methods" Wiley, Chichester, UK **2002**.
7. A. Kumar, *Chem Rev.*, **2001**, *101*, 1.
8. G. Metha, R. Uma. *Acc. Chem. Res.*, **2000**, *33*, 278.
9. Li Yun-Cheng, Zhang Jun-Min, Dong Li-Ting, *Chinese Journal of Chemistry*, **2006**, *24*, 929.
10. G. Jin, J. Zhao, J. Han, S. Zhu, J. Zhang, *Tetrahedron*, **2010**, *66*, 913.
11. E. Gál, C. Cristea, L. Silaghi-Dumitrescu, T. Lovász, A. Csámpai, *Tetrahedron* **2010**, *66* (52), 9938.
12. E. Gál, L. Găină, T. Lovász, C. Cristea, L. Silaghi-Dumitrescu *Studia Universitatis Babeş-Bolyai, Chemia*, **2009**, *4*, 17.
13. L. Gaina, T. Lovasz, I.A. Silberg, C. Cristea, S. Udrea, *Heterocycl. Commun.*, **2001**, *7*(6), 549.
14. V.A. Skorodumov, S.V. Zhuravlev, *Russian J. Org. Chem.*, **1965**, *2*(1), 363.
15. C. Imrie, P. Engelbrecht, C. Loubser, C.W. McClelland, V.O. Nyamori, R. Bogardi, D.C. Levendis, N. Tolom, J.L. van Rooyen, N. Williams, *J. Organomet. Chem.* **2002**, *65*, 645.
16. S.K. Pal, A. Krishnan, P.K. Das, A.G. Samuelson, *J. Organomet. Chem.*, **2000**, *604*, 248-259.
17. C. Imrie, V.O. Nyamori, T.I.A. Gerber, *J. Organomet. Chem.*, **2004**, *689*, 1617.
18. G. Öztürk, A. Petit, C. Kouklovsky, *Synthetic Communications*, **2008**, *38*, 2707.

PM6 MODELING OF ALPHA HELICAL POLYPEPTIDE STRUCTURES

ATTILA-ZSOLT KUN^a, ALEXANDRU LUPAN^a,
RADU SILAGHI-DUMITRESCU^a

ABSTRACT. This paper presents a computational study of an alpha-Gly₁₀ polypeptide (neutral and zwitterionic) using the PM6 semiempirical method and its variants implemented in Mopac2009 program. Statistical correlations with high level computational methods are discussed in all cases.

Keywords: glycine, alpha-helix, PM6, semiempirical calculation, optimization

INTRODUCTION

Computational study of proteins has been a challenging problem. This is due to their size and complex structure, based on weak interactions. High level computational methods such as “*ab initio*” and DFT are still computationally expensive although the computer evolution is tremendous. Less expensive approaches like molecular mechanics or the classical semiempirical methods, although easy in terms of computational effort, are not accurate enough in modeling large systems such as proteins [1].

The PM6 semiempirical method developed by Stewart [2] is a novel and more accurate among its class. It represents an update of the well-known NDDO method (core-core interactions and optimized parameters). Significant improvements of the predicted geometries as compared to the common AM1 and PM3 methods are also reported. In order to reduce the computational effort a new method of solving the self-consistent field equations has been proposed, namely Mozyme [3], which is a localized molecular orbital approach, much more efficient for large systems than the classical methods based on matrix algebra.

The Mopac2009 [4] implementation of the PM6 method and its augmented variants D2 and DH2 has been chosen here for studying a simple computationally-modeled Gly₁₀ polypeptide. The different optimization algorithms available in the program were tested to see their performance in energetic and structural terms. All calculations were done using the Mozyme SCF method specially designed for modeling large structures.

^a Babeş-Bolyai University, Faculty of Chemistry and Chemical Engineering, 11, Arany Janos Str., RO-400028 Cluj-Napoca, Romania, rsilaghi@chem.ubbcluj.ro; zak@chem.ubbcluj.ro

RESULTS AND DISCUSSIONS

The following tables show the different results obtained for the Gly₁₀ model (cf. Methods section). As seen in Table 1, for the Gly₁₀ neutral structure computed in vacuum the performance of the EF, EF-HESS1 and L-BFGS optimizers is roughly the same: the calculated heats of formation are roughly the same (within a difference of 1-2 kcal/mol), and the residual gradients of the optimized structures are low. The standard BFGS and DFP methods are giving poorer results in energy, with greater residual gradients. The change to precise optimization criteria has only little influence on the final energies.

Table 1. Heats of formation and residual gradients for the Gly₁₀ neutral form computed in vacuum. See also the Methods section

Model Hamiltonian	Optimization method	Normal calculation		Precise calculation		Δ energy
		Energy	Gradient	Energy	Gradient	
PM6	DFP	-468.581	55.38226	-476.200	24.74704	7.61849
PM6	EF	-483.601	1.26385	-484.186	0.75005	0.58480
PM6	EF-HESS1	-483.329	1.40090	-484.177	0.90926	0.84806
PM6	BFGS	-474.173	11.15584	-479.449	2.85466	5.27662
PM6	L-BFGS	-481.251	1.59716	-483.699	1.42570	2.44824
PM6-D2	DFP	-495.630	11.49224	-499.523	2.64713	3.89263
PM6-D2	EF	-504.138	1.52330	-505.804	0.94282	1.70246
PM6-D2	EF-HESS1	-504.145	1.53369	-505.745	0.76028	1.60008
PM6-D2	BFGS	-498.226	6.71154	-499.428	2.85579	1.20209
PM6-D2	L-BFGS	-504.099	1.57670	-504.742	2.02749	0.64335
PM6-DH2	DFP	-497.731	10.27741	-503.475	4.02141	5.74371
PM6-DH2	EF	-508.041	3.05565	-507.973	4.31984	-0.06739
PM6-DH2	EF-HESS1	-508.358	1.63295	-507.911	6.62062	-0.44659
PM6-DH2	BFGS	-500.591	14.10671	-500.801	15.08551	0.20989
PM6-DH2	L-BFGS	-507.982	1.52834	-509.030	5.44155	1.04775

For the Gly₁₀ neutral structure computed in vacuum the PM6 BFGS optimization method gives the correlation values closest to the M062X simulation with average bond differences of (0.3-0.4 Å). PM6-D2 DFP lays also in the same area of precision. Both PM6-D2 BFGS variants have a correlation coefficient of less than 0.9 but globally all four BFGS methods are in top five in terms of these comparisons. All the PM6-DH2 methods fail in terms of correlation coefficients and the maximum and average differences are greater.

PM6 MODELING OF ALPHA HELICAL POLYPEPTIDE STRUCTURES

Table 2. CO...NH hydrogen bond lengths and helix lengths for the Gly₁₀ neutral model form computed in vacuum. The order is from the N-terminal ending of the polypeptide chain. See also the Methods section for details

Neutral vacuum	1-5	2-6	3-7	4-8	5-9	6-10	CO...NH avg	Helix length	Correl	Max Dif	Avg Dif
Reference	2.51	2.13	2.15	2.23	2.68	3.08	2.46	14.90	-	-	-
PM6 DFP	1.85	2.01	1.95	1.90	1.92	2.17	1.97	14.10	0.55	0.91	0.50
PM6 DFP pr	1.97	1.99	2.10	1.99	2.06	2.30	2.07	14.33	0.74	0.78	0.40
PM6 EF	2.26	2.02	2.13	2.08	2.09	2.10	2.11	14.36	0.18	0.98	0.35
PM6 EF pr	1.97	1.99	2.10	1.99	2.06	2.30	2.07	14.33	0.74	0.78	0.40
PM6 EF HESS1	2.14	2.01	2.26	2.19	2.12	2.10	2.14	14.44	-0.22	0.98	0.36
PM6 EF HESS1 pr	2.27	2.04	2.07	2.05	2.07	2.21	2.12	13.77	0.61	0.87	0.35
PM6 BFGS	2.04	1.99	2.01	2.03	2.04	2.07	2.03	14.51	0.91	1.01	0.43
PM6 BFGS pr	2.13	2.06	2.10	2.09	2.20	2.37	2.16	14.79	0.97	0.71	0.31
PM6 L-BFGS	2.32	2.70	2.10	2.15	2.16	2.10	2.26	14.73	-0.44	0.98	0.40
PM6 L- BFGS pr	2.36	2.06	2.07	2.08	2.09	2.12	2.13	14.28	0.23	0.96	0.33
PM6 D2 DFP	1.90	1.97	2.01	1.97	2.02	2.17	2.01	14.24	0.70	0.91	0.46
PM6 D2 DFP pr	2.04	2.01	2.06	2.04	2.13	2.25	2.09	14.61	0.92	0.83	0.38
PM6 D2 EF	2.13	1.99	2.16	2.11	2.02	2.06	2.08	14.39	-0.20	1.02	0.39
PM6 D2 EF pr	2.28	1.99	2.04	2.03	1.96	2.72	2.17	12.94	0.79	0.72	0.29
PM6 D2 EF HESS1	2.12	2.00	2.17	2.10	2.00	2.09	2.08	14.26	-0.12	0.99	0.39
PM6 D2 EF pr HS1	2.36	1.99	2.01	2.37	1.95	2.74	2.24	12.97	0.65	0.73	0.27
PM6 D2 BFGS	1.98	1.98	2.07	2.03	2.11	2.42	2.10	14.41	0.84	0.66	0.37
PM6 D2 BFGS pr	2.04	2.00	2.05	2.01	2.10	2.41	2.10	14.55	0.89	0.67	0.36
PM6 D2 L-BFGS	2.17	1.99	2.18	2.10	2.02	2.06	2.09	14.32	-0.19	1.02	0.39
D2 L-BFGS pr	2.20	2.03	2.06	2.04	2.02	2.16	2.09	13.83	0.53	0.92	0.38
PM6 DH2 DFP	1.87	1.95	1.98	1.91	1.97	2.09	1.96	14.19	0.62	0.99	0.50
PM6 DH2 DFP pr	2.01	2.01	2.09	2.05	2.09	2.17	2.07	14.58	0.72	0.91	0.39
PM6 DH2 EF	2.09	2.02	2.33	2.18	2.00	2.03	2.11	14.53	-0.55	1.05	0.42
PM6 EF pr	2.11	2.02	2.32	2.22	2.00	2.04	2.12	14.55	-0.54	1.04	0.40
PM6 EF HESS1	2.11	1.99	2.29	2.18	2.03	2.03	2.11	14.47	-0.47	1.05	0.41
PM6 EF HESS1 pr	2.13	1.99	2.25	2.23	2.03	1.99	2.10	14.49	-0.56	1.09	0.39
PM6 DH2 BFGS	1.89	2.03	2.12	2.00	2.11	2.28	2.07	14.26	0.59	0.80	0.39
PM6 DH2 BFGS pr	1.90	2.04	2.12	2.00	2.12	2.32	2.08	14.27	0.63	0.76	0.38
PM6 DH2 L-BFGS	2.11	2.01	2.32	2.22	2.00	2.04	2.12	14.49	-0.52	1.04	0.40
PM6DH2L-BFGS pr	2.13	2.03	2.20	2.12	2.04	2.03	2.09	14.18	-0.52	1.05	0.39

On optimizing the Gly₁₀ neutral structure in water (Table 3.) the clear winner is the L-BFGS method, producing the best energies and residual gradients in all of the cases. The DFP optimizer is generally still the worst, producing poor energies and great residual gradients, but for the PM6-D2 Hamiltonian equals the other methods (in this case all the energies lie in a 2-3 kcal/mol interval). The use of precise optimization criteria does not influence severely the results, except for the PM6-DH2 Hamiltonian, where the energies are rising and the residual gradients are greater in this case. This can be the effect of the known limitation of the gradient calculation in current implementation:

the optimized geometry is not the exact minimum of PM6-DH2 energy. This can be ignored for weak H-bonds, but for many strong H-bonds as in a peptide may be a serious problem.

Table 3. Heats of formation and residual gradients for the Gly₁₀ neutral form computed in water. See also the Methods section

Model Hamiltonian	Optimization method	Normal calculation		Precise calculation		Δ energy
		Energy	Gradient	Energy	Gradient	
PM6	DFP	-535.427	50.61209	-535.734	61.14301	0.30768
PM6	EF	-540.011	6.54133	-540.014	13.14678	0.00287
PM6	EF-HESS1	-541.551	2.24855	-541.631	3.81095	0.08057
PM6	BFGS	-535.405	13.40674	-541.603	15.13316	6.19708
PM6	L-BFGS	-544.179	2.74499	-543.992	1.19717	-0.18779
PM6-D2	DFP	-559.642	8.42636	-560.376	8.87667	0.73325
PM6-D2	EF	-561.384	3.31497	-559.319	6.49577	-2.06447
PM6-D2	EF-HESS1	-560.526	5.35116	-561.698	3.35221	1.17194
PM6-D2	BFGS	-560.720	11.71167	-561.088	22.12513	0.36771
PM6-D2	L-BFGS	-563.167	2.08386	-562.861	1.25650	-0.30570
PM6-DH2	DFP	-565.760	14.20699	-565.226	27.70459	-0.53395
PM6-DH2	EF	-565.534	4.56001	-561.237	7.24253	-4.29728
PM6-DH2	EF-HESS1	-567.081	5.46998	-566.310	12.93433	-0.77113
PM6-DH2	BFGS	-558.271	32.45811	-565.573	32.06091	7.30236
PM6-DH2	L-BFGS	-574.409	1.51347	-570.567	2.23486	-3.84207

Table 4. CO...NH hydrogen bond lengths and helix lengths for the Gly₁₀ neutral model computed in water. The order is from the N-terminal ending of the polypeptide chain. See also the Methods section for details.

Neutral water	1-5	2-6	3-7	4-8	5-9	6-10	CO...NH avg	Helix length	Correl	Max Dif	Avg Dif
Reference	2.12	1.97	2.02	1.99	2.11	2.26	2.08	14.61	-	-	-
PM6 DFP	1.82	1.91	1.95	1.92	1.87	1.96	1.91	14.10	0.03	0.30	0.17
PM6 DFP pr	1.84	2.00	2.03	1.96	1.90	2.00	1.96	14.13	-0.21	0.28	0.14
PM6 Ef	1.90	1.95	1.98	1.96	1.98	2.05	1.97	14.30	0.54	0.22	0.11
PM6 EF pr	1.89	1.94	1.98	1.96	1.98	2.04	1.97	14.29	0.49	0.23	0.11
PM6 EF HESS1	1.98	1.94	2.00	1.96	2.01	2.04	1.99	14.50	0.86	0.22	0.09
PM6 EF HESS1 pr	1.94	1.96	1.97	1.96	2.01	2.09	1.99	14.46	0.80	0.18	0.09
PM6 BFGS	1.90	1.86	1.89	1.93	1.91	1.98	1.91	14.22	0.78	0.28	0.17
PM6 BFGS pr	1.98	1.97	2.01	2.00	2.02	2.15	2.02	14.45	0.84	0.14	0.06
PM6 L-BFGS	2.09	1.98	1.98	2.04	2.00	2.07	2.03	14.71	0.64	0.19	0.07
PM6 L-BFGS pr	2.03	1.94	1.98	1.99	1.96	1.96	1.98	14.30	0.07	0.30	0.10
PM6 D2 DFP	1.82	1.90	1.97	1.92	1.89	2.00	1.92	14.10	0.25	0.30	0.16
PM6 D2 DFP pr	1.84	1.90	1.94	1.94	1.93	2.00	1.93	14.13	0.38	0.28	0.15
PM6 D2 EF	1.90	1.93	1.97	1.95	1.96	2.04	1.96	14.30	0.61	0.22	0.12

PM6 MODELING OF ALPHA HELICAL POLYPEPTIDE STRUCTURES

Neutral water	1-5	2-6	3-7	4-8	5-9	6-10	CO...NH avg	Helix length	Correl	Max Dif	Avg Dif
PM6 D2 EF pr	1.87	1.90	1.93	1.92	1.93	1.98	1.92	14.23	0.54	0.28	0.16
PM6 D2 EF HESS1	1.90	1.90	1.95	1.93	1.95	1.97	1.93	14.37	0.56	0.29	0.15
PM6 D2 EF HS1 pr	1.92	1.93	1.95	1.93	1.97	2.04	1.96	14.37	0.81	0.22	0.12
PM6 D2 BFGS	1.83	1.93	2.00	1.96	1.93	2.03	1.95	14.14	0.19	0.29	0.13
PM6 D2 BFGS pr	1.85	1.92	1.98	1.96	1.94	2.03	1.95	14.16	0.33	0.27	0.13
PM6 D2 L-BFGS	1.99	1.92	1.94	1.93	1.99	2.12	1.98	14.49	0.98	0.14	0.10
PM6 D2 L-BFGS pr	1.97	1.91	1.94	1.93	2.00	2.15	1.98	14.50	0.96	0.15	0.10
PM6 DH2 DFP	1.82	1.86	1.99	1.92	1.90	1.97	1.91	14.16	0.19	0.30	0.17
PM6 DH2 DFP pr	1.81	1.85	1.95	1.87	1.88	1.97	1.89	14.14	0.41	0.31	0.19
PM6 DH2 EF	1.86	1.88	1.91	1.90	1.90	1.93	1.90	14.27	0.41	0.33	0.18
PM6 DH2 EF pr	1.82	1.82	1.84	1.84	1.84	1.86	1.84	14.15	0.61	0.40	0.24
PM6 DH2 EF HESS1	1.94	1.89	1.98	1.93	1.94	1.97	1.94	14.51	0.55	0.29	0.14
PM6 DH2 EF pr HS1	1.88	1.86	1.95	1.90	1.91	1.93	1.91	14.40	0.36	0.33	0.17
PM6 DH2 BFGS	1.76	1.81	1.86	1.82	1.81	1.85	1.82	14.02	0.07	0.41	0.26
PM6 DH2 BFGS pr	1.84	1.80	1.98	1.93	1.88	1.96	1.90	14.12	0.30	0.30	0.18
PM6 DH2 L-BFGS	1.96	1.96	1.95	1.98	2.03	1.84	1.95	13.77	-0.61	0.42	0.13
PM6 DH2 L-BFGS pr	1.93	1.91	1.99	2.03	1.98	1.97	1.97	14.55	-0.06	0.29	0.12

When passing to the neutral Gly₁₀ computed in water we notice that the correlations of the values as compared to the DFT computation are even better for the differences but worse for the correlation coefficient. The average of maximum difference for all methods is 0.27Å with a maximum of 0.42, and once again we notice the worst results for PM6-DH2 class. The two PM6-D2 L-BFGS variants stand the most precise of all, the best one with a correlation coefficient of 0.98, maximum difference of 0.14Å and average difference of 0.1Å.

Gly₁₀ zwitterionic structure optimized in vacuum (Table 5.) is a highly unrealistic situation. Albeit the DFP optimizer still gives the highest energies and greatest residual gradients. The EF variants and the L-BFGS are producing better energies and gradients – but sometimes locating different minima on the potential energy surface, not the initial α -helix. As the geometries are changing, the difference between normal and precise calculations is great.

Table 5. Heats of formation and residual gradients for the Gly₁₀ zwitterionic form computed in vacuum. See also the Methods section for details

Model Hamiltonian	Optimization method	Normal calculation		Precise calculation		Δ energy
		Energy	Gradient	Energy	Gradient	
PM6	BFGS	-328.555	16.25501	-478.472	2.10161	149.9168
PM6	DFP	-320.047	31.29806	-332.729	46.93261	12.68219
PM6	EF	-460.921	1.61288	-505.141	1.06650	44.22029
PM6	EF-HESS1	-471.336	1.71480	-460.808	1.34189	-10.52790
PM6	L-BFGS	-464.872	1.57470	-491.120	1.97629	26.24755
PM6-D2	BFGS	-371.332	22.11510	-493.162	5.88488	121.82980
PM6-D2	DFP	-362.805	12.16014	-463.076	12.07646	100.27150

Model Hamiltonian	Optimization method	Normal calculation		Precise calculation		Δ energy
		Energy	Gradient	Energy	Gradient	
PM6-D2	EF	-466.328	2.08065	-504.396	1.04559	38.06803
PM6-D2	EF-HESS1	-484.981	1.68821	-526.832	1.07549	41.85040
PM6-D2	L-BFGS	-455.669	1.61520	-507.447	1.20085	51.77824
PM6-DH2	BFGS	-382.392	9.40206	-383.229	5.57377	0.83670
PM6-DH2	DFP	-366.183	23.50733	-378.312	12.72887	12.12884
PM6-DH2	EF	-465.014	3.94958	-373.395	4.83304	-91.61840
PM6-DH2	EF-HESS1	-398.738	5.90495	-429.697	7.28087	30.95856
PM6-DH2	L-BFGS	-478.451	1.92075	-521.345	1.29656	42.89381

When performing the computations on the zwitterionic model in vacuum most of the methods fail so that table 6 presents only those methods that succeeded in maintaining the alpha helix. This is not surprising as for the reference density functional calculation in these conditions the alpha-helix is not stable. Even for the neutral form computed in vacuum the variation of helix length among all the options tested shows the imperfections of such approach. For all the options tested with a solvent model the geometry is more regular and the maximum deviation of helix length is less than 0.6Å.

Table 6. CO...NH hydrogen bond lengths and helix lengths for the Gly₁₀ zwitterion model computed in vacuum. The order is from the N-terminal ending of the polypeptide chain

Zwitterion vacuum	1-5	2-6	3-7	4-8	5-9	6-10	(CO...NH) _{av} _g	Helix length
DFP	1.94	1.98	1.98	2.06	2.11	2.43	2.08	14.19
DFP pr	2.09	1.97	2.35	2.39	2.31	2.71	2.30	14.37
BFGS	2.02	1.96	2.14	2.12	2.23	2.75	2.20	14.32
D2 DFP	2.25	2.03	2.23	2.39	2.55	3.18	2.44	14.66
D2 BFGS	2.73	2.22	3.22	3.09	3.85	5.07	3.36	15.12
DH2 DFP	2.25	2.05	2.21	2.36	2.57	3.42	2.48	14.73
DH2 DFP pr	2.68	2.12	2.14	2.83	3.33	3.69	2.80	15.33
DH2 EF pr	2.55	2.15	2.18	2.59	3.22	3.65	2.72	15.32
DH2 BFGS	2.81	2.14	2.99	2.82	3.60	5.31	3.28	15.49
DH2 BFGS pr	2.76	2.21	3.59	2.69	3.92	4.70	3.31	15.55

As in case of optimizing Gly₁₀ neutral structure in water, in case of the zwitterionic form in water (Table 7.), the L-BFGS optimizer produces the best results: lowest energies (in all cases) and smallest residual gradients (excepting one case). Surprisingly in this table, the standard EF method gives the worst results (excepting one case), and the DFP optimizer performs better, but still producing great residual gradients. The EF-HESS1 variant and the BFGS methods are producing intermediate results disputing the second place, with the latter giving generally greater residual gradients. The differences between normal and precise optimization criteria calculations are small - a few kcal/mol.

PM6 MODELING OF ALPHA HELICAL POLYPEPTIDE STRUCTURES

Table 7. Heats of formation and residual gradients for the Gly₁₀ zwitterionic form computed in water. See also the Methods section

Model Hamiltonian	Optimization method	Normal calculation		Precise calculation		Δ energy
		Energy	Gradient	Energy	Gradient	
PM6	BFGS	-554.153	6.84385	-551.934	30.19219	-2.21933
PM6	DFP	-547.085	39.02397	-551.908	15.07784	4.82284
PM6	EF	-539.728	11.73500	-539.541	11.36281	-0.18665
PM6	EF-HESS1	-551.387	11.60122	-552.919	10.75917	1.53230
PM6	L-BFGS	-557.027	2.26565	-557.941	2.01639	0.91368
PM6-D2	BFGS	-574.565	8.82374	-573.498	27.91870	-1.06748
PM6-D2	DFP	-571.552	12.20055	-566.640	27.55250	-4.91186
PM6-D2	EF	-561.899	15.35613	-561.669	11.35523	-0.22992
PM6-D2	EF-HESS1	-571.262	5.42663	-572.221	4.37181	0.95881
PM6-D2	L-BFGS	-578.515	2.10795	-577.025	3.96587	-1.48974
PM6-DH2	BFGS	-572.623	20.20676	-577.505	28.83444	4.88212
PM6-DH2	DFP	-575.463	16.35665	-574.727	29.94503	-0.73570
PM6-DH2	EF	-577.901	3.70453	-574.184	5.51010	-3.71653
PM6-DH2	EF-HESS1	-578.140	6.15222	-579.308	2.57518	1.16867
PM6-DH2	L-BFGS	-582.775	1.43065	-582.618	8.31848	-0.15647

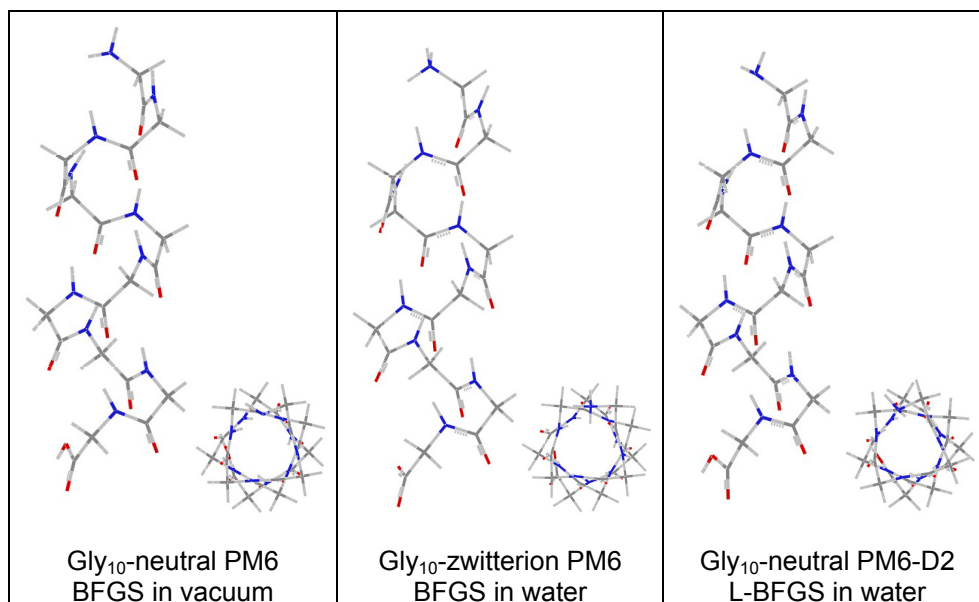


Figure1. Optimized structures of the best correlated optimized structures.

Table 8. CO...NH hydrogen bond lengths and helix lengths for the Gly₁₀ zwitterion model computed in water. The order is from the N-terminal ending of the polypeptide chain. See also the Methods section

Zwitterion water	1-5	2-6	3-7	4-8	5-9	6-10	CO...NH avg	Helix length	Correl	Max Dif	Avg Dif
Reference	2.25	2.04	2.02	2.01	2.28	2.65	2.21	14.85	-	-	-
PM6 DFP	1.87	1.87	1.99	1.89	1.97	1.98	1.93	14.15	0.41	0.67	0.28
PM6 DFP-pr	1.92	1.91	1.96	1.96	1.99	2.11	1.98	14.26	0.84	0.54	0.23
PM6 ef	1.84	1.83	1.84	1.85	1.85	1.89	1.85	14.12	0.87	0.76	0.36
PM6 EF pr	1.83	1.83	1.84	1.84	1.84	1.88	1.84	14.11	0.82	0.77	0.37
PM6 EF HESS1	1.97	1.91	1.98	1.98	1.95	2.08	1.98	14.42	0.77	0.57	0.23
PM6 EF pr HS1	1.99	1.92	1.96	1.97	1.98	2.06	1.98	14.40	0.91	0.59	0.23
PM6 BFGS	2.04	1.90	1.94	1.97	2.05	2.11	2.00	14.41	0.91	0.54	0.21
PM6 BFGS pr	1.94	1.91	1.98	1.97	1.99	2.08	1.98	14.28	0.80	0.57	0.23
PM6 L-BFGS	2.15	2.00	2.00	2.09	2.00	2.07	2.05	14.60	0.25	0.58	0.18
PM6 L-BFGS pr	2.12	1.92	2.05	2.04	1.95	3.04	2.19	12.06	0.87	0.39	0.17
PM6 D2 DFP	1.87	1.89	1.96	1.94	1.95	2.05	1.94	14.19	0.65	0.60	0.27
PM6 D2 DFP pr	1.84	1.89	1.94	1.90	1.86	1.94	1.90	14.09	0.13	0.71	0.31
PM6 D2 EF	1.83	1.83	1.84	1.85	1.84	1.89	1.85	14.11	0.77	0.76	0.36
PM6 D2 EF pr	1.83	1.82	1.84	1.84	1.84	1.88	1.84	14.11	0.82	0.77	0.37
PM6 D2 EF HESS1	1.95	1.90	1.97	1.96	1.92	2.08	1.96	14.40	0.75	0.57	0.25
PM6 D2 EF HS1 pr	1.95	1.93	1.91	1.92	1.96	2.10	1.96	14.36	0.97	0.55	0.25
PM6 D2 BFGS	2.03	1.86	1.90	1.96	2.03	2.07	1.98	14.35	0.83	0.58	0.23
PM6 D2 BFGS pr	1.95	1.89	1.96	1.97	2.00	2.09	1.98	14.29	0.85	0.56	0.23
PM6 D2 L-BFGS	2.02	1.95	2.01	2.03	1.90	1.96	1.98	14.20	-0.38	0.69	0.24
PM6 D2 L-BFGS pr	2.06	1.94	1.95	2.00	1.98	2.03	1.99	14.44	0.59	0.62	0.22
PM6 DH2 DFP	1.86	1.81	1.95	1.89	1.88	2.01	1.90	14.18	0.61	0.64	0.31
PM6 DH2 DFP pr	1.85	1.83	1.93	1.88	1.87	1.98	1.89	14.15	0.60	0.67	0.32
PM6 DH2 EF	1.95	1.90	1.92	1.92	1.93	2.03	1.94	14.40	0.94	0.62	0.27
PM6 DH2 EF pr	1.88	1.86	1.87	1.88	1.88	1.94	1.89	14.24	0.91	0.71	0.32
PM6 DH2 EF h1	1.98	1.90	1.94	1.92	1.94	2.02	1.95	14.50	0.89	0.63	0.26
PM6 DH2 EF pr h1	2.02	1.96	1.93	1.92	1.99	2.03	1.98	14.58	0.87	0.62	0.23
PM6 DH2 BFGS	1.92	1.83	1.83	1.88	1.86	1.98	1.88	14.20	0.87	0.67	0.33
PM6 DH2 BFGS pr	1.92	1.84	1.96	1.93	1.94	2.00	1.93	14.23	0.62	0.65	0.28
PM6 DH2 L-BFGS	2.08	1.90	1.97	2.05	2.02	1.98	2.00	14.66	0.11	0.67	0.22
PM6 DH2 L-BFGS pr	2.09	1.90	1.97	2.06	2.02	1.99	2.01	14.68	0.14	0.66	0.22

Table 8 summarizes the hydrogen bond lengths for the zwitterion species computed in water. We already notice that the precision as compared to the reference is better, the maximum hydrogen bond differences do not exceed 0.8Å with an average of just 0.6 while the average lies at 0.2 (never less than 0.21 or more than 0.37). The correlation coefficient would then be the only mean of discerning among methods although just correlating the computed values may not be a perfect criterion.

CONCLUSIONS

A complete study of PM6 semiempirical optimization of alpha-Gly₁₀ has been achieved in this paper. All the optimization methods available in Mopac2009 have been tested in all the possible situations (neutral and zwitterionic model in vacuum and in water). Most of the methods fail to model amfionic form in

vacuum while the neutral form results are still bad. For the calculations in water the neutral model gives correlation values better than the amfionic form. Classical PM6 approach results are comparable with the PM6-D2 class while PM6-DH2 methods are not performing well in this case. The PM6-D2 Hamiltonian and CPCM continuous solvent model (water) using L-BFGS optimization method with standard convergence criteria gives the best correlation as compared to a high level DFT optimization of the same structure.

METHODS - COMPUTATIONAL OPTIONS

The alpha-helical model of Gly₁₀ was built with the Spartan [5] program using the standard torsion angles. The model was either neutral (i.e. with the N- and C- terminal endings capped with hydrogen atoms to obtain -NH₂ or -COOH) or maintained as zwitterion (-COO⁻ and -NH₃⁺ respectively). The characteristic of an alpha-helix is the regularity imposed by the hydrogen bonds formed between CO and NH groups of different peptide bonds. Tables throughout manuscript show hydrogen bond lengths ordered starting from the N-terminal end. Geometry optimizations were performed either in vacuum or with a continuum solvent model (water). A high level computation (M062X/6-31G** [6] performed with Gaussian 09 [7]) is taken as reference geometry for statistical comparisons.

Tables depict for each optimization method the energy and the gradient for the normal and the precise calculation and the energy difference between these two is presented in the last column. All the CO...NH bond lengths are also presented as tables followed by detailed statistical analysis including:

- the average value of the six CO..NH bonds determining the alpha-helix.
- the length of the helix (measured each time between the C atom neighbouring the N-terminal end and the C atom neighbour to the C-terminal end).
- the correlation coefficient between the computed values and the reference (dft calculation) values computed by the statistical formula

$$Correl(x_{ref}, x_{calc}) = \frac{\sum (x_{ref} - \bar{x}_{ref})(x_{calc} - \bar{x}_{calc})}{\sqrt{\sum (x_{ref} - \bar{x}_{ref})^2 \sum (x_{calc} - \bar{x}_{calc})^2}}$$

- the maximum difference, i.e. the value representing the maximal difference between each computed alpha-helical H bond and the corresponding H bond of the reference structure.
- the average difference, i.e. the difference between the average alpha-helical H bond values of each optimization and the average of the corresponding reference structure.

Mopac2009 has implemented many methods, optimization algorithms and optional facilities designed to deal with a variety of systems.

Beside the basic PM6 method the Mopac2009 program has also two improved versions of this model Hamiltonian: PM6-D2 (augmented for dispersion interactions) and PM6-DH2 (augmented for dispersion and H-bond interactions) [8,9] which are parameterized to reproduce interaction energies for geometries obtained from high-level quantum mechanical calculations.

Five different geometry optimization algorithm variants present in Mopac2009 were tested. All geometry optimizations were done in Cartesian coordinates, as the system involves several big rings formed by hydrogen bonds, as using internal coordinates is often difficult in such cases. All energies (heat of formation, kcal/mol) and gradients (kcal/mol.Å) were recalculated in final single-point runs to prevent their alteration due to degradation of the wave function during optimization.

The default geometry optimizer in Mopac2009 is Baker's eigenvector following method [10]. Its performance was tested using the default starting Hess matrix (EF) and a calculated Hessian for the starting geometry (EF-HESS1). The full Hess matrix is constructed using single-sided derivatives, thus the calculation may be computationally prohibitive.

The Davidon-Fletcher-Powell (DFP) algorithm [11,12] was the first quasi-Newton generalized secant method implemented in Mopac. This method is superseded now by the Broyden-Fletcher-Goldfarb-Shanno (BFGS) procedure [13-16].

An advanced variant of the BFGS optimizer is the "Limited memory BFGS" function minimizer, which does not store the inverse Hessian, but instead calculates it as needed [17-19]. Because of this, the L-BFGS method uses very little storage, and is therefore suitable for optimizing very large systems. It is not as efficient as the other optimizers, but for large systems, it is often the only method that can be used. The Mopac2009 implementation (L-BFGS) is really the L-BFGS-B method, a variant which can handle box-constraints on the variables [20].

Different sets of calculations with normal and increased (PRECISE) convergence criteria were performed to estimate the usefulness of this computationally more demanding variant.

The structures were modeled in vacuum and in water, using the conductor-like screening model [21] as implemented in the program, using the dielectric constant of water 78.39 and solvent radius of 1.3 Å.

ACKNOWLEDGEMENTS

This work is supported by the Romanian Ministry for Education and Research (grant PCCE 312/2008).

The theoretical calculations are carried out using the resources of the Center for Molecular Modelling and Computational Quantum Chemistry acquired through a "Capacitati" program (Romanian Ministry for Education and Research, 130/14.09.2007).

REFERENCES

1. J.J.P. Stewart, *J. Mol. Model.*, **2009**, *15*, 765.
2. J.J.P. Stewart, *J. Mol. Model.*, **2007**, *13*, 1173.
3. J.J.P. Stewart, *Int. J. Quant. Chem.*, **1996**, *58*, 133.
4. Mopac2009, Version 10.153L, J. J. P. Stewart, Stewart Computational Chemistry, www.openmopac.net.
5. Spartan '06 Wavefunction Inc. 18401 Von Karman Avenue, Suite 370 Irvine, CA 92612 www.wavefun.com.
6. Y. Zhao, D.G. Truhlar, *Theor. Chem. Acc.*, **2008**, *120*, 215.
7. Gaussian 09, Revision A.02, Frisch, M.J., Trucks, G.W., Schlegel, H.B., Scuseria, G.E., Robb, M.A., Cheeseman, J.R., Montgomery, J., J.A., Vreven, T., Kudin, K.N., Burant, J.C., Millam, J.M., Iyengar, S.S., Tomasi, J., Barone, V., Mennucci, B., Cossi, M., Scalmani, G., Rega, N., Petersson, G.A., Nakatsuji, H., Hada, M., Ehara, M., Toyota, K., Fukuda, R., Hasegawa, J., Ishida, M., Nakajima, T., Honda, Y., Kitao, O., Nakai, H., Klene, M., Li, X., Knox, J.E., Hratchian, H.P., Cross, J.B., Bakken, V., Adamo, C., Jaramillo, J., Gomperts, R., Stratmann, R.E., Yazyev, O., Austin, A.J., Cammi, R., Pomelli, C., Ochterski, J.W., Ayala, P.Y., Morokuma, K., Voth, G.A., Salvador, P., Dannenberg, J.J., Zakrzewski, V.G., Dapprich, S., Daniels, A.D., Strain, M.C., Farkas, O., Malick, D.K., Rabuck, A.D., Raghavachari, K., Foresman, J.B., Ortiz, J.V., Cui, Q., Baboul, A.G., Clifford, S., Cioslowski, J., Stefanov, B.B., Liu, G., Liashenko, A., Piskorz, P., Komaromi, I., Martin, R.L., Fox, D.J., Keith, T., Al-Laham, M.A., Peng, C.Y., Nanayakkara, A., Challacombe, M., Gill, P.M.W., Johnson, B., Chen, W., Wong, M.W., Gonzalez, C., Pople, J.A., Gaussian, Inc., Wallingford CT, **2009**, www.gaussian.com.
8. M. Korth, M. Pitonák, J. Rezáč, P. Hobza, *J. Chem. Theory Comp.*, **2010**, *6*, 344.
9. J. Rezáč, J. Fanfrlík, D. Salahub, P. Hobza, *J. Chem. Theory Comp.*, **2009**, *5*, 1749.
10. J. Baker, *J. Comp. Chem.*, **1986**, *7*, 385.
11. W.C. Davidon, *SIAM J. Optimiz.*, **1991**, *1*, 1.
12. R. Fletcher, "Practical methods of optimization" (2nd ed.), John Wiley & Sons, New York, **1987**.
13. C.G. Broyden, *J. Inst. Math. Appl.*, **1970**, *6*, 222.
14. R. Fletcher, *Comp. J.*, **1970**, *13*, 317
15. D. Goldfarb, *Math. Comput.*, **1970**, *24*, 23.
16. D.F. Shanno, *Math. Comput.*, **1970**, *24*, 647.
17. H. Matthies, G. Strang, *Int. J. Num. Meth. Eng.*, **1979**, *14*, 1613.
18. J. Nocedal, *Math. Comput.*, **1980**, *35*, 773.
19. R.H. Byrd, J. Nocedal, R.B. Schnabel, *Math. Prog.*, **1994**, *63*, 4, 129.
20. C. Zhu, R.H. Byrd, J. Nocedal, *ACM Trans. Math. Soft.*, **1997**, *23*, 550.
21. A. Klamt, G. Schüümann, *J. Chem. Soc. Perkin Trans. 2*, **1993**, 799.